Modelling crystal growth from pure and impure solutions – a case study on sucrose

Pedro Miguel da Silva Martins

A thesis submitted in part fulfilment of the requirement for the degree of Doctor in the Faculty of Engineering, University of Porto, Portugal

This thesis was supervised by
Doctor Fernando Alberto Nogueira da Rocha, Departamento de Engenharia Química, Faculdade de Engenharia da Universidade do Porto, Porto, Portugal

Laboratório de Engenharia de Sistemas de Processos
Instituto de Sistemas e Robótica – Porto
Departamento de Engenharia Química
Faculdade de Engenharia da Universidade do Porto
Porto, Portugal

January, 2006

"Aquela criança olhava fascinada para o seu pai. O pai estava de joelhos na terra húmida, com as mãos enterrava e agora cobria aquela pedrinha – uma semente. Levantou os olhos para o filho e disse: "Vês aquela coisa grande, ali, alta, é uma árvore… e daqui vai nascer uma como aquela." A criança abria a boca de espanto e sorria. Acreditou. Não é que tivesse lógica, mas era o pai que dizia."

Vasco Pinto Magalhães, s.j.

Abstract

In this work, crystal growth from solution was investigated from an experimental and theoretical point of view. Particular emphasis was given to the crystallization of sucrose from pure and impure solutions. A progressive study of the factors influencing crystal growth was carried out, starting from industry oriented approaches and finishing at the molecular scale description of the phenomenon.

Accordingly, in the first part of the thesis, two methods were proposed for monitoring and management of sugar evaporative crystallizers. One of the methods is based in a set of equations balancing the amount of sucrose, impurities and water (mass balance method), whereas in the other, in situ images are captured and processed in order to determine the mean crystal size progress (image analysis method). Both methods were successfully applied to sugar boiling experiments carried out in a pilot vacuum pan with sugar cane syrups. The obtained evolution of parameters related with the crystal content, liquor purity and sucrose concentration, was subsequently used in equilibrium and kinetic studies. Sucrose growth rate curves were possible to be estimated under normal boiling conditions by representing the measured growth rates as a function of the liquor supersaturation during the experiments. Regardless of the significant practical interest of these results, their use in fundamental studies was at that time limited by the great number of variables in question.

In the subsequent chapters, most of those variables were independently assessed. Initially, sucrose growth experiments in a laboratory batch crystallizer were conceived to study the influence of the mass transfer resistance on the crystal growth rate. Soon it was noticed that existing diffusion-reaction theories would hardly explain the observed experimental evidences. The verified inconsistencies are probably related with the overlooked role of the interfacial adsorption in crystal growth from solution. As a result, an alternative physical and mathematical model was put forward, in which simultaneous occurrence of solute diffusion and adsorption is admitted to occur before the surface integration of adsorbed molecules. Contrarily to the classical theories, the new “parallel step model” demonstrated to be consistent with experimental results obtained at the laboratory and with published data regarding other systems than sucrose.

Next, crystal growth in the presence of impurities was investigated in the light of a new “competitive adsorption model”. This model emphasizes the competition between the crystallizing solute and the impurity for the occupation of active sites at crystal surface. By fitting the theoretical model to growth rate data measured at different supersaturations and impurity concentrations, it is possible to estimate the fraction of the crystal surface covered by the impurity and to characterize the impurity effectiveness on the growth rate lowering. The competitive adsorption model adequately explained unresolved mechanistic and kinetic evidences frequently reported in literature.

An important step forward was the proposal of a new atomistic theory called “spiral nucleation model” to look into the fundamental relationship between the crystal growth rate and key variables such as supersaturation, temperature, crystal size, interfacial properties, etc.

The introduced concepts derive from latest developments on the characterization of the surface phenomena using advanced microscopic techniques. With the spiral nucleation model, identified limitations of the two-dimensional nucleation models and of the Burton-Cabrera-Frank theory are responded, even though a common framework is shared by the new and the classical approaches. In a first application example of this model, important interfacial properties were possible to be calculated from the sucrose growth kinetics, and topological parameters of spiral growth were estimated without the use of microscopy.

In the concluding part of the thesis, the potential of the proposed models is illustrated in several application examples. By combining the parallel step model and the spiral nucleation model, an investigation was performed on the phenomenon of size dependent growth. Laboratory growth experiments were carried out in the batch crystallizer with crystals of different sizes. As expected by the new fundamental model, the integration rate was linearly dependent on crystal size. Consequently, a new formalism was proposed by expressing the mass deposition rate per crystal volume units. The "volumetric growth rate" demonstrated to be of great application to account for the kinetic effect of crystal size and in situations of unknown crystal number and size. This formalism was conveniently integrated in the competitive adsorption model to describe the effect of cane sugar impurities on the sucrose growth kinetics measured in the first part of the thesis. The theoretical model was found to be an excellent alternative to the empirical correlations traditionally used in sugar industry and a useful tool on the systematic characterisation of the impurities action. Finally, empirical, engineering and fundamental models were used in a unified vision of the effect of temperature and growth rate history on the sucrose growth kinetics. A relationship between the concepts of "true" and "apparent" activation energy was established according to the parallel step model. The temperature effect was further studied by performing innovative batch growth experiments, in which the crystal growth rates are continuously measured as the solution is cooled and at constant supersaturation. Different results were obtained by this method and by the conventional isothermal method; the spiral nucleation model suitably explained these differences according to different surface properties caused by the growth rate history in each case. The same arguments are believed to justify different growth rate curves measured in the batch crystallizer and in a fluidized bed crystallizer. This example additionally demonstrated how apparently divergent results can be rationally interpreted according to the new concepts introduced throughout this thesis.

Keywords: Crystal growth, Growth rate, Growth kinetics, Sucrose, Mass transfer, Impurities, Adsorption, Evaporative crystallizer.

Resumo

Neste trabalho investigou-se o crescimento cristalino sob os pontos de vista teórico e experimental, dando particular ênfase à cristalização da sacarose em soluções puras e impuras. Os factores que afectam o crescimento cristalino foram discutidos de uma forma progressiva, começando em perspectivas resultantes da indústria do açúcar e terminando com estudos fundamentais dos mecanismos de crescimento à escala molecular.

Assim sendo, na primeira parte da tese foram propostos dois métodos para a monitorização e gestão de cristalizadores evaporativos de açúcar. Um dos métodos baseia-se num conjunto de equações de balanço das quantidades de sacarose, impurezas e água (método dos balanços de massa), enquanto que no outro são captadas e processadas imagens *in situ* tendo em vista a determinação da evolução do tamanho médio dos cristais (método de análise de imagem). Ambos os métodos foram aplicados com sucesso em experiências de cristalização evaporativa de açúcar à escala piloto, usando xaropes industriais de cana. A evolução, daí resultante, de parâmetros relacionados com o conteúdo de cristais, pureza do licor e concentração de sacarose foi de seguida usada em estudos de equilíbrio e cinéticos. Através da representação das velocidades de crescimento de sacarose em função da sobressaturação do licor ao longo das experiências, foi possível estimar as curvas de crescimento em condições normais de cozedura do açúcar. Apesar do grande interesse prático destes resultados, o seu emprego em estudos fundamentais de crescimento foi na altura limitado pelo grande número de variáveis em jogo.

Nos capítulos que se seguiram, uma grande parte dessas variáveis foram descriminadamente analisadas. Numa primeira fase, experiências laboratoriais de crescimento de sacarose num cristalizador por partidas foram concebidas com a finalidade de estudar a influência da resistência de transferência de massa nas velocidades de crescimento cristalino. Depressa se notou que as teorias de difusão-reacção existentes dificilmente poderiam explicar as evidências experimentais observadas. Crê-se que a razão para as incoerências verificadas reside no papel, porventura desprezado, da adsorção interfacial. Consequentemente, foi sugerido um modelo físico e matemático alternativo, no qual se admite a ocorrência simultânea da difusão e adsorção do soluto, antes da integração à superfície das moléculas adsorvidas. Ao contrário do que aconteceu com as teorias clássicas, o novo "modelo dos passos em paralelo" provou ser consistente com os resultados experimentais obtidos no laboratório e com dados publicados referentes a outros sistemas que não a sacarose.

Seguidamente, o crescimento cristalino na presença de impurezas foi investigado à luz de um novo "modelo de adsorção competitiva". Este modelo enfatiza a competição que ocorre entre o soluto a cristalizar e a impureza pela ocupação dos sítios activos à superfície do cristal. Através do ajuste do modelo teórico a dados de velocidade de crescimento medidos a diferentes sobressaturações e concentrações de impureza, é possível estimar a fracção da superfície cristalina ocupada pela impureza e caracterizar a eficiência da impureza na diminuição das velocidades de crescimento. O modelo de adsorção competitiva permitiu esclarecer questões frequentemente colocadas na literatura, relacionadas com as cinéticas e mecanismos de crescimento em soluções impuras.

A proposta de uma nova teoria atomística denominada "modelo da nucleação em espiral" é considerada um significativo avanço, pois permite estabelecer uma relação fundamental entre a velocidade de crescimento cristalino e variáveis chave como sobressaturação, temperatura, tamanho do cristal, propriedades interfaciais, etc. Os conceitos introduzidos surgem na sequência de recentes desenvolvimentos na caracterização dos fenómenos de superfície usando técnicas microscópicas. Com o modelo da nucleação em espiral, é dada resposta a conhecidas limitações dos modelos de nucleação bi-dimensional e da teoria de Burton-Cabrera-Frank, ainda que, fundamentos comuns sejam partilhados pela nova abordagem e pelas teorias clássicas. Num primeiro exemplo de aplicação deste modelo, foi possível calcular propriedades interfaciais importantes a partir de cinéticas de crescimento de sacarose, bem como estimar parâmetros topológicos associados ao crescimento em espiral, sem recurso à microscopia.

Na parte final da tese, o potencial dos modelos propostos é ilustrado através de vários exemplos de aplicação. Combinando os modelos dos passos em paralelo e da nucleação em espiral, foi investigada a influência do tamanho dos cristais nas cinéticas de crescimento. As experiências laboratoriais de crescimento foram desta feita realizadas com cristais de diferentes tamanhos. Como esperado pelo novo modelo fundamental, a velocidade de integração variou linearmente com o tamanho do cristal. Por conseguinte, um novo formalismo foi proposto no qual a velocidade de cristalização é expressa por unidade de volume de cristal. A "velocidade de crescimento volumétrica" provou ser de grande aplicabilidade na caracterização do efeito cinético do tamanho dos cristais e em situações nas quais o número e tamanho dos cristais não são conhecidos. Este formalismo foi integrado com êxito no modelo de adsorção competitiva, na descrição do efeito das impurezas do açúcar de cana na cinética de crescimento da sacarose medida na primeira parte da tese. O modelo teórico demonstrou ser uma excelente alternativa às correlações empíricas tradicionalmente usadas na indústria do açúcar e uma ferramenta útil na caracterização sistematizada da acção das impurezas. A concluir, modelos empíricos, de engenharia e fundamentais foram usados numa visão unificada do efeito da temperatura e do historial de velocidades de crescimento na cinética de crescimento da sacarose. Usando o modelo dos passos em paralelo foi estabelecida uma relação teórica entre os conceitos de energia de activação "verdadeira" e "aparente". O estudo do efeito da temperatura foi complementado através da realização de experiências inovadoras, nas quais as velocidades de crescimento cristalino são continuamente estimadas à medida que a solução é arrefecida, a sobressaturação constante. Diferentes resultados foram obtidos através deste método e do método isotérmico convencional; tais diferenças foram adequadamente explicadas pelo modelo da nucleação em espiral com base nas diferentes propriedades superficiais causadas pelo historial de velocidades de crescimento em cada caso. Os mesmos argumentos foram depois usados para justificar diferentes curvas de crescimento medidas no cristalizador por partidas e num cristalizador de leito fluidizado. Este exemplo permitiu também demonstrar como resultados aparentemente divergentes podem ser racionalmente interpretados de acordo com os novos conceitos introduzidos ao longo da tese.

Palavras chave: Crescimento cristalino, Velocidade de crescimento, Cinética de crescimento, Sacarose, Transferência de massa, Impurezas, Adsorção, Cristalizador evaporativo.

Résumé

Dans ce travail, la croissance des cristaux en solution a été étudiée d'un point de vue expérimental et théorique, donnant une particulière attention à la cristallisation du saccharose en solutions pures et impures. Les facteurs qui affectent la croissance cristalline sont discutés d'une forme progressive, commençant dans les perspectives résultant de l'industrie du sucre et en finissant avec la description moléculaire du phénomène.

En conséquence, dans la première partie de la thèse, on a proposé deux méthodes pour la surveillance et la gestion des appareils à cuire pour la cristallisation du sucre. Une des méthodes est basée dans un ensemble d'équations évaluant la quantité du saccharose, les impuretés et l'eau (méthode de bilan de matière), tandis que dans l'autre, des images in situ sont capturées et traitées afin de déterminer le progrès de la dimension moyenne des cristaux (méthode d'analyse d'image). Les deux méthodes ont été appliqués avec succès dans des expériences de cristallisation évaporative de sucre à l'échelle pilote, utilisant sirops industriels de canne. L'évolution obtenue des paramètres rapportés avec le contenu de cristaux, pureté de la liqueur et concentration du saccharose a ensuite été utilisée dans des études d'équilibre et cinétiques. C'est à travers la représentation des vitesses de cristallisation du saccharose en fonction de la sursaturation de la liqueur au long des expériences, que ceci a été possible d'estimer les courbes de croissance dans des conditions normales de cuisson du sucre. Malgré le grand intérêt pratique de ces résultats, son emploi dans des études fondamentales de croissance a été à l'occasion limitée par le grand nombre de variables en question.

Dans les chapitres suivants, une grande partie de ces variables ont été indépendamment analysées. Au début, des expériences en laboratoire de croissance du saccharose dans un cristalliseur discontinu ont été conçues avec la finalité d'étudier l'influence de la résistance de transfert de masse dans les vitesses de cristallisation. Rapidement, on a remarqué que les théories de diffusion-réaction existantes difficilement pourraient expliquer les évidences expérimentales observées. On pense que la raison pour les incohérences vérifiées sont dues au papier, par hasard méprisé, de l'adsorption interfaciale. En conséquence, on a été suggéré un modèle physique et mathématique alternatif, dans lequel s'admet la présence simultanée de la diffusion et l'adsorption du soluté, avant l'intégration à la surface des molécules adsorbées. Contraire aux théories classiques, le nouveau "modèle des étapes en parallèle" a prouvé être cohérent avec les résultats expérimentaux obtenus dans le laboratoire et les données publiées concernant d'autres systèmes que le saccharose.

Ensuite, la croissance des cristaux en présence d'impuretés a été étudiée s'inspirant d'un nouveau "modèle d'adsorption concurrentielle". Ce modèle souligne la concurrence entre le soluté à cristalliser et l'impureté par l'occupation des lieus actifs à la surface du cristal. À travers l'ajustement du modèle théorique à des données de vitesse de croissance mesurés à différentes sursaturations et concentrations d'impureté, c'est possible d'estimer la fraction de la surface cristalline couverte par l'impureté et de caractériser l'efficacité de l'impureté dans la diminution des vitesses de cristallisation. Le modèle d'adsorption concurrentielle a permis d'éclaircir des questions fréquemment posées dans la littérature, rapportées avec les cinétiques et mécanismes de croissance en solutions impures.

La proposition d'une nouvelle théorie atomistique appelée "modèle de nucléation en spirale" est considérée comme étant une significative avance, qui permet d'établir une relation

fondamentale entre la vitesse de cristallisation et des variables clé comme la sursaturation, température, taille en cristal, propriétés interfaciales, etc. Les concepts présentés dérivent des récents développements dans la caractérisation des phénomènes de surface en utilisant techniques microscopiques. Avec le modèle de nucléation en spirale, des limitations identifiées des modèles bidimensionnels de nucléation et de la théorie Burton-Cabrera-Frank sont répondues, malgré cela, des fondements communs sont partagés par le nouvel abordage et par les théories classiques. Dans un premier exemple d'application de ce modèle, il a été possible de calculer des propriétés interfaciales importantes à partir de la cinétique de cristallisation de sucrose, ainsi que d'estimer des paramètres topologiques associés à la croissance en spirale, sans ressource à la microscopie.

En conclusion, le potentiel des modèles proposés est illustré dans plusieurs exemples d'application. En combinant les modèles des étapes en parallèle et de nucléation en spirale, une recherche a été effectuée sur l'influence de la taille des cristaux dans les cinétiques de cristallisation. Les expériences en laboratoire de croissance ont été cette fois réalisées avec des cristaux de différentes tailles. Comme attendu par le nouveau modèle fondamental, la vitesse d'intégration a varié linéairement avec la dimension du cristal. En conséquence, un nouveau formalisme a été proposé, dans lequel la vitesse de cristallisation est exprimée par unité de volume de cristal. La "vitesse de croissance volumétrique" a prouvé être de grande applicabilité dans la caractérisation de l'effet cinétique de la taille des cristaux, et dans les situations où le nombre et la dimension des cristaux ne sont pas connus. Ce formalisme a été intégré avec succès dans le modèle d'adsorption concurrentielle, dans la description de l'effet des impuretés du sucre de canne sur la cinétique de cristallisation du saccharose mesuré dans la première partie de la thèse. Le modèle théorique a démontré être une excellente alternative aux corrélations empiriques traditionnellement utilisées dans l'industrie du sucre et un outil utile dans la caractérisation systématisée de l'action des impuretés. Pour conclure, des modèles empiriques, d'ingénierie et fondamentaux ont été utilisés dans une vision unifiée de l'effet de la température et de l'histoire de vitesses de cristallisation dans la cinétique de croissance des cristaux du saccharose. Un rapport entre les concepts d'énergie d'activation "vraie" et "apparente" a été établi selon le modèle des étapes en parallèle. L'effet de la température a été encore étudié à travers la réalisation d'expériences innovatrices, dans lesquelles les vitesses de cristallisation sont mesurées sans interruption pendant que la solution est refroidie, à sursaturation constante. Différents résultats ont été obtenus par cette méthode et par la méthode isotherme conventionnelle; le modèle de nucléation en spirale a convenablement expliqué ces différences sur la base des différentes propriétés superficielles causées par l'histoire de vitesses de cristallisation en chaque cas. Les mêmes arguments ont été utilisés ensuite pour justifier les différentes courbes de croissance mesurées dans le cristalliseur discontinu et dans un cristalliseur de lit fluidisé. Cet exemple a permis aussi de démontrer comment des résultats apparemment divergents peuvent être rationnellement interprétés selon les nouveaux concepts présentés dans toute cette thèse.

Mots-clés: Croissance des cristaux, Vitesse de cristallisation, Cinétique de cristallisation, Saccharose, Transfert de masse, Impuretés, Adsorption, Appareil à cuire.

Aos meus Pais

À minha Irmã

Acknowledgments

A great part of this of this thesis is due to my supervisor Professor Fernando Rocha. I whish to thank him for his friendship and dedication, and for the freedom he gave me to take the risk of new research paths.

The time I spent at Audubon Sugar Institute (ASI) was very important for the thesis achievements. I would like to thank Doctor Peter Rein for welcoming me at the Institute and for his support. Many thanks to all the ASI staff, especially, to Julie King and Brian White for their prompt assistance.

Most of my experimental work at Engineering Faculty of University of Porto (FEUP) was carried out in the laboratory facility developed by Doctor Nuno Faria during his PhD. I am indebted to him for that, and for the support he gave me at the beginning of my research. I acknowledge Professor Romualdo Salcedo for his cooperation in many moments during the last 5 years.

I would like to thank Fundação para a Ciência e a Tecnologia for the financial support during 48 months (PhD scolarship SFRH/BD/3428/2000) and Fundação Calouste Gulbenkian for a 3 months grant in 2003. I thank the Process Systems Engineering Group for providing me very good working conditions at the Department of Chemical Engineering of FEUP.

I am grateful to Doctor Luís Bento and his wife Dina, for being my family in Louisiana.

I wish to thank Renato for his “lessons” on fluid flow software, Antonio and Pedro Mena for their help with image analysis software, and all the others “Feupianos” (Sarah, Vânia, Lúcia, Carina, Rosa, Tirzhá, Zé Luís, Rui, Luís, Nuno, ...) for their friendship.

I thank my only-geographically-distant friends Emilia Zettergren and Cameron Bradley for the good times I shared with them. I am also grateful to my good friends Ana, Denise and Manuel.

Particular thanks to Isabel, for giving me the privilege of being able to be myself.

I dedicate this thesis to all my family, in particular to my mother Augusta, to my father José and to my sister Susana.

Contents

Nomenclature

Roman Symbols

A	surface area of crystals
$\overline{A}$	average surface area of crystals
a	solute activity
a'	distance between two neighbouring adsorption positions
a_e	solute activity in equilibrium
a_n	peripheral area
C	constant of the BCF equation
C_1	constant of Eq. (7.34)
C_2	constant of Eq. (7.34)
C_A	molar concentration of solute A
CC	crystal content in the massecuite
c	solute concentration
c_i	interfacial solute concentration
c_i	impurity concentration
$\mathcal{D}_{AB}$	diffusion coefficient
D_{eq}	equivalent diameter of crystals
D_s	surface diffusion coefficient
E_A	apparent activation energy
E_D	activation energy for diffusion
E_T	true activation energy in the PSM
F	crystal shape factor
f	dimensionless supersaturation
f_e	equivalent dimensionless supersaturation
G	overall linear growth rate
G	Gibbs free energy
g	overall growth order
h	ratio between the kinetic and diffusional rates in the TSM
h	elementary height
J	current of molecules

K	parameter of the theoretical crystallization curve (Eq. (3.5))
K_0	empirical parameter in Eq. (3.16)
K_1	empirical parameter in Eq. (3.16)
K_2	empirical parameter in Eq. (3.16)
K_3	empirical parameter in Eq. (3.16)
K_G	overall growth constant
K_V	volumetric growth constant
K_{V0}	pre-exponential constant (Eq. (10.4))
K_a	Langmuir constant in the Kubota-Mullin model
K_i	Langmuir constant in the CAM
K_p	Langmuir constant in the CAM
k	Boltzmann constant
k_D	dissolution mass transfer coefficient
k_G	empirical kinetic constant in Eq. (7.31)
k_d	mass transfer coefficient during growth in the PSM
k_d'	mass transfer coefficient during growth in the TSM
k_{d0}	pre-exponential constant (Eq. (10.16))
k_e	equivalent kinetic constant in the PSM
k_i	parameter of the CAM ($k_i = K_i / (1 + K_p c^*)$)
k_i'	parameter of the CAM ($k_i c_i = k_i' (NS/W)$)
k_p	parameter of the CAM ($k_p = K_p c^* / (1 + K_p c^*)$)
k_r	kinetic constant in the PSM
k_r'	integration rate constant in the TSM
k_{r0}	pre-exponential constant in the PSM
k_{re}	kinetic constant in the PSM ($k_{re} = k_e \delta$)
k_{re}'	size-independent kinetic constant in the PSM ($k_{re}' = k_{re} / L$)
k_{si}	parameter of the CAM ($k_{si} = k_p / (1 + k_i c_i)$)
L	crystal size
L_a	average distance between active sites in a step
l	number of adsorbed layers (PSM)
$\overline{l}$	average distance between dislocations
l_i	average distance between adsorbed impurities in a step
M	unoccupied active sites (PSM)
MA	active sites occupied by the solute A (PSM)
m	mass of crystals

m_w	mass of water in the evaporative crystallizer
N	number of growing crystals
N	number of adsorbed molecules incorporating the crystal
N_A	molar flux of solute A
Nc	number of elements in a bounding polygon
NS/W	non-sucrose to water ratio
n	concentration of nuclei on the crystal surface
n_1	concentration of monomers on the crystal surface
n_c	concentration of critical sized 2D nuclei
n_e	density of molecular positions at crystal surface
n_s	density of surface adsorbed molecules
n_{se}	density of surface adsorbed molecules in equilibrium
n_{sp}	density of active spirals at the crystal surface
n_V	volumetric growth order
P_{abs}	absolute pressure
p	vapour pressure
p_e	vapour pressure in the equilibrium
R	growth rate perpendicular to the surface
R	ideal gas constant
R_0	growth rate perpendicular to the surface in pure systems
R^2	correlation coefficient
R_D	dissolution rate
R_G	overall growth rate
RS/A	reducing sugar to ash ratio
R_V	volumetric growth rate
R_{V0}	volumetric growth rate in pure systems
R_d	pure diffusional rate
R_p	radius of a spherical/cylindrical crystal
r	radial direction/radius
r	kinetic order in the PSM
r'	kinetic order in the TSM
r_f	radial distance from the crystal surface ($r_f = r_p - R_p$)
r_p	radial direction in the stagnant film
r_w	Wenzel roughness factor
S	supersaturation

SC	solubility coefficient
S_s	surface supersaturation ($S_s = n_s / n_{se} - 1$)
T	temperature
t	time
t_b	massecuite temperature
t_{bw}	vapour temperature in the evaporative crystallizer
u	particle-solution velocity
V	step advancing velocity
V_f	stagnant film volume
v	vibrational frequency
v_n	surface nucleus volume
W	evaporation energy in vapour growth
W	adsorbing energy in solution growth
w	percentage of solids in the massecuite
x	dimensionless coordinate direction
x	solute molar fraction
x_2	solute molar fraction in Eq. (7.32)
x_e	solute molar fraction in equilibrium
x_s	mean displacement of adsorbed molecules
y	distance from the midpoint between two steps
y_0	interstep distance
z	coordinate direction

Greek symbols

α	volume shape factor
α	impurity effectiveness factor in the Kubota-Mullin model
α	proportionality factor ($y_0 = \alpha r_{c2D}$)
β	surface area shape factor
β	impurity effectiveness factor in CAM
β	parameter of the SNM to distinguish solution growth and vapour growth
Γ_2	Gibbs excess concentration
γ	interfacial tension
Δ	difference/variation
δ	stagnant film thickness

ε	number of dislocation sources
η	effectiveness factor in the PSM
η	viscosity
η_C	effectiveness factor in the TSM
θ	angle (polar coordinate)
θ_l	coverage of adsorption sites by impurities in a step
θ_s	overall surface coverage
κ	crystal shape factor defined by Eq. (4.35)
λ	density of dislocations at the crystal surface
ρ	solution density
ρ	radius of curvature of a step
ρ_s	crystal density
τ_s	mean life time of adsorbed molecules
ϕ	ratio between the kinetic and diffusional rates in the PSM
ϕ_g	generalized value of ϕ defined by Eq. (4.45)
χ	constant of the BCF equation
ψ	differential supersaturation ($\psi = S - S_s$)
Ω	molecular volume
ω	proportionality factor ($\omega = k_d / k_D$)

Indices and exponents

$2D$	two-dimensional
adj	fitted to experimental data
ads	adsorption
b	in the bulk
c	critical
chem	chemical regime
diff	diffusional regime
f	final
i	initial
int	integration of adsorbed molecules
med	median
mig	migration of adsorbed molecules
min	minimum

pol	convex bounding polygon area
proj	projected area
s	seeds
*	saturation
∞	straight step

Acronyms

BCF	Burton, Cabrera and Frank
CAM	competitive adsorption model
CCD	charge-coupled device
CSD	crystal size distribution
DS	dissolved solids in the massecuite
PSM	parallel step model
SL	solid-liquid
SNM	spiral nucleation model
TDS	total dry solids in the massecuite
TSM	two step model

Dimensionless numbers

Da	Damköhler number ($Da = h$ in the TSM and $Da = \phi^2/2$ in the PSM)
Sc	Schmidt number ($Sc = \eta/(\mathcal{D}_{AB}\rho)$)
Sh	Sherwood number ($Sh = k_D L/\mathcal{D}_{AB}$)
Re_p	Reynolds number of particle ($Re_p = \rho u L/\eta$)

List of Figures

List of Tables

1. Introduction

1.1 Motivation and aim

When, in 1973, Ohara and Reid discussed the applicability and feasibility of sophisticated crystal growth models of surface diffusion growth and two-dimensional nucleation [1], they probably would not anticipate that the same theories would remain the fundamental basis of crystal growth science more than 50 years after their introduction. In fact, the means and instrumentation available nowadays regularly lead to important new findings that have not been considered in the classical models update. This is valid for both the physical premises of the crystal growth mechanisms and for the critical evaluation the growth models against experimental results. At the beginning of this study in 2001, the transfer of impurities into crystals in solution growth was the primary subject of study, as a natural sequence of previous works of Faria [2], Gonçalves [3] and Chorão [4] within the sugar system, and following the current trend in many research groups on industrial and fundamental crystallization. Nevertheless, as the work progressed, it became clear that considerable research in pure systems would have to be done before centering the attention on the impurity uptake. The alternative could be an essentially experimental work describing several pure solute/impurity systems; although interesting from a practical point of view, such a work would always have a limited application field. Presently, a great number of experimental data are published documenting the growth of crystals in the most diverse systems, by employing several growth techniques, and focusing the majority of growth variables. In so doing, the main emphasis is not anymore on the indiscriminate measurement of additional kinetic data of crystallization but instead on the development of new theoretical tools for their interpretation. This was a major conclusion from the panel discussion “Towards the Future of Industrial Crystallization” presented by Roger Davey, John Garside and Ronald

Rousseau in the last day of the 16th International Symposium on Industrial Crystallization held in Dresden, Germany [5]. In a time when this thesis was nearly finished (September of 2005), it was satisfying to realize that the guidelines for forthcoming studies appointed by those recognized authors, corresponded to the main objective envisaged by us during 2001: To combine the new experimental insights and the accepted theoretical grounds on the development of new crystal growth models that are able to shorten the existing gap between theory and practice. In so doing, the ultimate goal of estimating crystal growth rates a priori would be gradually accomplished.

The objectives outlined are manifestly challenging. Yet, in a first phase, the concrete problems found in the design, operation and management of industrial crystallizers were thought to be more effectively approached through pilot scale experimental investigation. The established cooperation with the Audubon Sugar Institute at Louisiana State University would make possible to perform sugar crystallization experiments in a pilot evaporative crystallizer, thus providing the proper starting point for increasingly sophisticated studies. As suggested by Ohara and Reid, the development and verification of any crystal growth theory should be based on kinetic data documenting the influence of specific independent variables [1]. According to the same authors, the most important variables are supersaturation, temperature, crystal size, mass transfer, and impurity type and level. More recently, the growth rate history and the energetics of the crystal faces have also been found to have a considerable role during growth. Unfortunately, few experiments have been reported where all the main variables were considered. Moreover, growth rates measured at similar experimental conditions can diverge significantly, when different growth techniques are employed [6, 7]. As a consequence, laboratory growth experiments under well-defined conditions are still required to evaluate the isolated influence of some of the above mentioned variables.

In this regard, the mass transfer studies during crystal growth are an illustrative case: although this subject is been considered in many works, only a small fraction of these are suitable to be used in the rational assessment of diffusion-integration models. This happens because the evaluation of the mass transfer resistances is often merely qualitative, or else, their quantification is based on doubtful simplifying hypothesis. As illustrated by the well-known series of 3 papers of Garside and Mullin dated from 1967/8 [8-10], the comprehensive modeling of the problem requires considerable amounts of growth and dissolution rate data, over a wide range of crystal-solution velocities. By this way, the relationship between the diffusional resistances during growth and dissolution can be clarified and, on the other hand,

important indications can be provided on how mass transfer is affected by surface adsorption during growth. The existence of a multilayered adsorption phase at the surface of growing crystals is admitted by many authors (see for example the revision made by Tai et al. [11]), but the incorporation of this concept in the crystal growth theories has not been effective [12-14]. The adsorption step is also thought to play an important role on the growth of crystals in the presence of impurities. In this field of study, numerous authors are in accordance about the kinetic patterns obtained, even though the existing theories do not completely explain those evidences. It is considered that further investigation has to be performed on the competitive nature of surface adsorption when the crystallizing solute and the impurity are involved. The demand for new theoretical growth models results, to a great extent, from the perspectives provided by modern microscopic techniques on the molecular mechanism of crystal growth [15]. This is, therefore, an important source to be explored on the fundamental research envisaged for this thesis.

1.2 Thesis layout

In this work, crystal growth from solution is progressively discussed from industrial, engineering and scientific perspectives. Following this order, new experimental methods and theoretical models are presented in the first three parts of the thesis, and in the last part, illustrative examples are given where the new concepts are jointly applied to crystallization data.

Part I, named “macro scale approach”, comprises Chapters 2 and 3 and deals with the evaporative crystallization of sucrose at pilot scale. In **Chapter 2**, new industry-oriented methods are purposed and applied to sugar boiling runs. The results obtained are then used in **Chapter 3** on the estimation of the respective sucrose growth kinetics.

In Part II, “new engineering models” are introduced to describe diffusion-affected growth in pure solutions (Chapters 4 and 5) and crystal growth in the presence of impurities (Chapter 6). **Chapter 4** is purely theoretical, providing the physical and mathematical concepts of the “parallel step model”. In **Chapter 5** the validation of the model is made against experimental data taken from literature and obtained in sucrose growth experiments at laboratory scale. **Chapter 6** is concerned with the proposal and validation of the “competitive adsorption model” about the effect of impurities on the crystal growth rates.

Part III is named “crystal growth science”, since new fundamental perspectives documented in literature are discussed in the light of a new “spiral nucleation model”. In **Chapter 7** the theoretical basis of the model is introduced and the model practical interest is pointed out. In **Chapter 8**, the phenomenon of size dependent growth is studied according to the spiral nucleation model.

The three chapters of Part IV consist in “application examples and conclusions”. In **Chapter 9** the influence of cane sugar impurities on the sucrose growth kinetics is investigated using the kinetic data obtained in Part I and the theoretical background provided by the competitive adsorption model and the spiral nucleation model. In **Chapter 10**, a synthesis of the several approaches discussed in the thesis is made through their use on the interpretation of sucrose growth rate data. In particular, the effect of temperature and growth rate history on the crystallization kinetics is analyzed, and the importance of the growth rate measurement technique is discussed. Finally, in **Chapter 11** the general conclusions and future work suggestions are referred.

All the main chapters are initiated with an overview of the theme and with a review of the respective state-of-the-art. After that, the novelty of the chapter is introduced and, in the case of experimental works, the experimental details and procedures are outlined. The results obtained experimentally or taken from the literature, are then presented and discussed. Finally, the main conclusions are summarized.

References

[1] M. Ohara and R. C. Reid, Modelling crystal growth rates from solution, Prentice-Hall, Inc., New Jersey, **1973**.

[2] N. Faria, Quantificação da morfologia de cristais de açúcar e sua aplicação ao estudo das cinéticas de cristalização, PhD Thesis, Faculdade de Engenharia da Universidade do Porto / Institut Nationale Polytechnique de Lorraine, Porto, **2002**.

[3] M. J. Gonçalves, Modelização e simulação computacional de uma unidade industrial de cristalização de açúcar, PhD Thesis, Faculdade de Engenharia da Universidade do Porto, Porto, **1996**.

[4] J. M. N. Chorão, Operação assistida por computador de um cristalizador evaporativo industrial de açúcar, PhD Thesis, Faculdade de Engenharia da Universidade do Porto, Porto, **1995**.

[5] R. Davey, J. Garside, and R. Rousseau, in *16th International Symposium on Industrial Crystallization*, Dresden, Germany, **2005**.

[6] M. Kohl, F. Puel, J. P. Klein, C. Hoff, and O. Monnier, Investigation of the growth rate of [beta]-cyclodextrin in water during both flow-cell and batch experiments. *J. Cryst. Growth*, **2004,** 270, 633-645.

[7] J. Garside, A. Mersmann, and J. Nyvlt, Measurement of Crystal Growth and Nucleation Rates, 2nd ed.; EFCE Working Party on Crystallization, IChemE, Rugby, **2002**.

[8] J. W. Mullin and J. Garside, Crystallization of aluminium potassium sulphate: a study in the assessment of crystallizer design data: I: - Single crystal growth rates. *Trans. Inst. Chem. Eng.*, **1967,** 45, T285-T290.

[9] J. W. Mullin and J. Garside, Crystallization of aluminium potassium sulphate: a study in the assessment of crystallizer design data: II: - Growth in a fluidized bed crystallizer. *Trans. Inst. Chem. Eng.*, **1967,** 45, T291-T295.

[10] J. W. Mullin and J. Garside, Crystallization of aluminium potassium sulphate: a study in the assessment of crystallizer design data: III: - Growth and dissolution rates. *Trans. Inst. Chem. Eng.*, **1968,** 46, T11-T18.

[11] C. Y. Tai, J.-F. Wu, and R. W. Rousseau, Interfacial supersaturation, secondary nucleation, and crystal growth. *J. Cryst. Growth*, **1992,** 116, 294-306.

[12] N. Kubota, M. Yokota, N. Doki, L. A. Guzman, S. Sasaki, and J. W. Mullin, A mathematical model for crystal growth rate hysteresis induced by impurity. *Cryst. Growth Des.*, **2003,** 3, 397-402.

[13] T. A. Land, T. L. Martin, S. Potapenko, G. T. Palmore, and J. J. De Yoreo, Recovery of surfaces from impurity poisoning during crystal growth. *Nature*, **1999,** 399, 442-445.

[14] L. N. Rashkovich and N. V. Kronsky, Influence of Fe3+ and Al3+ ions on the kinetics of steps on the {1 0 0} faces of KDP. *J. Cryst. Growth*, **1997,** 182, 434-441.

[15] A. A. Chernov, Notes on interface growth kinetics 50 years after Burton, Cabrera and Frank. *J. Cryst. Growth*, **2004,** 264, 499.

PART I

MACRO SCALE APPROACH

2. Vacuum pan monitoring by mass balance and image analysis methods

Overview

Sugar boiling experiments are carried out in a pilot vacuum pan with the aim of developing new methods for monitoring and estimation of important variables in industrial crystallization. A mathematical model based on mass balances is applied, using typical on-line data recorded during the boiling runs, to determine the evolution of parameters related to the crystal content and liquor purity. The conclusions resulting from the application of the mass balance method will be used in following chapters to study the crystal growth kinetics of sucrose in industrial and synthetic syrups. In a different approach, in situ images are captured and processed for the purpose of estimating the mean crystals size progress at the early stages of the strike – image analysis method. A strategy is proposed to solve the problems associated with the identification of crystals in images taken directly from the suspension. The results obtained by the two methods are compared, showing good agreement both in the range of the crystal sizes and in the way crystal size changes.

2.1 Vacuum pan monitoring

The change in the main properties and parameters during industrial crystallization is not always followed accurately because of the absence of suitable on-line measurements. This affects the product final quality, crystal yield, and the overall efficiency of the process. Consider, for example, the measurement of the degree of supersaturation. At a given temperature, a solution is supersaturated when the solute concentration is higher than saturation. In industry, supersaturation is achieved by evaporating the solvent, evaporative crystallization, or by cooling the solution, cooling crystallization. In either case, operators are still far from having a quantitative knowledge of this key parameter, and their actions are commonly empirically based. However, the temperature of the solutions is easily followed and the on-line measurement of solute concentration is well-established. The main difficulties in measuring the degree of supersaturation are related to the variation of variables that directly or indirectly alter the equilibrium conditions, as the crystallization advances. Namely, few alternatives are available to quantify the gradual drop of solution purity or the increase in crystal content. Two methods are here proposed for better monitoring and understanding of the process. The methods were applied to the evaporative crystallization of sugar from cane syrups.

2.1.1 Recent developments

At a given pressure, the boiling point of solutions is increased by the presence of non-volatile solutes. This basic principle has been used for a long time in the sugar industry for on-line measuring of the dissolved dry solids in liquors, correlating their concentration with the boiling point elevation and purity [1, 2]. The influence of the liquor purity on the boiling point elevation is considered a drawback of this inexpensive method, because such data are often unavailable. Refractometry is a classical analytical technique among sugar technologists. With the arrival of on-line refractometers [3], the amount of dissolved solids in the crystallizers can be measured independently of the amount of crystal, although impurity concentration has a small influence on the refractive index. Since the second half of the 1990s, a new technique has been introduced in the sugar industry, based on microwave technology [4]. The microwave concentration corresponds to the total quantity of dry substance, so no differentiation is made between the dissolved solids and the crystallized matter. Other traditional techniques based on physical and electrical properties of the

massecuite (conductivity, radio frequency conductivity, viscosity/consistency, and density) are used as an indicative help to the pan boiler. Difficulties in quantifying the relative contribution of the several process variables are associated with these techniques.

The research on monitoring techniques has been recently focused on two important crystallization parameters: crystal content and supersaturation [5]. At the industrial level, those properties are traditionally followed by sample extractions or by approximate relations with other measurements [3]. Sometimes, the estimations are based on the experience and feel of the operators who relate the massecuite viscosity with crystal content and supersaturation. Attempts have been made to employ more sophisticated technology. For example, Vaccari et al. [6] utilized an NIR (near infrared) technique in the cooling crystallization of pure sugar, as a first approach to automatic crystallization management. Schultz and Edye [7] continuously measured the crystal content in a pilot vacuum pan using low resolution NMR (nuclear magnetic resonance) instrumentation. In their experiments, massecuite was continuously drawn from the vacuum pan, flowing through a cell for the NMR measurements, before returning to the pan. Rozsa [3] developed a mathematical model to be used with on-line refractometers for supersaturation measurements. In this method, the values of the liquor purity were approximated according to a presupposed profile of the crystal content.

Image analysis is an emerging technique, whose potential in particle size and shape detection is being applied to crystallization. A review of the main steps on particle morphology characterization using image analysis was made by Pons et al. [8]. Tadeo et al. [9] processed the images taken during sugar crystallization to identify the phases of the process. The morphology of sucrose crystals was studied by Faria et al. [10] using an automated image analysis procedure. In that work, the degree of agglomeration of crystal samples was quantified. Lionnet [11] measured by image analysis the length and width of crystals at the end of sugar boiling runs, for crystal growth rates measurements. Off-line crystal size distributions were calculated from image processing by Monnier et al. [12] for adipic acid crystallization in water. This information was used together with on-line calorimetry and laser granulometry for batch cooling crystallization modelling.

2.2 Experimental section

Sugar boiling runs were conducted in the 50 L pilot vacuum pan shown in Figure 2.1 at Audubon Sugar Institute, Louisiana.

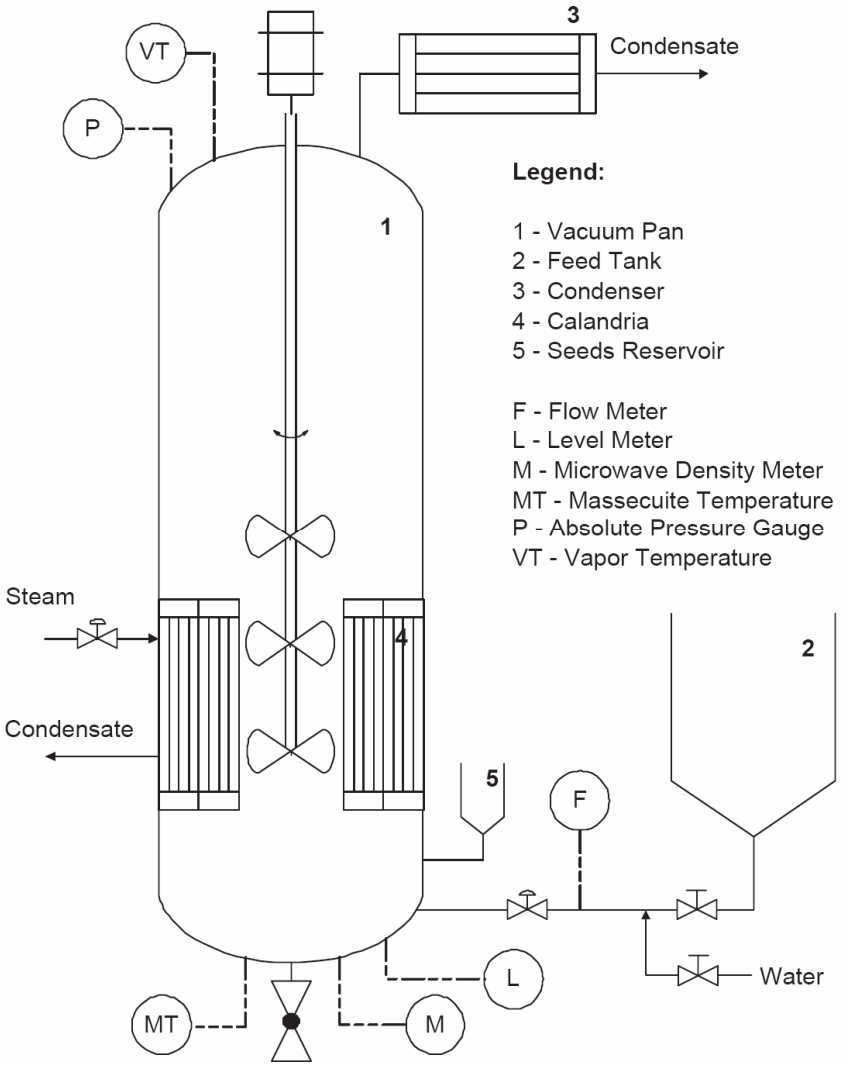

Figure 2.1. Scheme of the pilot vacuum pan.

Typical process parameters were controlled, displayed, and recorded by means of an Allen Bradley programmable control system and Rockwell automation software. The percentage of total dry solids in the massecuite (w_{TDS}) was measured through the microwave density readings provided by a Pro-M-tec GmbH device, model uWA-2.5. The dissolved solids' concentration (w_{DS}) was calculated from the boiling point elevation (Δt_b), according to the integrated form of the Clausius-Clapeyron equation with the parameters found by Saska in similar conditions [2],

$$\Delta t_b = 0.1660\left(\frac{w_{DS}}{100-w_{DS}}\right)^{1.1394}\left(\frac{273+t_{bw}}{100}\right)^{1.9735}\left(\frac{Purity}{100}\right)^{0.1237} \tag{2.1}$$

where $\Delta t_b = t_b - t_{bw}$. The massecuite temperature (t_b) was measured with a calibrated PT100 sensor located in the bottom of the pan. The vapour temperature (t_{bw}) is calculated as a function of the absolute pressure (P_{abs}) [2]:

$$t_{bw}(\text{ºC}) = 3.3374 P_{abs}(\text{inHg}) + 40.746 \quad (2.2)$$

The value of the liquor purity required in Eq. (2.1) was continuously updated according to the mass balance method (see below).

The experimental procedure was planned according to the conditions required for the solubility and kinetic studies that will be presented in the Chapter 3. It is intended to perform successive crystal growth and dissolution experiments until near saturation and at a controlled amount of water. A typical run consisted of the following sequence of steps:

1. Filling up. The absolute pressure inside the vacuum pan is set to a constant value ~17 kPa. The juice solenoid valve is then opened, allowing the syrup to enter until it reaches the desired level (~50 cm $H_20_{25ºC}$).

2. Concentration phase. The mechanical agitation is turned on, and the steam pressure controller is started. The concentration of dry solids begins to increase because of the evaporation of water.

3. Seeding. A suspension (5.0 ml) of sucrose crystals (seeds) in n-propanol was introduced in the vacuum pan, by opening the seed solenoid valve. The right moment to perform this action was determined by the concentration of dissolved dry solids in the mother liquor; usually seeding was made when the percentage of dissolved solids was near 75%.

4. Building up. The automatic control of microwave density is started, and the seeds are allowed to grow at constant water content. Consequently, the admission of water is automatically controlled to balance the evaporation rate. Because of crystal growth, the concentration of dissolved sucrose decreases until near saturation. The transition to another growth experiment is made by changing the set point of w_{TDS} to a higher value; the admission of water is suppressed, and the rise in supersaturation causes the crystals to grow. In some runs, dissolution experiments were made by the inverse process: after the growth period had finished, a lower value of the w_{TDS} set point was established and water was fed to the pan. Undersaturation is established and the crystals start to dissolve.

In all runs, industrial syrup with the same origin (Cora Texas mill) was used–apparent purity = 87.75% (sucrose content measured by the polarization method), brix = 65.42% (dissolved solids content measured by refractomery), glucose content = 1.12% (HPLC), fructose content = 1.16% (HPLC), and ash content = 2.22%. The propeller agitation speed was 650 rpm in all experiments. The concentration of seed in the n-propanol suspension was 0.411 kg/L. The

volume mean diameter (L_s) was measured by laser diffraction. The value found (13.33 μm) was used to estimate the number of crystals (N) inside the pan according to the introduced mass of seeds (m_s):

$$N = \frac{m_s}{\alpha \rho_s L_s^3} \tag{2.3}$$

In this equation, where ρ_s is the density of sucrose crystals, the volume shape factor found by Bubnik and Kadlec [13], using a characteristic dimension that is a function of the crystal linear dimensions ($\alpha = 0.31$), was used.

2.3 New Methods of sugar crystallization management

2.3.1 Mass balance method

This method relies on a set of equations that balance the amount of sucrose, impurities, and water in a vacuum pan during the crystallization of sugar. The syrup fed to the pan is the only source of sucrose and impurities, as long as the water used to control the total dry solids' concentration is pure. In the massecuite, sucrose can be either dissolved in the mother liquor or crystallized, while the non-sucrose compounds are assumed to be all in the mother liquor, therefore neglecting the small amount transferred into crystals. Water is continuously evaporated and is supplied both in the syrup, at the beginning of the run, and at the stage of the water content control.

Crystal content (CC), defined as the mass fraction of crystals in the massecuite, is calculated from the information of the total dry solids' concentration (w_{TDS}), given by the microwave concentration readings, and from the dissolved solids' concentration (w_{DS}) in the mother liquor, estimated from the boiling point elevation measurements. To calculate the mass of crystals, it is necessary to know, besides their fraction, the overall mass of the massecuite in the pan, which was determined from the massecuite level measurements.

Liquor purity corresponds to the percentage of sucrose in the total amount of dissolved dry solids. As the crystallization advances, sucrose concentration decreases, and thus, the liquor becomes less pure. The estimation of the liquor purity at any stage of the strike was done by evaluating the mass of crystals relative to the initial amount of dissolved sucrose.

Therefore, the initial purity of the used syrup had to be known. The non-sucrose to water ratio (NS/W) was also followed, since this is a parameter often required for solubility studies. The calculation used the value of the syrup purity and the microwave readings to determine the amount of impurities introduced in the pan and the water mass fraction.

2.3.2 Image analysis method

Images from the inside of the vacuum pan were captured with a CCD (charge-coupled device) camera during the boiling runs, and then they were analyzed using a professional image analysis package (Visilog 5.4, Noesis, les Ulis, France). The 752×480 pixel RGB images were processed in order to correct differences in light intensity and to enhance the crystals edges (Figure 2.2a, b).

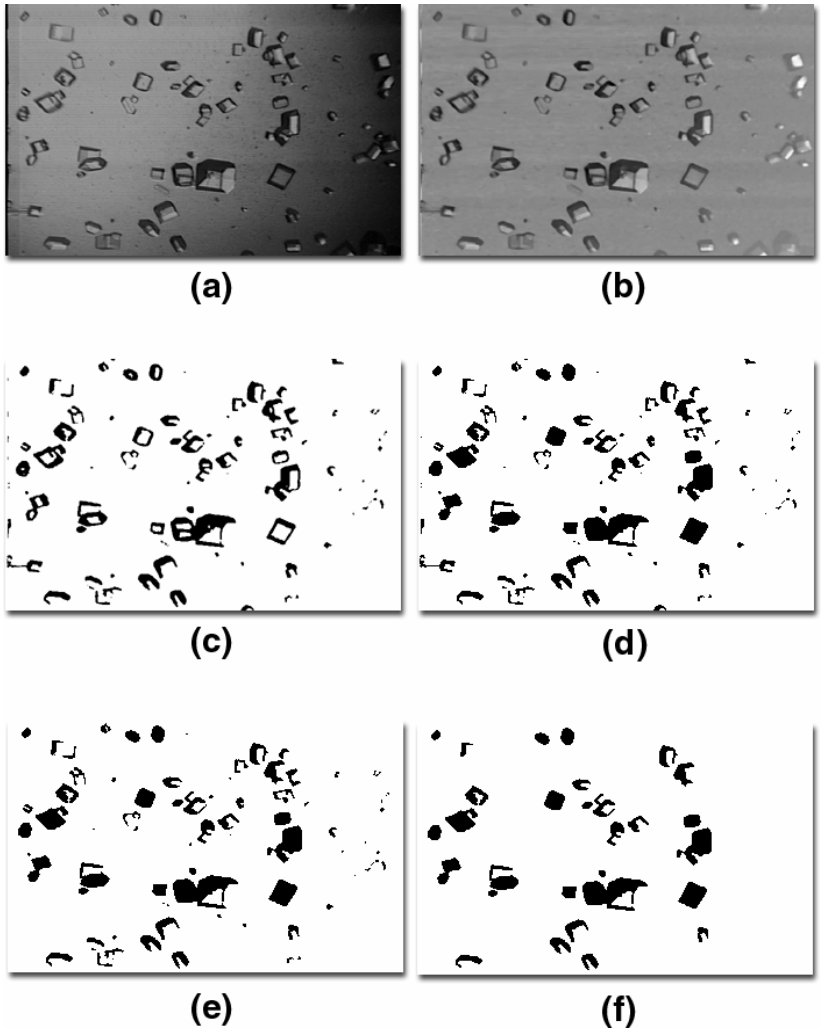

Figure 2.2. Sequence of the main actions performed on the images taken from inside of the vacuum pan. The original image was captured 37 min after seeding (05/12GI experiment).

This phase involves the use of image filters and the adjustment of the background by subtracting to the original images the one taken before each seeding (without crystals). As the images are taken directly from the process without any kind of sample preparation, their quality improvement by software can affect the results significantly. The resulting images were converted into 256 grey levels and then, the individual crystals are separated from the background in a binary image – image segmentation (Figure 2.2b, c). An automatic segmentation algorithm based on a three-zone entropic criterion was used. After that, a series of classical image processing functions were applied [8], including the elimination of crystal transparencies by hole filling (Figure 2.2c, d), elimination of the objects in contact with the image frame (Figure 2.2d, e) and debris cleaning by erosion/reconstruction (Figure 2.2e, f). At that point, the several objects were identified. Before measuring the silhouette surface, two problems needed to be solved: (i) the incomplete silhouettes of crystals exemplified by objects number 2 and 3 in Figure 2.3 and (ii) the occurrence of overlaid crystals as in the case of objects number 4 and 5 in the same figure. These troubles are associated with the limited image acquisition conditions in features such as the angle of the incident light, which cannot be ideal for all the moving crystals, or the existence of various planes of crystal flowing.

Figure 2.3. Identification of different types of silhouettes, from which, crystal equivalent diameters were calculated.

The procedure adopted for the equivalent mean diameter estimation is illustrated in Figure 2.4 for the different types of elements pointed out in Figure 2.3. The complete silhouette of crystals was forecasted by creating the convex bounding polygon [10, 14]. Estimating the projected area (A_{proj}) of individual crystals by means of the area of the convex bounding polygon (A_{pol}) introduces an error by defect in the cases where the edges are poorly defined. This is possible to see in Figure 2.4b by comparing the original picture of the crystal (I) with the silhouette of the respective convex bounding polygon (III). The equivalent diameter is given by

$$D_{eq} = 2\sqrt{\frac{A_{pol}}{\pi}} \tag{2.4}$$

As shown in Figure 2.4a, for well-differentiated crystals the projected silhouette before the individual measurements (II) is equivalent to the silhouette of the convex bounding polygon (III): $A_{proj} = A_{pol}$.

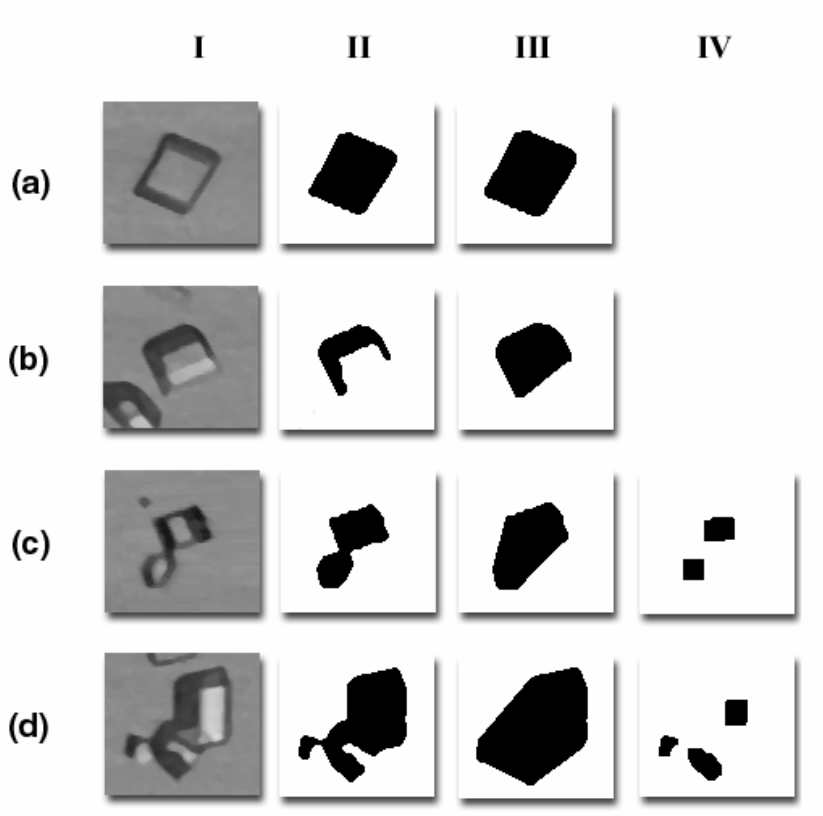

Figure 2.4. Comparison between the (I) original picture of individual elements and (II) the silhouettes corresponding to the measurements of the projected area, (III) convex bounding polygon area and (IV) number of crystals within each element – (a) well defined crystal; (b) poorly defined crystal; (c) two joined crystals; (d) three joined/overlapped crystals.

The same procedure was adopted in a first phase to solve the problem of the joined/overlapped crystals (Figure 2.4c, d). Here, the area of the polygon can be either higher or lower than the sum of the individual crystals areas, depending on the degree of overlap. The number of crystals contained in each bounding polygon (Nc) was then estimated by means of the number of different zones with the same gray level in the object (Figure 2.4c, d, step IV). Finally, a mean equivalent diameter was calculated as

$$D_{eq} = \frac{2\sqrt{\frac{A_{pol}}{\pi}}}{Nc} \tag{2.5}$$

When $Nc = 1$, this equation reduces to Eq. (2.4), meaning that Eq. (2.5) is applicable to all types of objects shown in Figure 2.3.

2.4 Results and discussion

Figures 2.5 and 2.6 show typical properties measured during the runs. Figure 2.5 shows the good automatic control of total dry solids' concentration (w_{TDS}) attained for all conditions, by controlling the water flow rate (see Figure 2.6).

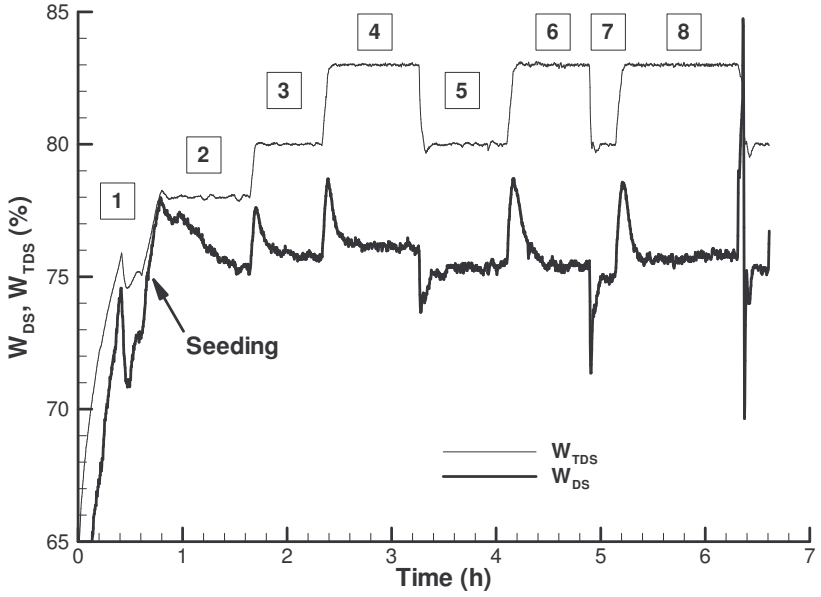

Figure 2.5. Record of the dissolved and total dry solids' concentrations in the massecuite during the 05/12 run. The numbers in the boxes represent several stages and experiments: 1-

Concentrating phase and stabilization; 2- 05/12GI experiment; 3- 05/12GII experiment; 4- 05/12GIII experiment; 5- 05/12DI experiment; 6- 05/12GIV experiment; 7- 05/12DII; 8- 05/12GV experiment.

In the majority of the runs, good agreement was obtained between w_{TDS} and w_{DS}, once past the period of conditions stabilization after the vacuum pump start-up. This is expected in the absence of crystals. Every plateau on the value of w_{TDS} corresponds to growth or dissolution experiments at constant mass fraction of water. The experiments are named by (i) the day and month of the run, (ii) the letters "G" or "D", depending on if it is a growth or dissolution experiment, respectively, and (iii) a Roman numeral corresponding to the chronological order at which they were performed (03/12DII is the second dissolution of the run of the 3rd of December).

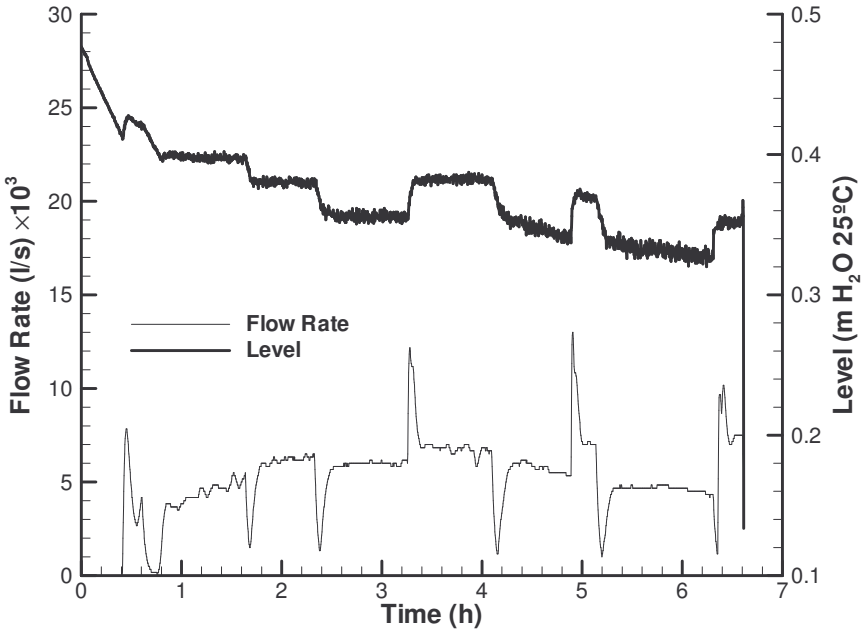

Figure 2.6. Record of the water flow rate and massecuite level during the 05/12 run.

Data resulting from the mass balance method are presented in Figures 2.7 and 2.8. To obtain these results, the experimental data shown in Figures 2.5 and 2.6, and the initial purity of the mother liquor were used. The derived equations can be implemented for on-line monitoring of CC, mass of crystals, liquor purity, and NS/W without making use of the historical record of the measurements. This way, the accumulation of systematic errors is minimized. The results are obviously affected by the quality of the measurements; for example, fluctuations in the

concentration measurement are reproduced and even amplified in the resulting *CC* and liquor purity profiles of Figures 2.7 and 2.8. Because of the scatter in the purity results, moving averages for 40 points were calculated and presented in Figure 2.8.

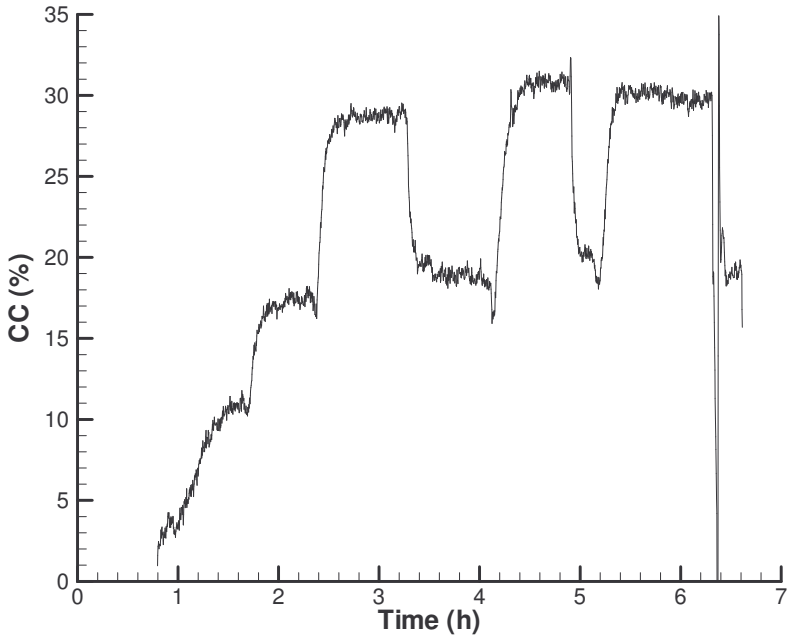

Figure 2.7. Variation of the crystal content in the massecuite during the 05/12 run.

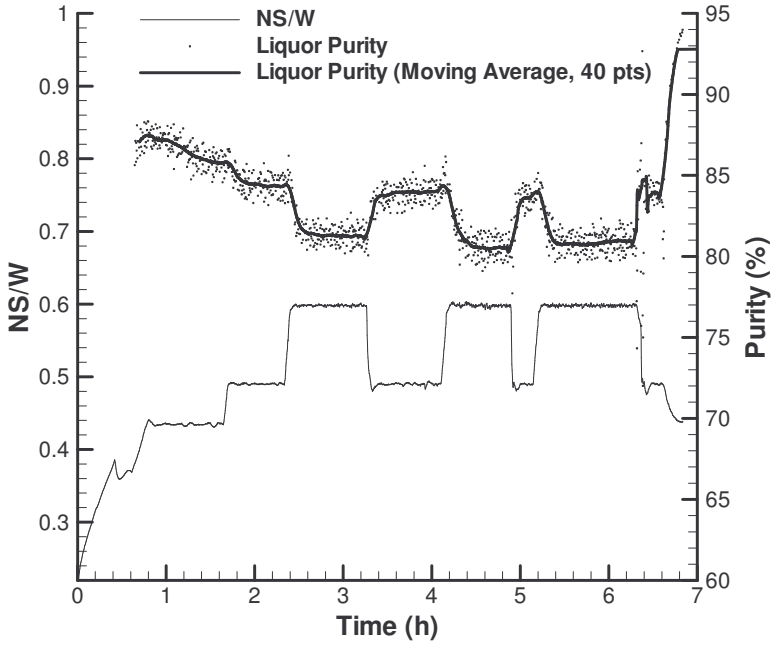

Figure 2.8. Variation of the liquor non-sucrose to water ratio and purity during the 05/12 run.

The image analysis method was applied to four growth experiments under similar experimental conditions. The results are shown in Figure 2.9. Each point of the graphic corresponds to the arithmetic mean of the crystals equivalent diameters, measured in 5 min intervals. Sometimes, bubbles and other foreign elements appear in the images, affecting the crystal size measurements. The Chauvenet rejection criterion was applied to eliminate these elements from the population of crystals [15]. The satisfactory agreement between the profiles of Figure 2.9 is good evidence of the consistency of the method.

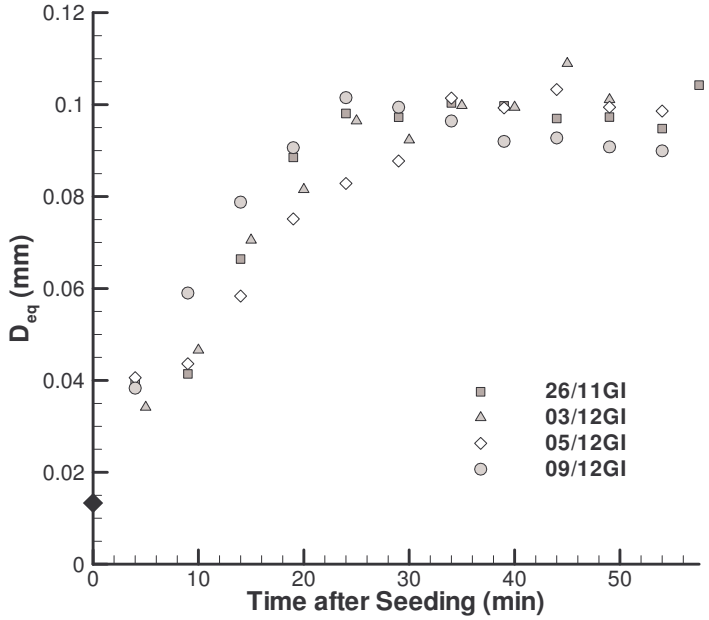

Figure 2.9. Evolution of the mean equivalent crystal diameter obtained by the Image Analysis Method during four growth experiments. ◆ - mean seed diameter obtained by laser light diffraction.

The measurements by image processing were only possible for the first growth experiments (GI) of the runs, because high mass fractions of solid matter seriously affect the quality of the images. As explained in the method description, the difficulties in analyzing in situ images due to incomplete crystal silhouettes and joined/overlapped crystals were solved by estimating the approximate individual areas. Preferably, the number of these cases should be much lower than the well-defined isolated crystals, although as the crystals grow, the percentage of extrapolated silhouettes and joined units also increase (Figure 2.10).

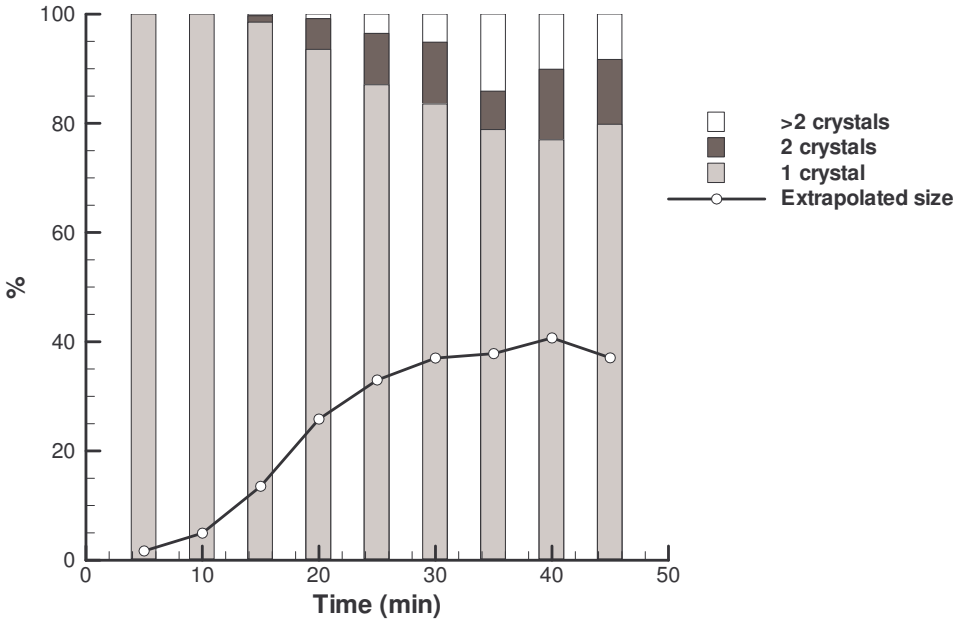

Figure 2.10. Percentage of different types of particles along the time for the 03/12GI experiment. The bars refer to single and joined/overlapped crystals and the line to incomplete silhouettes.

In Figure 2.10, "extrapolated size" corresponds to the percentage of isolated crystals whose extrapolated area is higher than the initial incomplete silhouette by more than 10%. In the first 15-20 min of growth, the small crystals seldom appear joined or overlapped, but at the end, the percentage of isolated crystals decreases to 80%. The uncertainty of the measurements is, therefore, higher at the end of the GI experiments. Even so, in all experiments a clear maximum size limit was visible without significant scatter.

Image analysis techniques can be an important tool to describe the change in crystal size distribution (CSD) during crystallization and, consequently, can contribute to a better understanding of the process. Studies on crystal growth dispersion, nucleation, and agglomeration, among others, can be made from the dynamic CSDs and the statistical parameters of these distributions. The image analysis method was used to calculate the population density distributions with time, as shown in Figure 2.11.

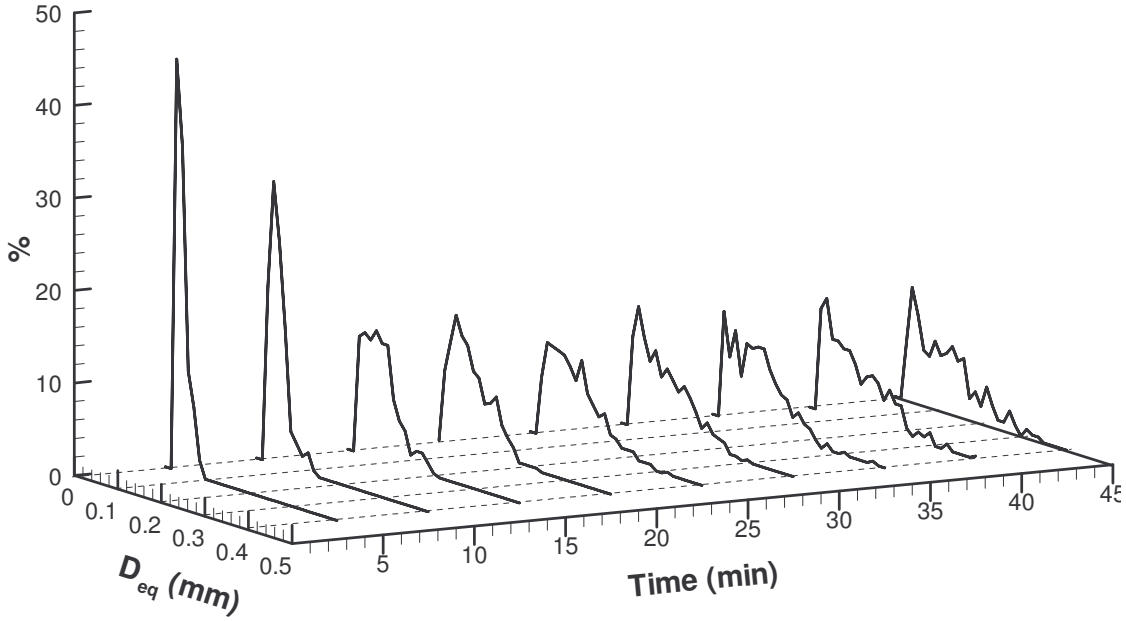

Figure 2.11. Change in the crystal size distribution during the 03/12GI experiment.

As the growth advances, CSD, expressed in Figure 2.11 by the number fraction of crystals with equivalent diameters comprised within a differential size fraction, becomes broader. Considering the specific experimental conditions at which the results were obtained, with low CC and small crystals, the increasing spread of the CSD is a predictable consequence of the growth rate dispersion and of the size-dependent growth phenomena. Other events associated with this behavior, such as secondary nucleation, crystal breakage, and agglomeration, are less probable to occur to any extent under these boiling conditions.

In some of the trials, the mass balance method and the image analysis method were simultaneously employed. To compare the results of both methods, the evolution of the mean equivalent crystal diameter was determined. To do that, it is necessary to know the number of growing crystals inside the pan and to find in the literature an adequate volume shape factor. The mean equivalent diameter of the crystals is calculated from their mass according to

$$D_{eq} = \left(\frac{m}{\alpha \rho_s N} \right)^{1/3} \tag{2.6}$$

The number of crystals in the pan was approximately calculated as described in the Experimental Section. There is no unanimity in the literature about the volume shape factors of sugar crystals, simply because, depending of the method of size measuring, this parameter

has different values. From the review made, the value found by Bubnik and Kadlek [13] of $\alpha = 0.750$ led to the best results. In that work, the mass of crystals was related with a linear dimension consisting of the mean aperture of sieves. Apparently, other shape factors determined by image analysis techniques would be more suitable to compute D_{eq}, but in those cases, the crystals are observed at their most stable position [11, 13]. This is a significant difference from the method here used, since the on-line images taken from the pan show the crystals flowing downward in the liquor, therefore assuming a variable position. With the values of α and N, and knowing from literature the density of sugar crystals $\rho_s = 1587\,\mathrm{kg/m^3}$ [13], it was possible to compare the two methods (see Figures 2.12–2.14). The confidence intervals of each mean equivalent diameter measured by image processing at a level of significance of 5% are represented by error bars. The number of crystals analyzed changed from ~50 to 400 per each 5 min interval. Increasing this number, which could be done by increasing the image capture frequency, the confidence interval would decrease, but at the same time, the possibility of analyzing repeated crystals would be higher.

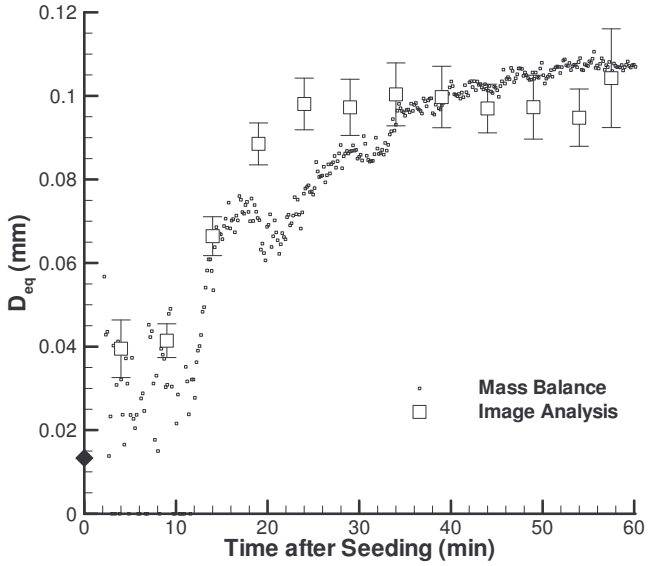

Figure 2.12. Comparison between the mean equivalent diameters obtained by the Image Analysis Method and by the Mass Balance Method, for the 26/11GI experiment. ◆ - mean seed diameter obtained by laser light diffraction.

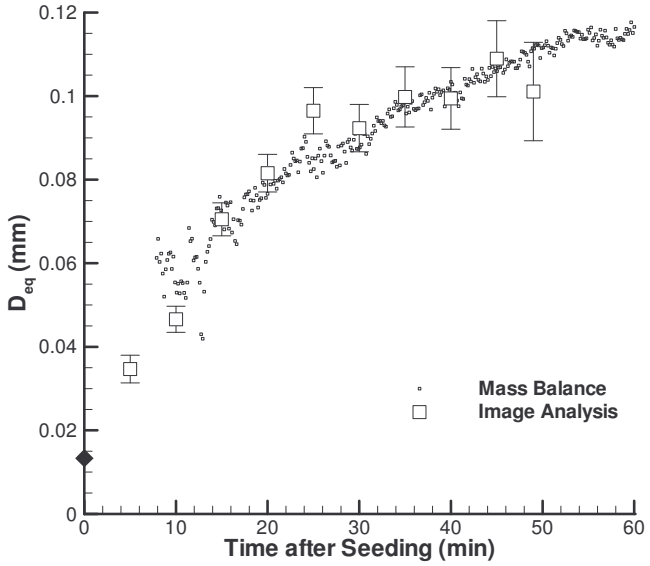

Figure 2.13. Comparison between the mean equivalent diameters obtained by the Image Analysis Method and by the Mass Balance Method for the 03/12GI experiment. ◆ - mean seed diameter obtained by laser light diffraction.

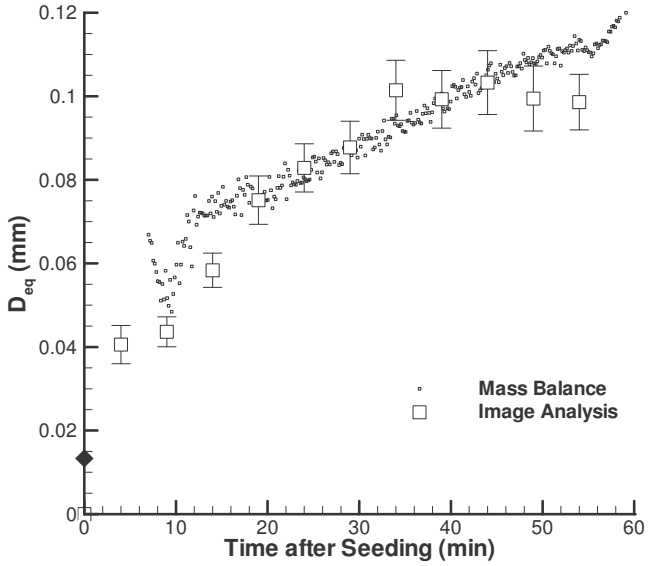

Figure 2.14. Comparison between the mean equivalent diameters obtained by the Image Analysis Method and by the Mass Balance Method for the 05/12GI experiment. ◆ - mean seed diameter obtained by laser light diffraction.

Considering the approximations made, good agreement between the methods was obtained, both in the range of the measured crystal size and in the way the crystal size changes. There is

a period of unstable conditions that follows seeding, caused by the effect of air entrance on the absolute pressure control. Disturbances of this kind have a strong impact on the calculation of the mass of crystals by the mass balance method, especially for low CC. Consequently, representative values of D_{eq} for the first minutes of the GI experiments were only possible to be obtained by the image analysis method.

2.5 Conclusions

Two methods were proposed for vacuum pan monitoring:

- By the mass balance method, the evolution of the crystal content, mass of crystals, liquor purity and liquor non-sucrose to water ratio during sugar boiling runs was determined. The information required consists of the purity of the syrup and typical boiling conditions. The robustness and applicability of this method make it suitable to be implemented for on-line measurements.

- By the image analysis method, images from the massecuite taken during the boiling runs were processed to calculate the mean crystal size. The applicability of this method was limited to small crystal contents; otherwise, the quality of the images gets too poor to be processed. In this work, the method was employed for crystal contents between 0 and 10%, approximately, and mean crystal sizes below 0.1 mm. Image analysis is a tool of growing interest in crystallization, since it also permits more fundamental studies based on the change of crystal size distribution with time.

A good agreement was found when comparing the crystal size profiles obtained by the two methods.

References

[1] P. W. Van der Poel, H. Schiweck, and T. Schwartz, Sugar Technology, Bartens, Berlin, **1998**.

[2] M. Saska, Boiling point elevation of technical sugarcane solutions and its use in automatic pan boiling. *Int. Sugar J.*, **2002,** 104, 500-507.

[3] L. Rozsa, Sucrose solubility in impure cane sugar solutions. *Int. Sugar J.*, **2000,** 102, 230-235.

[4] K.-H. Theisen and T. Diringer, in *Sugar Industry Technologists 62nd Annual Meeting*, Hamilton Island, Australia, **2003**.

[5] D. J. Love, Dynamic modelling and optimal control of sugar crystallisation in a multi-compartment continuous vacuum pan, Ph.D. Thesis, University of Natal, Durban, South Africa, **2002**.

[6] G. Vaccari, E. Tamburini, S. Tosi, G. Sgualdino, and T. Bernardi, In-line control and automatic management of industrial crystallizations using NIR technique. *Chem. Eng. Technol.*, **2003,** 26, 273-276.

[7] A. C. Schultz and L. A. Edye, in *Sugar Industry Technologists 59th Annual Meeting*, New Orleans, USA, **2000**.

[8] M. N. Pons, H. Vivier, K. Belaroui, B. Bernard-Michel, F. Cordier, D. Oulhana, and J. A. Dodds, Particle morphology: From visualization to measurement. *Powder Technol.*, **1999,** 103, 44-57.

[9] F. Tadeo, D. Matia, D. Laya, F. Santos, T. Alvarez, and S. Gonzalez, in *International Conference on Image Processing, Vol III, Proceedings*, Thessaloniki, Greece, **2001**.

[10] N. Faria, M. N. Pons, S. Feyo de Azevedo, F. A. Rocha, and H. Vivier, Quantification of the morphology of sucrose crystals by image analysis. *Powder Technol.*, **2003,** 133, 54-67.

[11] G. R. E. Lionnet, Interfacial model for the transfer of impurities into the sucrose crystal. *Chem. Eng. Res. Des.*, **1998,** 76, 803-808.

[12] O. Monnier, G. Fevotte, C. Hoff, and J. P. Klein, Model identification of batch cooling crystallizations through calorimetry and image analysis. *Chem. Eng. Sci.*, **1997,** 52, 1125-1139.

[13] Z. Bubnik and P. Kadlec, Sucrose crystal shape factors. *Zuckerindustrie*, **1992,** 117, 345-350.

[14] B. Bernard-Michel, M. N. Pons, and H. Vivier, Quantification, by image analysis, of effect of operational conditions on size and shape of precipitated barium sulphate. *Chem. Eng. J.*, **2002,** 87, 135-147.

[15] J. P. Holman, Experimental Methods for Engineers, 7th ed.; McGraw-Hill, Singapore, **2001**.

3. Investigation into crystal growth kinetics and solubility

Overview

A methodology to calculate sucrose saturation concentration under normal conditions of evaporative crystallization of sugar was adopted and will be presented. Its practical application is supported in the sugar boiling experiments that were described in the previous chapter. The calculated profiles of mass of crystals and supersaturation with time are used to determine the crystal growth kinetics of sucrose, at different stages of the strikes. Published data confirm the equilibrium and kinetic results obtained for pure sucrose and industrial cane syrups. Increasing non-sucrose to water ratios in the molasses clearly lowered the sucrose solubility coefficients. A similar effect on the crystal growth rate was harder to identify, since other parameters, like the ones related with hydrodynamic conditions and crystal size, are known to also influence it. The methods proposed proved to be robust and of direct application to sugar process crystallization.

3.1 Sucrose solubility in cane molasses

As a parameter quantifying the deviation from the equilibrium conditions of the solutions, supersaturation requires the knowledge of solute solubility. Many experimental equations correlating solubility and temperature are available for the most common solutes. Depending on their nature and concentration, impurities can have a dramatic influence on the saturation limit, either increasing or decreasing it. This is well-known in the sugar industry, where the wide variability and quantity of non-sucrose compounds make accurate supersaturation measurements a difficult task. The variation of the sucrose saturation limit with purity is well-described for beet sugar molasses (concentrated impure solutions of sucrose) by the solubility coefficient (SC), defined as the quotient of the sucrose solubilities (expressed by (g of sucrose)/(100 g of water)) in impure and pure solutions. Cane sugar solutions are a more problematic system. For this case, there are fewer equilibrium studies and there is a wide dispersion of results, as the review made by Love confirms (Figure 3.1) [1].

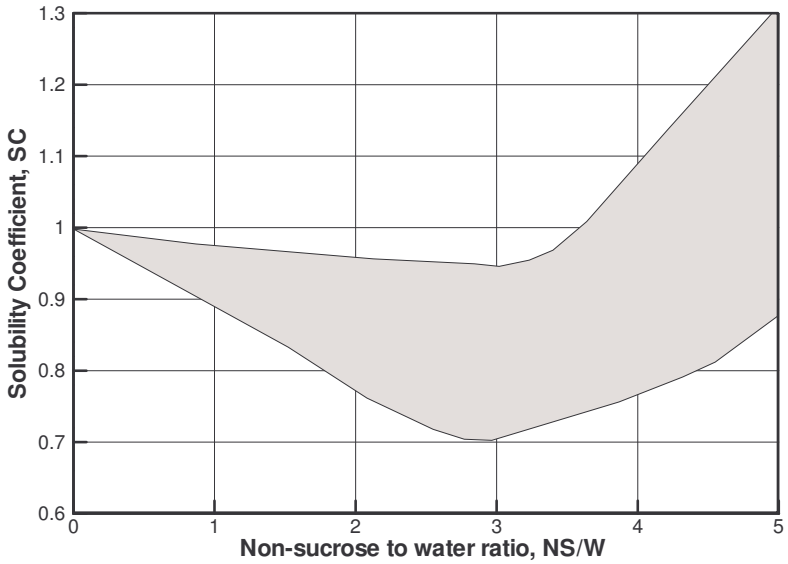

Figure 3.1. Range of sucrose solubility coefficients in impure cane solutions (adapted from the review made by Love [1]).

Sucrose solubility coefficients in cane molasses are often related to the non-sucrose to water ratio (NS/W) and also to the reducing sugar to ash (inorganic constituents) ratio, contrary to

what happens for beet molasses, where only the first ratio is used. Also, cane molasses composition is less predictable than that in the beet case. The unpredictability of the equilibrium conditions makes it desirable for sugar technologists to be able to do periodic solubility tests. Unfortunately, the time and means required for these analyses make this an impracticable objective.

Crystal growth kinetics have an important role in the design and management of industrial crystallizers. Kinetic data determined in the laboratory may be used in industry. However, scale-up problems may result from this procedure, as it often occurs in the case of sucrose crystallization. In this work, crystal growth rate curves were obtained in a pilot plant pan, making use of the calculated profiles of supersaturation and mass of crystals.

3.2 Estimation of solubility from crystallization curves

Solubility at a given temperature can be experimentally determined by allowing crystals to grow or dissolve until saturation is reached and measuring the solution concentration at that point. These experiments can take days, depending on the system studied and the technique chosen. A new procedure is proposed, which may be applied rapidly under normal crystallization conditions (e.g., application to evaporative crystallization). A typical crystallization curve is shown in Figure 3.2.

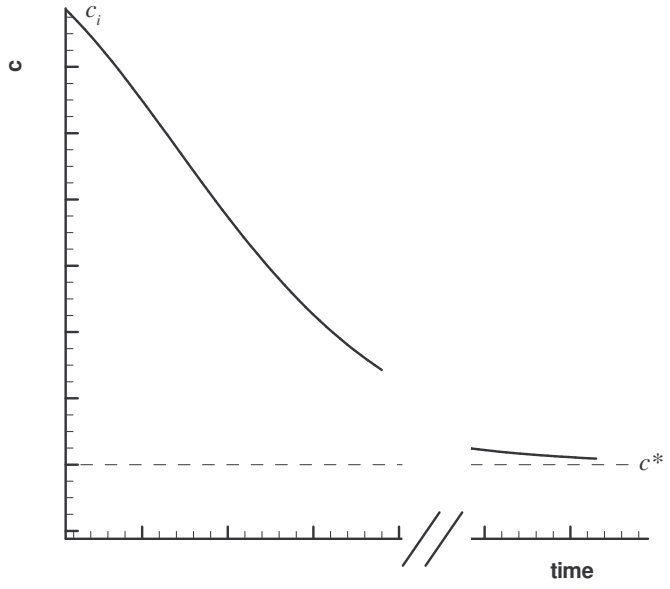

Figure 3.2. Crystallization curve.

The solute concentration starts to decrease when the crystallization begins (c_i) and gradually tends toward saturation. Saturation is represented by the concentration at that point (c^*). The idea behind the new method is to describe mathematically the progression of crystallization, so that it is not necessary to wait for saturation. Solubility can be estimated when the extent of the experiment is enough to adequately describe all the parameters of the concentration profile.

The following analysis will be done assuming a constant mass of water (m_w), which makes it valid for cooling crystallization or for evaporative crystallization with automatic control of the water content. For convenience sake, the solute concentration (c) will be expressed in terms of mass of solute per mass of water, so its variation can be easily related with the change of the mass of crystals (m) with time (t):

$$\frac{dm}{dt} = -m_w \frac{dc}{dt} \tag{3.1}$$

If no nucleation occurs, the crystal mass increase per time and per unit area is given by a growth law, generally defined by a power law equation,

$$\frac{1}{A}\frac{dm}{dt} = K_G \left(c - c^*\right)^g \tag{3.2}$$

where K_G and g are kinetic parameters. Combining Eqs. (3.1) and (3.2) gives

$$-\frac{m_w}{A}\frac{dc}{dt} = K_G (c - c^*)^g \tag{3.3}$$

This equation can be solved numerically after expressing the surface area of the crystals (A) as a function of time. It would be more suitable to have instead an analytical solution that could be fitted to experimental data to obtain c^*. With that aim, a simplification will be made assuming a constant average crystal surface area ($\bar{A}$) over the growth period. The consequences of this approximation will be discussed below, but it immediately simplifies the integration of Eq. (3.3):

$$\int_{c_i}^{c} \frac{dc}{\left(c - c^*\right)^g} = -\frac{\bar{A}}{m_w} K_G \int_0^t dt \tag{3.4}$$

resulting from that the following concentration profile:

$$c = \left[-K\left(1-g\right)t + \left(c_i - c^*\right)^{1-g} \right]^{\frac{1}{1-g}} + c^* \tag{3.5}$$

with

$$K = \frac{\overline{A}}{m_w} K_G \tag{3.6}$$

The saturation concentration c^*, and the other two parameters of Eq. (3.5) (g and K) can now be obtained by minimizing the differences between the experimental c vs t curve and the calculated one. Maurandi et al. [2] calculated the sucrose saturation concentrations from crystallization curves using an analogous equation. However, in this case, the regression parameters obtained were essentially empirical, corresponding to a particular case of Eq. (3.5) when $g = 2$.

It is important to establish the reliability of the value found for c^*, since it is calculated from an approximate solution assuming invariant crystal surface area. For doing that, the differential equation, which in fact describes the process (Eq. (3.3)), was numerically solved for several sets of parameters. These solutions, obtained with variable area, will be called "true profiles". Equation (3.5) was fitted to the true profile and the resulting parameters (c^*_{adj}, g_{adj}, and K_{adj}) were compared to the ones adopted when computing the differential equation (see Figure 3.3).

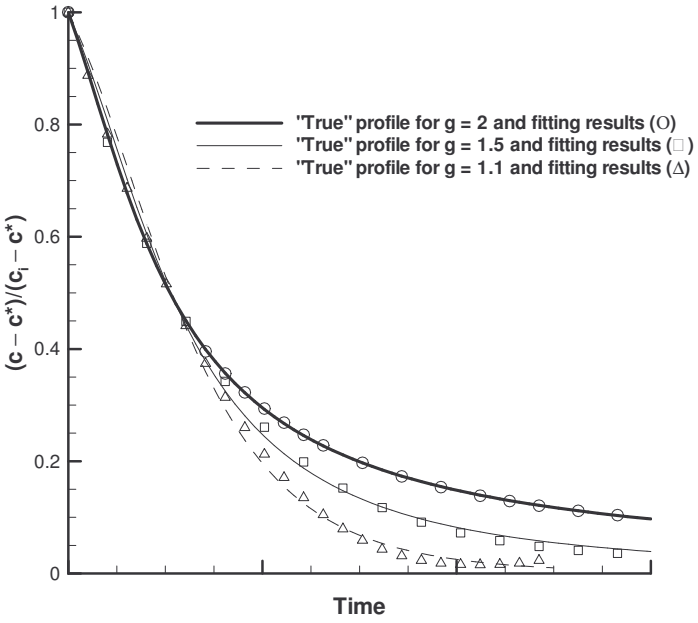

Figure 3.3. Numerical solution of Eq. (3.3) ("True" profile) and representation of its best fit, using Eq. (3.5).

The calculated solubility (c^*_{adj}), was in all cases, in close agreement with the assumed c^* (relative differences ~1%). The same cannot be said for the other parameters, since little differences in the adjustment, like the ones reported in Figure 3.3, considerably affect these parameters. From this, one can conclude that Eq. (3.5) may be useful for solubility estimation, as it is intended in this work.

When predicting c^* from a segment of the chart, the error of the extrapolation will be higher as the distance from equilibrium increases. Consider, for example, the case of Figure 3.4, where only the data comprised between 60% and 90% of the full range of variation of c are used to fit Eq. (3.5). The errors found on the calculation of c^*, using the range of data considered, are ~5%, which is an acceptable result for engineering purposes. Nevertheless, the value of c^* will be more reliable if the time interval is longer and approaches saturation more closely. Solubility data can, therefore, be extrapolated from partial crystallization curves both for pure and impure solutions.

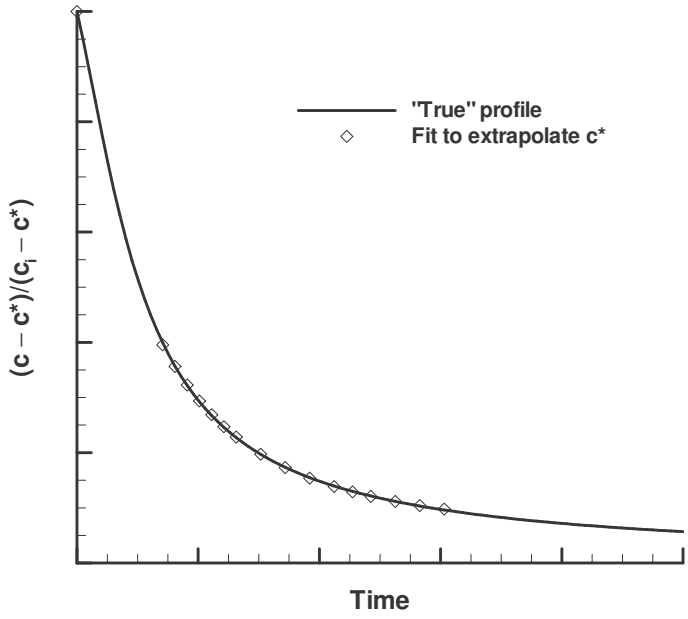

Figure 3.4. Extrapolation of c^* from a segment of the normalized crystallization curve.

Certainly, the accuracy of the results will always depend on the instrumentation employed to measure the solute concentration and on temperature control. In this work, the proposed method will be applied to determine the solubility coefficients of sucrose in sugar cane solutions under normal boiling conditions. A similar approach was used by Lionnet and Rein [3] to evaluate solubility coefficients. However, they applied a model to cooling

crystallization of massecuites (mixture of sucrose crystals and their mother liquor during the crystallization process) with much higher non-sucrose to water ratios.

3.2.1 Results and discussion

Solubilities were calculated for growth and dissolution experiments according to the method described above. The experimental data were obtained during the sugar boiling runs described in Chapter 2. An application example is given in Figure 3.5, where Eq. (3.5) was fitted to the sucrose crystallization curve to determine c^*.

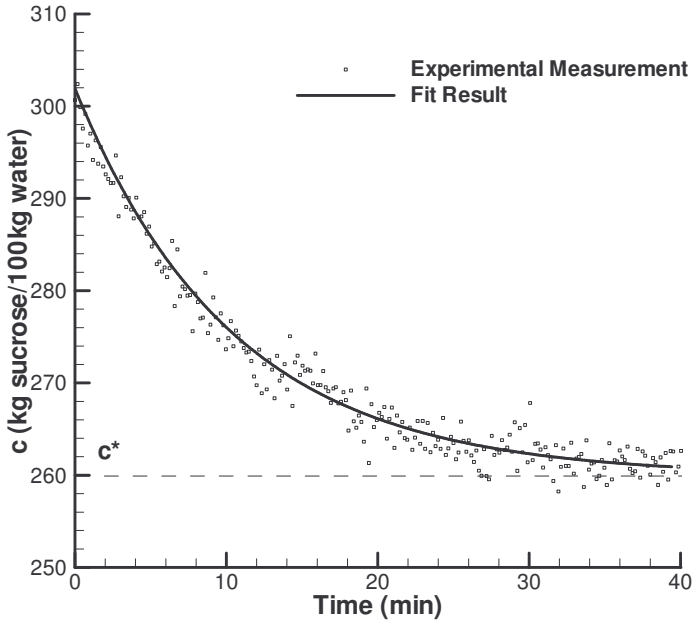

Figure 3.5. Plot of the dissolved sucrose concentration during the 05/12GII experiment and of the fit of Eq. (3.5). The solubility found, $c^* = (259.9\,\text{kg sucrose})/(100\,\text{kg water})$, is represented by the dashed line.

Experimental results were considered after the automatic control of the amount of water was stabilized. The sucrose concentration at that moment corresponds to the c_i parameter of Eq. (3.5). In the case of Figure 3.5, $c_i = (301.9\,\text{kg sucrose})/(100\,\text{kg water})$. The sucrose solubility coefficients corresponding to the values of c^* obtained were then calculated, taking into account the sucrose solubilities in pure solutions given in the literature for the operating temperature [4]. The results were plotted against the non-sucrose to water ratio, as shown in Figure 3.6. Several experiments were performed for three levels of NS/W : 0.434, 0.490, and 0.596. These values correspond to the chosen steps on the total dry solids'

concentration of 78.0%, 80.0%, and 83.0%, respectively. Each confidence interval of Figure 3.6 is estimated with the sucrose solubility coefficients resulting from more than 6 different experiments.

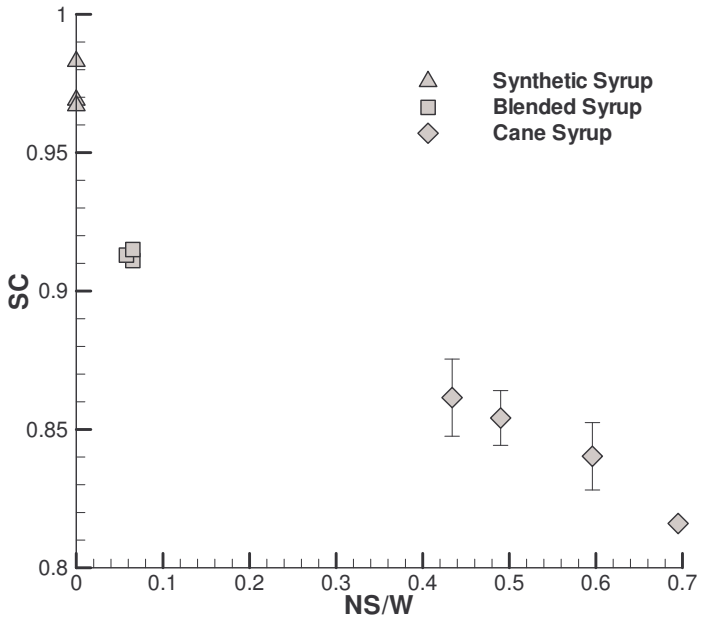

Figure 3.6. Influence of NS/W on the measured sucrose solubility coefficients for three syrups. Confidence intervals of SC at a level of significance of 5%, are represented for the three levels of NS/W at which experiments with cane syrup were most often carried out.

For the range of non-sucrose to water ratios considered, SC in cane solutions is expected to decrease with NS/W, tending to unity when $NS/W = 0$ (Figure 3.1). This is confirmed by Figure 3.6. The values of SC obtained for synthetic syrup are slightly lower than 1. This could be explained by the existence, in small quantities, of impurities present in the commercial sugar and in the tap water used to prepare the synthetic syrup. The sucrose solubility coefficients obtained with cane syrups are lower than expected from the study summarized in Figure 3.1. For example, the lower value of SC expected in that review for $NS/W = 0.434$ is ~0.95, while the average value found here was 0.86. The differences reported may have their cause in the method used for SC determinations. The published values are generally determined in the laboratory under experimental conditions that are very distinct from the ones at normal vacuum pan boiling. Schultz and Edye [5], using an innovative analytical technique (NMR) have also found SC values lower than other literature data (Figure 3.7). The non-equilibrium conditions during vacuum pan boiling and the

existence of systematic errors on calculating the solubility coefficients were admitted by the authors as possible explanations to those findings.

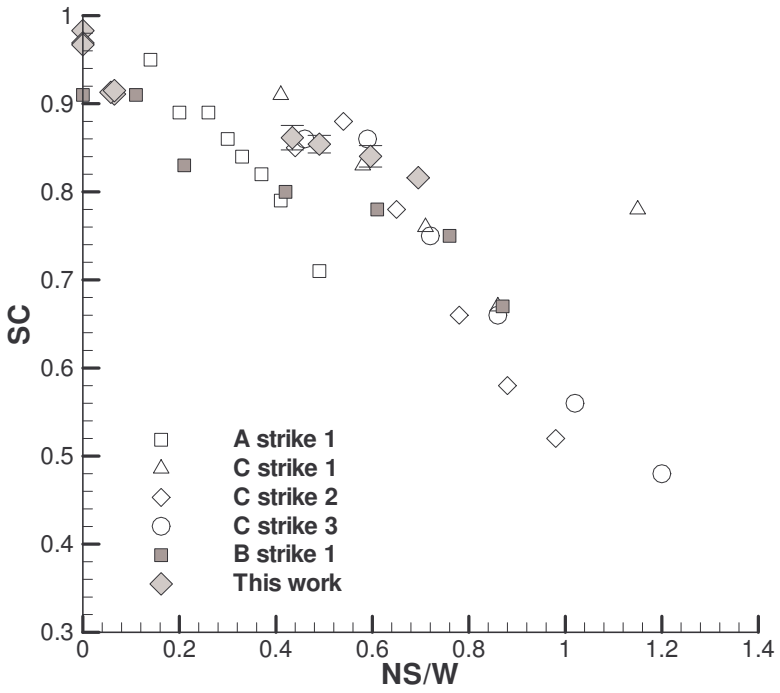

Figure 3.7. Comparison between the sucrose solubility coefficients found in this work and the results of Schultz and Edye [5]. The literature values were obtained with cane liquor and molasses of different grades (A, B and C).

Moreover, according to Figure 3.7, it seems that different SC vs NS/W correlations can be obtained depending on the grade of the syrup/molasses boiled. The results of Figure 3.6 also suggest this, since the equilibrium coefficients obtained with cane syrups suggest higher SC values than those registered with blended syrup. This may be related to other factors influencing the sucrose solubility in sugar cane solutions, like the reducing sugar to ash ratio (RS/A) [6]. It is known in the cane sugar industry that sucrose solubility coefficients decrease as RS/A increases.

3.3 Growth rate measurement

A means of calculating crystal growth kinetics will be described here and its application exemplified for the case of the evaporative crystallization of sugar. Information

about the change in the concentration of solute and mass of crystals with time must be available. Other prerequisites are the sucrose solubility (to calculate the supersaturation) and the parameters of crystals, such as their number and shape factors.

Crystal growth rate (R_G) is conventionally defined in terms of mass deposition per unit time and per unit crystal area:

$$R_G = \frac{\Delta m}{A \Delta t} \tag{3.7}$$

Existing experimental methods of growth rate measurement use the mass increment in a small time interval Δt to calculate R_G. In these cases, the crystal surface area is assumed to remain constant for that period of growth [7]. The use of a mean surface area was suggested by Ang and Mullin [8] for significant crystal size variation. A new approach is now proposed where such approximations are not needed. The surface area is expressed in terms of the mass of crystals according to the definitions of volume and surface area shape factors (α and β, respectively),

$$A = N^{1/3} \beta \left(\frac{m}{\rho_s \alpha} \right)^{2/3} \tag{3.8}$$

where N is the number and ρ_s the density of crystals. Substituting this equation in Eq. (3.7) gives

$$R_G = \frac{(\rho_s \alpha)^{2/3}}{N^{1/3} \beta} \frac{\Delta m}{m^{2/3} \Delta t} \tag{3.9}$$

this reduces to

$$R_G = 3 \frac{(\rho_s \alpha)^{2/3}}{N^{1/3} \beta} \frac{\Delta m^{1/3}}{\Delta t} \tag{3.10}$$

This way, the average growth rate for the period Δt is given as a function of the change in the mass of crystals raised to the power of $1/3$. If data for the average supersaturation during the same period are available, crystal growth kinetics can be determined, representing R_G as a function of supersaturation. An analogous practice will be necessary for dissolution rates (R_D) determination, but in this case,

$$R_D = -3\frac{(\rho_s \alpha)^{2/3}}{N^{1/3}\beta}\frac{\Delta m^{1/3}}{\Delta t} \tag{3.11}$$

Improved accuracy of results arises when the time intervals considered in Eqs. (3.10) and (3.11) correspond to small variations in supersaturation. However, the quality of the analytical techniques ultimately determines the choice of interval extent, since short increments can amplify measurement errors. When growth experiments are carried out at constant supersaturation, Eq. (3.10) is integrated to give

$$R_G = 3\frac{(\rho_s \alpha)^{2/3}}{N^{1/3}\beta}\cdot\frac{1}{t_f}\left[\left(m_f\right)^{1/3} - \left(m_i\right)^{1/3}\right] \tag{3.12}$$

This result is well-known from literature for crystal growth rate measurements in fluidized beds [9].

3.3.1 Results and discussion

Crystal growth and dissolution rates were calculated according to Eqs. (3.10) and (3.11), respectively, for the sugar boiling experiments considered in the preceding solubility study. Examples of the results and the experimental conditions are summarized in Table 3.1.

Table 3.1. Experimental conditions for the sucrose growth and dissolution experiments.

Experiment	Syrup	Absolute Pressure (kPa)	Average Temperature (ºC)	Mass of Massecuite (kg)	*CC* (%)		*NS*/*W*
					Min	Max	
26/11GI	Cane	18.56	65.7	31.8	0	8.1	0.434
26/11GII	Cane	18.56	65.6	30.2	8.1	16.9	0.490
26/11GIII	Cane	18.56	66.1	28.0	16.9	23.8	0.596
05/12GI	Cane	17.20	64.5	35.1	0	6.3	0.434
05/12GII	Cane	17.20	64.2	34.2	6.3	17.0	0.490
05/12GIII	Cane	17.20	64.5	32.9	17.0	28.1	0.596
11/12GI	Synthetic	15.58	62.3	36.2	0	13.6	0
11/12GII	Synthetic	15.58	62.3	34.1	13.6	22.5	0
03/12DII	Cane	17.85	64.6	36.1	9.3	16.2	0.434
05/12DI	Cane	17.20	63.7	34.2	18.1	28.1	0.490
15/12DI	Cane	15.24	62.0	36.0	18.5	28.9	0.490
15/12DII	Cane	15.24	63.3	36.0	20.2	31.0	0.490

The sucrose crystal properties are represented by the crystal shape factor, F, defined as,

$$F = \frac{\beta}{(\alpha \rho_s)^{2/3}} \tag{3.13}$$

The average value of F found by Bubník and Kadlec [10] (4.47 $mm^2mg^{2/3}$) was used. The number of growing crystals was calculated using the seed mean diameter measured by laser light diffraction (see Chapter 2), and it is assumed to remain constant during the growth/dissolution. Through the mass balance method, the change in the mass of crystals during the experiments was calculated. As is shown in Figure 3.8, the experimental results have a certain degree of scatter. Therefore, moving averages of $m^{1/3}$ and c were calculated using a variable number of data points, depending on the overall duration of the experiment. This value corresponds to the number of readings in the time interval Δt chosen to evaluate the crystal growth and dissolution rates. In the example considered, the mass of sucrose crystals increased from m_t to $m_{t+\Delta t}$ at an average crystal growth rate of R'_G that is given by Eq. (3.10). The corresponding average sucrose concentration is, as Figure 3.8b illustrates, c'. Following this methodology, information was gathered in order to determine the kinetic curves representing the influence of supersaturation (and undersaturation) on the crystal growth (and dissolution) rates. Supersaturation is here defined by $\Delta c = c - c^*$, where c^* is the sucrose solubility found for each experiment according to the method formerly presented

.

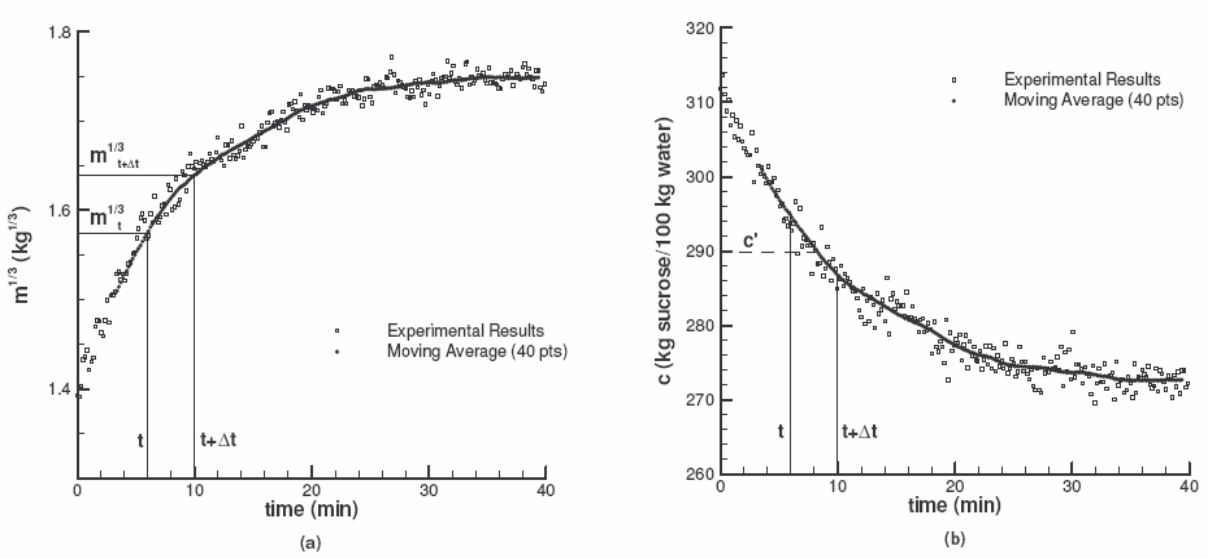

Figure 3.8. Representation of (a) the mass of crystals raised to the power of 1/3 and (b) sucrose concentration during the 05/12GII experiment, and the respective 40 point moving averages.

Crystal growth kinetics presented in Figure 3.9 were obtained from the experimental data represented in Figure 3.8.

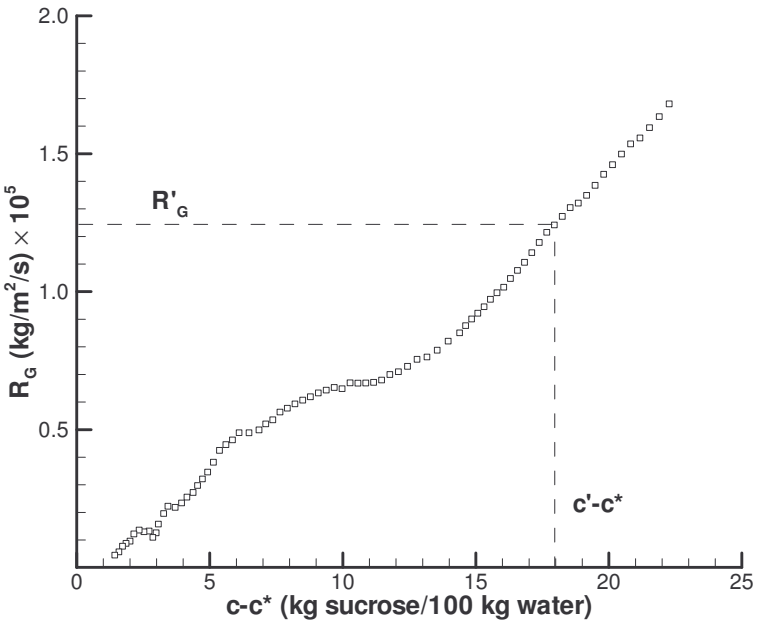

Figure 3.9. Crystal growth rates of sucrose calculated from the boiling data of the 05/12GII experiment (experimental conditions in Table 3.1).

In general, the kinetic behaviour depicted is expected from growth theories. The observed curve fluctuations may be caused by gradients on the massecuite temperature, which affect the concentration estimation through the boiling point elevation and, indirectly, the calculation of the mass of crystals by mass balance. Deviations from homogeneous conditions inside the pan will aggravate these effects. It should be noticed that each curve is obtained under varying experimental conditions of solid matter content, mother liquor purity, and other physical properties of the massecuite. For instance, the growth rates of Figure 3.9 corresponding to higher supersaturations were obtained at the beginning of the experiment, when the crystal content, crystal size, and impurity concentration in solution were the lowest. The differences on the operating conditions are more notorious among experiments carried out at different stages of the strike. The kinetic consequences are, however, difficult to distinguish, as in the case represented in Figure 3.10. It can be seen that growth rates are in fair agreement throughout the run, despite the different experimental conditions summarized in Table 3.1.

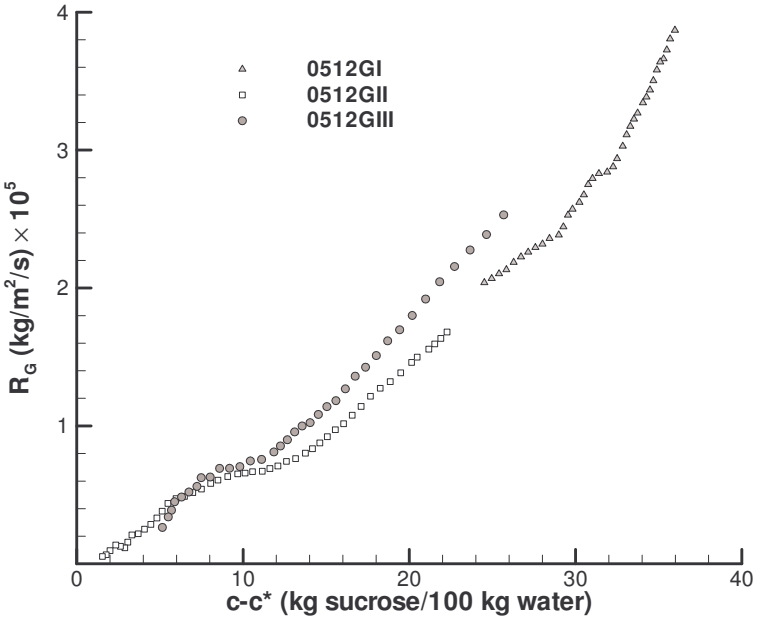

Figure 3.10. Crystal growth rates of sucrose obtained during the run of 05/12 (experimental conditions in Table 3.1).

The impurity concentration in the mother liquor exponentially decreases the growth rate [11]:

$$\frac{R_{G_1}}{R_{G_2}} = \exp\left\{-1.75\left[\left(\frac{NS}{W}\right)_1 - \left(\frac{NS}{W}\right)_2\right]\right\} \tag{3.14}$$

Following that, for the same supersaturation, the rates measured at $NS/W = 0.434$ (05/12GI) should be 10% higher than the ones at $NS/W = 0.490$ (05/12GII) and 30% higher than the ones at $NS/W = 0.596$ (05/12GIII). Instead, the last experiment had the faster growth kinetics of the run, certainly as a consequence of other variables influencing the process. Below, it is shown that crystallization was also affected by diffusional limitations and, therefore, by the pan circulation. Hydrodynamic conditions are a complex function of variables such as crystal content, overall mass of massecuite, evaporation rate, efficiency of the mechanical stirring, massecuite density and viscosity, etc. In brief, as the run evolves, the increasing mass fraction of solids turns the massecuite thicker, decreasing the rate of mass transfer. Bigger crystals are frequently assumed to grow faster [12, 13], so the enlargement of the crystals during the run also will favor the growth kinetics.

Definitive conclusions on the effect of each process variable, separately, are not easily taken because of other interactions, like secondary nucleation or agglomeration. These disturbances will become more significant for high contents of solid matter. Even so, the kinetic results for cane syrups showed a good general agreement in all runs. The values taken from literature of crystal growth rate in pan operation (Table 3.2) fall in the range of the measured rates summarized in Figure 3.10. Linear growth rates (G) were gathered from the literature, at comparable experimental conditions of temperature and mother liquor purity, and converted into overall mass growth rates (R_G) according to the following expression,

$$R_G = 3\frac{\alpha\rho_s}{\beta}G \tag{3.15}$$

using the shape factors found by Bubník and Kadlec [10].

Table 3.2. Literature values of linear and mass growth rates of sucrose crystals, for the evaporative crystallization of sugar.

Source	G (μm/hr)	$R_G \times 10^5$ (kg/m^2/s)
Wright [14]	150	3.0
Miller and Broadfoot [15]	52 – 121	1.0 – 2.4
Lionnet [16]	40 – 144	0.8 – 2.9

As mentioned by Georgieva et al. [17], there are few studies describing the sucrose growth rate under industrial conditions. Wright and White [11] summarized the effect of supersaturation (S), temperature (T), and non-sucrose to water ratio on the crystallization rate in vacuum pans through a general equation:

$$G = K_1\left(S - \left(1 + K_0\right)\right)\exp\left(K_2 - K_3\frac{NS}{W}\right) \tag{3.16}$$

The constant K_2 is an Arrhenius-type function of the temperature and activation energy. It was found that the original parameters K_0, K_1, K_2, and K_3 overestimate the crystal growth rates [1]. Using, instead, the values found by Li-Wu and Corripio [18] ($K_0 = 0.005$; $K_1 = 6000\,\mu$m/h; $K_2 = 0.37$; $K_3 = 2.45$) for the same parameters, the predicted growth rates are still above the measured ones, as illustrated in Figure 3.11 for the run of 26/11. The differences found are not surprising, taking into account all the factors affecting the final kinetics, namely differences in experimental conditions.

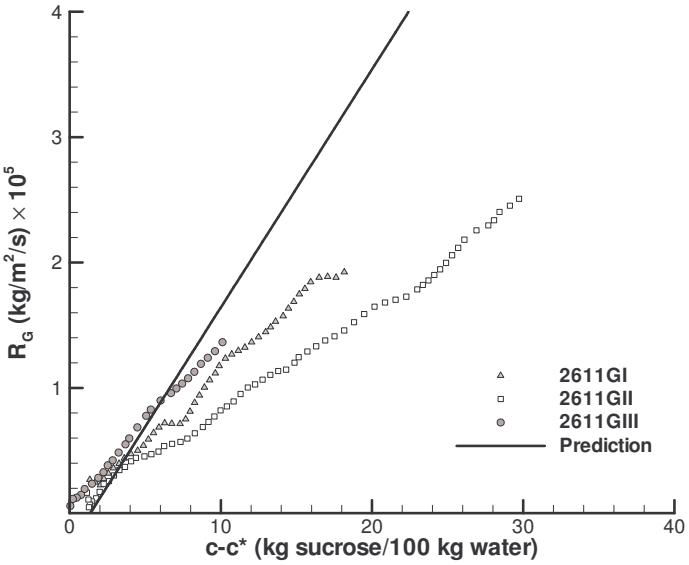

Figure 3.11. Crystal growth rates of sucrose obtained during the run of 26/11 (experimental conditions in Table 3.1) and predicted curve according to Eq. (3.16) ($T = 66$ ºC and $NS/W = 0.490$) with the parameters found by Li-Wu and Corripio [18].

The results obtained in the run performed with synthetic syrup show good agreement with the laboratory data taken from Smythe [19] (see Figure 3.12).

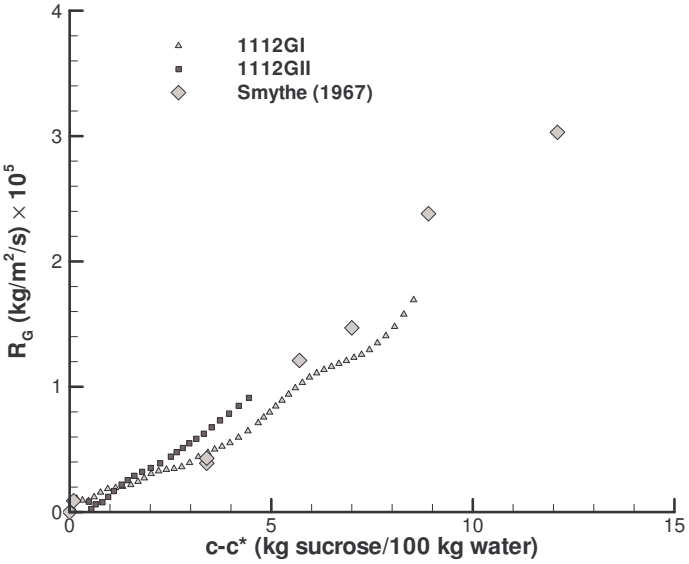

Figure 3.12. Comparison between crystal growth rates of sucrose obtained during the run of 11/12 (experimental conditions in Table 3.1) and the results found by Smythe [19] at 60.5 ºC.

The literature values were obtained at slightly lower solution temperature (60.5 ºC) and for small diffusional resistances (stirring speed = 3000 rpm). When "pure" syrup was used, crystal growth rates were higher than those obtained with factory liquors. Comparing the growth rates at the same supersaturation of the 1112GI (synthetic syrup) and 0512GII (cane syrup) experiments, it was found that the former are $2-2.5\times$ faster. According to Eq. (3.14), the expected rate increase when changing from $NS/W = 0.490$ to $NS/W = 0$ is $2.36\times$. The range of supersaturations covered during the 11/12 run (Figure 3.12) is smaller than that in the experiments with impure syrups as a consequence of the higher solubilities found in that case.

The measurement of the dissolution rates was not always possible, because of the rapidity of the process when the crystal surface area is high. Sometimes substantial dissolution occurred before the control of the amount of water was fully stabilized. The kinetic curves obtained are represented in Figure 3.13, showing significant agreement between the data of different runs. As conventionally assumed by theories of mass transfer, the results are well-described by straight lines passing through the origin. This evidence supports not only the method of calculation of crystal growth/dissolution rates but also the calculation of sucrose solubilities.

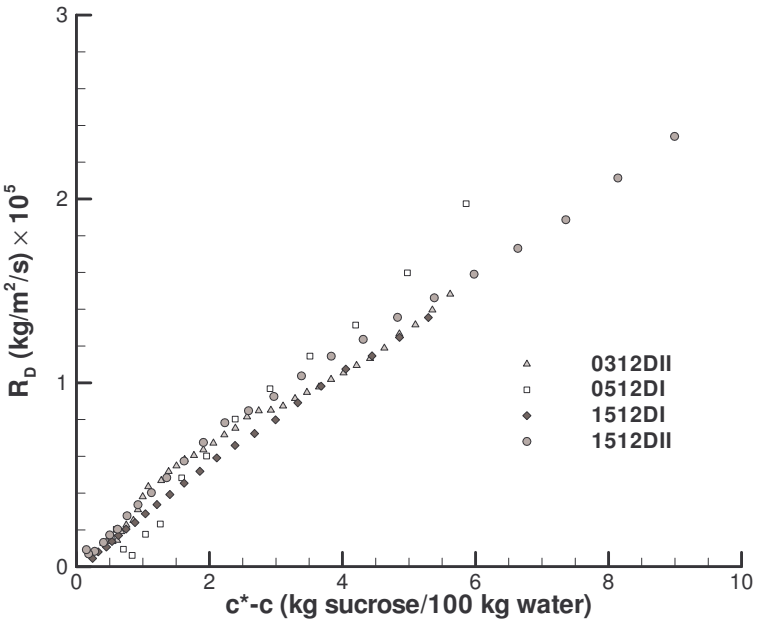

Figure 3.13. Dissolution rates of sucrose crystals obtained during different boiling experiments (experimental conditions in Table 3.1).

Comparing with the other dissolutions experiments, the 03/12DII experiment corresponds to lower NS/W and crystal mass fraction. Nevertheless, the results are very close, indicating that different hydrodynamic and purity conditions did not appear to have an effect on the dissolution rate.

The results show that crystals dissolve faster than they grow. Considering the 0512DI and 0512GII experiments, the R_D/R_G ratio evaluated for an undersaturation/supersaturation of $(5\,\text{kg of sucrose})/(100\,\text{kg of water})$ is 4.5. Under these circumstances, the surface integration resistance is dominant, but diffusion can have an influence on the sucrose crystal growth, especially at higher driving forces [20].

3.4 Conclusions

Experiments on evaporative crystallization of sugar were carried out in a pilot vacuum pan using synthetic and industrial syrups. The results obtained by the mass balance method presented in Chapter 2 were used to determine equilibrium data and growth and dissolution rates.

Sucrose solubilities, and hence the solubility coefficients, were determined using the concentration profiles fitted to an appropriate model. The effect of the non-sucrose to water ratio on the sucrose solubility coefficient was investigated. Increasing the non-sucrose to water ratio from 0 to 0.6 decreased the sucrose solubility coefficient from near 1.0 to ~0.84. These results compare well with literature data for similar experimental conditions.

Crystal growth rates were determined from the increase in the crystal mass with time. The equation used was derived taking into account the variation of the crystal surface area, instead of assuming a mean surface area. Values up to 2×10^{-5} kg/m^2/s were found with industrial syrups, while with pure syrup, the crystal growth rates were 2 to 2.5× faster. Growth kinetic curves were obtained that represent the crystal growth rates as a function of sucrose supersaturation. The growth rates showed reasonable agreement with data in the existing literature.

Dissolution rates determined for different experiments are close, indicating that, for the experimental conditions used, different hydrodynamic and purity values did not appear to have a significant effect on the dissolution rate.

The new methodologies proposed to calculate sucrose saturation concentrations and dissolution and growth rates proved to be robust and of direct application to sugar process crystallization. The results of this work were obtained under normal boiling conditions; their straightforward application to industrial conditions can be done with less scale-up problems than seen with conventional data measured at laboratory.

References

[1] D. J. Love, Dynamic modelling and optimal control of sugar crystallisation in a multi-compartment continuous vacuum pan, Ph.D. Thesis, University of Natal, Durban, South Africa, **2002**.

[2] V. Maurandi, G. Vaccari, G. Mantovani, and A. Rossi, Kinetic Variations in Sucrose Crystallization for Different Inter-Crystal Distances. *Zuckerindustrie*, **1989,** 114, 562-566.

[3] R. E. Lionnet and P. Rein, in *Proc. Int. Soc. Sugar Cane Technol.*, South Africa, **1980**.

[4] V. Maurandi, G. Mantovani, G. Vaccari, and A. Rossi, Kinetics and technology of low boiling massecuite exhaustion. *Zuckerindustrie*, **1988,** 113, 791-794.

[5] A. C. Schultz and L. A. Edye, in *Sugar Industry Technologists 59th Annual Meeting*, New Orleans, USA, **2000**.

[6] G. Vavrinecz, The Formation and Composition of Beet Molasses. *Sugar Technol. Rev.*, **1978,** 6, 117-305.

[7] J. Garside, A. Mersmann, and J. Nyvlt, Measurement of Crystal Growth and Nucleation Rates, 2nd ed.; EFCE Working Party on Crystallization, IChemE, Rugby, **2002**.

[8] H. M. Ang and J. W. Mullin, Crystal growth rate determinations from desupersaturation measurements: Nickel ammonium sulphate hexahydrate. *Trans. Instn. Chem. Engrs*, **1979,** 57, 237-243.

[9] J. W. Mullin, Crystallization, 4th ed.; Butterworth-Heinemann, Oxford, **2001**.

[10] Z. Bubnik and P. Kadlec, Sucrose crystal shape factors. *Zuckerindustrie*, **1992,** 117, 345-350.

[11] P. G. Wright and E. T. White, in *Proc. Int. Soc. Sugar Cane Technol.*, Australia, **1974**.

[12] A. A. Zekic and M. M. Mitrovic, Dependence of growth rate on initial crystal size. *J. Cryst. Growth*, **2003,** 258, 204-210.

[13] L. Guimarães, S. Sá, L. S. M. Bento, and F. Rocha, Investigation of crystal growth in a laboratory fluidized bed. *Int. Sugar J.*, **1995,** 97, 199-204.

[14] P. G. Wright, Pan and pan stage control. *Sugar Technol. Reviews*, **1983,** 10, 39-76.

[15] K. F. Miller and R. Broadfoot, in *Proc. Int. Soc. Sugar Cane Technol.*, Australia, **1997**.

[16] G. R. E. Lionnet, Interfacial model for the transfer of impurities into the sucrose crystal. *Chem. Eng. Res. Des.*, **1998,** 76, 803-808.

[17] P. Georgieva, M. J. Meireles, and S. Feyo de Azevedo, Knowledge-based hybrid modelling of a batch crystallisation when accounting for nucleation, growth and agglomeration phenomena. *Chem. Eng. Sci.*, **2003,** 58, 3699-3713.

[18] Q. Li-Wu and A. B. Corripio, Experimental verification of a dynamic model of a vacuum pan. *J. Amer. Soc. Sugar Cane Technol.*, **1985,** 5, 77-84.

[19] B. M. Smythe, Sucrose Crystal Growth.I. Rate of Crystal Growth in Pure Solutions. *Aust. J. Chem.*, **1967,** 20, 1087-1095.

[20] J. Mydlarz and A. G. Jones, Growth and dissolution kinetics of potassium sulphate crystals in aqueous 2-propanol solutions. *Chem. Eng. Sci.*, **1989,** 44, 1391-1402.

PART II

NEW ENGINEERING MODELS

4. Parallel step model

Overview

In this chapter, the theoretical analysis of the factors influencing crystal growth is started. Conventional theories of mass diffusion and solute integration into the crystal lattice are the basis of a new model on the influence of the diffusional resistance on the crystal growth rate. Here, two resistances are assumed to coexist in parallel (solute diffusion and adsorption) before the integration step. The new arrangement of the processes involved and the estimation of crystallization kinetics as a function of what is adsorbed are thought as being the main differences of the parallel step model relatively to the classical diffusion-reaction theories. The physical concepts are presented in the first part of the chapter, following a methodology comparable to well-known derivations of adsorption isotherms. Supported on that theoretical background, shell mass conservation balances are formulated, with resulting second-order differential equations for the concentration profile around the crystals. The model characteristic equations are then derived for different crystal geometries, diffusional resistances and kinetic orders. Finally, a simplified growth rate equation is deduced, providing a generic way of relating the crystallization variables.

4.1 Introduction

Crystal growth theories and catalytic reaction mechanisms share common fundamentals on mass transfer, and the integration of solute in the crystal lattice is frequently seen as a chemical reaction with its characteristic kinetic parameters. In crystallization, it is admitted that the molecules adsorb at the crystal surface before being incorporated into the lattice and after being transported from the bulk of the solution. However, the weight of this intermediate adsorption step on the formulation of theoretical models is not the same in those two types of heterogeneous systems. It is recognized that the development of concepts like chemisorption and physisorption was a significant contribution to the understanding of catalytic kinetics, not only for the cases where the adsorption is rate controlling, but also for relating superficial to bulk concentrations, establishing overall reaction kinetics and characterizing solid surface properties [1]. On the opposite, adsorption has been vaguely considered on the major models describing the development of crystals in solution, remaining as a theoretical concept that is not clearly related to the process. Recent progresses on the characterization of growth kinetics of crystals in the presence of impurities renewed the interest on this phenomenon. For example, Kubota and Mullin suggested the use of a Langmuir adsorption isotherm for quantifying the coverage of the active sites at the crystal surface by impurities [2]. Based on the pinning mechanism originally proposed by Cabrera and Vermilyea [3], it was established how the amount of adsorbed impurities interferes with the growth rate of the crystal. Further developments of this model considered a non-equilibrium adsorption model, where the coverage is calculated as a function of time [4]. Reported cases of crystal growth rate hysteresis could be explained by slow adsorption kinetics [5, 6]. In other works, different equations describing the adsorption equilibrium of the impurities, such as Temkin isotherms and Freundlich isotherms were also studied [7, 8]. In this work, the adsorption of the solute itself on the faces of the growing crystal will be considered, and a new physical and mathematical model for crystal growth from pure solutions will be presented. The mathematical treatment here presented shares common features with classical diffusion-reaction theories of crystal growth. Nevertheless, instead of the typical association in series of the diffusional and kinetic resistances, the proposed model considers two resistances coexisting in parallel (diffusion and adsorption) followed by the surface integration of adsorbed units into the crystal structure. In the subsequent chapter, the

practical consequences and benefits arising from this new theoretical concept are emphasized by testing it against experimental results on crystal growth kinetics.

4.1.1 Two step model

It is generally considered that crystal growth from solution is the result of the existence of two steps in series: bulk or volume diffusion through a hypothetical stagnant film (diffusional step), followed by the integration of growth elements into the crystal lattice ("kinetic" step or surface "reaction" step). The associated resistances will determinate the overall growth rate:

$$R_G = \rho k_d' (c_b - c_i) \tag{4.1}$$

$$R_G = \rho k_r' \left(c_i - c^*\right)^{r'} \tag{4.2}$$

In the case of simple integration kinetics, it is possible to find an analytical relation between R_G and the overall concentration driving force, $\Delta c_b = c_b - c^*$ [9]. Yet, a semi-empirical overall growth rate equation is frequently employed:

$$R_G = K_G \Delta c_b^g \tag{4.3}$$

This equation has no theoretical background and the role of the kinetic and diffusional parameters is not established. In 1971, a way to quantify the involved resistances adopting the concept of "effectiveness factor" (η_C) from reactions on porous catalyst and non-catalytic gas-solid reactions to crystal growth was introduced [9]. This parameter can be defined as the ratio between the measured growth rate and the one expected in the absence of significant diffusional resistance, i.e., in the bulk conditions. The generally unknown interfacial concentration c_i, can be eliminated by combining Eqs. (4.1) and (4.2):

$$R_G = k_r' \left[\Delta c_b - \frac{R_G}{k_d'} \right]^{r'} \tag{4.4}$$

which can be rewritten as follows

$$\frac{R_G}{k_r' \Delta c_b^{r'}} = \left[1 - \frac{R_G}{k_d' \Delta c_b} \right]^{r'} \tag{4.5}$$

and, at the same time, an equation for η_C is obtained:

$$\eta_C = \left(1 - h\eta_C\right)^{r'} \tag{4.6}$$

where,

$$h = \frac{k_r' \Delta c_b^{r'}}{k_d' \Delta c_b} \tag{4.7}$$

This parameter is also known as "Damköhler number" [10, 11]. The so-called "two step model" is of great application for chemical engineering purposes, providing a simple and intuitive arrangement of the processes involved. Despite of that, difficulties in the scale up of crystallizers are often reported, due to uncertainties in the prediction of growth rates.

The main issues of an alternative diffusion-adsorption-integration theory will now be developed in a physical and mathematical point of view. Ideally, the proposed crystal growth model should eliminate the limitations and inconsistencies of the two step model, without significant losses in the simplicity of the concepts.

4.2 Parallel step model – physical fundamentals

The adsorption of molecules at the crystal surface is of key importance in this model – the existence of non-compensate attractive forces leads to the existence of an adsorbed phase that works as a precursor of the incorporation of growth elements into the solid. The interactions should be essentially van der Waals forces, diminishing rapidly with the crystal surface distance. Based on that, a multi-layer adsorption disposition is assumed, where the sorbate concentration is considerably higher in the superficial layers than in the outer ones.

A connection between adsorption kinetics and crystal growth velocities can be demonstrated. For doing that, let us assume the following approximations for the adsorbed layers:

1. The adsorption occurs in a defined number of places called "active sites".

2. Each active site can only accommodate one adsorbed unit.

3. All active sites are energetically equivalent.

4. There is no interaction between adsorbed units on neighbouring active sites.

These hypotheses can be found in typical adsorption isotherms derivations such as the Langmuir isotherm and the Brunauer-Emmett-Teller (BET) isotherm [1, 12, 13]. Representing by *MA* the active sites occupied by the solute *A* and by *M* the unoccupied ones, it can be said that the adsorption rate in each layer (J_n^{+ads}) is proportional to the concentration of *A* in solution and to the number of unoccupied active sites, *M*. On the other hand, the velocity of the inverse process of desorption (J_n^{-ads}) increases with the *MA* concentration. Schematically this equilibrium can be represented for the *n*th layer by

$$A_n + M_n \underset{J_n^{-ads}}{\overset{J_n^{+ads}}{\rightleftarrows}} MA_n$$

where $n = 1,\ 2,\ \ldots l$, and l is the total number of adsorbed layers. Consider now two successive layers, n and $n+1$. It is expected that the tendency of transferring adsorbed units from the $(n+1)$th to the nth layer (J_n^{+mig}) will increase as the MA_{n+1} and/or M_n concentrations increase. The migration of adsorbed solute in the opposite direction (J_n^{-mig}) is promoted by high MA_n concentrations:

$$MA_{n+1} + M_n \underset{J_n^{-mig}}{\overset{J_n^{+mig}}{\rightleftarrows}} MA_n$$

In addiction to this, in the first layer, the integration of the adsorbed units into the crystal structure should be taken into account. The higher the occupation of adsorption active sites, the faster the crystal grows, which leads to higher integration velocity (J^{int}):

$$MA_1 \xrightarrow{J^{\text{int}}} Crystal$$

This step is described in the literature through mechanisms like mononuclear two-dimensional nucleation, polynuclear two-dimensional nucleation or surface diffusion [14, 15]. Under steady state, the total number of occupied sites (and therefore, the total number of unoccupied sites) remains unchangeable. This means that

$$\begin{aligned} &\sum_{n=1}^{l}\left(\frac{d\left[MA_n\right]}{dt}\right)_{ss} = 0 \Leftrightarrow \\ &\Leftrightarrow \sum_{n=1}^{l}\left\{\begin{array}{l}\left(J_n^{+ads} - J_n^{-ads}\right) + \left(J_n^{+mig} - J_n^{-mig}\right) - \\ -\left(J_{n-1}^{+mig} - J_{n-1}^{-mig}\right) - J^{\text{int}}\end{array}\right\} = 0 \end{aligned} \tag{4.8}$$

with J_0^{+mig}, J_0^{-mig}, J_l^{+mig} and $J_l^{-mig} = 0$. Therefore

$$J^{\text{int}} = \sum_{n=1}^{l} \left(J_n^{+ads} - J_n^{-ads} \right) \tag{4.9}$$

Equation (4.9) will be very important on the physical support of the mathematical model. From it, one can infer that:

1. The crystallization rate corresponds to the sum of the net adsorption velocities in every adsorbed layer.

2. In each layer, the number of adsorbed units is certainly influenced by the proximity of the crystal; however, the integration velocity of the molecules into the crystal lattice could also have a role on it.

3. Unlike what happens in the two step model, there is not a strict differentiation between the stagnant film and the adsorbed layer. Indeed, in the stagnant film the solute units are assumed to be in a diffusive movement, but also, in an adsorbing/desorbing equilibrium with the crystal surface.

The same conclusions could have been drawn from the steady state balance to the free active sites, M. On the other hand, care must be taken when balancing the non-adsorbed solute A because, in this case, there is an additional source that takes into account the diffusional transport from the bulk of the solution.

4.3 Mathematical model

From the preceding hypothesis of the physical model and using basic principles of mass conservation, the objective is now to obtain the model characteristic equations. Relations between crystal growth rate and factors like bulk supersaturation, temperature and hydrodynamic parameters should be clarified.

Some approximations or simplifying hypothesis will be assumed in this derivation. Despite of its frequent usage on mass transfer characterization, the stagnant film concept is an example of such idealizations [16]. Mass balances will be applied to an infinitesimal portion of that film, with the purpose of deriving concentration and flux profiles:

$$\left\{\begin{matrix}\textit{Input of}\\ \textit{solute A}\\ \textit{per time unit}\end{matrix}\right\}-\left\{\begin{matrix}\textit{Output of}\\ \textit{solute A}\\ \textit{per time unit}\end{matrix}\right\}= \\ =\left\{\begin{matrix}\textit{Amount of}\\ \textit{solute A adsorbed}\\ \textit{per time unit}\end{matrix}\right\} \tag{4.10}$$

Some considerations should be taken into account regarding the quantification of Eq. (4.10):
1. The chemical species A enters and leaves the shell by a diffusive movement through the binary mixture of A and B, according to Fick's first law:

$$N_A = x_A\left(N_A + N_B\right) - \mathcal{D}_{AB}\frac{dC_A}{dz} \tag{4.11}$$

When the molar fraction of solute is low enough, one can write:

$$N_A = -\mathcal{D}_{AB}\frac{dC_A}{dz} \tag{4.12}$$

In crystallization this is true only for sparingly solutes. It is likely that solute molecular diffusion during crystal growth can be affected by the existence of the adsorbed layer, especially in the cases of big molecules and thick adsorbed layers.

2. For the conditions considered, there is a lack of theoretical foundations describing the transfer of solute from the solution to the adsorbed phase. As in similar situations, the right term of the material balance can be described via a kinetic law:

$$\left\{\begin{matrix}\textit{Mass fraction of}\\ \textit{solute A adsorbed}\\ \textit{per time unit}\end{matrix}\right\} = k_r \Delta c^r \tag{4.13}$$

3. The kinetic constant k_r is temperature and distance-to-surface dependent. The former relation is given by an Arrhenius-type equation:

$$k_r = k_{r0}\exp\left(-\frac{E_T}{RT}\right) \tag{4.14}$$

However, the function relating k_r and the position in the film is more difficult to find. A solution to this problem will be suggested below.

4. Crystal geometry will affect the mass and flux distributions [10, 17]. A simple geometric approach will be assumed, followed by a generalization with respect to the crystal shape.

4.3.1 Flat face growth

Consider in a first stage, the simplest situation of flat face growth (Figure 4.1), with a linear kinetic law.

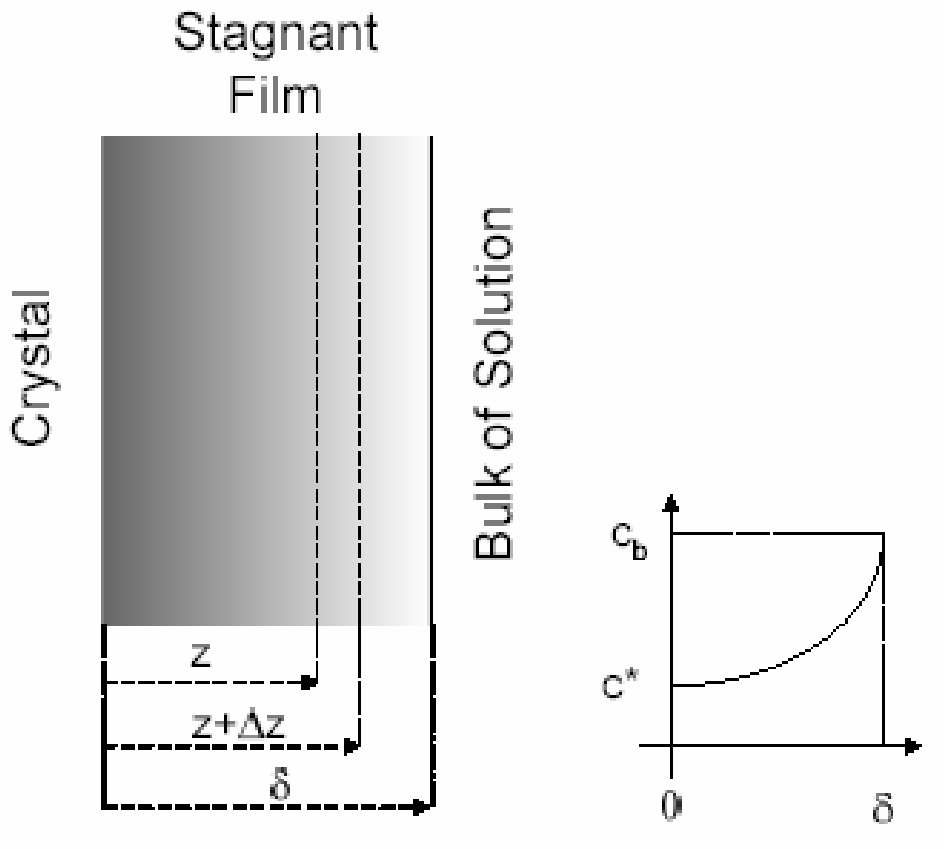

Figure 4.1. Growth of a crystal with a flat face. Sketch of the concentration profile in the stagnant film.

For this geometry the area of mass transfer remains constant along the stagnant film. The mass balance applied to a slab of volume comprised between z and $z+\Delta z$ is:

$$A\,\mathcal{D}_{AB}\left(\frac{d\Delta c}{dz}\right)_{z+\Delta z} - A\,\mathcal{D}_{AB}\left(\frac{d\Delta c}{dz}\right)_{z} = k_r \Delta c\; A\,\Delta z \tag{4.15}$$

In the limiting situation, when $\Delta z \to 0$, it becomes:

$$\frac{d^2\Delta c}{dz^2}-\frac{k_r}{\mathcal{D}_{AB}}\Delta c=0 \tag{4.16}$$

or in dimensionless form:

$$\frac{d^2 f}{dx^2}=\frac{k_r\delta^2}{\mathcal{D}_{AB}}f \tag{4.17}$$

with $x=z/\delta$ and $f=\Delta c/\Delta c_b$. The boundary conditions refer to the concentration at the crystal-solution interface ($z=0$), which is assumed to be the equilibrium saturation concentration ($c=c^*$), and at the stagnant film-solution interface ($z=\delta$), where the concentration is the same as in the bulk of solution ($c=c_b$):

$$\begin{cases} f=1\left(\Delta c=\Delta c_b\right),\ x=1\ (z=\delta) \\ f=0\left(\Delta c=0\right),\ x=0\ (z=0) \end{cases} \tag{4.18}$$

The overall growth rate is the integral of the solute transfer rate over the volume of the stagnant film (V_f):

$$R_G=\frac{\rho}{A}\int_0^{V_f}k_r\Delta c dV_f=\rho\int_0^{\delta}k_r\Delta c dz=\rho\delta\Delta c_b\int_0^1 k_r f dx \tag{4.19}$$

The solution of Eq. (4.17) is only possible after knowing the function $k_r(x)$. Therefore, information about the change in the adsorption rate with the crystal distance would be necessary. As such is not possible, an equivalent kinetic constant k_e will be considered, that gives the same overall growth rate but with the difference of being constant along the film:

$$R_G=\rho\delta\Delta c_b\int_0^1 k_r f dx=\rho\delta\Delta c_b k_e\int_0^1 f_e dx \tag{4.20}$$

In the previous equation, $f_e(x)$ is the equivalent supersaturation profile, obtained from the following material balance

$$\frac{d^2 f_e}{dx^2}-\frac{k_e\delta^2}{\mathcal{D}_{AB}}f_e=0 \tag{4.21}$$

The solution of the differential equation, for the boundary conditions given in Eq. (4.18), is

$$f_e=\frac{\sinh(\phi x)}{\sinh(\phi)} \tag{4.22}$$

where ϕ is a dimensionless parameter, representing the kinetic step/diffusional step ratio:

$$\phi = \sqrt{\frac{k_e \delta^2}{\mathcal{D}_{AB}}} = \sqrt{\frac{k_e \delta}{\mathcal{D}_{AB}/\delta}} = \sqrt{\frac{k_{re}}{k_d}} \tag{4.23}$$

This definition has analogies with the Hatta number used in gas-liquid reactions and with the Thiele modulus well known in heterogeneous catalysis [13]. Furthermore, there is a correspondence between ϕ and the parameter h of Eq. (4.7). The overall rate equation results from Eqs. (4.20) and (4.22):

$$R_G = \rho k_{re} \Delta c_b \cdot \frac{1}{\phi} \left\{ \frac{1}{\tanh(\phi)} - \frac{1}{\sinh(\phi)} \right\} \tag{4.24}$$

This equation establishes both the relation R_G vs Δc_b and the role of the parameters k_{re} and k_d in the process.

4.3.2 Influence of diffusional limitations

Diffusional limitations can be accounted through parameter ϕ. High ϕ values mean slow diffusion comparatively with the kinetic step (diffusional regime). On the other hand, when the diffusional resistance is negligible the value of ϕ is low (chemical regime). The thickness of the adsorbed layer would be related to the relative rates of diffusion and surface integration [18]. Growth rate equations for the limiting situations can be calculated from Eq. (4.24):

In the diffusional regime, $\phi \to \infty$, therefore

$$R_{G_{diff}} = \rho k_{re} \Delta c_b \cdot \frac{1}{\phi} \tag{4.25}$$

In chemical regime, $\phi \to 0$, and

$$R_{G_{chem}} = \rho k_{re} \Delta c_b \cdot \frac{1}{2} \tag{4.26}$$

Diffusion-affected growth rate can be compared with the one predicted for chemical regime, through an effectiveness factor:

$$\eta = \frac{R_G}{R_{G_{chem}}} \tag{4.27}$$

For the current case of a slab crystal and a first order kinetics, this is the same as:

$$\eta = \frac{\rho k_{re} \Delta c_b \int_0^1 f_e dx}{\rho k_{re} \Delta c_b \cdot \frac{1}{2}} = 2\int_0^1 f_e dx = \\ = \frac{2}{\phi}\left\{\frac{1}{\tanh(\phi)} - \frac{1}{\sinh(\phi)}\right\} \tag{4.28}$$

For chemical regime, $\eta_{chem} = 1$, and when strong diffusional limitations are imposed, $\eta_{diff} = 2/\phi$.

4.3.3 Generalized growth rate equations - Crystal geometry factor

The equations derived so far are for the planar case; the corresponding results for spherical and cylindrical crystals will now be considered. Applying the continuity equation to a spherical shell (Figure 4.2), gives

$$\left[4\pi r_p^{\,2} \mathcal{D}_{AB}\left(\frac{d\Delta c_e}{dr_p}\right)\right]_{r_p+\Delta r_p} - \\ -\left[4\pi r_p^{\,2} \mathcal{D}_{AB}\left(\frac{d\Delta c_e}{dr_p}\right)\right]_{r_p} = k_e \Delta c_e 4\pi r_p^{\,2} \Delta r_p \tag{4.29}$$

Similarly to what was done for the flat face growth, a kinetic constant that is independent of the position in the stagnant film is assumed. Again the concentration profiles are called "equivalent", since they lead to the same growth rate as for the case of the true kinetic constant, k_r. Simplifying Eq. (4.29) and letting $r_f = r_p - R_p$, one obtains

$$\frac{d^2\Delta c_e}{dr_f^2} + \frac{2}{r_f + R_p}\frac{d\Delta c_e}{dr_f} - \frac{k_e}{\mathcal{D}_{AB}}\Delta c_e = 0 \tag{4.30}$$

Rendering this equation dimensionless, by setting $f_e = \Delta c_e / \Delta c_b$, $x = r_f / \delta$, and using Eq. (4.23) becomes

$$\frac{d^2 f_e}{dx^2} + \frac{2}{x + R_p/\delta}\frac{df_e}{dx} - \phi^2 f_e = 0 \tag{4.31}$$

Applying the same procedure to an infinitely long cylindrical crystal gives

$$\frac{d^2 f_e}{dx^2} + \frac{1}{x + R_p/\delta}\frac{df_e}{dx} - \phi^2 f_e = 0 \tag{4.32}$$

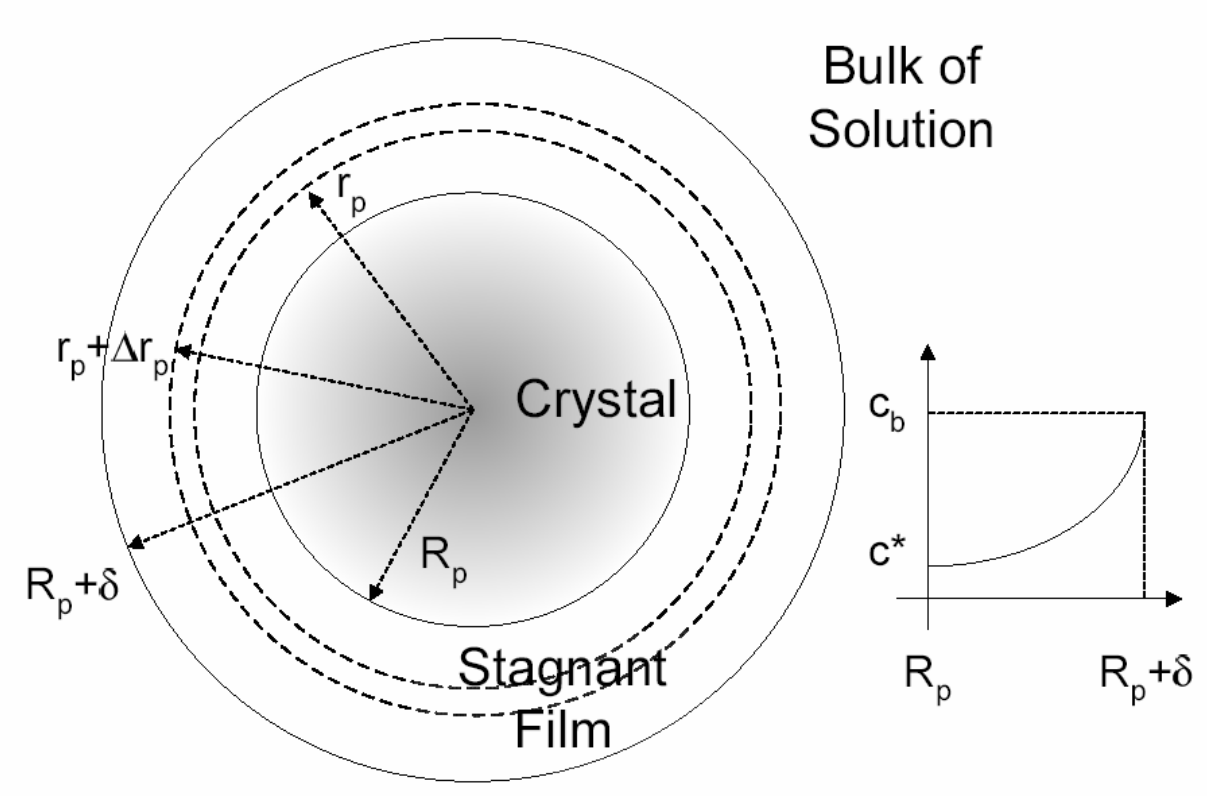

Figure 4.2. Growth of a spherical crystal. Sketch of the concentration profile in the stagnant film.

Complicated analytical growth equations can be deduced for spherical and cylindrical crystals expressions. Comparing Eqs. (4.21), (4.31) and (4.32) it is possible to deduce a general second-order differential equation, valid for the crystal shapes under study:

$$\frac{d^2 f_e}{dx^2} + \frac{\kappa}{x + R_p/\delta}\frac{df_e}{dx} - \phi^2 f_e = 0 \tag{4.33}$$

where

$$x = \frac{z \text{ or } r_f}{\delta} \tag{4.34}$$

and κ is a function of the shape factor for each geometry,

$$\kappa = \frac{\text{Area}}{\text{Volume}} \cdot \left(L \text{ or } R_p\right) - 1 \tag{4.35}$$

The boundary conditions are defined by Eq. (4.18). For a given value of ϕ, the differences between equivalent concentration profiles, and consequently between effectiveness factor profiles for each geometry, arise from the values of κ and R_p/δ considered (Figure 4.3).

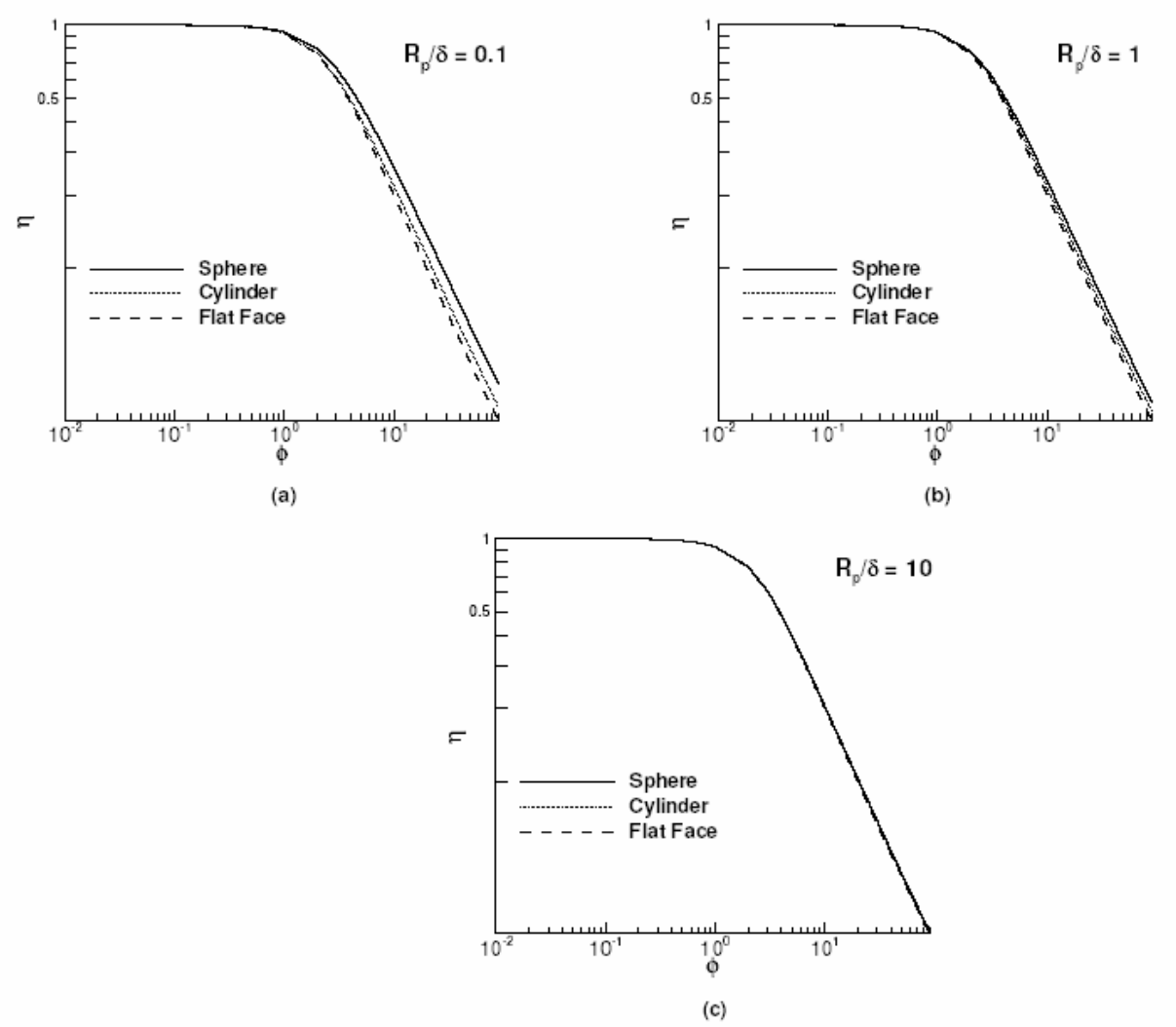

Figure 4.3. Effectiveness factor versus ϕ for presented geometries and R_p/δ values.

The overlapping profiles of Figure 4.3c can be understood from Eq. (4.33), since for high values of R_p/δ, the relative weight of the second term of this equation becomes negligible. It is believed that this is the common case in crystal growth since, for the majority of experimental conditions, high values of the Sherwood number are reported (at least $Sh = 2$, for natural convection conditions) [11] and

$$Sh = \frac{k_d}{\mathcal{D}_{AB}} L = \frac{L}{\delta} \approx R_p/\delta \tag{4.36}$$

It is, therefore, a good approximation to use the equations derived for flat face growth in any crystal geometry.

4.3.4 Generalized growth rate equations - Kinetic order factor

Consider now a generalized kinetic order r. For a sufficiently high value of R_p/δ, the mass conservation law in the dimensionless form is

$$\frac{d^2 f_e(x)}{dx^2} - \phi^2 \Delta c_b^{r-1} f_e^r = 0 \tag{4.37}$$

and the boundary conditions are defined by Eq. (4.18). In this case there is not an analytical solution, although it is possible to find an expression of η (and therefore of R_G) accounting the asymptotic limits [19].

In the diffusional regime, ϕ is high and

$$\left(\frac{df_e}{dx}\right)_{x=0} = 0 \tag{4.38}$$

On the other hand, from Eqs. (4.27) and (4.37),

$$\begin{aligned} \eta &= (r+1)\int_0^1 f_e^r dx = (r+1)\int_0^1 \frac{d^2 f_e}{dx^2}\frac{1}{\phi^2 \Delta c_b^{r-1}} dx = \\ &= \frac{r+1}{\phi^2 \Delta c_b^{r-1}}\left[\left(\frac{df_e}{dx}\right)^{x=1} - \left(\frac{df_e}{dx}\right)_{x=0}\right] \end{aligned} \tag{4.39}$$

and the following expression can be derived

$$\eta_{diff} = \frac{r+1}{\phi^2 \Delta c_b^{r-1}}\left(\frac{df_e}{dx}\right)^{x=1} \tag{4.40}$$

Manipulating the differential equation, becomes

$$\begin{aligned} &\frac{d^2 f_e}{dx^2}\frac{df_e}{dx} dx = \Delta c_b^{r-1} \phi^2 f_e^r df_e \Rightarrow \\ &\Rightarrow \frac{1}{2}\left(\frac{df_e}{dx}\right)^2\Bigg|_{x=0}^{x=1} = \frac{\Delta c_b^{r-1}\phi^2}{r+1} f_e^{r+1}\Big|_{x=0}^{x=1} \end{aligned} \tag{4.41}$$

and,

$$\left(\frac{df_e}{dx}\right)^{x=1} = \phi\sqrt{\frac{2}{r+1}\Delta c_b^{r-1}} \tag{4.42}$$

Replacing Eq. (4.42) in Eq. (4.40), results that

$$\eta\big|_{diff} = \frac{1}{\phi}\sqrt{\frac{2(r+1)}{\Delta c_b^{r-1}}} \tag{4.43}$$

This equation can be re-written in a form that is similar to the definition of η_{diff} when $r=1$:

$$\eta_{diff} = 2/\phi_g \tag{4.44}$$

with

$$\begin{aligned}\phi_g &= \sqrt{\frac{2}{r+1}\cdot\frac{k_e\delta^2}{D_e}\Delta c_b^{r-1}} = \\ &= \sqrt{\frac{2}{r+1}\cdot\frac{k_{re}}{k_d}\Delta c_b^{r-1}} = \phi\sqrt{\frac{2}{r+1}\Delta c_b^{r-1}}\end{aligned} \tag{4.45}$$

In the chemical regime, the solution is independent of the kinetic order r, i.e., $\phi \to 0$ and $\eta = 1$.

The limiting cases obtained for a given kinetic order r, are comparable with what was deduced when $r=1$. An approximate equation for the effectiveness factor can therefore be obtained by analogy with Eq (4.28):

$$\eta = \frac{2}{\phi_g}\left\{\frac{1}{\tanh(\phi_g)} - \frac{1}{\sinh(\phi_g)}\right\} \tag{4.46}$$

As illustrated in Figure 4.4, the major differences between the preceding equation and the true profile obtained numerically from Eqs. (4.37) and (4.39) occur for intermediate values of ϕ_g The generalized growth rate equation results from Eq. (4.27) and from Eq. (4.46),

$$R_G = \rho k_{re}\Delta c_b^r \cdot \frac{2}{r+1}\frac{1}{\phi_g}\left\{\frac{1}{\tanh(\phi_g)} - \frac{1}{\sinh(\phi_g)}\right\} \tag{4.47}$$

This equation can be widely used despite of experimental conditions and crystal shapes.

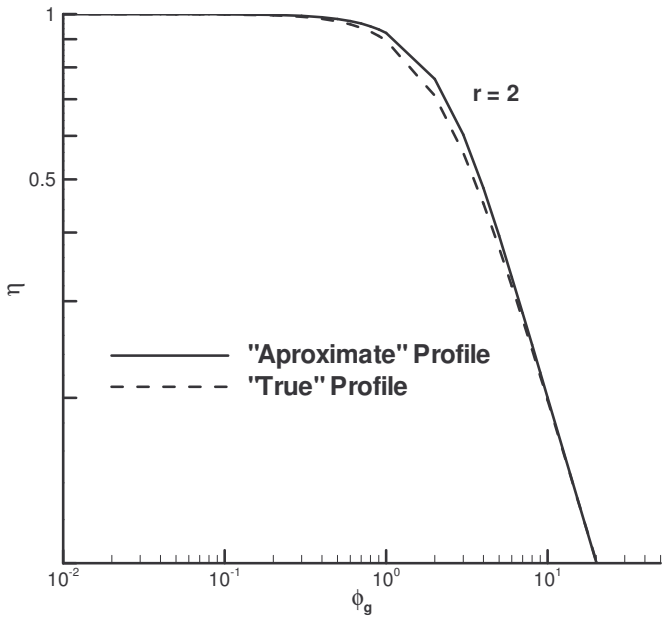

Figure 4.4. Approximate effectiveness factor (Eq. (4.46)) and the true effectiveness factor (numerical solution) vs ϕ_g .

4.4 Conclusions

An alternative model characterizing the physical processes during crystallization is presented. The Langmuir theory for monolayer surface adsorption is extended to the multilayer case following a method which can be related to the derivation of the BET equation. With this approach, the crystal growth rate corresponds to the net adsorption velocities extended to all adsorbed layers. The mathematical description of the process assumes the simultaneous occurrence of solute diffusion and adsorption, followed by the surface integration of the adsorbed molecules. The equivalent concentration profiles and growth rate equations are estimated. From the analysis of different cases concerning crystal shape, kinetic law, and diffusional resistance, a generalized overall growth rate equation is obtained – Eq. (4.47).

References

[1] J. J. Carberry, Chemical and catalytic reaction engineering, McGraw-Hill, New York, **1976**.

[2] N. Kubota and J. W. Mullin, A Kinetic model for crystal growth from aqueous solution in the presence of impurity. *J. Cryst. Growth*, **1995,** 152, 203-208.

[3] N. Cabrera and D. A. Vermilyea, in *Growth and perfection of crystals*, (R. H. Doremus, B. W. Roberts, D. Turnbull, eds.), Wiley, New York, **1958**.

[4] N. Kubota, M. Yokota, and L. A. Guzman, in *Separation and purification by crystallization*, (G. D. Botsaris, K. Toyokura, eds.), American Chemical Society, Washington, DC, **1997**.

[5] L. A. Guzman, N. Kubota, M. Yokota, A. Sato, and K. Ando, Growth hysteresis of a potassium sulfate crystal in the presence of chromium(III) impurity. *Cryst. Growth Des.*, **2001,** 1, 225-229.

[6] N. Kubota, M. Yokota, N. Doki, L. A. Guzman, S. Sasaki, and J. W. Mullin, A mathematical model for crystal growth rate hysteresis induced by impurity. *Cryst. Growth Des.*, **2003,** 3, 397-402.

[7] K. Sangwal, Kinetic effects of impurities on the growth of single crystals from solutions. *J. Cryst. Growth*, **1999,** 203, 197-212.

[8] K. Sangwal and E. Mielniczek-Brzoska, Effect of Cr(III) ions on the growth kinetics of ammonium oxalate monohydrate crystals from aqueous solutions. *J. Cryst. Growth*, **2002,** 242, 421-434.

[9] J. Garside, The concept of effectiveness factors in crystal growth. *The concept of effectiveness factors in crystal growth*, **1971,** 26, 1425-1431.

[10] J. Garside, in *Advances in industrial crystallization*, (J. Garside, R. J. Davey, A. G. Jones, eds.), Butterworth Heinemann, Oxford, **1991**.

[11] J. W. Mullin, Crystallization, 3rd ed.; Butterworth-Heinemann, **1992**.

[12] D. M. Ruthven, Principles of adsorption and adsorption processes, John Wiley & Sons, Inc., New York, **1984**.

[13] G. F. Froment and K. B. Bischoff, Chemical reactor analysis and design, John Wiley & Sons, Inc., New York, **1990**.

[14] M. Ohara and R. C. Reid, Modelling crystal growth rates from solution, Prentice-Hall, Inc., New Jersey, **1973**.

[15] W. K. Burton, N. Cabrera, and F. C. Frank, The Growth of Crystals and the Equilibrium Structure of their Surfaces. *The Growth of Crystals and the Equilibrium Structure of their Surfaces*, **1951,** 243, 299-358.

[16] J. Garside, Advances in the Characterisation of Crystal Growth. *Advances in the Characterisation of Crystal Growth*, **1984,** 80, 23-38.

[17] W. R. Paterson and A. N. Hayhurst, Mass or heat transfer from a sphere to a flowing fluid. *Chem. Eng. Sci.*, **2000,** 55, 1925-1927.

[18] C. Y. Tai, J.-F. Wu, and R. W. Rousseau, Interfacial supersaturation, secondary nucleation, and crystal growth. *Interfacial supersaturation, secondary nucleation, and crystal growth*, **1992,** 116, 294.

[19] J. Villermaux, Génie de la réaction chimique - conception et fonctionnement des réacteurs, TEC & TOC - Lavoisier, Paris, **1993**.

5. Interpretation of diffusion-affected growth rate data

Overview

Experimental results on crystal growth and dissolutions kinetics are taken from literature to test the novel parallel step model (PSM) and the well-established two step model (TSM). The chosen literature data allowed calculating the mass transfer coefficients during crystal growth, for different hydrodynamic conditions. The obtained results are compared with estimates from the mass transfer theories. According to the TSM, the measured crystal growth kinetics can only be explained by means of an unrealistic variation of the mass transfer coefficient with the relative crystal-solution velocity. Conversely, mass transfer coefficients obtained by the PSM were confirmed by appropriate semi-theoretical correlations, both in their order of magnitude and in their behaviour. In addition, crystal growth and dissolution experiments of sucrose were carried out at 40 ºC in a batch crystallizer for different agitation speeds. The resulting kinetics are used to test the PSM in a system that is significantly different from the inorganic salts used in the analysed literature works. As predicted by this model, the existence of an adsorbed layer in the crystal surrounding is likely to affect the solute molecular diffusivity in the medium. Based on this premise, the results obtained with sucrose are well described by the PSM.

5.1 The role of diffusion during crystal growth

The growth of crystals from solution is known to be affected by mass transport processes. When mass transfer resistances are strong, changes in the hydrodynamic conditions of the solution will have a direct impact on the crystallization kinetics. The several theoretical models considering this subject admit the existence of a diffusive flux of the solute towards the crystal, according to Fick's first law of diffusion. Yet, the way this step is related with other phenomena occurring during crystal growth (solute adsorption, surface diffusion, integration in crystal lattice, etc) is described by distinct viewpoints. More fundamental approaches depart from the work of Burton, Cabrera and Frank [1], where the growth of crystals at low supersaturations was successfully explained by the spiral movement of steps originated from surface imperfections. The original model was derived for crystals growing from vapour with dominant resistances taking place at their surface. In subsequent modifications to the Burton, Cabrera and Frank theory, the role of volume diffusion was further discussed [2, 3]. Despite of the theoretical and mechanistic interest of the atomic-scale models, soon it was noticed that their complexity would not facilitate the practical analysis of experimental data [4]. Instead, the use of empirical mass transfer relations between the Sherwood number (Sh), the crystal Reynolds number (Re_p) and the solution Schmidt number (Sc) was preferred for engineering purposes. This procedure is still adopted nowadays [5].

Typically, crystals dissolve faster than they grow and the respective rates depend differently on the concentration driving force. These experimental evidences suggest that crystallization is not a pure mass transfer process (or a reciprocal process of dissolution), and so, care must be taken when analysing the overall kinetics through mass transfer correlations alone. The simple arrangement in series of the volume diffusion step followed by the solute integration at crystal surface ("kinetic" step) has found great applicability on the interpretation of crystal growth rates from solution. According to the already described two step model (TSM), the crystal growth rate (R_G) is related with the kinetic (k_r' and r') and diffusional parameters (k_d') through the following equation (see Chapter 4):

$$\frac{R_G}{k_r' \Delta c_b^{r'}} = \left[1 - \frac{R_G}{k_d' \Delta c_b} \right]^{r'} \tag{5.1}$$

The isolated role of supersaturation ($\Delta c_b = c_b - c^*$) on the crystal growth rate is usually given by a semi-theoretical law:

$$R_G = K_G \Delta c_b^g \tag{5.2}$$

For a given system, the parameters K_G and g would assume different values depending on the temperature and diffusional resistance at which crystal growth rates were measured. Sometimes, the latter experimental condition is neglected or non-specified leading to reproducibility problems. As seen in Chapter 4, the mass transfer resistance during crystal growth can be quantified by means of the "effectiveness factor" (η_C), defined as the ratio between the measured growth rate and the one expected in the absence of significant diffusional resistance [6]:

$$\eta_C = \frac{R_G}{R_{G_{chem}}} = \frac{K_G \Delta c_b^g}{k_r' \Delta c_b^{r'}} \tag{5.3}$$

As demonstrated, Eq. (5.1) can be conveniently rearranged in order to include the preceding definition, so that:

$$\eta_C = \left(1 - h \cdot \eta_C\right)^{r'} \tag{5.4}$$

and h represents the ratio between the kinetic and the diffusional steps (Chapter 4):

$$h = \frac{k_r' \Delta c_b^{r'}}{k_d' \Delta c_b} \tag{5.5}$$

The concept of effectiveness factor is been widely used, not only as a direct measure of the mass transfer influence on crystal growth, but also on the study of the growth kinetics change due to the presence of impurities [7-12].

The effectiveness factor corresponding to a given overall crystal growth can be calculated by one of the following alternatives:

I. If the crystal growth rate without diffusional limitations is known, η_C can be computed from Eq. (5.3).

II. If the mass transfer coefficient (k_d') is known, the true kinetic parameters (k_r' and r') can be determined by curve fitting of Eq. (5.1) to the crystal growth rate data. Once determined all the parameters, η_C is again given by Eq. (5.3).

These two cases will be hereafter called "type I" and "type II" problems. Type II problems are more often found, since dissolution experiments carried out under equivalent conditions of the

crystal growth give a prompt estimation of k_d' (the validity of this estimation will be later discussed). On its turn, true kinetic parameters are more demanding to obtain from crystal growth experiments. Previous studies must be made on when crystal growth rates start to be independent of the diffusional resistance. Type I problems are, consequently, less common.

An alternative perspective on the role of the diffusional resistance during crystal growth was presented in the preceding chapter. According to the new parallel step model (PSM), the following generalized growth rate expression can be used to relate R_G with supersaturation, mass transfer coefficient (k_d) and the true kinetic parameters associated to the adsorption rate (k_{re} and r):

$$R_G = \rho k_{re} \Delta c_b^r \cdot \frac{\eta}{r+1} \tag{5.6}$$

with ρ being the solution density and η the PSM effectiveness factor,

$$\eta = \frac{R_G}{R_G\big|_{chem}} = \frac{2}{\phi_g}\left\{\frac{1}{\tanh\left(\phi_g\right)} - \frac{1}{\sinh\left(\phi_g\right)}\right\} \tag{5.7}$$

and

$$\phi_g = \sqrt{\frac{2}{r+1} \cdot \frac{k_{re}}{k_d} \Delta c_b^{r-1}} \tag{5.8}$$

As indicated by Eqs. (5.3) and (5.7), the meaning of the effectiveness factor is the same independently if the model considered is the TSM (η_C) or the PSM (η). What differentiates the two models is how the several variables and parameters affect the effectiveness factor, and hence, how they affect the crystal growth rate. For a better understanding of the different behaviours, the so-called Damköhler number (Da), relating the growth rate in absence of diffusional limitation ("chemical" regime) with the pure diffusional rate (R_d) will now be used:

$$Da = \frac{R_G\big|_{chem}}{R_d} \tag{5.9}$$

In what concerns with the TSM, the Damköhler number corresponds to the parameter h defined in Eq. (5.5). As a consequence, Eq. (5.4) relating η_C with h is also valid for Da:

$$\eta_C = \left(1 - Da \cdot \eta_C\right)^{r'} \tag{5.10}$$

In the case of the PSM, it should be noted that,

$$\phi_g = \sqrt{2Da} \tag{5.11}$$

And so,

$$\eta = \frac{2}{\sqrt{2Da}}\left\{\frac{1}{\tanh\left(\sqrt{2Da}\right)} - \frac{1}{\sinh\left(\sqrt{2Da}\right)}\right\} \tag{5.12}$$

The two definitions of effectiveness factor given by Eqs. (5.10) and (5.12) are represented in Figure 5.1.

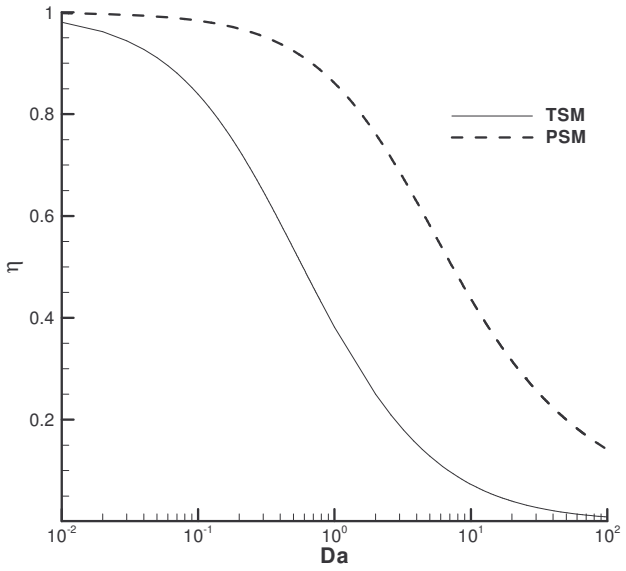

Figure 5.1. Influence of the Damköhler number on the effectiveness factor according to Eq. (5.10) (TSM) and to Eq. (5.12) (PSM).

As shown, the region of low Da values where the crystal growth rate is insensitive to changes in the mass transfer coefficient is smaller in the TSM case. In fact, the growth rate slowing down effect caused by the progressive increase of the boundary layer thickness is expected to occur much sooner by the TSM than by PSM. For example, if $Da = 0.5$ the crystal growth rate predicted by the TSM will be only 54% of the one expected in chemical regime, while by the PSM this percentage increases to 92%.

In the following section it will be investigated which of theoretical predictions represented in Figure 5.1 is closer to typical experimental evidences taken from literature. Additionally, experiments on the influence of hydrodynamics on sucrose crystal growth and

dissolution rates were carried out and the resulting data will be interpreted in the light of the PSM.

5.2 Analysis of literature data

Many experimental works have been published on the factors influencing crystal growth such as supersaturation, temperature, impurities concentration, crystal size, hydrodynamic conditions, etc. However, most of the resulting conclusions are not suitable to compare the TSM against PSM. For example, very distinct effectiveness factors would result from each model if they were applied to a type II problem (where mass transfer coefficients obtained from dissolution experiences are used to estimate the weight of the diffusional resistance during crystal growth); however, it would not be possible to know if any of the solutions would be the correct one. To compare the models, crystal growth data obtained under different and well-defined diffusional conditions have to be known. Ideally, information on the limiting cases (pure chemical and diffusional regimes) should also be available. Variations on the growth behaviour due to different hydrodynamics could this way be compared with the two theoretical predictions. Among the experimental studies that were consulted, the comprehensive work of Mullin and Garside on the crystallization of aluminium potassium sulphate (potash alum) [13-15] appears to be indicated for these purposes. The effect of the solution velocity on the linear growth rate of the (111) faces measured in a single crystal growth cell [13] is of particular interest to determine the mechanism of growth. These results were obtained for the pure system, at constant temperature (32.0 ºC) and for crystal sizes around 2 mm. As both TSM and PSM admit, growth rate increased with solution velocity – Figure 5.2 and Table 5.1. For higher solution velocities this effect became less evident indicating that, under those conditions, the process started to be controlled by the kinetic step. The estimated crystal growth rate in absence of diffusional resistances was given by,

$$\frac{R_{G_{chem}}}{\rho_s} = (17.4 \pm 0.2) \times 10^{-5} \Delta c_b^{(1.62 \pm 0.02)} \tag{5.13}$$

where ρ_s is the crystal density.

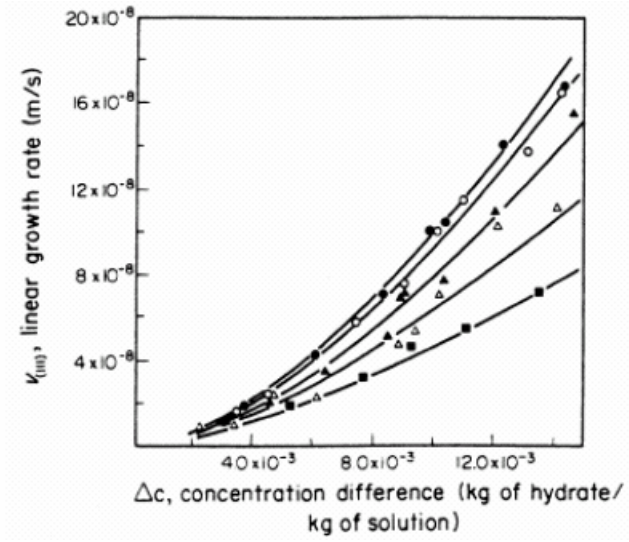

Figure 5.2. Effect of solution velocity on the growth rates of single crystals of potash alum at 32.0 ºC. Solution velocity (m/s): ● = 0.217, ○ = 0.120, ▲ = 0.064, Δ = 0.022, ■ = 0.006 [13].

Table 5.1. Parameters of the Eq. (5.2) (empirical growth rate law) that best fit the experimental results represented in Figure 5.2 [13].

u (m/s)	$K_G/\rho_s \times 10^5$ (m/s)	g ± standard error
0.006	2.93	1.39 ± 0.09
0.022	4.31	1.41 ± 0.12
0.064	14.4	1.63 ± 0.09
0.120	16.4	1.62 ± 0.02
0.217	19.4	1.65 ± 0.05

Information provided by Eq. (5.13) and Table 5.1 allows calculating the effectiveness factor for each set of experimental conditions (type I problem),

$$\eta_C \text{ or } \eta = \frac{R_G}{R_{G_{chem}}} = \frac{K_G}{17.4\times10^{-5}\,\Delta c_b^{(1.62-g)}} \tag{5.14}$$

According to the previous equation, crystal growth rate is more influenced by diffusional limitations at higher supersaturations. This effect is more pronounced in diffusional regime, when $g \ll 1.62$. Type I problems lead to the same effectiveness factor values, independently if the model considered is the TSM or the PSM. Despite of that, distinct consequences arise from each of the situations in terms of the importance of the mass transfer resistance. Recalling the two profiles represented in Figure 5.1, for a given value of effectiveness factor

it is expected the Damköhler number to be smaller when calculated through the TSM equations. Table 5.2 shows the effectiveness factors calculated for each solution velocity by using Eq. (5.14) and the corresponding values of Da given by Eq. (5.10) (TSM) and by Eq. (5.12) (PSM). At same time, the definition of Damköhler number (Eq. (5.9)) is used to compute the mass transfer coefficients at the considered driving force of $(0.010\,\text{kg hydrate})/(\text{kg solution})$.

Table 5.2. Values of effectiveness factor, Damköhler number and mass transfer coefficient obtained by the TSM and PSM for each solution velocity. The driving force for diffusion and crystallization was in all cases, $\Delta c_b = (0.010\,\text{kg hydrate})/(\text{kg solution})$.

u (m/s)	η or η_C	TSM		PSM	
		Da	k_d' (kg/m^2·s)	Da	k_d (kg/m^2·s)
0.006	0.486	0.741	0.0238	7.860	0.0022
0.022	0.652	0.357	0.0493	3.573	0.0049
0.064	0.790	0.171	0.1028	1.679	0.0105
0.120	0.943	0.038	0.4622	0.370	0.0475
0.217	0.971	0.018	0.9514	0.180	0.0978

Mass transfer coefficients obtained by the TSM were higher and more steeply dependent of the solution velocity than the ones given by the PSM. Semi-theoretical correlations for mass transfer in liquid-solid systems will be used to interpret the results of Table 5.2. Dissolution experiments were carried out with potash alum in a fluidized-bed crystallizer to determine the correlations parameters that best describe the dissolution rate data [15]. The results obtained with mean crystal sizes between 510 and 1750 μm and at different temperatures (between 15 and 47 ºC) were well described by the following equation:

$$Sh = 0.37\,Sc^{0.33}\,Re_p^{0.62} \tag{5.15}$$

This relationship allows estimating mass transfer coefficients for the set of experimental conditions and solution physical properties of the crystal growth experiments. Although crystallization and dissolution data were measured by different techniques (single crystal growth cell and fluidized-bed crystallizer, respectively), it has been concluded that the crystal growth behaviour obtained by one of the methods can be directly predicted by the results of the other [14]. Accordingly, mass transfer coefficients resulting from the growth experiments

(Table 5.2) were compared with the estimations of Eq. (5.15) at the same solution velocity. The obtained results are shown in Figure 5.3.

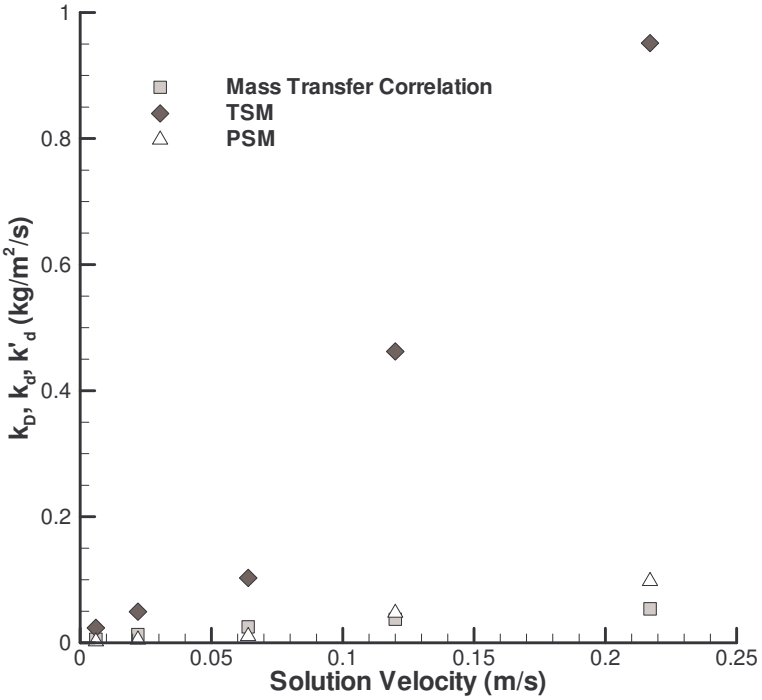

Figure 5.3. Comparison of mass transfer coefficients estimated from dissolution (k_D) and growth (k_d' and k_d) experiments.

Considering the degree of uncertainty associated to the determination of diffusional parameters, a good agreement was found between mass transfer coefficients calculated by the PSM (k_d) and by mass transfer correlations (k_D). Contrarily, values resulting from the TSM (k_d') were always higher than k_D, with the differences getting significantly higher as the solution velocity increases. The order of magnitude of the calculated k_D (and k_d) was in all cases below 10×10^{-2} kg/m^2·s, corresponding approximately to the range of experimental values obtained during dissolutions in the fluidized bed crystallizer [15]. Comparatively, the evolution of mass transfer coefficients foreseen by the TSM do not seem realistic, with k_d' rapidly increasing to near 100×10^{-2} kg/m^2·s for higher solution velocities.

From these results it is evident that mass transfer coefficients obtained from semi-theoretical correlations or directly from dissolution data should not be used to describe the diffusion step during crystal growth as conceived by the TSM. Garside and Mullin have drawn a similar conclusion by comparing the results from crystal growth and dissolution measurements in the fluidized-bed crystallizer [15]. Yet, besides supersaturation and

hydrodynamics, size dependent growth is an additional factor that should be accounted on the interpretation of those results. It is likely that the observed growth rate enhancement with increasing crystal sizes is not exclusively due to higher solution velocities (required to suspend bigger crystals) but also to variations on the surface integration kinetics.

In a later work, Clontz et al. [16] also employed the growth cell technique to measure crystal growth rates of magnesium sulphate heptahydrate. Kinetic and diffusional parameters of the TSM were determined for the (110) faces according to the procedure previously described for potash alum. Again, the obtained mass transfer coefficients were considerably above the values indicated by standard mass transfer correlations. Moreover, mass transfer resistances provided by the TSM are unusually influenced by hydrodynamics by means of a rapid increase of k_d' with solution velocity. Both indications coincide with the behaviour observed in Figure 5.3, for the potash alum system. A number of potential causes for the reported differences have been suggested in literature. Mullin and Garside [15] admit that electrostatic charges attracting solute molecules towards the crystal surface would accelerate the diffusion rate during crystal growth. Other processes occurring in the surroundings of crystal surface, such as desolvation and partial ordering of growth units, might as well affect this step [17]. It is also possible that dissolution is not a purely diffusional phenomenon due to the existence of a surface disintegration step [7, 15]. Despite of all the evidences supporting the non-correspondence between standard mass transfer coefficients and the diffusional parameter of the TSM, it is a common procedure to admit the contrary. The inexistence of a practical alternative to predict crystal growth rates at different operating conditions is probably the main reason why that happens. From the preliminary tests against crystal growth and dissolution data taken from literature, the recently introduced parallel step model have confirmed to be a credible option to fulfil this gap. The adequacy of the PSM to experimental evidences was quantitatively and qualitatively demonstrated with the potash alum and the magnesium sulphate heptahydrate systems, respectively.

An interesting divergence arises from the two conceptions of crystal growth provided by the TSM and the PSM: while in the first case it is physically impossible the overall crystal growth rate to be faster than the rate of the diffusional step, by the PSM this hypothesis is perfectly admissible. This happens because by the TSM the only way the solute is transported to crystal surface is by the diffusional movement. If by some hypothetical reason the diffusive flux was stopped the integration of units into crystal lattice would also stop. According to the PSM, the adsorption of solute in the vicinity of the crystal is an additional way to carry the

solute to the surface. In this case, even for very small diffusion rates, crystal growth can be assured by the adsorptive flux. In the above mentioned work of Clontz et al. [16], the TSM surface integration coefficients were calculated for the (111) faces of magnesium sulphate heptahydrate crystals. A simplified expression was used resulting from the fact that the measured crystal growth rates were linearly dependent on supersaturation:

$$k_r^{'} = \frac{k_d^{'} K_G}{k_d^{'} - K_G} \tag{5.16}$$

Surprisingly, negative surface integration coefficients resulted from those calculations. From Eq. (5.16) this means that $k_d^{'} < K_G$. At that time this physical impossibility was considered to be caused by the use of an inappropriate mass transfer coefficient. Perhaps the adopted value of $k_d^{'}$ would not be applicable to the (111) faces since it was obtained from the growth experiments performed with the (110) faces. Nevertheless, as it was referred by the authors it does not seem likely that the diffusion conditions in the two faces would greatly differ [16]. Using mass transfer coefficients given by typical correlations would not solve the problem since, as it was previously mentioned, these values were even lower than $k_d^{'}$. In accordance with the PSM the obtained results can be seen from another perspective. Possibly this is one of the cases where the diffusion step is indeed slower than the overall crystal growth rate. In other words, if k_d and k_D are admitted to be equivalent, crystals will grow faster than they dissolve for the same driving force and for the considered operating conditions. Definitive conclusions about the validity of such argument need further experimental confirmation.

5.3 Experimental section

Growth and dissolution rates of sucrose crystals were measured at 40.0 ± 0.1 ºC, in the 3 L jacketed batch crystallizer represented in Figure 5.4, at different agitation speeds. Solutions were prepared at 60 ºC by dissolving refinery white sugar in ultra-pure water. Supersaturation was obtained by cooling down the solutions to the working temperature. Once the temperature was stable, an accurately known weight of seed crystals (about 5 g) with sieve sizes between 0.250 and 0.300 mm was introduced into the crystallizer. In all experiments, the initial percentage of dissolved sucrose was of 73.4% in weight. The crystals were allowed to grow, leaving the sucrose concentration to decrease until near the saturation. The concentration profile was continuously followed by an on-line refractometer. Each growth experiment took near 15 h, although, the calculation of the growth rate is limited to a

period of ~5 h, which was preceded by a pre-growth period of about 40 min. At the end of the growth, the approximate mass fraction of sucrose crystals was 10.4%. Dissolution experiments immediately followed these periods by adding to the slightly supersaturated solution a rigorously weighted amount (about 100 g) of ultra-pure water at the working temperature. An initial drop on the sucrose concentration occurs due to the introduction of water and the solution becomes undersatureated. The subsequent crystals dissolution gradually increases the dissolved sucrose concentration. As expected for the sucrose system, dissolution experiments were much faster than the preceding crystal growth. Generally, saturation was possible to be achieved in about 1 h. The percentage of dissolved sucrose corresponding to the steady conditions was 69.98% in weight. This value is close to the solubility sucrose in water at 40 ºC (70.01%) obtained in literature [18]. During the dissolution experiments the mass fraction of sucrose crystals decreased from 10.4% to 5.1%. Experiments were carried out at different agitation speeds.

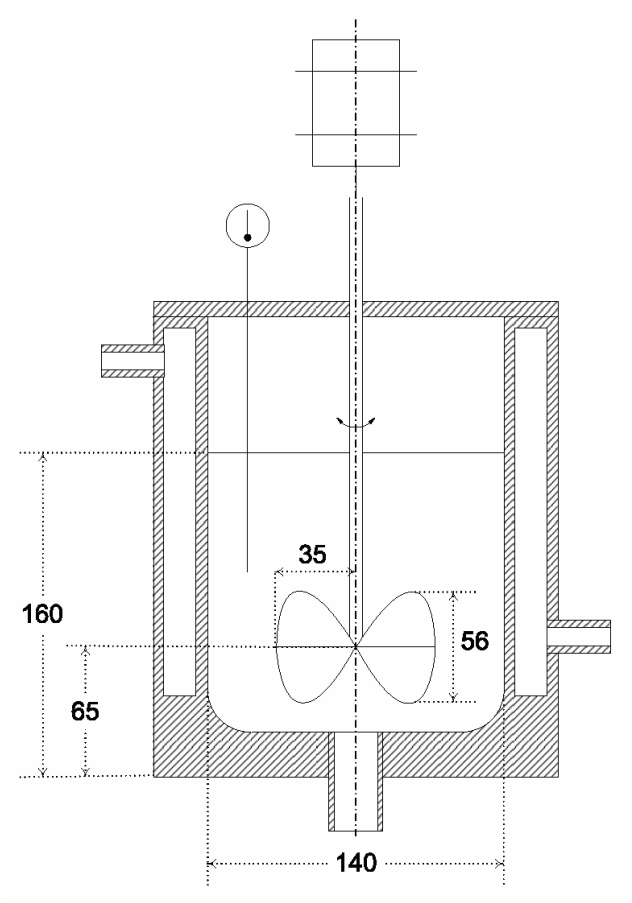

Figure 5.4. Crystallizer used for growth and dissolution experiments (all dimensions in mm).

The amount of crystallized matter was continuously calculated from the change of the solution concentration throughout the experiments [19]. The respective profiles are represented for a given experiment in Figure 5.5.

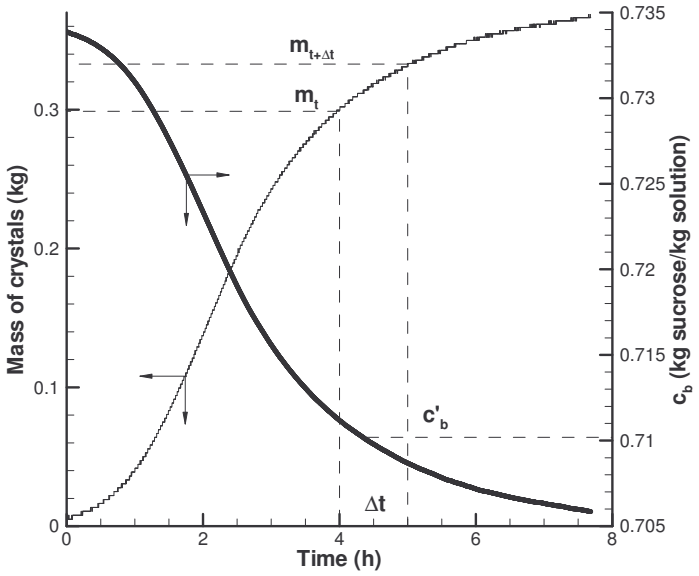

Figure 5.5. Experimental data used to compute crystal growth kinetics. Evolution of the mass of crystals and sucrose concentration during a growth experiment.

Crystal growth and dissolution kinetics were determined based on this information. In a given period Δt, the average crystal growth rate at which the mass of crystals increases from m_t to $m_{t+\Delta t}$ is given by:

$$R_G = 3\frac{(\rho_s \alpha)^{2/3}}{N^{1/3}\beta}\frac{\Delta m^{1/3}}{\Delta t} \tag{5.17}$$

where α and β are volume and surface area shape factor and N the number of crystals. This equation was previously derived in Chapter 3 to account for the variation of the crystals surface area during Δt. According to Figure 5.5, the corresponding average solute concentration during the same period is c_b' (average supersaturation $\Delta c_b' = c_b' - c^*$). Repeating this procedure all over the chosen range of concentrations, information is gathered about the influence of supersaturation (and undersaturation) on the crystal growth (and dissolution) rates. The physical properties of sucrose crystals to be used in Eq. (5.17) were taken from the work of Bubnik and Kadlek [20]. The number of growing/dissolving crystals is assumed to remain constant during the experiments (significant nucleation, crystal breakage or agglomeration is not admitted to occur). The estimation of this number was based on the mass

of seeds (m_s) and on their mean size obtained from sieve fractions (L_s), so that $N = m_s \big/ \left(0.75 \rho_s L_s^3\right)$ [20].

5.4 Results and discussion

Figure 5.6a shows the variation of overall growth rate at 40 ºC with the concentration driving force, for different sets of hydrodynamic conditions. Only results corresponding to equally spaced supersaturations are represented. The average difference between successive supersaturations is approximately $(5\times10^{-4}$ kg sucrose)/(kg solution). Dissolution experiments were performed once finished the growth period, after adding 100 g of water to the crystallizer content. The obtained dissolution rates (R_D) are shown in Figure 5.6b.

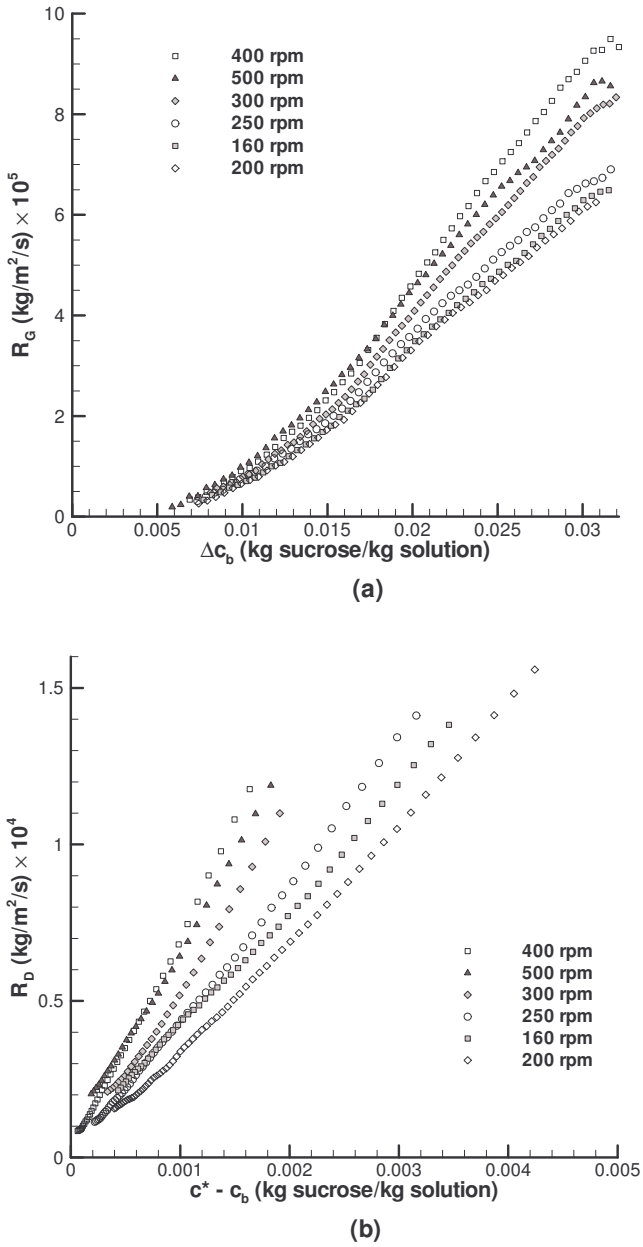

Figure 5.6. Effect of the agitation speed on the (a) growth and (b) dissolution rates of sucrose in a batch crystallizer at 40 ºC.

Growth and dissolution rates of sucrose generally increased with agitation speed. The exceptions to this tendency are probably due to mixing phenomena. Still, every time the hydrodynamics promoted the dissolution rates, crystal growth was also promoted. Differences between crystallization rates measured at approximate stirring speeds are sometimes hardly distinguishable. From the reproducibility analyses made, even these small differences can be attributed to changes in the crystal-solution velocity. In fact, very good accordance is obtained when the experimental conditions are kept constant. An example is given in Figure 5.7 where

the crystal growth rates measured at 300 rpm are confirmed by the results obtained in a replicate experience.

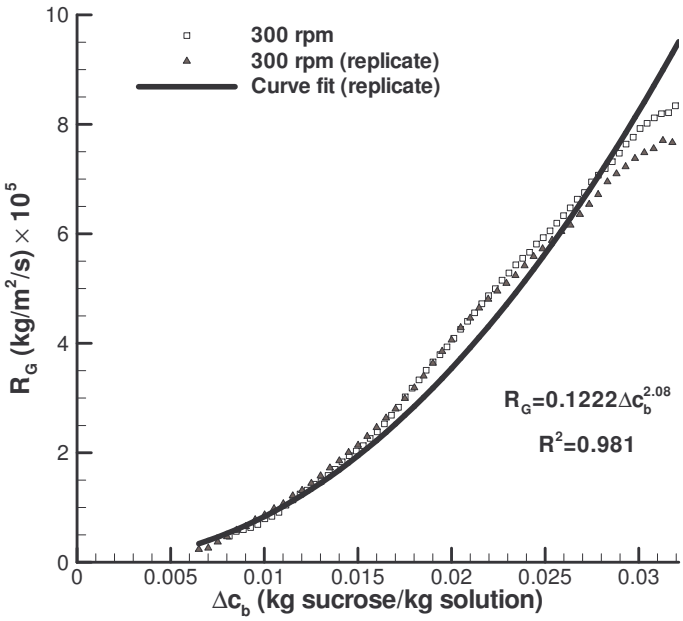

Figure 5.7. Comparison between two growth kinetics obtained at equivalent experimental conditions. Eq. (5.2) is used to fit the results from one of the experiments (replicate).

In the same figure, Eq. (5.2) is represented for the set of parameters K_G and g that best fit one of the experimental growth curves. It can be seen that the power-law equation does not give a completely satisfactory representation of the results. Apparently, the growth kinetics changes throughout the supersaturation range. An overall parabolic ($g = 2$) relation between crystal growth rate and supersaturation was obtained, however, for low Δc_b, $g > 2$ and for high Δc_b, $g < 2$. The same behaviour was verified with the other curves represented in Figure 5.6a.

According to the Burton Cabrera and Frank theory [1] the growth rate law is expected to change from parabolic to linear with increasing supersaturation. Therefore, the variation of the apparent kinetic order with supersaturation may possibly be explained by different integration kinetics. Other probable causes are related with the adopted method of growth rate measurement. Results obtained at high supersaturations correspond to the beginning of the experiences, with small crystals and low crystals mass fractions. During growth there is a significant change of the suspension conditions and crystals more than duplicate their size. It is likely that the changing kinetics observed in each curve results from the changing

experimental conditions at which they were measured. Figure 5.8a shows the initial and final crystal size distributions measured by laser light diffraction. The grown crystals were filtered, washed successively with a saturated sucrose solution and with pure ethanol, and then dried at room temperature. Particles in Figure 5.8a with sizes above 1.5 mm are essentially conglomerates formed during this process. The population of crystals with sizes below 0.4 mm results from the occurrence of primary nucleation and crystal breakage. The small percentage of these cases (in Figure 5.8, less than 5% in volume during a growth period of 5h) does not significantly affect the growth rate results. With Figure 5.8b it is intended to emphasize the role of crystals size on growth kinetics. The distributions shown are obtained by normalizing the horizontal axis of Figure 5.8a by the corresponding volume median size ($L_{med} = 0.314$ mm before the experiment and $L_{med} = 0.802$ mm after it). In these scaled representations the traditional spread of crystal size distributions after the growth is no longer evident.

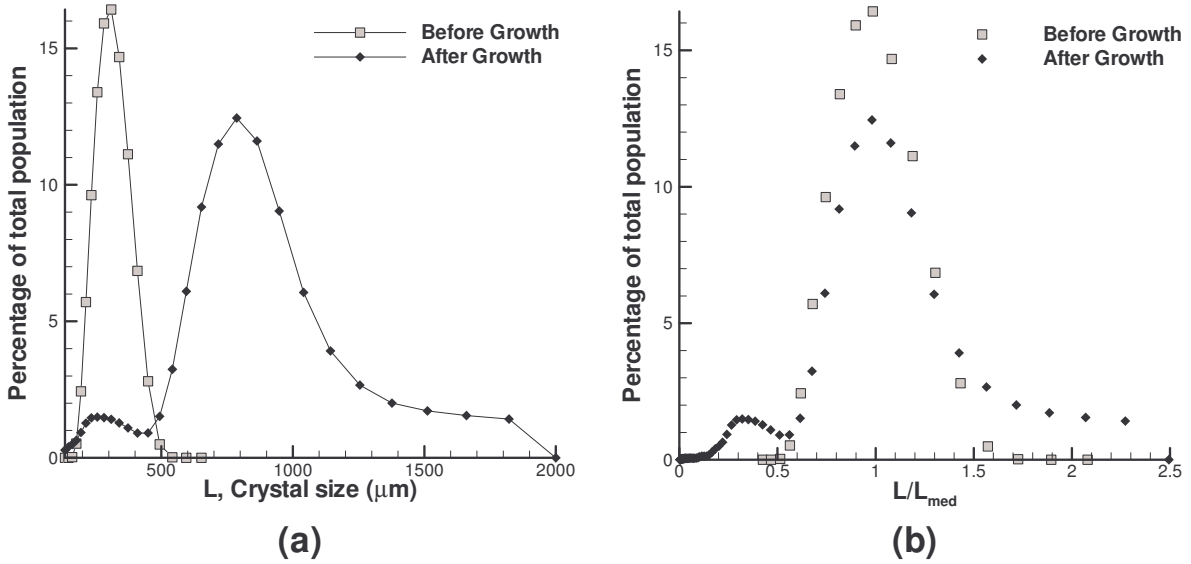

Figure 5.8. (a) Crystal size distributions in a volume basis and (b) scaled size distributions measured by laser light diffraction, before and after a typical growth experiment.

Apparently, if conglomerates and nucleated/broken crystals were eliminated, the distributions of sieved seeds and grown crystals would be superimposed. Such evidence was previously reported in sugar crystallization [21]. From it, one can conclude that crystals grow proportionally to their size, i.e., R_G seems to vary linearly with L. The variation of crystals size during the experiments affect differently the growth kinetics, leading to deviations from the power law rate equation as reported in Figure 5.7.

Despite the effect of the hydrodynamic conditions on the sucrose crystallization and dissolution being clearly visible in Figure 5.6, the test of theoretical crystal growth models with these experimental results cannot be done in the same terms as in a preceding section, when literature data were used. On the one hand, growth rate curves were obtained under changing kinetic constrains, disallowing the determination of the models parameters. On the other hand, crystal growth rates in chemical regime were not possible to obtain: changes in the diffusional conditions always led to changes in the crystallization rate. The approach that will be adopted consists in the study of the relative kinetics of growth, by comparing the values of R_G measured at same supersaturation. Since the initial sucrose concentration and seed size were the same in all experiments, these relative rates are as well evaluated at equivalent conditions of crystals size and mass fraction. Table 5.3 shows the mean growth and dissolution rate ratios calculated in relation to the slowest kinetics (obtained with an agitation speed of 200 rpm).

Table 5.3. Mean ratios between crystal growth (and dissolution) rates measured at different agitation speeds and the ones measured at 200 rpm.

Agitation Speed (rpm)	$R_G / R_{G\ 200rpm}$	$R_D / R_{D\ 200rpm}$	$\sqrt{R_D / R_{D\ 200rpm}}$
200	1	1	1
160	1.03	1.13	1.06
250	1.12	1.25	1.12
300	1.24	1.54	1.24
500	1.42	1.88	1.37
400	1.42	2.01	1.42

The given values did not change considerably along the supersaturation (and undersaturation) range. Their magnitude is exclusively due to the effect of agitation speed (all other factors remain unchanged). Dissolution rate ratios are greater than the corresponding values for growth. The influence of hydrodynamics was consequently more marked in the former case. Although not so strong as during dissolutions, the increase of the growth rate ratios with the agitation speed was also significant. Comparing the second and fourth columns of Table 5.3 it appears that R_G varies in the same proportion of the square root of R_D. Such dependence of R_G on the diffusional conditions means that the results are far from the chemical regime,

independently of the theoretical model considered. Apparently, this is in contradiction with the fact that dissolution rates are more than 20× higher than the crystal growth rates evaluated at same driving force and agitation speeds; for this situation it would be expected R_G to remain almost insensible to changes in the mass transfer resistance. The contradiction found suggests that mass transfer coefficients during crystal growth are not equivalent to the ones found for dissolution. As previously demonstrated, such correspondence is only admissible to happen in the light of the PSM. Nevertheless, on the derivation of the PSM it was also admitted that the existence of an adsorbed layer may influence the diffusivity of the molecules in the medium (Chapter 4). In systems with the specificity of the sucrose solutions (high solubility, high viscosity, strongly non-ideal solute, etc.) an effective mass transfer coefficient should be considered for crystallization, in order to account with the extra resistance caused by the adsorbed molecules ($k_d = \omega \times k_D$). In the case of moderately soluble substances, the movement of elements towards the surface is not significantly affected by the solution conditions around the growing crystals and the proportionality factor ω is 1 (see the examples previously given in the analysis of literature data). The values of k_d will not be determined for the sucrose system because of the lack of information about the crystal growth kinetics in chemical regime. Even so, according to the PSM, the effective mass transfer coefficient during crystal growth will have to be much lower than k_D, since the results shown in Table 5.3 correspond to a situation of diffusional regime. To demonstrate it, consider the crystal growth rate equation for high mass transfer resistances ($R_{G_{diff}}$):

$$R_{G_{diff}} = \rho k_{re} \Delta c_b^r \cdot \frac{2}{r+1} \frac{1}{\phi_g} = \rho \sqrt{\frac{2 k_{re} k_d}{r+1} \Delta c_b^{r+1}} \tag{5.18}$$

When calculating the ratio between two crystal growth rates measured at same supersaturation and temperature, it will result that

$$\frac{R_{G1}\big|_{diff}}{R_{G2}\big|_{diff}} = \sqrt{\frac{k_{d1}}{k_{d2}}} \tag{5.19}$$

or, as $k_d = \omega \times k_D$ and generally, $R_D = k_D \Delta c_b$:

$$\frac{R_{G1}\big|_{diff}}{R_{G2}\big|_{diff}} = \sqrt{\frac{R_{D1}}{R_{D2}}} \tag{5.20}$$

Results of Table 5.3 confirm what is expected by the previous equation. Indeed, the growth rate ratios were independent of the value of supersaturation and correspond to the square root

of the dissolution rate ratios. This was valid even for higher agitation speeds, so it is admitted that all the experiences were carried out under diffusional regime. If the mass transfer resistances continued to be decreased, it would be expected R_G to become progressively less interrelated with R_D. Once reached the chemical regime, R_G would be totally independent of changes in the mass transfer coefficient.

5.5 Conclusions

Theoretical models such the TSM are generally used to interpret crystal growth kinetics without guarantees of being adequate for that purposes. To test the validity of those models, the experimental data required goes beyond the conventional relation between crystal growth rates and supersaturation. In this work, the TSM and the recently introduced PSM were tested against experimental data taken from literature. Particular emphasis was given to the works of Mullin and Garside on the influence of hydrodynamics on crystal growth and dissolution kinetics. Mass transfer coefficients obtained by the two models from the published results were interpreted taking into account standard mass transfer theories. According to the TSM, the measured growth rate increase with the relative crystal-solution velocity can only be explained by means of an unrealistic behaviour of the mass transfer coefficient during crystallization. On the contrary, mass transfer coefficients obtained by the PSM were confirmed by appropriate semi-theoretical correlations. The coefficients were in agreement both in their order of magnitude and in the way they were influenced by the relative crystal-solution velocity. The PSM was further tested against sucrose crystal growth kinetics at 40 ºC, measured in a batch crystallizer at different hydrodynamic conditions. This system significantly differs from the inorganic salts used in the literature works here analysed. Although the dissolution rates were several times faster than growth rates, a significant influence of the mass transfer resistance was possible to be identified on the crystal growth kinetics. Following the physical arrangement provided by the PSM, the existence of an adsorbed layer in the crystal surroundings is likely to have changed the molecular diffusivity of sucrose in that medium. This way the mass transfer resistance during growth is considerably higher than the expected from the dissolution rates. Based on this premise, the results were well described by the PSM. As predicted by this model for diffusional regime, the relative growth rates were independent of supersaturation and correspond to the square root of the dissolution rate ratios.

References

[1] W. K. Burton, N. Cabrera, and F. C. Frank, The growth of crystals and the equilibrium structure of their surfaces. *Phil. Trans. Roy. Soc. London*, **1951,** 243, 299-358.

[2] A. A. Chernov, The spiral growth of crystals. *Soviet Physics Uspekhi*, **1961,** 4, 116-148.

[3] G. H. Gilmer, R. Ghez, and N. Cabrera, An analysis of combined surface and volume diffusion processes in crystal growth. *J. Cryst. Growth*, **1971,** 8, 79-93.

[4] M. Ohara and R. C. Reid, Modelling crystal growth rates from solution, Prentice-Hall, Inc., New Jersey, **1973**.

[5] T. A. Graber, M. E. Taboada, M. N. Alvarez, and E. H. Schmidt, Determination of mass transfer coefficients for crystal growth of nitrate salts. *Cryst. Res. Technol.*, **1999,** 34, 1269-1277.

[6] J. Garside, The concept of effectiveness factors in crystal growth. *Chem. Eng. Sci.*, **1971,** 26, 1425-1431.

[7] S. Al-Jibbouri and J. Ulrich, The growth and dissolution of sodium chloride in a fluidized bed crystallizer. *J. Cryst. Growth*, **2002,** 234, 237-246.

[8] S. Al-Jibbouri and J. Ulrich, Impurity adsorption mechanism of borax for a suspension growth condition: A comparison of models and experimental data. *Cryst. Res. Technol.*, **2004,** 39, 540-547.

[9] O. Sahin, Effect of borax on the crystallization kinetics of boric acid. *J. Cryst. Growth*, **2002,** 236, 393-399.

[10] M.-H. Sung, J.-S. Kim, W.-S. Kim, I. Hirasawa, and W.-S. Kim, Modification of crystal growth mechanism of yttrium oxalate in metastable solution. *J. Cryst. Growth*, **2002,** 235, 529-540.

[11] J. Mydlarz and A. G. Jones, Growth and dissolution kinetics of potassium sulphate crystals in aqueous 2-propanol solutions. *Chem. Eng. Sci.*, **1989,** 44, 1391-1402.

[12] S. U. Tanrikulu, I. Eroglu, A. N. Bulutcu, and S. Ozkar, The growth and dissolution of ammonium perchlorate crystals in a fluidized bed crystallizer. *J. Cryst. Growth*, **1998,** 194, 220-227.

[13] J. W. Mullin and J. Garside, Crystallization of aluminium potassium sulphate: a study in the assessment of crystallizer design data: I: - Single crystal growth rates. *Trans. Inst. Chem. Eng.*, **1967,** 45, T285-T290.

[14] J. W. Mullin and J. Garside, Crystallization of aluminium potassium sulphate: a study in the assessment of crystallizer design data: II: - Growth in a fluidized bed crystallizer. *Trans. Inst. Chem. Eng.*, **1967,** 45, T291-T295.

[15] J. W. Mullin and J. Garside, Crystallization of aluminium potassium sulphate: a study in the assessment of crystallizer design data: III: - Growth and dissolution rates. *Trans. Inst. Chem. Eng.*, **1968,** 46, T11-T18.

[16] N. A. Clontz, R. T. Johnson, W. L. McCabe, and R. W. Rousseau, Growth of magnesium sulphate heptahydrate crystals from solution. *Ind. Eng. Chem. Fundam.*, **1972,** 11, 368-373.

[17] J. Garside, J. W. Mullin, and S. N. Das, Growth and dissolution kinetics of potassium sulfate crystals in an agitated vessel. *Ind. Eng. Chem. Fundam.*, **1974,** 13, 299-305.

[18] D. F. Charles, The solubility of pure sucrose in water. *Int. Sugar J.*, **1960,** 62, 125-131.

[19] J. Garside, A. Mersmann, and J. Nyvlt, Measurement of Crystal Growth and Nucleation Rates, 2nd ed.; EFCE Working Party on Crystallization, IChemE, Rugby, **2002**.

[20] Z. Bubnik and P. Kadlec, Sucrose crystal shape factors. *Zuckerindustrie*, **1992,** 117, 345-350.

[21] E. T. White, D. L. Mackintosh, B. K. Butler, H. Zhang, and M. R. Johns, in *Proceedings of the Australian Society of Sugar Cane Technologists*, (D. M. Hogarth, ed.), **1998**.

6. On the kinetic effect of impurities – the competitive adsorption model

Overview

A mathematical model describing the growth of crystals in impure solutions is presented. Evidences of competitive surface adsorption involving the crystallizing solute and impurities are discussed in terms of the adsorption isotherm in equilibrium and of the mechanism of occupation of active sites for growth. The impurity effect on the crystal growth rates is characterized by the Langmuirian adsorption constants, and by the parameter β measuring the ability of the foreign species to move across the surface and occupy a stable position at the surface steps. Experimental growth rate data taken from literature is used to test the proposed competitive adsorption model (CAM). The reported effects of the impurity concentration on the crystal growth rate at constant supersaturation are quantitatively interpreted. Additionally, growth rate curves obtained in pure and impure solutions are used to investigate the influence of supersaturation on the relative growth rates. Several examples are considered concerning the impurity adsorption extension and the impurity activity. In all cases the CAM adequately describes the experimental data.

6.1 Introduction

The occupation by impurities of preferential places for solute incorporation into the crystal lattice is known to have a strong effect on crystal growth. Small quantities of specific impurities can suppress the growth, while others, being crystallographic face-selective, can be used as habit modifiers. Cabrera and Vermilyea introduced the pinning mechanism to explain the action of the impurities on the advancement of the surface steps [1]. They depart from the representation of crystal growth from pure solution by the addition of new molecules at active sites (kinks) in the steps. When the impurity is adsorbed at those places, the steps flowing at crystal surface are hindered and tend to curl around. If the average distance between adsorbed impurities along the step is smaller than $2\times$ the critical radius for two-dimensional nucleation ($l_i < 2\rho_c$) the step will stop. The relationship between the velocity of advancement of steps and the radius of curvature is given by the also-called Gibbs-Thomson formula:

$$\frac{V_\rho}{V_\infty} = 1 - \frac{\rho_c}{\rho} \tag{6.1}$$

where V_∞ stands for the movement of a straight step. At low supersaturations ($S \ll 1$) ρ_c is given by

$$\rho_c = \frac{\gamma\Omega}{kT}\frac{1}{S} \tag{6.2}$$

When, in Eq. (6.1) $\rho = l_i/2$, a minimum step velocity is reached ($V_{\min}$). Originally, Cabrera and Vermilyea considered the average step velocity during the time of step squeezing as the geometric mean of V_∞ and $V_{\min}$ ($V = \sqrt{V_\infty V_{\min}}$) [1], so that,

$$\frac{V}{V_\infty} = \sqrt{1 - 2\frac{\rho_c}{l_i}} \tag{6.3}$$

More recently, Kubota and Mullin proposed the use of an arithmetic mean of the same limit velocities to describe V ($V = \left(V_\infty + V_{\min}\right)/2$) [2]. In this case,

$$\frac{V}{V_\infty} = 1 - \frac{\rho_c}{l_i} \tag{6.4}$$

and $l_i \geq \rho_c$. By assuming (1) the step advancement velocity, V, to be proportional to the face growth rate, R, and (2) infinite radius of curvature of the steps in pure system ($V_0 = V_\infty$), one can express Eq. (6.4) in terms of the growth rate ratio in impure and pure systems ($V / V_\infty \sim R / R_0$). The second assumption is open to criticism, particularly if spiral growth mechanisms are assumed [3]. From simple geometric considerations, one can say that the equilibrium coverage of adsorption sites by impurities (θ_l) corresponds to the ratio of the average distance between active sites to the average distance between neighboring adsorbed impurities, $\theta_l = L_a / l_i$. This fraction is commonly given by a Langmuirian adsorption isotherm:

$$\theta_l = \frac{K_a c_i}{K_a c_i + 1} \tag{6.5}$$

Nevertheless, Temkin isotherms [4] and Freundlich isotherms [5] have been also used. The typical form of the Kubota-Mullin equation is obtained by rewriting Eq. (6.4) as follows:

$$\frac{R}{R_0} = 1 - \alpha \frac{K_a c_i}{K_a c_i + 1} \tag{6.6}$$

with α being the "impurity effectiveness factor", defined as

$$\alpha = \frac{\gamma \Omega}{k T L_a} \frac{1}{S} \tag{6.7}$$

According to the value of α, equally adsorbed impurity species can affect very differently the growth kinetics. The determination of α and K_a is generally done by fitting the model equations to experimental data on the influence of c_i and S on the relative growth rates. Alternatively, K_a can be determined by performing independent adsorption experiments, where the impurity uptake into crystal is measured as a function of c_i [6, 7].

Despite the current interest in this field of crystallization, the existing theories are not yet capable to answer to all questions [8-10]. In this paper, a new engineering approach is proposed and validated against experimental growth rate data in the presence of impurities. The new model is believed to contribute for a better understanding of the mechanism by which impurities affect crystal growth from solution.

6.2 Competitive adsorption model

In the competitive adsorption model (CAM), crystal growth in the presence of an impurity is seen as a competition between the crystallizing solute units and the foreign species for the preferential adsorption sites. The factors determining the success of each type of molecules are related with their concentration, mobility and physico-chemical affinity with the crystal surface. When a simple Langmuir adsorption isotherm is considered (Eq. (6.5)), θ_l is assumed to be exclusively dependent of the impurity concentration. This is not likely to be true since the number of kink sites occupied by impurities is certainly lowered as the supersaturation increases. For high supersaturation all the active sites would be occupied by the crystallizing solute, and $\theta_l \sim 0$. The new perspectives on the impurity adsorption mechanism provided by the CAM will be complemented by an alternative description of the impurity effect on the crystal growth rate. This new approach considerably differs from the pinning mechanism proposed by Cabrera and Vermilyea and developed by Kubota and Mullin. In this regard, recent atomic force microscopy evidences go against the validity of the Gibbs-Thomson formula (Eq. (6.1)) upon which the pinning mechanism is based [11-13]. Instead of a gradual increase of v with ρ, an abrupt increase of v occurs when the step exceeds a critical dimension (ρ_c). The CAM is concerned with the impurity kinetic effect and not with modifications of the solution properties by the impurity.

The Langmuir adsorption isotherm is conventionally used to quantify the fraction of the solid surface covered by a monolayer of adsorbed species. As referred, crystal growth in impure solution comprises a multicomponent sorption phenomenon, where the adsorption sites are disputed by both the impurity and the pure solute. In equilibrium, the fraction of the surface occupied by impurities is given by the extension of the basic Langmuir model to competitive adsorptions [14]:

$$\theta_s = \frac{K_i c_i}{K_i c_i + K_p c + 1} \tag{6.8}$$

Expressing this equation as a function of supersaturation ($S = c/c^* - 1$) gives

$$\theta_s = \frac{k_i c_i}{k_i c_i + k_p S + 1} \tag{6.9}$$

where $k_i = K_i \big/ \left(1 + K_p c^*\right)$ and $k_p = K_p c^* \big/ \left(1 + K_p c^*\right)$. Low surface impurity coverage ($\theta_s \ll 1$) is expected when the dimensionless concentration. $k_i c_i$ is also low. Even in these

cases of barely adsorbed impurities, crystal growth rates can be drastically affected by impurities. This is certainly related with the mechanism of surface integration, and in particular, with the surface mobility of the different molecules.

According to the so-called Kossel model of a growing crystal face in pure solution, molecules entering a terrace near a step can be loosely adsorbed, diffuse across the surface and reach an energetically favorable place (kink) to integrate the crystal. Although well-established in crystal growth from vapour, the existence of significant surface diffusion during solution growth is open to discussion [15-17]. In the case of crystal growth in impure solution the kinetic effect of an impurity involves three analogous stages [4]:

1. Surface adsorption of the impurity molecules diffusing from solution.

2. Migration of impurity molecules across the surface.

3. Step/kink adsorption of impurity molecules migrating on the surface.

Each of these stages has an associated thermodynamic energy change, whose relative values determine if and how adsorption occurs. The coverage of active sites by an impurity (θ_l) will be proportional to the corresponding overall surface coverage (θ_s):

$$\theta_l = \beta\theta_s \tag{6.10}$$

The parameter β here introduced, takes higher values when the second and third stages are thermodynamically favorable relatively to the first one. For very mobile impurities, β is much greater than 1, i.e., impurities will be mainly concentrated in the preferential adsorption sites. Conversely, in the case of favorable surface adsorption and low mobility of the adsorbed impurities, β is expected to take small positive values. The density of adsorbed molecules of crystallizing solute at the surface (n_s) is generally thought to decrease toward the equilibrium concentration n_{se} as we approach the step. The intrusion of impurities on the adsorption equilibrium at the step will decrease from n_{se} to $n_{se}\left(1-\theta_l\right)$, and consequently, the growth rate perpendicular to the surface defined as [3]

$$R_0 = n_{se}\frac{\chi h D_s}{n_e x_s^2}\left(\frac{S^2}{C}\right)\tanh\left(\frac{C}{S}\right) \tag{6.11}$$

will decrease in the same proportion. Equation (6.11) results from the Burton Cabrera and Frank surface diffusion mechanism, wherein the constant C is defined by

$$C = \frac{2\pi\gamma\Omega}{kTx_s} \tag{6.12}$$

In accordance to what is stated, the ratio between growth rates in impure and pure solution is given by the following equation:

$$\frac{R}{R_0} = 1 - \theta_l \tag{6.13}$$

which, according to Eqs. (6.9) and (6.10) can be rewritten as

$$\frac{R}{R_0} = 1 - \beta \frac{k_i c_i}{k_i c_i + k_p S + 1} \tag{6.14}$$

New perspectives about the role of important variables in crystal growth from impure solutions (supersaturation, impurity concentration, temperature, surface mobility, etc) arise from Eq. (6.14). Nevertheless, evidences of competitive adsorption have been previously reported (Sangwal 2000). For example, crystal growth stoppage after previous dissolution in contaminated solutions suggests the occupation by impurities of the active sites for pure solute integration [18, 19]. The observation of different growth rates when experiments are carried out at increasing or decreasing supersaturation, indicates, not only the existence of non-steady state impurity adsorption [20], but also the competitive nature of this step and the crystallizing species attachment.[21] Indeed, the theoretical treatment of the growth rate hysteresis proposed by Guzman et al. [20] and Kubota et al. [8] points out a time constant for impurity adsorption "τ" that is supposed be a function of supersaturation. Such dependence can only be explained assuming that the adsorption isotherm is also a function of the crystallizing solute concentration [8]. In the present study, we will not be concerned with non-steady state adsorption, therefore, equilibrium conditions are assumed.

6.3 Analysis of literature data

In the following analysis it is not intended to carry out a general review of the published work in the field (for this purpose, see the works of Kubota [22], and Sangwal [23, 24]) but instead a selection of typical trends on the influence of supersaturation and impurity concentration on the relative growth rates R/R_0. Our main emphasis is on the CAM differences and common aspects to existing theories, as well as, on the contribution of the

new model to solve unanswered questions. In a first phase, the case of weak impurity adsorption (low θ_s) is studied, since its quantitative treatment is analogous to the one followed in the Kubota-Mullin model. The novelty of the CAM is then highlighted by analyzing the growth rate dependence on the impurity concentration and supersaturation, when strong impurity adsorption occurs.

6.3.1 Barely adsorbed impurity

According to the definition of θ_s given in Eq. (6.9), low surface coverage is expected when the impurity affinity with crystal is low (low k_i), when the solubility of the crystallizing solute is high (high c^*, high k_p and low k_i) and for small impurity concentration (low c_i). If the conditions are such that $k_p S \gg (k_i c_i + 1)$, Eq. (6.14) simplifies to

$$\frac{R}{R_0} \approx 1 - \beta \frac{k_i c_i}{k_p S} \tag{6.15}$$

For this combination of factors, the relative growth rate measured at constant supersaturation is linearly dependent on c_i. This corresponds to the case shown in Figure 6.1a, about the crystal growth of sucrose in the presence of raffinose [25]. As expected, deviations from the linearity start to be pronounced at low supersaturations and high c_i. From Eq. (6.15) it also arises that relative growth rates measured at constant c_i would be linearly dependent on the reciprocal of supersaturation (Figure 6.1b). The effect that trace amounts of raffinose have on R/R_0 is explained by the strong capacity of the impurity to occupy the active sites for growth, at the surface of the sucrose crystal (high β value). To provoke similar sucrose growth rate lowering, other impurities such as invert sugars, inorganic salts, oligosaccharides and carbohydrates would have to occur in solution in much higher concentrations [26]. The behavior shown in Figure 6.1 was also identified for potassium sulfate growing in the presence of iron(III) [27], for trinitrotoluene in the presence of 2,2-dinitropropane (R/R_0 vs c_i relationship) [28], and for $NaClO_3$ in the presence of $S2O_6^{2-}$ (R/R_0 vs $1/S$ relationship) [29]. These results are as well explained by the Kubota-Mullin model, assuming $K_a c_i \ll 1$ in Eq. (6.5).

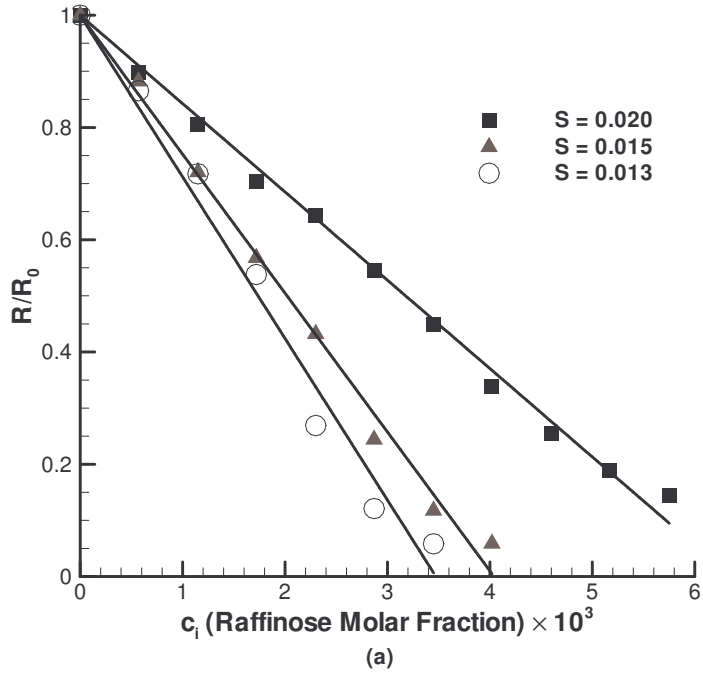

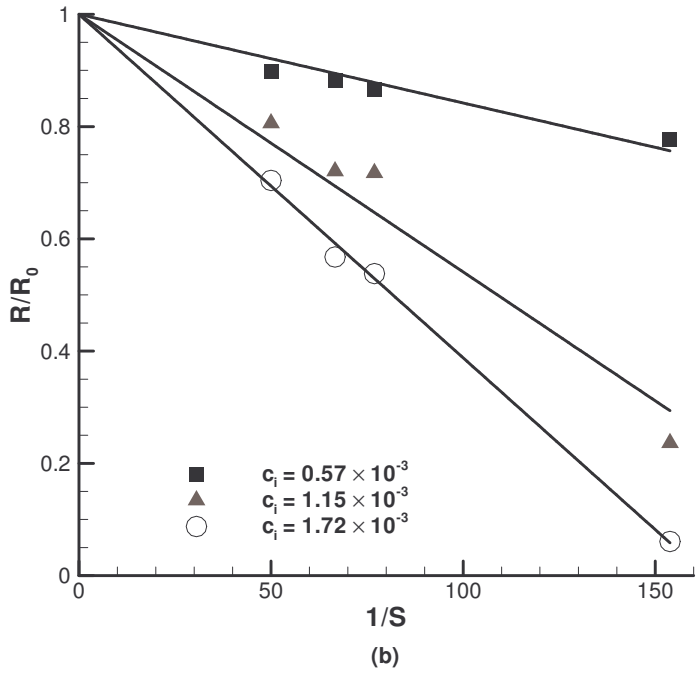

Figure 6.1. Effect of (a) the raffinose concentration and (b) the reciprocal of supersaturation on the relative growth rate of sucrose at 30 ºC [25].

6.3.2 Widespread impurity adsorption

Deviations from linearity on the representation of R/R_0 as a function of c_i are indicative of significant impurity adsorption at the crystal surface. When the crystal surface is

extensively covered by the impurity (high θ_s), even moderately active impurities (low β) would influence the growth kinetics. In these cases, $k_i c_i$ is of comparable order of magnitude of $k_p S + 1$ in Eq. (6.9). The concept of competitive adsorption is here properly used since there is not a clear dominance of any of the adsorbates at the surface. Distinct supersaturation dependences of R/R_0 at constant c_i are expected by the CAM and by non-competitive adsorption models, while the parameters of the Kubota-Mullin can be re-interpreted in the light of the CAM when analyzing the influence of c_i on R/R_0 at constant supersaturation.

Let us consider in first place the example of Figure 6.2 about the influence of c_i on the relative growth rates of trinitrotoluene growing in the presence of two distinct impurities [28].

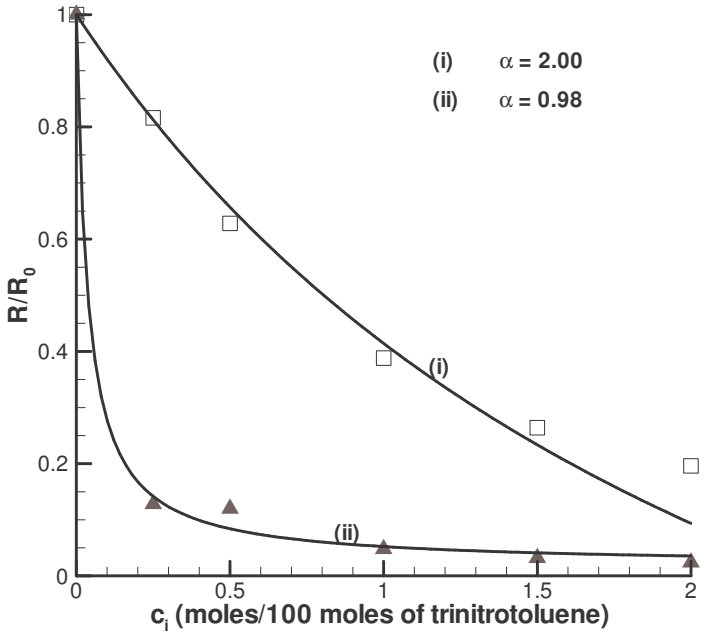

Figure 6.2. Effect of different additives on the relative growth rates of trinitrotoluene at 74.0 ºC [28], and respective fit to Eq. (6.6): (i) 2,4,6-trinitrodiphenyl ether; (ii) 2-chloro-2,4,6-trinitrostilbene.

As shown, the results follow the trend expected by Eq. (6.6) (Kubota-Mullin model) and the obtained value of α more than duplicates from one additive to the other. The difference between the obtained effectiveness factors should not be surprising, since different physico-chemical properties of the additives are expected to influence differently the growth rate mechanism. Nevertheless, if we attend to the definition of the impurity effectiveness factor given in Eq. (6.7), α is a function of the molecular volume of the crystallizing solute, of the

crystal surface and interfacial properties, and of temperature and supersaturation, but is not supposed to change with any characteristic property of the impurity. In other words, according to its classical definition, α is not expected to vary significantly with the impurity type. An alternative perspective of the physical meaning of α and K_a results from the competitive adsorption theory. At constant supersaturation, Eq. (6.14) of the CAM can be rewritten assuming $k_p S$ as another constant:

$$\frac{R}{R_0} = 1 - \beta \frac{\dfrac{k_i}{k_p S + 1} c_i}{\dfrac{k_i}{k_p S + 1} c_i + 1} \tag{6.16}$$

By comparing this equation with the Kubota-Mullin definition given in Eq. (6.6), one realizes that $\alpha = \beta$ and $K_a = k_i / \left(k_p S + 1 \right)$. The equivalence between the impurity effectiveness factor and the parameter β solves the dilemma of unchanging α among impurities. As referred, in the CAM β is a function of specific properties of the impurity (e.g., surface mobility), and thus it can be considered an intrinsic effectiveness factor of the pure solute-impurity system. The competitive adsorption constants k_p and k_i can be estimated either by fitting Eq. (6.14) to additional growth data on the influence of S on R/R_0 at constant c_i or by performing separate adsorption experiments.

When extensive impurity adsorption occurs, contrasting positions on the supersaturation dependence of the crystal growth rate result from the pinning mechanism theories and the CAM. The concept of critical supersaturation (S_c), defined by Kubota et al. [21] as the limit supersaturation below which $R = 0$, can be conveniently used to illustrate the differences. In the Kubota-Mullin model, S_c is obtained by setting $R/R_0 = 0$ in Eq. (6.6), and using the definition of α given in Eq. (6.7), so that

$$S_c = \frac{\gamma \Omega}{kTL} \frac{K_a c_i}{K_a c_i + 1} \tag{6.17}$$

The stronger is the impurity kinetic effect, the wider is the supersaturation range of no growth, $0 \le S \le S_c$. The relative growth rate is easily expressed as a function of S_c using Eqs. (6.17) and (6.7):

$$\frac{R}{R_0} = 1 - \frac{S_c}{S} \tag{6.18}$$

In Figure 6.3, the type-1 curve represents the theoretical influence of an active impurity on the crystal growth kinetics as stated by the Kubota-Mullin model; crystals would start to grow at supersaturations above S_c, and for $S \gg S_c$ the growth rate curve is approximately parallel to the one of the pure system. In the example given, a second order rate equation was used for pure system. The behavior illustrated by type-1 curve can be found in literature when very active impurities are investigated, such in the case of ammonium oxalate monohydrate growing in the presence of Cr(III) ions [5], or the already mentioned example of the sucrose-raffinose impurity system [25]. Even so, the other type of impurity-affected kinetics exemplified in Figure 6.3 (type-2 curve) is also frequently reported in literature [26, 30-32]. Despite of the marked growth rate lowering ($R/R_0 < 1$), there is not a clear supersaturation limit below which growth stops, which makes $S_c = 0$. This fact is not explained by pinning mechanism theories. Following, for example, the Kubota-Mullin model, if $S_c = 0$ it results from Eq. (6.18) that $R = R_0$, whichever the supersaturation considered.

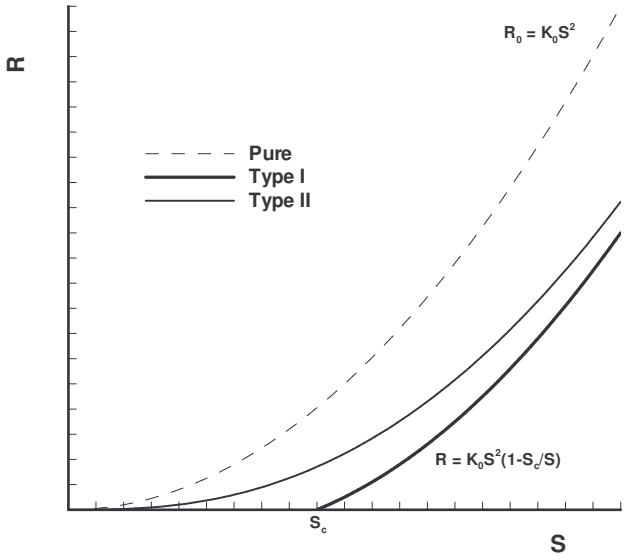

Figure 6.3. Typical growth rate curves in the presence of impurities.

Considering now the new model, the CAM mathematical definition of critical supersaturation is obtained by setting $R/R_0 = 0$ in Eq. (6.14),

$$S_c = \frac{k_i c_i (\beta - 1) - 1}{k_p} \tag{6.19}$$

By combining this equation with Eq. (6.14), an alternative equation for R/R_0 results:

$$\frac{R}{R_0} = 1 - \frac{1 + k_{si} S_c}{1 + k_{si} S} \tag{6.20}$$

with

$$k_{si} = \frac{k_p}{1 + k_i c_i} \tag{6.21}$$

From Eq. (6.19) one can establish two distinct situations: (i) if besides being extensively adsorbed (high $k_i c_i$ product), the impurity is also active ($\beta > 1$), S_c will assume positive values; (ii) if the impurity is slightly active, $\beta < 1$, and the critical supersaturation given by Eq. 19 will be negative. The first case roughly corresponds to type-1 curve in Figure 6.3. As for the Kubota-Mullin model, there is a zone of no growth for $S < S_c$ and for $S \gg S_c$, R tends to be parallel to R_0. Despite of the common limit cases, distinct supersaturation dependences of R are expected by the two theoretical models for intermediate supersaturations. Comparing Eqs. (6.18) and (6.20), one finds that a linear R/R_0 vs $1/S$ relationship is expected by the Kubota-Mullin model, while in the CAM, the relative growth rates decrease with $1/S$ in a more gradual way. Both trends are represented in Figure 6.4 for the case of sodium chloride growing in the presence of lead(II) [6].

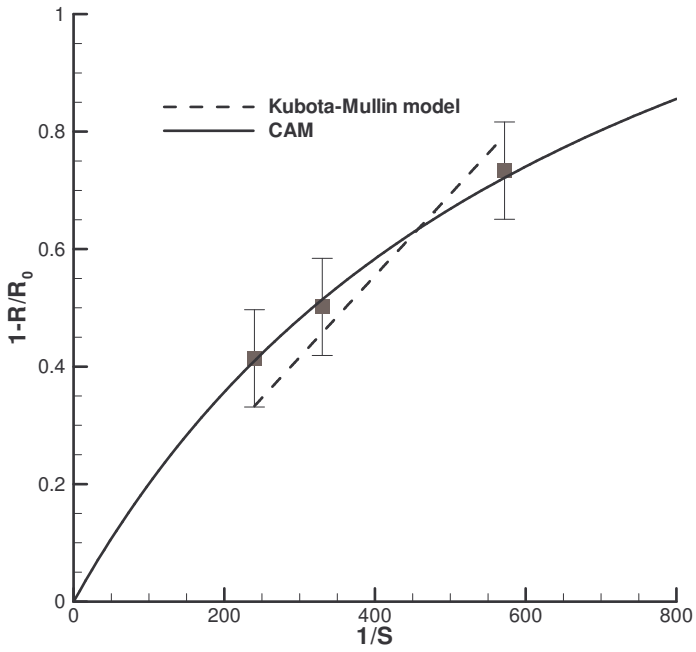

Figure 6.4. Representation of Eqs. (6.18) (Kubota-Mullin model) and (6.20) (CAM) for the set of parameters that best fit the data of Kubota et al. [6] on the effect of lead(II) on the growth of sodium chloride crystals at 35 ºC. The results are estimated for $c_i = 0.25 \times 10^{-6}$ mol/dm^3. The vertical error bars indicate standard errors.

The other situation resulting from the CAM definition of critical supersaturation corresponds to poorly active impurities, so that $\beta \leq 1$ and $S_c \leq 0$. In physical terms, negative critical supersaturations mean that growth will always occur at positive supersaturations, even if at growth rates much smaller than R_0 (see type-2 curve in Figure 6.3). As mentioned before, this behavior is not expected by the traditional pinning mechanisms, even though the great number of published data reporting it. Examples of type-2 curves can be found for the sodium chloride growth in the presence of impurities like $MgCl_2$, $PbCl_2$, $K_4Fe(CN)_6{\cdot}H_2O$, [30] for potassium sulphate growth in the presence of chromium(III) [31], for hydroxyapatite (0001) face growth in the presence of magnesium and zinc [32], and for sucrose crystal growth in the presence of several poorly active impurities [26]. A particular case of impurity affected growth curves is observed when the growth kinetic order remains unchanged in pure and impure solutions, i.e., when R/R_0 is independent of supersaturation, even at low S. In Chapter 9, one of these situations will be used to illustrate the CAM applicability to industry purposes.

6.4 Conclusions

An expression establishing the dependence of the relative growth rates in impure and pure solutions on supersaturation and impurity concentration is proposed (Eq. (6.14)). A mechanism of competitive adsorption is assumed, where the crystallizing solute and the impurity dispute (1) the coverage of the crystal surface and (2) the occupation of energetically favourable places at surface steps. The first stage is quantified by a Langmuir isotherm for competitive adsorption, while the second is a function of the thermodynamic energy change of the surface processes. According to classical theories of crystal growth, the growth rate varies in the same proportion of the number of adsorbed molecules at the step. At a given surface coverage, the impurity activity reflects the tendency to replace the crystallizing solute at the active sites and is measured by means of the parameter β. In systems exhibiting $\beta > 1$ the fraction of active sites occupied by the impurity is higher than the surface coverage. This can lead to crystal growth suppression at supersaturation below a critical limit given by Eq. (6.19). For $\beta < 1$, crystal growth can be slowed by the presence of impurities, but is not suppressed. The role of supersaturation and impurity concentration on the crystal growth rates significantly changes with the impurity adsorption extension and impurity activity. Published experimental data showing different types of impurity-affected kinetics was adequately described by the CAM. Differences and common aspects between the new competitive model

and existing theories based on the pinning mechanism were discussed, and the CAM contribution to solve unanswered questions was highlighted.

References

[1] N. Cabrera and D. A. Vermilyea, in *Growth and perfection of crystals*, (R. H. Doremus, B. W. Roberts, D. Turnbull, eds.), Wiley, New York, **1958**.

[2] N. Kubota and J. W. Mullin, A kinetic model for crystal growth from aqueous solution in the presence of impurity. *J. Cryst. Growth*, **1995,** 152, 203-208.

[3] W. K. Burton, N. Cabrera, and F. C. Frank, The growth of crystals and the equilibrium structure of their surfaces. *Phil. Trans. Roy. Soc. London*, **1951,** 243, 299-358.

[4] K. Sangwal, Kinetic effects of impurities on the growth of single crystals from solutions. *J. Cryst. Growth*, **1999,** 203, 197-212.

[5] K. Sangwal and E. Mielniczek-Brzoska, Effect of Cr(III) ions on the growth kinetics of ammonium oxalate monohydrate crystals from aqueous solutions. *J. Cryst. Growth*, **2002,** 242, 421-434.

[6] N. Kubota, H. Otosaka, N. Doki, M. Yokota, and A. Sato, Effect of lead(II) impurity on the growth of sodium chloride crystals. *J. Cryst. Growth*, **2000,** 220, 135-139.

[7] M. Rauls, K. Bartosch, M. Kind, S. Kuch, R. Lacmann, and A. Mersmann, The influence of impurities on crystallization kinetics - a case study on ammonium sulfate. *J. Cryst. Growth*, **2000,** 213, 116-128.

[8] N. Kubota, M. Yokota, N. Doki, L. A. Guzman, S. Sasaki, and J. W. Mullin, A mathematical model for crystal growth rate hysteresis induced by impurity. *Cryst. Growth Des.*, **2003,** 3, 397-402.

[9] L. N. Rashkovich and N. V. Kronsky, Influence of Fe3+ and Al3+ ions on the kinetics of steps on the {1 0 0} faces of KDP. *J. Cryst. Growth*, **1997,** 182, 434-441.

[10] T. A. Land, T. L. Martin, S. Potapenko, G. T. Palmore, and J. J. De Yoreo, Recovery of surfaces from impurity poisoning during crystal growth. *Nature*, **1999,** 399, 442-445.

[11] L. N. Rashkovich, N. V. Gvozdev, M. I. Sil'nikova, I. V. Yaminski, and A. A. Chernov, Dependence of the step velocity on its length on the (010) face of the orthorhombic lysozyme crystal. *Cryst. Rep.*, **2001,** 46, 860-863.

[12] H. H. Teng and P. M. Dove, Thermodynamics of calcite growth: baseline for understanding biomineral formation. *Science*, **1998,** 282, 724-727.

[13] A. A. Chernov, Notes on interface growth kinetics 50 years after Burton, Cabrera and Frank. *J. Cryst. Growth*, **2004,** 264, 499-518.

[14] D. M. Ruthven, Principles of adsorption and adsorption processes, John Wiley & Sons, Inc., New York, **1984**.

[15] M. Ohara and R. C. Reid, Modelling crystal growth rates from solution, Prentice-Hall, Inc., New Jersey, **1973**.

[16] T. Nishinaga, Understanding of crystal growth mechanisms through experimental studies of semiconductor epitaxy. *J. Cryst. Growth*, **2005,** 275, 19.

[17] T. A. Land, J. J. De Yoreo, and J. D. Lee, An in-situ AFM investigation of canavalin crystallization kinetics. *Surf. Sci.*, **1997,** 384, 136.

[18] N. Kubota, I. Uchiyama, K. Nakai, K. Shimizu, and J. W. Mullin, Change of solubility of potassium sulfate in water caused by traces of chromium(III). *Ind. Eng. Chem. Res.*, **1988,** 27, 930-934.

[19] A. A. Chernov and A. I. Malkin, Regular and irregular growth and dissolution of (101) ADP faces under low supersaturations. *J. Cryst. Growth*, **1988,** 92, 432.

[20] N. Kubota, M. Yokota, and L. A. Guzman, in *ACS Symposium Series*, (G. D. Botsaris, K. Toyokura, eds.), **1997**.

[21] N. Kubota, M. Yokota, and J. W. Mullin, Supersaturation dependence of crystal growth in solutions in the presence of impurity. *J. Cryst. Growth*, **1997,** 182, 86-94.

[22] N. Kubota, Effect of impurities on the growth kinetics of crystals. *Cryst. Res. Technol.*, **2001,** 36, 749-769.

[23] K. Sangwal, Effects of impurities on crystal growth processes. *Prog. Cryst. Growth Charact. Mater.*, **1996,** 32, 3-43.

[24] K. Sangwal, Growth kinetics and surface morphology of crystals grown from solutions: Recent observations and their interpretations. *Prog. Cryst. Growth Charact. Mater.*, **1998,** 36, 163-248.

[25] N. Albon and W. J. Dunning, Growth of sucrose crystals: determination of edge energy from the effect of added impurity on rate of step advance. *Acta Cryst.*, **1962,** 15, 474-476.

[26] B. M. Smythe, Sucrose crystal growth.I. Rate of crystal growth in the presence of impurities. *Aust. J. Chem.*, **1967,** 20, 1097-1114.

[27] N. Kubota, K.-i. Katagiri, M. Yokota, A. Sato, H. Yashiro, and K. Itai, Impurity effect of iron(III) on the growth of potassium sulfate crystal in aqueous solution. *J. Cryst. Growth*, **1999,** 196, 156-163.

[28] W. A. Gey, E. R. Dalbey, and R. W. Van Dolah, Studies on the linear crystallization of TNT systems[1]. *J. Am. Chem. Soc*, **1956,** 78, 1803-1810.

[29] R. Ristic, B. Y. Shekunov, and J. N. Sherwood, Growth of the tetrahedral faces of sodium chlorate crystals in the presence of dithionate impurity. *J. Cryst. Growth*, **1994,** 139, 336-343.

[30] S. Al-Jibbouri and J. Ulrich, The influence of impurities on crystallization kinetics of sodium chloride. *Cryst. Res. Technol.*, **2001,** 36, 1365-1375.

[31] W. Omar and J. Ulrich, Influence of crystallization conditions on the mechanism and rate of crystal growth of potassium sulphate. *Cryst. Res. Technol.*, **2003,** 38, 34-41.

[32] N. Kanzaki, K. Onuma, G. Treboux, S. Tsutsumi, and A. Ito, Effect of impurity on two-dimensional nucleation kinetics: Case studies of magnesium and zinc on hydroxyapatite (0001) face. *J. Phys. Chem. B*, **2001,** 105, 1991-1994.

PART III

CRYSTAL GROWTH SCIENCE

7. Spiral nucleation model

Overview

In the preceding chapters, new theories were proposed with the aim of quantifying and understand the effect of the diffusional resistance and of the impurity concentration on the crystal growth rate. Nevertheless, crystal growth is known to be influenced by a number of other factors related with physical fundamentals that go beyond what is comprised in engineering models. Examples of these factors are, among others, crystal-solution interface properties, growth rate history, crystal topological properties and crystal size. In this chapter, classical concepts of two dimensional nucleation and spiral growth are used together with recent findings on the dynamics of dislocation spirals to derive a new fundamental crystal growth model. Hopefully, this new theory would contribute for the clarification of the "fundamental factors" affecting crystal growth. In a first application example, the crystallization kinetics of sucrose measured at 40 ºC is interpreted in the light of the new perspectives resulting from the proposed model. Using the measured experimental data, the variation of the sucrose interfacial tension with supersaturation was estimated, and topological parameters of growing crystals such as the height and length of the surface steps were able to be predicted. The validation of the new model will proceed in the following chapters by analysing the influence of additional crystal growth variables.

7.1 Introduction

The atomistic representation of crystal growth has been subject of many studies in the past half century. The thermodynamic and kinetic theories on two-dimensional (2D) nucleation [1] and especially, the dislocation mechanism of Burton, Cabrera and Frank (BCF) [2] were key advances leading to nowadays understanding of the phenomenon.

In the 2D nucleation models, the growth of a new layer on a flat face starts with the formation of 2D islands on the surface. To be stable, the initial nucleus must be constituted by a given number of molecules below which it would disintegrate. The critical number corresponds to a critical nucleus size (r_c) that can be determined based on the calculation of the Gibbs free energy change. The overall free energy difference (ΔG) between the elements of the nucleus and the solute molecules in the supersaturated solution results from the sum of the surface excess free energy (positive quantity) and the volume excess free energy (negative quantity) [3]:

$$\Delta G = a_n \gamma - v_n \frac{kT}{\Omega} \ln(1+S) \tag{7.1}$$

The first term accounts for the isothermal compression when packing the solute molecules on the surface in a nucleus of peripheral area a_n, and is proportional to the solid-liquid interfacial tension, γ. The volume excess free energy refers to the transfer of molecules from the supersaturated solution (solute activity, a_b) to a saturated state at crystal surface (solute activity, a_e). Supersaturation is defined by $S = a_b/a_e - 1$, k is the Boltzmann constant and T the temperature. The number of molecules transferred is given by the ratio v_n/Ω, where v_n is the nucleus volume and Ω is the molecular volume. Conventionally, the nucleus is assumed to be a circular disc of radius r and height h (Figure 7.1a), so the area and volume in Eq. (7.1) are given by $a_n = 2\pi rh$ and $v_n = \pi r^2 h$. As Figure 7.1b shows, ΔG will initially increase with r until reaching the critical size. In this range, the process spontaneously evolves in the direction of decreasing r. Above r_c, more molecules will tend to integrate the nucleus, since the free energy decreases with r. Setting $d\Delta G/dr = 0$, the value of r_c for 2D nucleation is given by:

$$r_{c\,2D} = \frac{\gamma\Omega}{kT\ln(1+S)} \tag{7.2}$$

From this equation, the critical radius of the nucleus is expected to be progressively smaller as the supersaturation increases. Replacing this result in Eq. (7.1) one obtains the amount of energy necessary to form a stable nucleus:

$$\Delta G_{c_{2D}} = \pi h \frac{\gamma^2 \Omega}{kT \ln(1+S)} \tag{7.3}$$

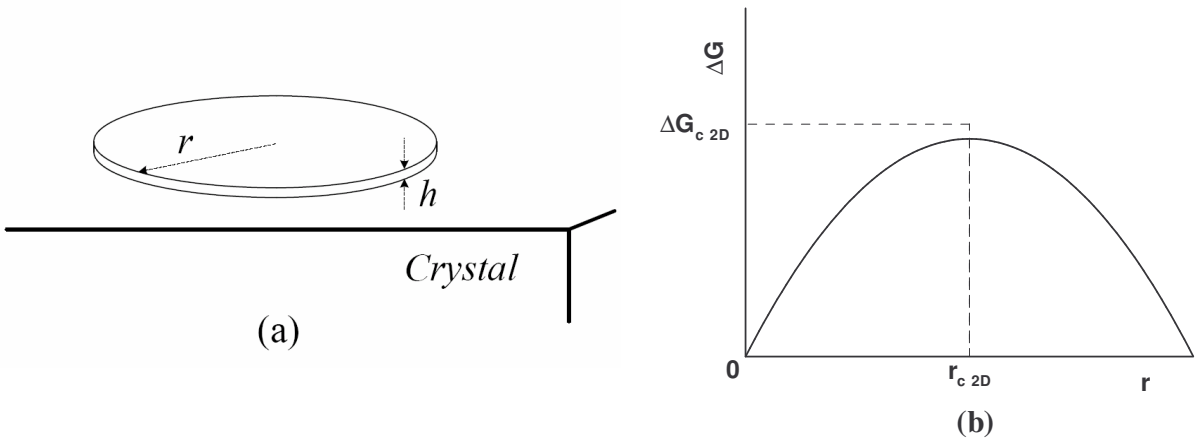

Figure 7.1. Two-dimensional nucleation. (a) 2D nucleus on the crystal surface. (b) Free energy diagram reporting the existence of a critical size of the nucleus.

The thermodynamic basis of the 2D nucleation theory is used to estimate the equilibrium concentration of critical sized nuclei (n_c) as a function of the concentration of monomer on the surface (n_1) [4]:

$$n_c = n_1 \exp\left(-\frac{\Delta G_{c_{2D}}}{kT}\right) \tag{7.4}$$

In its turn, n_c is an important parameter on the determination of the rate of nuclei formation and subsequently, of the growth rates in the perpendicular direction to the surface. Depending on the model assumed to describe the spreading of the 2D islands on the surface, different crystal growth rates are obtained. Ohara and Reid [1] comprehensively revised the different 2D nucleation models (mononuclear model, polynuclear model, birth and spread model, etc.) and the approximations taken on the derivation of the respective equations. The major limitation of all 2D nucleation theories is related with the energy requirements for the growth to occur. At low supersaturation the 2D nucleation barrier ΔG_c is too high for admitting the occurrence of significant crystal growth. This is in contradiction with most of the experimental facts, leading many investigators to loose interest in two dimensional models [1, 3]. Further modifications of the Polynuclear model [5, 6] have proven to adequately describe

experimental growth rates. According to Liu et al. [7], the occurrence of foreign particles on growing surfaces induces a special type of surface instability that could explain crystal growth at low supersaturations. Two-dimensional nucleation mechanisms are currently used on the determination of fundamental parameters like the interfacial tension [8-10] and on the characterization of crystal growth in conjunction with other mechanisms [11].

With the BCF dislocation mechanism the dilemma caused by crystal growth at low supersaturations was solved by postulating that sources of surface steps would exist in real crystals due the presence of imperfections (dislocations) in their lattice. When dislocations have a screw component, the existence of steps in the surface would be assured during growth [12], obviating the necessity of surface nucleation. Growth would occur by the incorporation of molecules into steps disposed in spirals, in a self-perpetuating process (Figure 7.2).

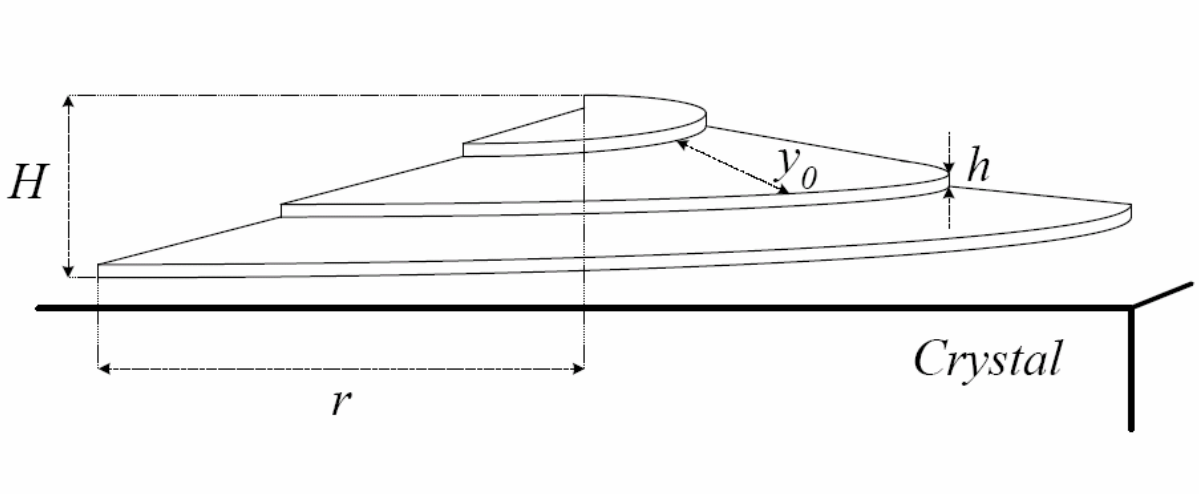

Figure 7.2. Spiral growth.

The advancing velocity of steps (V) was determined assuming that the rate limiting process is the surface diffusion of adsorbed molecules. The Gibbs-Thomson formula was used to relate the velocity of the step with its radius of curvature (ρ):

$$\frac{V}{V_\infty} = 1 - \frac{\rho_c}{\rho} \tag{7.5}$$

where V_∞ refers to a straight step and ρ_c corresponds to the critical radius of the 2D nucleus given by Eq. (7.2). From very early the validity of this equation was questioned because of its tenuous theoretical grounds and lack of experimental verification [1]. Recently, its inconsistency was demonstrated by using atomic-force microscopy on the investigation of the spirals structure [13-16].

Considering a parallel sequence of steps separated by a constant distance of y_0, the two dimensional equations for surface diffusion were solved to obtain an expression for V_∞ [2]:

$$V_\infty = 2\chi S x_s v \exp\left(-\frac{W}{kT}\right)\tanh\left(\frac{y_0}{2x_s}\right) \tag{7.6}$$

In this equation, χ is a factor accounting the possibility of non-equilibrium state, x_s is the mean displacement of adsorbed molecules, v the vibrational frequency of the surface adsorbed molecule and W the evaporation energy (in the case of growth from vapour). The growth rate perpendicular to the surface (R) was obtained taken into account Eqs. (7.5) and (7.6), and the geometry of the rotating spirals:

$$R = \chi h v \exp\left(-\frac{W}{kT}\right)\left(\frac{S^2}{C}\right)\tanh\left(\frac{C}{S}\right) \tag{7.7}$$

with,

$$C = \frac{2\pi\gamma h}{kTx_s} \tag{7.8}$$

According to the BCF relationship, the dependence of R on supersaturation is expected to change from parabolic to linear as the supersaturation increases. The remarkable importance of the BCF theories is recognized until nowadays [17, 18] and it is demonstrated by the great number of experimental data on growth kinetics that are still interpreted based on these concepts [19-21].

In spite of all fundamental advancements in the crystal growth science, several unsolved issues do not allow crystallization results to be predicted under specific growth conditions [18, 22]. In the following section, general principles of the 2D nucleation and BCF mechanisms are used to derive a new molecular-kinetic model in which the inconsistencies of existing theories are avoided and recent experimental findings are taken into account.

7.2 Spiral nucleation model

The advent of atomic force microscopy (AFM) made possible to infer the mechanisms of crystal growth from the examination of growth features on crystal surfaces. By Employing

this technique, Rashkovich et al. [15] followed the process of formation of a dislocation spiral on the (010) face of a potassium hydrogen phthalate crystal. From their observations, important conclusions were drawn concerning the relation between the velocity of segments of steps and their length. The movement of a given segment only started after a critical length was reached and the rate of elongation of each segment was also determined by the displacement of the neighbouring segments. As already referred, the Gibbs-Thomson Eq. (7.5) was not in conformity with the experimental results. The identification of a critical length of the segments is also surprising, since the steps having their origin in screw dislocations are traditionally thought to move freely, once provided that supersaturation is created [2]. The idea of an energy-activated spiral growth is the basis for the spiral nucleation model (SNM) here proposed. Screw dislocations are considered privileged points to start crystal growth due to the smaller energy required to activate the process relatively to the case of flat "perfect" face. A representation of the mechanism would initially consist in the organization of the adsorbed molecules in a spiral, induced by the screw component of the lattice imperfection. Comparatively to the classical 2D nucleation models, the initial island on the surface is no longer assumed to be a circular disc but, instead, a conical spiral (hillock). Besides being consistent with AFM observations of the surface morphology of growing crystals at low supersaturations, this geometric formalism has significant consequences in terms of the energy barrier to form a critical sized nucleus. For simplicity, let us consider an Archimedean-type spiral (polar equation $r = y_0\theta / 2\pi$) circumscribed in a hillock of radius r (Figure 7.2). The peripheral area of the hillock is given by

$$a_n = \frac{y_0}{4\pi}\left[\theta\sqrt{1+\theta^2} + \ln\left(\theta + \sqrt{1+\theta^2}\right)\right]h \tag{7.9}$$

where h is the step elementary height and y_0 is the distance between steps ($h \ll y_0$), and the hillock volume corresponds to

$$v_n = \frac{\pi r^3}{3}\frac{h}{y_0} \tag{7.10}$$

The Gibbs free energy change on the formation of this nucleus is given by Eq. (7.1), using the geometric definitions of the spiral:

$$\Delta G = \frac{y_0}{4\pi}\left[\theta\sqrt{1+\theta^2} + \ln\left(\theta + \sqrt{1+\theta^2}\right)\right]h\gamma - \frac{\pi r^3}{3}\frac{h}{y_0}\frac{kT}{\Omega}\ln\left(1+S\right) \tag{7.11}$$

Such as it was described for the 2D nucleation, there is a minimum size r_c above which the nuclei continue to grow. This dimension corresponds to a critical number of spiral turns $\theta_c / 2\pi$ that can be determined by maximizing Eq. (7.11) with respect to θ. For a given value of θ_c, the energetic barrier for spiral nucleation is as well influenced by the separation between steps, hereafter expressed in relation to the size of the 2D nucleus:

$$y_0 = \alpha r_{c2D} \tag{7.12}$$

where α is a proportionality factor. The combined effect of θ and α on the normalized Gibbs free energy change is shown in Figure 7.3.

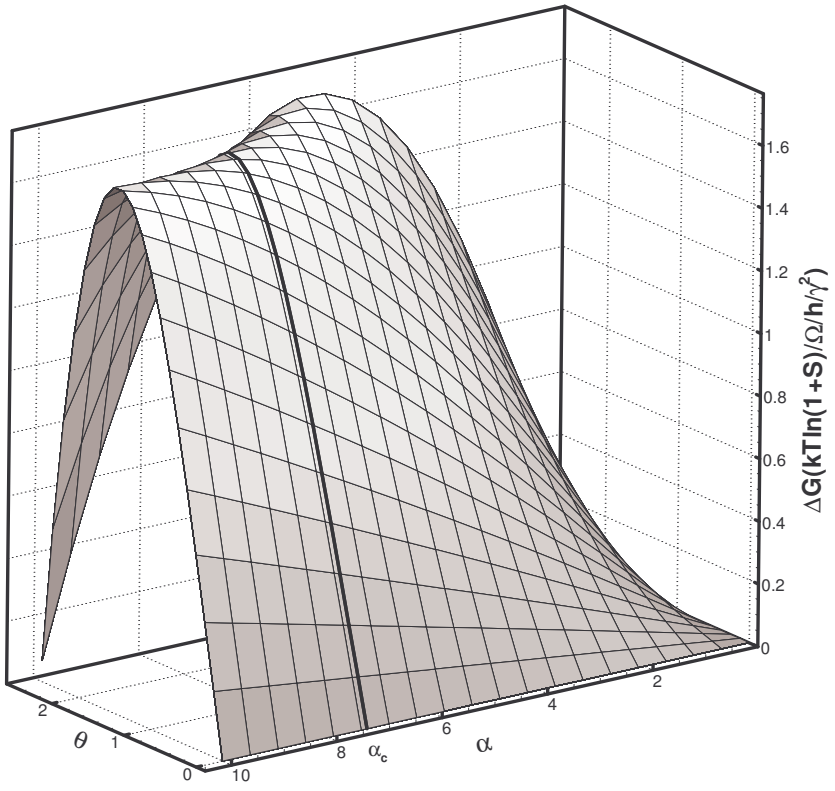

Figure 7.3. Influence of θ and α on the normalized Gibbs free energy change according to Eq. (7.11) and the definitions of y_0 and $r_{c_{2D}}$.

For the range of α values considered, the maximum free energy change takes place when θ is about 2 (114º). Under these conditions, there is an optimum interstep distance corresponding to $\alpha = 7.26$ (highlighted in the figure) that leads to minimum critical free energy change. This value is considerably lower than the result of $\alpha = 19$, obtained from admitting direct correspondence between velocity of advance and radius of curvature of the

step (Eq. (7.5)) [1]. At the optimum conditions for the formation of the spiral, $\theta_c = 1.95$ independently of the system studied, $r_c = 2.25 r_{c_{2D}}$ and

$$\Delta G_c = 1.64 h \frac{\gamma^2 \Omega}{kT \ln(1+S)} \tag{7.13}$$

Comparing this result with Eq. (7.3) one obtains that the energy required for 2D nucleation is about two times higher than the one needed for spiral nucleation. Therefore, the formation of nuclei at crystal surface is expected to occur preferentially by a spiral growth mechanism.

Once established the thermodynamics of the SNM, the derivation of the relation between the crystal growth rate and growth affecting variables will follow. After the formation of stable spirals, crystal growth occurs by the integration of adsorbed units into their steps. To start, let us consider the rate at which molecules integrate a particular spiral, from a geometrical point of view. The variation of the number of incorporated molecules (N) during an infinitesimal time interval dt is proportional to the corresponding increase of the peripheral area,

$$\frac{dN}{dt} = \frac{h}{\Omega} \frac{da}{dt} \tag{7.14}$$

In the case of a well developed spiral hillock (high θ) it results from Eq. (7.9) that

$$\frac{da}{dt} = \frac{2\pi r h}{y_0} \frac{dr}{dt} \tag{7.15}$$

with dr/dt corresponding to the rate of advancement of the step (V). Combining Eqs. (7.14) and (7.15), and assuming V to be independent of the spiral size one obtains that the incorporation rate is higher for bigger hillocks, i.e., dN/dt increases with r:

$$\frac{dN}{dt} = \frac{2\pi r h^2}{\Omega y_0} V \tag{7.16}$$

Although the Gibbs-Thomson Eq. (7.5) predicts V to be directly dependent of ρ, it has been recently demonstrated that the step velocity abruptly changes to a maximum (V_∞) once surpassed the segment critical size [14, 16]. Accordingly [18],

$$V = \begin{cases} 0, & r < r_c \\ V_\infty & r > r_c \end{cases} \tag{7.17}$$

The dependence of dN/dt on r and y_0 leads us to the importance of understanding the disposition of spirals on the surface and how spirals originated from different dislocations coexist. Apparently, the behaviour of a crystal face with many dislocations is the same as if it had just one. Nevertheless, from topological considerations Burton et al. [2] demonstrated that the activity of a group of dislocations is greater than that of a dislocation alone by a factor of ε, which can be approximated to the number of dislocations. With the activity enhancement, the distance y_0 between steps decreases ε times and the number of steps passing in a given point increases in the same proportion. From what was said, the general case of spiral growth due to a group of dislocations can be described considering a single spiral, after correcting the distance between steps by the number of dislocations. For convenience, let us assume a crystal with a circular face of radius L, covered by a group of ε sources of active spirals. The incorporation rate is here given by the corrected form of Eq. (7.16):

$$\frac{dN}{dt} = \frac{2\pi L h^2}{\Omega y_0}\varepsilon V \tag{7.18}$$

Note that if the distance between steps was measured, for example by AFM, the obtained value would correspond to y_0/ε. Converting the previous expression in order to obtain the more conventional mass deposition rate per surface area units, R_G, one gets

$$R_G = \frac{2\pi\rho_s L h^2}{y_0} n_{sp} V \tag{7.19}$$

Where ρ_s is the crystal density and n_{sp} the number of active spiral sources per surface area units. This number corresponds to the fraction of the total number of dislocations per m^2 (λ), whose resulting spirals reached the thermodynamic barrier ΔG_c defined in Eq. (7.13) and continued on growing. If the dislocations centres are closer together than half of the radial distance between successive turns ($y_0/2$), the activity of the group of dislocations is changed in a factor of approximately $y_0/2\bar{l}$, where $\bar{l}$ is the average distance between dislocations [2]. Consequently, the density of stable spirals in equilibrium is given by

$$n_{sp} = \frac{\lambda y_0}{2\bar{l}} \exp\left(-\frac{\Delta G_c}{kT}\right) \tag{7.20}$$

This expression is similar to Eq. (7.4), used to estimate the concentration of critical sized nuclei in the classical 2D nucleation mechanism. In the derivation of the BCF theory it was found that, in spite of the activity of a group can be several times greater than that of a single

dislocation, a maximum on the activity enhancement with the number of dislocations in a group is obtained. Indeed, as a consequence of the key role that surface diffusion has in that model, the rate of step advancement was established to decrease as the distance between steps decreases [2]. Distinct kinetic approaches to the movement of steps will be considered in the SNM depending if crystals grow from solution or from vapour. The importance of surface diffusion considerably differs from one growth processes to the other. In the case of growth from solution the velocity of advancement of steps is not expected to decrease with the proximity of steps. Hence, according to Eq. (7.19), the new proposed model expects R_G to increase as the number of dislocations contained in a group increases. Such behaviour is in accordance with what is experimentally known [23, 24]. Later modifications to the BCF model were introduced to quantify the growth rate enhancement caused by groups of dislocations [25] and to take into account the level of strains in the crystal [26].

To conclude the SNM crystal growth rate expression it is necessary to quantify the forward speed of a step, V , in Eq. (7.19). The mechanism that will be adopted describing the integration of units into the crystal is, in the case of growth from solution, roughly comparable to the adhesive growth pattern and, in the case of growth from vapour, similar to the lateral growth pattern [27]. In this approach, the volume diffusion resistance will not be considered on the derivation of the kinetic equations, that is to say, the integration step is analysed separately from the mass transfer step.

Starting with crystal growth from solution, molecules leave the solution and reach the crystal surface at a maximum rate given by the Wilson-Frenkel relation (or by the Hertz-Knudsen formula, in the case of vapour) [27]. The corresponding current of molecules J_{max} (molecules/m/s) entering in a given terrace of length y_0/ε is

$$J_{max} = \frac{n_{se} S}{\tau_s} \frac{y_0}{\varepsilon} \tag{7.21}$$

where n_{se} is the number of adsorbed molecules in equilibrium, per unit of surface area, and τ_s is the mean life time of an adsorbed molecule before desorbing, so that:

$$\frac{n_{se}}{\tau_s} = n_e v \exp\left(-\frac{W}{kT}\right) \tag{7.22}$$

Here, n_e corresponds to the number of molecular positions on the surface per m^2 and W is the energy of adsorbing onto the surface (as previously seen, W corresponds to the

evaporation energy when considering growth from vapour). Unless the crystals planes are very rough, growth will take place at a rate below J_{max}. This should be the most common situation since rough, uneven surfaces tend to disappear and only flat, slow growing surfaces remain. The fraction of J_{max} integrating the crystal lattice accounts for the molecules that have reached a position in the terrace near the step. The other adsorbed molecules do not have enough mobility to achieve a more energetically favourable position within a mean time interval τ_s and become desorbed. Assuming that no significant surface diffusion occurs, the active area for incorporation into the step would be the perimeter of the spiral ($\pi\varepsilon L^2/y_0$) multiplied by the molecular length (approximately, h). The active area to total surface area ratio ($\varepsilon h/y_0$) corresponds therefore to the probability of integration of a molecule arriving from solution. The velocity of step is then $J_{max}\varepsilon h/(y_0 n_e)$, or, using Eqs. (7.21) and (7.22),

$$V = v\exp\left(-\frac{W}{kT}\right)hS \tag{7.23}$$

The existence of significant surface diffusion during growth from solution is hard to conceive [1, 18, 28]. Nevertheless, Land et al. [29] explained the homogenization of initially nonuniform double step current through the occurrence of surface diffusion during canavalin crystal growth. For these cases, larger active area for incorporation would be expected, and consequently, the obtained velocity of step advancement would be higher than the one predicted by Eq. (7.23).

Contrarily to what happens in crystal growth from solution, the existence of surface diffusion during growth from vapour is well-established. Here, molecules reaching a terrace can diffuse across the surface and integrate into the step in an energetically favourable place, following the so-called Kossel mechanism [27]. The steady state continuity equation for surface diffusion regarding the density of adsorbed molecules is given by,

$$x_s^s \frac{d^2\psi}{dy^2} = \psi \tag{7.24}$$

where ψ is the difference between the supersaturation in the vapour and on the surface, $\psi = S - S_s$ and x_s is the average distance that molecules diffuse during the residence time τ_s. The vapour supersaturation is defined in terms of the actual vapour pressure (p) and the equilibrium value (p_e), $S = p/p_e - 1$, and the surface supersaturation is defined by means of the actual and equilibrium density of adsorbed molecules (n_s and n_{se}, respectively),

$S_s = n_s / n_{se} - 1$. Considering a parallel sequence of steps separated by equal distances y_0/ε, the boundary conditions of Eq. (7.24) are:

$$\begin{cases} y = 0, & \psi = S \\ y = \dfrac{y_0}{2\varepsilon}, & \psi = 0 \end{cases} \tag{7.25}$$

In this situation, y is the distance from the midpoint between two steps ($y_0/(2\varepsilon)$). The current of molecules, J (molecules/m/s), integrating the crystal lattice can be obtained from the gradient at the step position:

$$J = 2D_s \left.\frac{dn_s}{dy}\right|_{y=\frac{y_0}{2\varepsilon}} \tag{7.26}$$

Replacing the solution of Eq. (7.24) in the previous equation one gets

$$J = \frac{2n_{se}D_s S}{x_s} \tanh\left(\frac{y_0}{2\varepsilon x_s}\right) \tag{7.27}$$

where D_s is the surface diffusion coefficient. Using the Einstein's expression $D_s \tau_s = x_x^2$ and knowing the total number of molecules reaching the terrace J_{max} from Eq. (7.21), Eq. (7.27) can be rewritten as

$$J = J_{max} \frac{2\varepsilon x_s}{y_0} \tanh\left(\frac{y_0}{2\varepsilon x_s}\right) \tag{7.28}$$

Figure 7.4 shows the expected influence of the average step semi-distance to the average diffusion distance ratio ($y_0/(2\varepsilon x_s)$) on the fraction of adsorbed molecules integrating the step (J/J_{max}).For a given system, diminishing the distance between steps will progressively increase the J/J_{max} ratio until reaching the unity. As shown in Figure 7.4, for $y_0/(2\varepsilon x_s) < 0.1$ the current integrating the step reaches its maximum and becomes practically insensitive to variations in the interstep distance. Estimations of the order of magnitude of x_s and y_0/ε make us believe that the integration current would frequently correspond to J_{max}. In fact, for a surface of large interplanar distance in a face-centred cubic crystal, Burton et al. estimated $x_s \sim 3\times10^3 a'$, where a' is the distance between two neighbouring adsorption positions. At the ambient temperature, a' corresponds practically to the diameter of the growth unit, h [30]. Assuming as a reference AFM measurements of interstep distances taken from literature $y_0/\varepsilon \sim (30 \text{ to } 400)h$ [31, 32], the dimensionless

parameter in the *x*-axis of Figure 7.4 will range from 0.005 to 0.07 and $J/J_{max} \sim 1$. For close-packed surfaces x_s is much lower than the value of $3\times10^3 a'$ and so, higher values of the $y_0/(2\varepsilon x_s)$ parameter are expected. Even for these surfaces of low morphological importance [33], the fraction of integrating molecules would be more than 80% of the estimated maximum flux. In the general case, the velocity of advancement of step during growth from vapour is

$$V = \frac{J}{n_e} = 2x_s v \exp\left(-\frac{W}{kT}\right)\tanh\left(\frac{y_0}{2\varepsilon x_s}\right)S \tag{7.29}$$

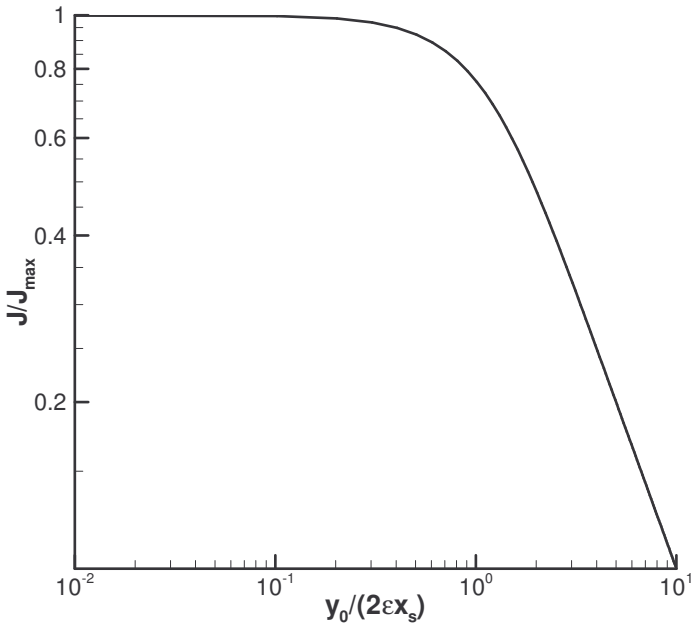

Figure 7.4. Variation on a log-log scale of the J/J_{max} ratio as a function of the $y_0/(2\varepsilon)$ to x_s ratio, according to Eq. (7.28).

At this point we are able to obtain the generalized crystal growth rate equation by replacing the derived definitions of step advancement velocity in Eq. (7.19):

$$R_G = \frac{2\pi\rho L h^2}{y_0} n_{sp} v \exp\left(-\frac{W}{kT}\right)\beta S \tag{7.30}$$

The parameter β is here introduced to distinguish solution growth ($\beta = h$) from vapour growth ($\beta = 2x_s \tanh\left(y_0/(2\varepsilon x_s)\right) \approx y_0/\varepsilon$). The density of spirals n_s is a function of supersaturation, temperature and physical properties of the crystal (Eq. (7.20)). New insights on the role of supersaturation, temperature, crystal size, topological parameters of the crystal,

number of surface dislocations, interfacial tension, etc., result from the SNM growth rate equation. Hopefully the resulting conclusions will contribute for a better understanding of unresolved problems in crystal growth science such as spirals formation and development, step bunching, abnormal growth kinetics, size-dependent growth or growth rate dispersion. In the following section an example of application of the SNM to sucrose crystal growth kinetics will be given. It is intended to determine the sucrose interfacial tension and to calculate topological parameters from the measured dependence of R_G/L on the supersaturation.

7.3 Application of the SNM to growth rate data

In this section, the interpretation of crystallization data according to the SNM will be exemplified using the sucrose growth curve obtained at 40 ºC and 300 rpm in the batch growth experiments described in Chapter 5. Crystal growth rates are normalized by the instantaneous equivalent size of the crystals given by mass balance. This procedure is based on the assumption of linear $R_G(L)$ dependence suggested in Eq. (7.30), and afterwards confirmed in Chapter 6. In conformity with the same equation, supersaturation is expressed as a function of the solute molar fraction, using the measured sucrose solubility at 40 ºC ($x_e = 0.1093$), so that $S = x_b / x_e - 1$. Figure 7.5 shows the sucrose growth curve calculated accordingly. The average difference between successive mean supersaturations is approximately 2.3×10^{-3}.

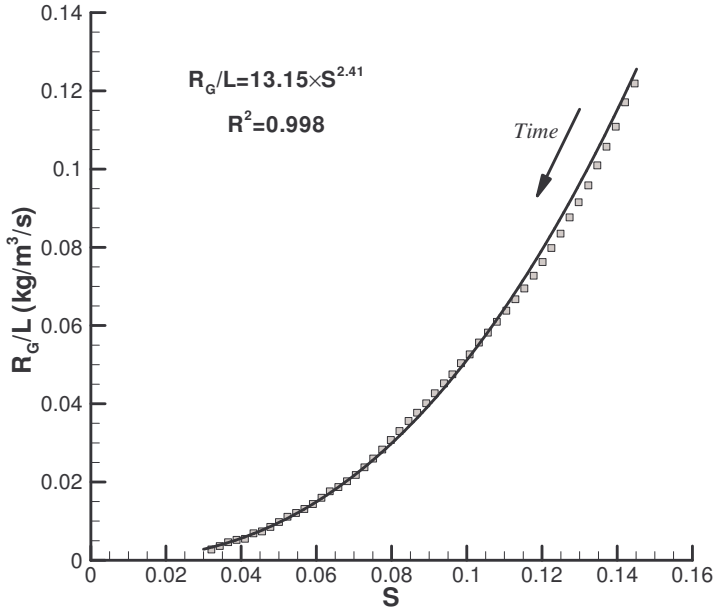

Figure 7.5. Effect of supersaturation on the normalized sucrose growth rates in batch crystallization experiments at 40 ºC. A power law equation is used to fit the data.

The volume median size measured by laser light diffraction changed from 0.314 mm to 0.802 mm during the growth experiment. Crystal growth rates obtained at high supersaturations correspond to the beginning of the experiment and to smaller crystals. As shown in Figure 7.5, the results were well fitted by the following empirical equation:

$$\frac{R_G}{L} = k_G S^{n_V} \tag{7.31}$$

where k_G and n_V are the empirical kinetic constant and kinetic order, respectively. The parameters of Eq. (7.31) can be interpreted in the light of the SNM and of the respective fundamental growth rate expression, given by Eq. (7.30). This correspondence will be used to estimate the influence of supersaturation on the interfacial tension between sucrose crystals and the supersaturated sucrose solutions. Other existing methods for interfacial tension determination using crystallization kinetics were previously reviewed by Wu and Nancollas [10]. Usually, the experimentally determined kinetic order n_V is compared with the $\gamma-$ dependent theoretical expression corresponding to the growth mechanism accepted. On the derivation of the $n_V(\gamma)$ relations, the interfacial tension is assumed to be independent of supersaturation. According to the Gibbs adsorption isotherm theory, this has to be considered

a gross approximation. For ideal systems, the variation of the interfacial tension with solute concentration is given by [34-36]:,

$$\left(\frac{\partial \gamma}{\partial \ln x_2}\right)_{p,T} = -\Gamma_2 RT \tag{7.32}$$

where x_2 is the solute mole fraction, R is the gas constant and Γ_2 is the Gibbs excess concentration of solute on the interface (mol/m^2). The Gibbs adsorption isotherm is often applied on liquid-fluid interfaces to calculate the solute adsorption, since the interfacial tension can be measured. On solid-fluid interfaces the same isotherm is used to calculate the interfacial tension, because adsorption can be measured [37]. Bearing in mind that γ is not constant over a range of supersaturations, the slope of the log-log plot of the normalized growth rate R_G / L against S is, in the case of the SNM,

$$n_V = \frac{\partial \ln\left(R_G / L\right)}{\partial \ln S} = 1 + 1.64 \frac{h\Omega}{\left(kT\right)^2} \gamma \left(\frac{\gamma}{S} - 2\frac{d\gamma}{dS}\right) \tag{7.33}$$

This equation results from Eq. (7.30) for solution growth, from the definitions of n_{sp}, y_0 and ΔG_c and from the approximation $\ln\left(1+S\right) \approx S$. In its turn, the inclination of growth hillocks, $p = h\varepsilon / y_0$ is proportional to $S^{n_V - 1}$ because of its dependence on the $\exp\left(-\Delta G_c / kT\right)$ factor. Frequently the value of n_V is comprised between 1 and 2, so, p can be nearly constant or vary linearly with S, depending on the growth kinetic order. This is consistent with AFM observations of the topology of the (101) face of KDP made by De Yoreo et al. [38, 39], over the range of supersaturation between $S = 0.03$ and $S = 0.30$, and with the subsequent analysis of published data made by Sangwal [40]. Evidences of both linear [41] and sublinear [42] $p(S)$ dependence were also found by applying in-situ Michelson interferometry to study the (001) and the (101) ADP face, respectively.

The data shown in Figure 7.5 indicate that $n_V = 2.41$ over the supersaturation range considered. As a result, the inclination of the growth hillocks for sucrose at 40 ºC should increase with supersaturation according to a power law with an exponent of 1.41. Replacing the measured value of n_V in Eq. (7.33) one obtains a first-order ordinary differential equation (ODE) relating γ and S, with no analytical solution. Setting instead the condition of constant kinetic order over the range of supersaturation in study ($\partial n_V / \partial S = 0$), one obtains the following analytical solution from the second-order ODE:

$$\gamma = \sqrt{C_1 S - C_2 S \ln S} \tag{7.34}$$

Where C_1 and C_2 are constants. The value of C_2 can be directly obtained by replacing the derived $\gamma(S)$ relation in Eq. (7.33), so that

$$n_V = 1 + 2\frac{1.64h\Omega}{(kT)^2}C_2 \tag{7.35}$$

Using $\Omega = 715.04\times10^{-30}$ m^3 [43] and letting $h \approx \Omega^{1/3}$, it results that $C_2 = 1.08\times10^{-5}$ for the system in study. Note that n_V is independent of the value of C_1 and, for $n_V = 1$, the crystal growth kinetics from solution is not affected by the interfacial tension. The knowledge of C_1 is, however, essential to determine the behaviour of the interfacial tension for changing supersaturation. Figure 7.6 is a representation of Eq. (7.34) assuming $C_1 = 9.75\times10^{-4}$. This value was chosen in order to reproduce rough estimations taken from literature indicating that $\gamma \approx 5\times10^{-3}\,N/m$ for saturated sucrose solutions [44]. As shown, the interfacial tension markedly increases with supersaturation. According to the Gibbs adsorption isotherm given by Eq. (7.32), the Gibbs excess concentration of sucrose is a negative value ($\Gamma_2 < 0$), i.e., for a given supersaturation, the concentration of sucrose on the crystal surface decreases relatively to solution. Since $\partial\gamma/\partial \ln x_2 \approx \partial\gamma/\partial S$ and Γ_2 is a constant, the Gibbs adsorption isotherm predicts the interfacial tension to vary linearly with supersaturation.

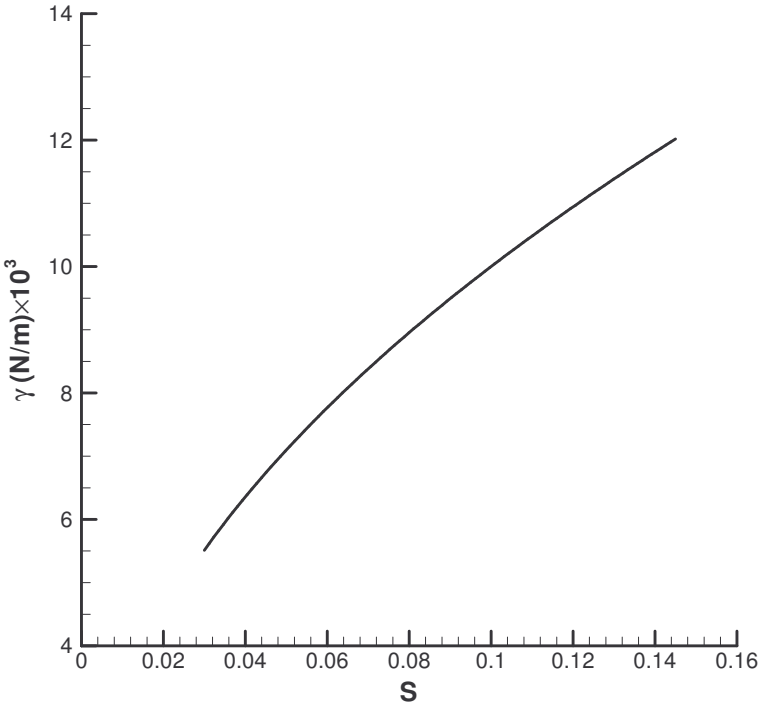

Figure 7.6. Influence of supersaturation on the interfacial tension between sucrose crystals and aqueous solutions of sucrose at 40 ºC according to Eq. (7.34).

The slope of the $\gamma(S)$ curve shown in Figure 7.6 decreases as the supersaturation increases, indicating that the sucrose system at 40 ºC diverges from the ideal behaviour. After the influence of supersaturation on the interfacial tension is established, critical parameters of the SNM such as the critical radius of the nuclei or the energetic barrier for the nuclei formation can be determined for the operating conditions. An application example will follow, where the influence of supersaturation on the ratio between the interstep distance of spirals resulting from one dislocation source and the step height (y_0 / h) is determined. The profile shown in Figure 7.7 results from the definition $y_0 = 7.26 r_{c_{2D}}$ and from Eqs (7.2) and (7.34). Increasing the supersaturation would decrease the y_0 / h ratio, because of the lower energetic barrier to form a spiral nucleus. The range of values represented in Figure 7.7 compares well with the average ratio measured by AFM on (100) faces of KDP grown from aqueous solutions at $S = 0.03$ [31]. Under those conditions, the average value of y_0 / h was approximately 200. Observations of lower step length-to-height ratio are, however, likely to occur due to the phenomenon of step bunching and to multiple-source steps.

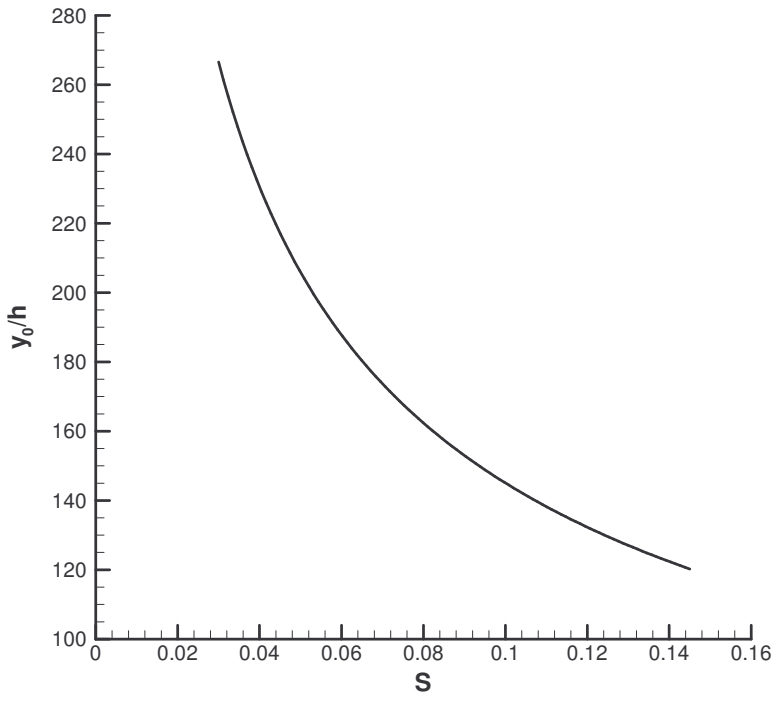

Figure 7.7. Influence of supersaturation on the step length-to-height ratio of spirals resulting from one dislocation source.

Presently, there is a renewed interest on the determination of interfacial tension at solid-liquid interfaces [10] and a great number of works have been published about the topological properties of the surface of growing crystals. More than accurately determine these parameters, the example here presented has the purpose of illustrating how they can be

estimated from crystallization data using the SNM growth equation. Better estimations of the interfacial properties would have to account for the deviations from ideality of the water-sucrose mixture [34, 35]. Moreover, the crystal growth rates of sucrose are known to be affected by volume diffusion resistances that are not considered in present approach. In following chapters, the combined use of the SNM with diffusion-reaction models will be illustrated. In spite of the simplifications made, the SNM has proven to be a valuable tool for characterizing the interface phenomena during crystal growth and on the determination of the morphology of growing hillocks by a non-microscopic method.

7.4 Conclusions

The formation and development of surface dislocation spirals during crystal growth was revised from the thermodynamic and kinetic point of view. Spiral growth is not seen as a spontaneous process in supersaturated media, although the energy requirements for the formation of the initial nuclei are considerably lower than in other energy-activated models. Following recent AFM observations of the growth mechanism, the velocity of step advancement was calculated independently of the step radius of curvature. Conversely, it was found that the overall integration rate increases with the number of surface dislocations and with the interface size. It is believed that the distance between steps resulting from the same dislocation source is independent of supersaturation. However, increasing the supersaturation, the number of cooperating active sources may increase and consequently decrease the measured interstep distance. Because of the low mobility of the adsorbed molecules during solution growth, only a small fraction of the current reaching the crystal surface is integrated into the steps. The contrary happens during vapour growth, where high mean displacements of condensed molecules lead to high integration efficiencies. Eq. (7.30) provides a generalized relation between crystal growth rate and the main variables that are recognized to influence it. The spiral nucleation model was used to calculate the influence of supersaturation on the interfacial tension from the measured crystal growth kinetics of sucrose at 40 ºC. Other interfacial phenomena such as solute adsorption were also analyzed, and the morphology of growth hillocks was possible to be inferred without using microscopic techniques. The consistency of the proposed model was demonstrated in terms of general microscopic evidences and of growth kinetic behaviour. The potential of the spiral nucleation mechanism will continue to be explored on the interpretation of some unresolved questions in crystal growth science.

References

[1] M. Ohara and R. C. Reid, Modelling crystal growth rates from solution, Prentice-Hall, Inc., New Jersey, **1973**.

[2] W. K. Burton, N. Cabrera, and F. C. Frank, The growth of crystals and the equilibrium structure of their surfaces. *Phil. Trans. Roy. Soc. London*, **1951,** 243, 299-358.

[3] J. W. Mullin, Crystallization, 4th ed.; Butterworth-Heinemann, Oxford, **2001**.

[4] W. A. Tiller, The Science of Crystallization: Microscopic Interfacial Phenomena, Cambridge University Press, Cambridge, **1991**.

[5] J. Christoffersen and M. R. Christoffersen, A revised theory for the growth of crystals by surface nucleation. *J. Cryst. Growth*, **1992,** 121, 608.

[6] J. Christoffersen, J. Dohrup, and M. R. Christoffersen, The importance of formation of hydroxyl ions by dissociation of trapped water molecules for growth of calcium hydroxyapatite crystals. *J. Cryst. Growth*, **1998,** 186, 275.

[7] X. Y. Liu, Heterogeneous 2D nucleation-induced surface instability. *J. Cryst. Growth*, **2002,** 237-239, 101.

[8] H. Hao, J. Wang, and Y. Wang, Determination of induction period and crystal growth mechanism of dexamethasone sodium phosphate in methanol-acetone system. *J. Cryst. Growth*, **2005,** 274, 545.

[9] I. Liszi, M. Hasznosne-Nezdei, B. G. Lakatos, T. J. Sapundzhiev, and R. G. Popov, Determination of the crystal growth mechanism of KCl in ethanol-water system. *J. Cryst. Growth*, **1999,** 198-199, 1330.

[10] W. Wu and G. H. Nancollas, Determination of interfacial tension from crystallization and dissolution data: a comparison with other methods. *Adv. Colloid Interface Sci.*, **1999,** 79, 229.

[11] A. E. Nielsen, Electrolyte crystal growth mechanisms. *J. Cryst. Growth*, **1984,** 67, 289.

[12] F. C. Frank, The influence of dislocations on crystal growth. *Discuss. Faraday Soc.*, **1949,** 5, 48-54.

[13] S. R. Higgins, D. Bosbach, C. M. Eggleston, and K. G. Knauss, Kink dynamics and step growth on barium sulfate (001): A hydrothermal scanning probe microscopy study. *J. Phys. Chem. B*, **2000,** 104, 6978-6982.

[14] L. N. Rashkovich, N. V. Gvozdev, M. I. Sil'nikova, I. V. Yaminski, and A. A. Chernov, Dependence of the step velocity on its length on the (010) face of the orthorhombic lysozyme crystal. *Cryst. Rep.*, **2001,** 46, 860-863.

[15] L. N. Rashkovich, E. V. Petrova, O. A. Shustin, and T. G. Chernevich, Formation of a Dislocation Spiral on the (010) Face of a Potassium Hydrogen Phthalate Crystal. *Phys. Solid State*, **2003,** 45, 400-407.

[16] H. H. Teng and P. M. Dove, Thermodynamics of Calcite Growth: Baseline for Understanding Biomineral Formation. *Science*, **1998,** 282, 724-727.

[17] P. Bennema, Spiral growth and surface roughening: Developments since Burton, Cabrera and Frank. *J. Cryst. Growth*, **1984,** 69, 182.

[18] A. A. Chernov, Notes on interface growth kinetics 50 years after Burton, Cabrera and Frank. *J. Cryst. Growth*, **2004,** 264, 499.

[19] F. Farhadi and M. B. Babaheidary, Mechanism and estimation of Al(OH)3 crystal growth. *J. Cryst. Growth*, **2002,** 234, 721.

[20] R. Mohan and A. S. Myerson, Growth kinetics: a thermodynamic approach. *Chem. Eng. Sci.*, **2002,** 57, 4277.

[21] D. Sun, X. Yu, Y. Wang, and Y. Fu, Growth kinetics on the (100) and (001) faces of TGS crystals. *Prog. Cryst. Growth Charact. Mater.*, **2000,** 40, 227.

[22] A. A. Chernov, Crystal growth science between the centuries. *J. Mater. Sci. Mater. Electron.*, **2001,** 12, 437.

[23] C. M. Jones and M. A. Larson, Characterizing growth-rate dispersion of NaNO3 secondary nuclei. *AIChE J.*, **1999,** 45, 2128-2135.

[24] R. I. Ristic, J. N. Sherwood, and T. S. Shripathi, in *Advances in Industrial Crystallization*, (J. Garside, R. J. Davey, A. G. Jones, eds.), Butterworth-Heinemann, Oxford, **1991**.

[25] J. Garside and R. J. Davey, Secondary contact nucleation: kinetics, growth and scale-up. *Chem. Eng. Commun.*, **1980,** 4, 393-424.

[26] C. M. Jones and M. A. Larson, Using dislocations and integral strain to model the growth rates of secondary nuclei. *Chem. Eng. Sci.*, **2000,** 55, 2563.

[27] T. Irisawa, in Crystal Growth Technology (K. Byrappa, T. Ohachi, eds.), William Andrew Publishing, Noyes, **2002**, pp. 25-54.

[28] T. Nishinaga, Understanding of crystal growth mechanisms through experimental studies of semiconductor epitaxy. *J. Cryst. Growth*, **2005,** 275, 19.

[29] T. A. Land, J. J. De Yoreo, and J. D. Lee, An in-situ AFM investigation of canavalin crystallization kinetics. *Surf. Sci.*, **1997,** 384, 136.

[30] S. Koutsopoulos, Kinetic study on the crystal growth of hydroxyapatite. *Langmuir*, **2001,** 17, 8092-8097.

[31] K. Sangwal, J. Torrent-Burgues, P. Gorostiza, and F. Sanz, AFM Study of the Behaviour of Growth Steps on the (100) Faces of KDP Crystals and the Tapering Phenomenon. *Cryst. Res. Technol.*, **1999,** 34, 667-675.

[32] K. Sangwal, J. Torrent-Burgues, F. Sanz, and P. Gorostiza, Atomic force microscopic study of step bunching and macrostep formation during the growth of L-arginine phosphate monohydrate single crystals. *J. Cryst. Growth*, **1997,** 172, 209.

[33] P. Bennema, On the crystallographic and statistical mechanical foundations of the forty-year old Hartman-Perdok theory. *J. Cryst. Growth*, **1996,** 166, 17.

[34] H. Kahl, T. Wadewitz, and J. Winkelmann, Surface Tension and Interfacial Tension of Binary Organic Liquid Mixtures. *J. Chem. Eng. Data*, **2003,** 48, 1500-1507.

[35] H. Kahl, T. Wadewitz, and J. Winkelmann, Surface tension of pure liquids and binary liquid mixtures. *J. Chem. Eng. Data*, **2003,** 48, 580-586.

[36] N. Matubayasi, S. Matsuyama, and R. Akizuki, Surface properties of aqueous amino acid solutions: II. Leucine-leucine hydrochloride and leucine-sodium leucinate mixtures. *J. Colloid Interface Sci.*, **2005,** 288, 402-406.

[37] A. D. Rey, Thermodynamic model of surfactant adsorption on soft liquid crystal interfaces. *Langmuir*, **2004,** 20, 11473-11479.

[38] J. J. De Yoreo, T. A. Land, and J. D. Lee, Limits on surface vicinality and growth rate due to hollow dislocation cores on KDP {101}. *Phys. Rev. Lett.*, **1997,** 78, 4462-4465.

[39] J. J. De Yoreo, T. A. Land, L. N. Rashkovich, T. A. Onischenko, J. D. Lee, O. V. Monovskii, and N. P. Zaitseva, The effect of dislocation cores on growth hillock vicinality and normal growth rates of KDP {1 0 1} surfaces. *J. Cryst. Growth*, **1997,** 182, 442.

[40] K. Sangwal, On the mechanism of crystal growth from solutions. *J. Cryst. Growth*, **1998,** 192, 200-214.

[41] A. A. Chernov, L. N. Rashkovich, and A. A. Mkrtchan, Solution growth kinetics and mechanism: Prismatic face of ADP. *J. Cryst. Growth*, **1986,** 74, 101.

[42] P. G. Vekilov, Y. G. Kuznetsov, and A. A. Chernov, The effect of temperature on step motion; (101) ADP face. *J. Cryst. Growth*, **1992,** 121, 44.

[43] D. Aquilano, M. Franchini-Angela, M. Rubbo, G. Mantovani, and G. Vaccari, Growth morphology of polar crystals: A comparison between theory and experiment in sucrose. *J. Cryst. Growth*, **1983,** 61, 369-376.

[44] P. Walstra, Physical Chemistry of Foods, Marcel Dekker Inc., New York, **2003**.

8. Size-dependent growth

Overview

The effect of crystal size on the growth rate of sucrose at 40 ºC is investigated from a theoretical and an experimental point of view. Based on the principles of the spiral nucleation model, crystal growth rates are expressed in terms of mass deposition per time and crystal volume units. This alternative definition is demonstrated to be size-independent over the considered supersaturation range. The conventional overall growth rate expressed per surface area units is found to be linearly dependent on crystal size. The advantages of the "volumetric" growth rate concept are discussed. Sucrose dissolution rates were measured under reciprocal conditions of the growth experiments in order to investigate the two-way effect of crystal size on the mass transfer rates and on the integration kinetics. Both effects are adequately described by combining a well-established diffusion-integration model and the spiral nucleation mechanism.

8.1 Introduction

In systems exhibiting size-dependent growth (SDG), crystal growth rates are influenced by the size of crystals. A good understanding of SDG is essential on the analysis of crystal growth kinetics and crystal size distributions [1], on the interpretation of growth rate dispersion [2] and to develop better seeding policies [3]. The influence of crystal size on the growth rates has been mainly described through empirical formulations. Most of these correlations were previously reviewed in the works of Abegg et al. [4], Mitrovic et al. [5] and White et al. [6]. Garside and Jancic [1] suggested that for larger crystals higher crystal collisions and mechanical stress would increase the surface dislocation density and consequently enhance the crystal growth rate. In fact, according to the classical Burton Cabrera and Frank (BCF) theory [7, 8] the growth rate perpendicular to the surface (*R*) can be enhanced by a factor of ε, which is proportional to the number of dislocations in a group, so that

$$R = \chi h v \exp\left(-\frac{W}{kT}\right)\left(\frac{\varepsilon S^2}{C}\right)\tanh\left(\frac{C}{\varepsilon S}\right) \tag{8.1}$$

where

$$C = \frac{2\pi\gamma h}{kTx_s} \tag{8.2}$$

and k is the Boltzmann constant, T is the temperature, W is the energy of adsorbing onto the surface (in the case of growth from solution), χ is a factor accounting the possibility of non-equilibrium state, h is the step height, v is the vibrational frequency of the surface adsorbed molecule, γ is the solid-liquid interfacial tension and x_s is the mean displacement of adsorbed molecules. Supersaturation is defined by $S = a_b / a_e - 1$, where a_b and a_e are the solute activity in the supersaturated solution and in the equilibrium, respectively. Using the BCF equation and assuming the number of dislocations in a dominant group to be proportional to the initial crystal size, Zeckic and Mitrovic [9] concluded that the mean growth rate is directly proportional to the mean initial crystal sizes at low supersaturation. This was experimentally confirmed for crystals belonging to one growth rate distribution maximum [10].

In the previous chapter, a new fundamental crystal growth model was derived taking into account recent findings on the dynamics of dislocation spirals and classical concepts of two dimensional nucleation and spiral growth. In this spiral nucleation model (SNM), the mass deposition rate per surface area units (R_G) is explicitly given as a function of the crystal size (L) and of other variables such as the density of activated spirals (n_{sp}) and the interstep distance (y_0):

$$R_G = \frac{2\pi\rho_s L h^3}{y_0} n_{sp} v \exp\left(-\frac{W}{kT}\right) S \tag{8.3}$$

Here, ρ_s is the crystal density and n_{sp} is a function of the total number of dislocations per m^2 (λ) and of the critical energy required for the formation of a stable spiral (ΔG_c),

$$n_{sp} = \frac{\lambda y_0}{2\bar{l}} \exp\left(-\frac{\Delta G_c}{kT}\right) \tag{8.4}$$

with,

$$\Delta G_c = 1.64 h \frac{\gamma^2 \Omega}{kT \ln(1+S)} \tag{8.5}$$

Equation (8.3) sets that growth rates of crystals having similar dislocation density and topological properties are in direct proportion to crystal size. Although linear dependences of R_G on the crystal size are often reported in the literature, it is also common to use more complex empirical relations. According to Mitrovic et al. [5] there is no reason for their use. Deviations from linearity may well result from the procedures adopted when measuring and analysing crystal growth kinetics in features like the duration of the experiments, the use of initial, instantaneous or mean crystal size over the runs, the way the mean crystal size is estimated, etc. This was illustrated by the work of Laguerie et al. [11] with citric acid monohydrate, when remarkably different R_G vs L relations were obtained by treating differently the experimental data. To avoid this kind of ambiguities one proposes to express the crystal growth rates in terms of mass deposition rate per unit of crystal volume (R_V). The "volumetric" growth rate can be directly computed from the variation of the crystal mass (m) in a given period Δt, regardless of the size, number and surface area of crystals during the experiments:

$$R_V = \frac{1}{V}\frac{\Delta m}{\Delta t} = \frac{\rho_s}{m}\frac{\Delta m}{\Delta t} = \rho_s \frac{\Delta \ln m}{\Delta t} \tag{8.6}$$

where V is the crystal volume. Assuming the validity of the SNM and of Eq. (8.3), R_V can be seen as the inherent growth rate of crystals having similar dislocation densities, since it can be calculated for a given temperature and supersaturation independently of the crystals size:

$$R_V = \frac{\beta}{\alpha}\frac{R_G}{L} = \frac{\beta}{\alpha}\frac{2\pi\rho_s h^3}{y_0} n_{sp} v \exp\left(-\frac{W}{kT}\right) S \tag{8.7}$$

where α and β are the volume and surface area shape factors. In a first application example of the SNM, interfacial properties were estimated from the measured dependence of R_G / L on the supersaturation (Chapter 7). In this chapter, the potential of this model will continue to be explored on the interpretation of SDG data of sucrose at 40 ºC.

8.2 Experimental section

Crystal growth and dissolution rates of sucrose were measured at 40.0 ± 0.1 ºC, in a 3 L jacketed batch crystallizer for different crystal sizes. The detailed experimental apparatus and procedures are described in Chapter 5. Briefly, an accurately known weight of seed crystals (~ 5 g) was introduced into the supersaturated solution and were allowed to grow at an agitation speed of 300 rpm and at controlled temperature during approximately 15 h. At the end of the growth period, the mass fraction of sucrose crystals was approximately 10%. Dissolution experiments immediately followed these periods by adding to the slightly supersaturated solution a rigorously weighted amount (about 100g) of ultra-pure water at the working temperature. An initial drop on the sucrose concentration occurs due to the introduction of water and the solution becomes undersaturated. Dissolution experiments were much faster than the preceding crystal growth. Generally, saturation was possible to be achieved in about 1 h.

The sucrose concentration was followed by an on-line refractometer and the mass of crystals was continuously computed by mass balance. Experiments were carried out with "small" seed crystals (sieve sizes between 0.125 and 0.250 mm), "medium" seed crystals (sieve sizes between 0.250 and 0.300 mm), and "large" seed crystals (sieve sizes between 0.300 and 0.425 mm). The instantaneous mean equivalent size of the crystals (L) was calculated every 10 seconds interval using the shape factors of sucrose crystals found by Bubnik and Kadlec [12]. The respective profiles are shown in Figure 8.1 for the three classes of seeds.

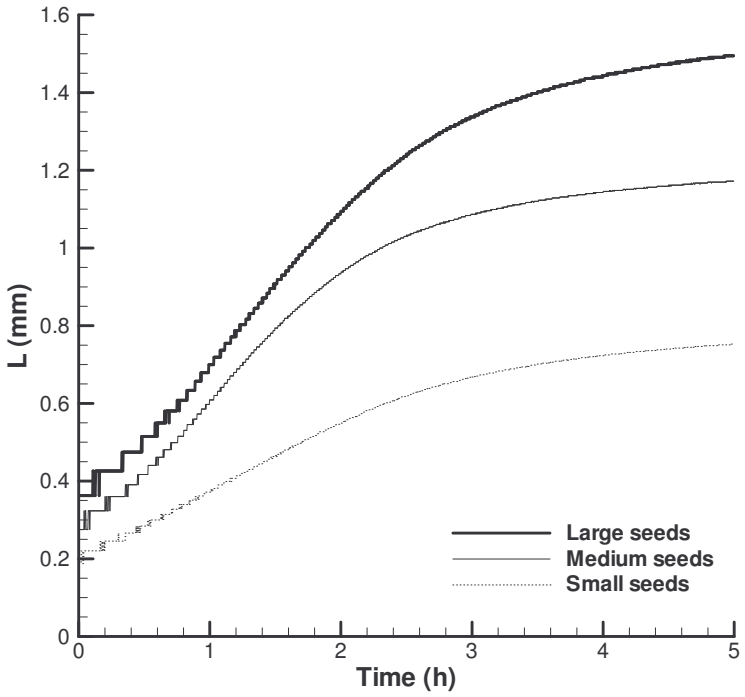

Figure 8.1. Evolution of the mean equivalent size of crystals during the growth experiments.

The overall crystal growth rate for a given time interval Δt was calculated considering the variation of the mass of crystals during that period, the crystal shape factors and the number of introduced crystals (N):

$$R_G = 3\frac{(\rho_s \alpha)^{2/3}}{N^{1/3}\beta}\frac{\Delta m^{1/3}}{\Delta t} \tag{8.8}$$

In its turn, the volumetric growth rate R_V was calculated using Eq. (8.6). The corresponding supersaturation for the period Δt was estimated from the average mole fraction (x_b) during that period and from the measured sucrose solubility at 40 ºC ($x_e = 0.1093$). Significant nucleation, crystal breakage and/or agglomeration were not found to have occurred.

8.3 Results and discussion

Figure 8.2 shows that both growth and dissolution rates increase with crystal size. The interpretation of SDG data of Figure 8.2a should not be detached from the effect of crystal size on mass transfer rates shown in Figure 8.2b.

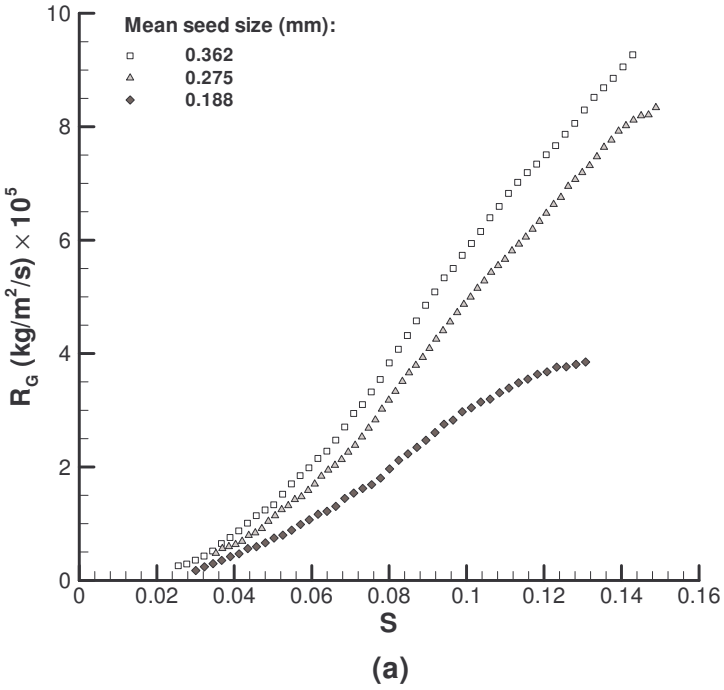

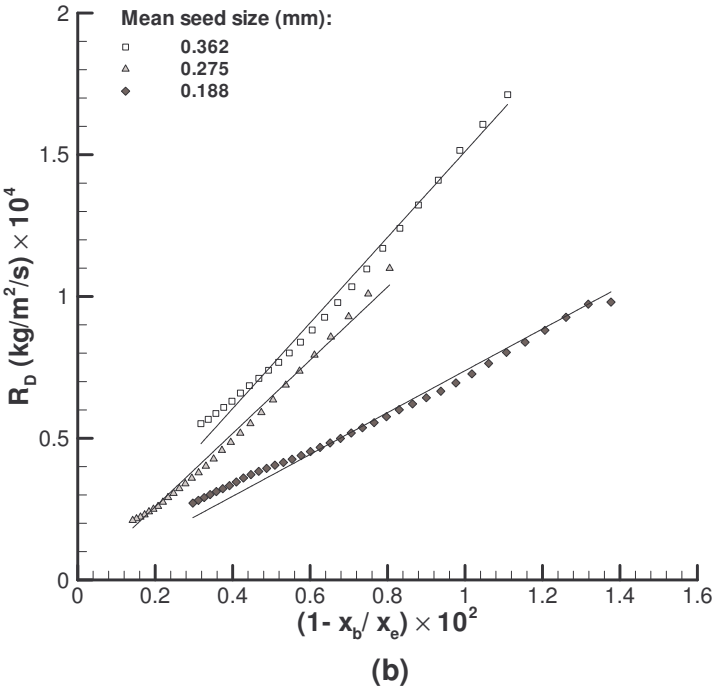

Figure 8.2. (a) Growth and (b) dissolution rates of sucrose in a batch crystallizer at 40ºC for different crystal sizes.

In Chapter 5, the importance of the diffusional resistance during growth of sucrose at 40 ºC was investigated by performing several growth and dissolution experiments of equally sized

crystals at different agitation speeds. It was found that crystal growth rates vary with agitation speed in the same proportion of the square root of the corresponding dissolution rates, i.e.,

$$\frac{R_{G_1}}{R_{G_2}} = \sqrt{\frac{R_{D_1}}{R_{D_2}}} \tag{8.9}$$

where the subscripts "1" and "2" correspond to two sets of hydrodynamic conditions and R_D is the dissolution rate. Based on this premise, one can conclude from Figure 8.2 that crystal size influences not only the system hydrodynamics but also the surface integration step during growth. If only the first effect was considered, the variation of the growth rate with crystal size (Figure 8.2a) would be smoother than the correspondent variation of the dissolution rates (Figure 8.2b). Instead of that, R_G strongly increases as the crystal size increases, suggesting a size-dependent integration kinetics. This is in accordance with other evidences previously reported by other authors [1, 13-16] and goes against the initial justification of SDG by means of variations on the diffusional resistance, alone [17].

With the purpose of quantifying the role of crystal size on the crystallization kinetics, the experimental results were expressed in terms of the volumetric growth rate (Figure 8.3).

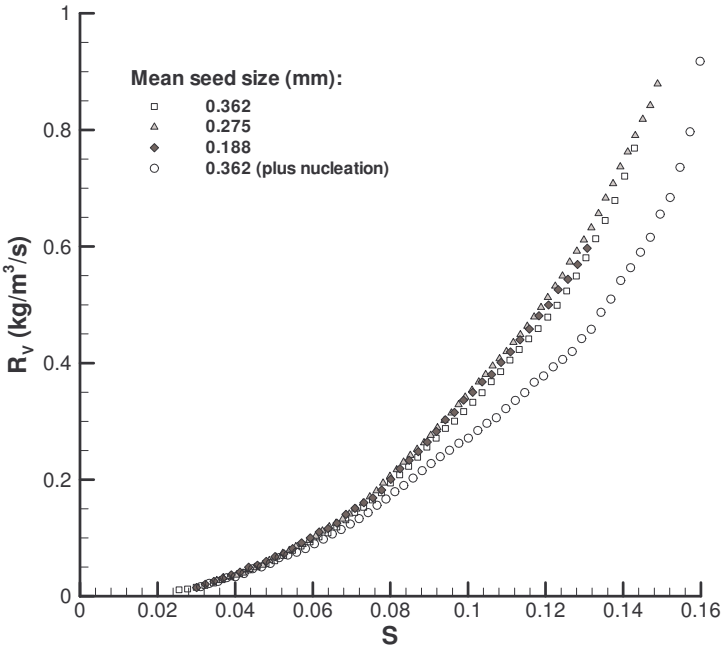

Figure 8.3. Volumetric growth rates of sucrose for different crystal sizes. One of the curves was obtained after the occurrence of spontaneous nucleation in the beginning of the experiment.

As shown in the figure, besides the experiments already presented in Figure 8.2, an additional growth result was considered, in which spontaneous nucleation have occurred at the beginning of the experiment. In this case, the initial crystal size distribution was strongly affected by the generation of new micro-particles at high supersaturation. After the abrupt crystal mass increase (and supersaturation decrease), R_V was possible to be computed taking into account the variation of the mass of crystals with time. The applicability of volumetric growth rates can therefore be extended to a great number of practical situations where the number and size of crystals are not known.

Changing the crystal size did not affect significantly the volumetric growth rate in the absence of nucleation. Contrarily to the strong dependence of R_G on the crystal size (Figure 8.2a), R_V is apparently size-independent over the considered range of supersaturation. The growth experiment preceded by spontaneous nucleation was the only exception to the apparent agreement between the results of Figure 8.3. Relatively to the standard growth experiments, the hydrodynamic conditions of the suspension were significantly altered by the presence of a great number of micro-crystals in solution, leading to much higher diffusional resistances during growth (see below). From the apparent independence of R_V on L and since $R_G = \alpha L R_V / \beta$, one concludes that the overall growth rate, R_G, is linearly dependent of crystal size. A similar conclusion can be drawn by analysing the variation of the particle size distributions through a growth experiment. Figure 8.4 shows the size distributions at the beginning (medium seed crystals) and the end of an experiment, after normalizing the crystal sizes by the corresponding median size ($L_{med} = 0.314$ mm before the experiment and $L_{med} = 0.802$ mm after it). Grown crystals for which $L / L_{med} < 0.5$ result from the occurrence of primary nucleation and crystal breakage. The small percentage of these cases does not significantly affect the growth rate results. Crystals having $L / L_{med} > 1.5$ are essentially conglomerates formed during the filtration, washing and drying of the grown crystals. Apparently, if one excludes these abnormal particles, the distributions of sieved seeds and grown crystals would be superimposed. The relation between growth rates of different sized crystals within a population corresponds, therefore, to the relation between the respective overall growth rates [18]. Once more, the linear correspondence between R_G and L is confirmed.

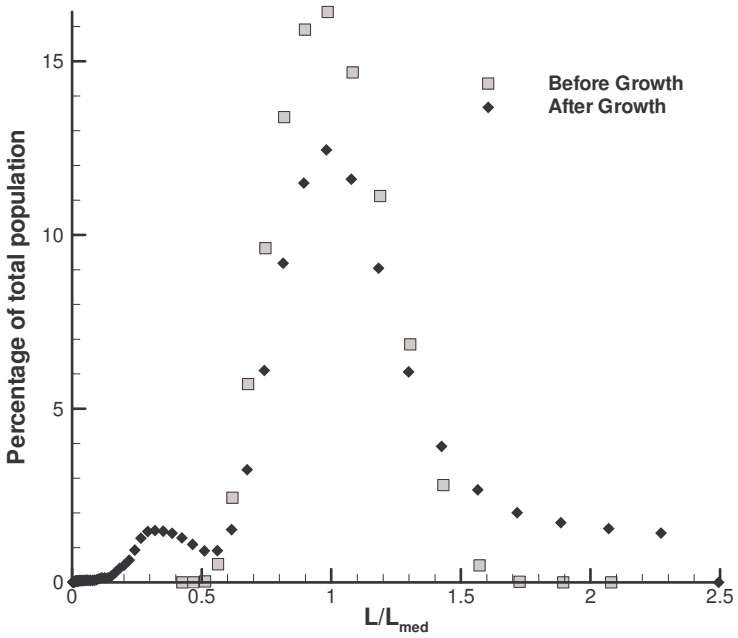

Figure 8.4. Scaled size distribution in a volume basis measured by laser light diffraction, before and after a growth experiment.

Empirical equations are commonly used to describe crystal growth kinetics in a straightforward way. Of the experimental curves shown in Figure 8.2 (R_G) and Figure 8.3 (R_V), only the latter ones are well described by a conventional power-law equation:

$$R_V = K_V S^{n_V} \tag{8.10}$$

where K_V and n_V are the empirical kinetic constant and kinetic order, respectively. Figure 8.5a illustrates the behaviour of the R_G vs. S curves. Although the overall rate equation is parabolic the apparent kinetic order is higher than 2 for low S and lower than 2 for high S. The observed changing growth kinetics is certainly related with the variation of crystal size during the experiments. Expressing the growth rates in terms of R_V one normalizes the kinetic effect of crystal size, with resulting invariant power-law rate equation over the supersaturation range (Figure 8.5b). Table 8.1 lists the fitting results for all growth experiments.

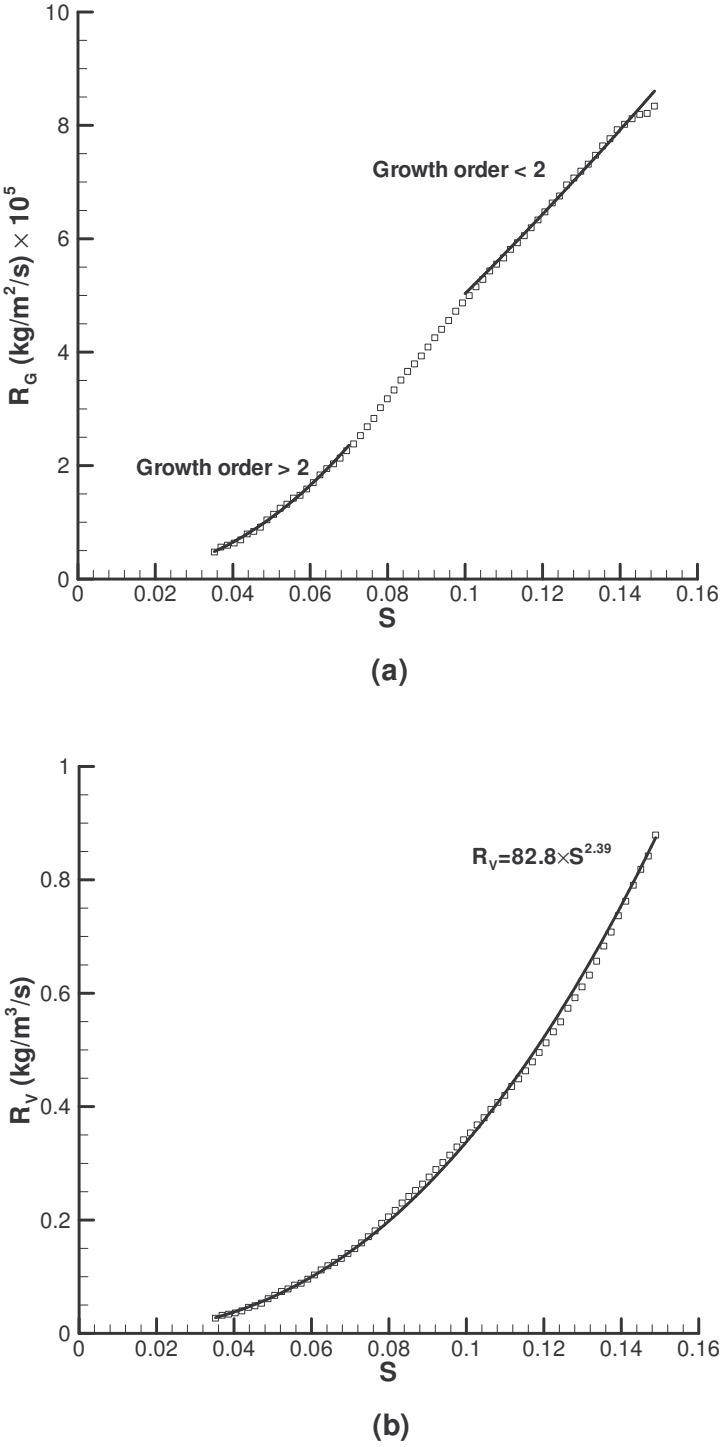

Figure 8.5. Plots of the (a) conventional and (b) volumetric growth rate of sucrose at 40 ºC and of the respective fits to a power-law equation. Seed crystals with sieve sizes between 0.250 and 0.300 mm were used.

Table 8.1. Parameters of Eq. (8.10) that best fit the experimental results presented in Figure 8.3.

Mean seed size (mm)	K_V	n_V	R^2
0.362	85.6	2.43	0.998
0.275	82.8	2.39	0.999
0.188	81.8	2.39	0.997
0.362	43.0	2.21	0.997

The concept of volumetric growth rate follows from the recently introduced spiral nucleation model (SNM) establishing a linear dependence of the integration rate on the crystal size. This model characterizes crystal growth without taking into account eventual mass transfer limitations, which in the case of sucrose at 40 ºC are known to exist. The relative weight of the kinetic and mass transfer steps are, however, well established for this system in Chapter 5. In the absence of significant diffusional resistances the crystal growth rate would be given by an equation of the type

$$R_G = \frac{k_{re}}{r+1} S^r \tag{8.11}$$

where k_{re} and r are the kinetic constants. Nevertheless, by comparing growth and dissolution kinetics measured under different hydrodynamic conditions, the crystal growth rate of sucrose was found to be considerably affected by the mass transfer coefficient during growth (k_d), so that

$$R_G = \sqrt{\frac{2k_{re}k_d}{r+1} S^{r+1}} \tag{8.12}$$

In Chapter 5, the successive growth experiments were performed keeping the same conditions of crystal size and number, with the purpose of avoiding SDG to interfere on the study of diffusional resistances during growth. Admitting now the validity of the SNM, the influence of crystal size on the kinetic step can be emphasized by letting $k_{re} = k'_{re} L$, where k'_{re} is a function of the physical and topological parameters of the crystal, and temperature. As a result, the relationship between growth rates obtained at same supersaturation and temperature but for different crystal size and hydrodynamic conditions will be given by

$$\frac{R_{G_1}}{R_{G_2}} = \sqrt{\frac{k_{d_1} L_1}{k_{d_2} L_2}} = \sqrt{\frac{R_{D_1} L_1}{R_{D_2} L_2}} \qquad (8.13)$$

where the second equality results from considering the mass transfer coefficients during growth and dissolution to be correspondent (see Chapter 5 for more details). Note that the equation previously used to investigate whether the influence of crystal size on the sucrose growth rate was merely diffusional or also kinetic (Eq. (8.9)) is a particular case of Eq. (8.13) when $L_1 = L_2$, i.e., when growth rates of equivalent sized crystals are compared. Rewriting Eq. (8.13) in order to obtain the corresponding ratio between volumetric growth rates, gives

$$\frac{R_{V_1}}{R_{V_2}} = \sqrt{\frac{R_{D_1}/L_1}{R_{D_2}/L_2}} \qquad (8.14)$$

The verification of this relationship will be done by comparing the R_V vs. S curves presented in Figure 8.3 with the corresponding dissolution kinetics recalculated in terms of the R_D/L ratio:

$$\frac{R_D}{L} = -\frac{\alpha \rho_s}{\beta} \frac{\Delta \ln m}{\Delta t} \qquad (8.15)$$

This definition can as well be used when the number and size of crystals are not known. The obtained dissolution data are shown in Figure 8.6.

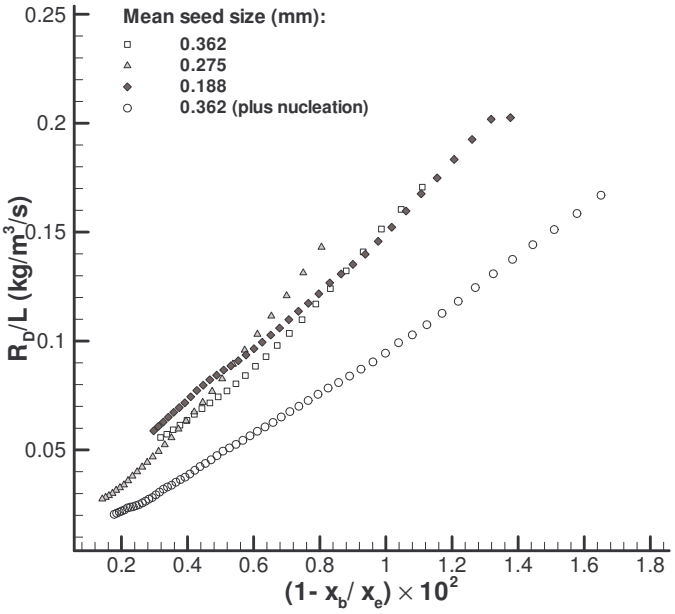

Figure 8.6. Representation of the dissolution rates of sucrose normalized by the mean equivalent crystal size, for different crystal sizes and for the nucleation-preceded experiment.

An equation of the type $R_D/L = K_D\left(1 - x_b/x_e\right)$ was used to fit the results – Table 8.2.

Table 8.2. Dissolution coefficients that best fit the experimental results shown in Figure 8.6.

Mean seed size (mm)	K_D	R^2
0.362	0.151	0.990
0.275	0.168	0.993
0.188	0.155	0.969
0.362	0.097	0.998

The influence of crystal size on the normalized dissolution rate is hardly distinguishable among experiences with controlled crystal size and number. This pattern entirely confirms what would be expected from Eq. (8.14) and from the growth kinetics shown in Figure 8.3. In fact, the small differences between the dissolution rates of Figure 8.6 are even smaller in the corresponding representation of volumetric growth rates. The differences found in each plot may well be interrelated by the square-root factor expected by Eq. (8.14). An additional confirmation of this equation results from the relation between growth and dissolution rates obtained after the occurrence of spontaneous nucleation: using the kinetic constants of Table 8.1 corresponding to large seeds, with and without nucleation one obtains

$$\frac{R_{V,\ without\ n.}}{R_{V,\ with\ n.}} = \sqrt{\frac{K_{D,\ without\ n.}}{K_{D,\ with\ n.}}} = 1.2 \tag{8.16}$$

for a reference supersaturation of 0.1. This example illustrates how the crystallization of sucrose at 40 ºC can be successfully explained in terms of the influence of supersaturation, diffusional resistance and crystal size on the growth rate by combining an engineering model concerned with the relative importance of the mass transfer and kinetic steps, with the fundamental perspective of crystal growth given by the SNM.

Summing up, the characterization of SDG started by using Eq. (8.9) to identify this phenomenon in the results of Figure 8.2a; the origin of the different growth kinetics obtained was shown to be diffusional and kinetic. Then, the overall growth rate was found to increase about linearly with crystal size according to the representation of the volumetric growth rates (Figure 8.3) and subsequently, from the normalized crystal size distributions shown in Figure 8.4. Finally, the confirmation of Eq. (8.14) proved that, besides the overall growth rate, the

integration step rate is also linearly dependent of the crystal size in accordance to what is expected by the SNM. Other theoretical models admitting this correspondence only partially explain the obtained results. In particular, in the BCF mechanism as seen by Zeckic and Mitrovic [9] the direct influence of crystal size on R_G is restricted to a limit case of the growth rate equation (Eq. (8.1)). As shown in the analysis of Figure 8.2a and Figure 8.3, the linearity of the $R_G(L)$ dependence was verified in spite of the supersaturation range and kinetic behaviour.

8.4 Conclusions

In the present work, the influence of the crystal size on the growth kinetics of sucrose at 40 ºC is characterized in a systematic way. Crystal size has a two-way effect on the mass transfer rate and on the integration mechanism during growth. The introduced spiral nucleation model provides a fundamental basis for the latter effect, proposing a linear dependence of the integration rate on the crystal size. Accordingly, an alternative growth rate definition is put forward, where the mass deposition rate is expressed per crystal volume units. Besides being theoretically consistent, the volumetric growth rate concept is of great practical interest since crystal growth kinetics can be calculated in situations of unknown crystal number and size. The growth data of sucrose expressed in terms of the volumetric growth rates are size-independent at comparable hydrodynamic conditions. This shows that the overall growth rate varies linearly with the crystal characteristic dimension. The same can be confirmed from the superposition of the normalized crystal size distributions before and after the growth experiments. By combining the spiral nucleation model with an established diffusion-integration engineering model, the crystallization of sucrose at 40 ºC was successfully explained in terms of the combined influence of supersaturation, diffusional resistance and crystal size.

References

[1] J. Garside and S. J. Jancic, Growth and dissolution of potash alum crystals in the subsieve size range. *AIChE J.*, **1976,** 22, 887-894.

[2] M. W. Girolami and R. W. Rousseau, Size-dependent crystal growth - A manifestation of growth rate dispersion in the potassium alum-water system. *AIChE J.*, **1985,** 31, 1821-1828.

[3] B. LoI Mi Lung-Somarriba, M. Moscosa-Santillan, C. Porte, and A. Delacroix, Effect of seeded surface area on crystal size distribution in glycine batch cooling crystallization: a seeding methodology. *J. Cryst. Growth*, **2004,** 270, 624-632.

[4] X. F. Abegg, J. D. Stevens, and M. A. Larson, Crystal size distributions in continous crystallizers when growth rate is size dependent. *AIChE J.*, **1968,** 14, 118-122.

[5] M. M. Mitrovic, A. A. Zekic, and M. M. Napijalo, Correlation between the crystal size and crystal growth rate of KDP and Rochelle salt crystals. *J. Cryst. Growth*, **2000,** 216, 437.

[6] E. T. White, L. L. Bending, and M. A. Larson, in *Analysis and design of crystallization processes*, (R. W. Rousseau, M. A. Larson, eds.), AIChE Symposium Series, New-York, **1976**.

[7] W. K. Burton, N. Cabrera, and F. C. Frank, The growth of crystals and the equilibrium structure of their surfaces. *Phil. Trans. Roy. Soc. London*, **1951,** 243, 299-358.

[8] J. Garside and R. J. Davey, Secondary contact nucleation: kinetics, growth and scale-up. *Chem. Eng. Commun.*, **1980,** 4, 393-424.

[9] A. A. Zekic and M. M. Mitrovic, Dependence of growth rate on initial crystal size. *J. Cryst. Growth*, **2003,** 258, 204-210.

[10] M. M. Mitrovic, A. A. Zekic, and Z. Z. Ilic, Connection between the growth rate distribution and the size dependent crystal growth. *Chem. Phys. Lett.*, **2002,** 361, 312.

[11] C. Laguerie, G. Muratet, and H. Angelino, Choix d'une methode de determination des vitesses de croissance cristalline en couche fluidisee: Application a la croissance de cristaux d'acid. *The Chem. Eng. J.*, **1977,** 14, 17.

[12] Z. Bubnik and P. Kadlec, Sucrose crystal shape factors. *Zuckerindustrie*, **1992,** 117, 345-350.

[13] J. Garside, J. W. Mullin, and S. N. Das, Growth and dissolution kinetics of potassium sulfate crystals in an agitated vessel. *Ind. Eng. Chem. Fundam.*, **1974,** 13, 299-305.

[14] J. Garside, V. R. Phillips, and M. B. Shah, On size-dependent crystal growth. *Ind. Eng. Chem. Fundam.*, **1976,** 15, 230-233.

[15] J. Mydlarz and A. G. Jones, Growth and dissolution kinetics of potassium sulphate crystals in aqueous 2-propanol solutions. *Chem. Eng. Sci.*, **1989,** 44, 1391-1402.

[16] V. R. Phillips and N. Epstein, Growth of nickel sulfate in a laboratory-scale fluidized-bed crystallizer. *AIChE J.*, **1974,** 20, 678-687.

[17] W. L. McCabe and R. P. Stevens, *Chem. Eng. Progr.*, **1951,** 47, 168-174.

[18] E. T. White, D. L. Mackintosh, B. K. Butler, H. Zhang, and M. R. Johns, in *Proceedings of the Australian Society of Sugar Cane Technologists*, (D. M. Hogarth, ed.), **1998**.

PART IV

APPLICATION EXAMPLES AND CONCLUSIONS

9. Effect of cane sugar impurities on the sucrose growth kinetics

Overview

In Chapter 6, the effect of impurities on the crystal growth rate was described by means of a new kinetic model called “competitive adsorption model” (CAM). The validation of this theory was made with experimental data taken from literature reporting several examples on how impurities can interfere with the growth mechanism. In this chapter, the CAM is applied to the sucrose growth kinetics measured in a pilot evaporative crystallizer, under industry-like conditions. In accordance with the general pattern expected by empirical correlations used in sugar industry, crystal growth rates decrease as the non-sucrose concentration increases. The kinetic effect of the impurities existing in cane sugar solutions is characterized from a fundamental point of view, by estimating the corresponding average CAM parameters. The obtained results indicate that this type of impurities can be greatly adsorbed at the sugar crystal surface, even though their effectiveness on the growth rate lowering is low.

9.1 Introduction

According to the competitive adsorption model (CAM), the action of a given impurity during crystal growth is mainly dependent on its capability of adsorbing at crystal surface and on the capacity of the adsorbed molecule to migrate across the surface and occupy potential active sites for the crystallizing solute integration. The first step is quantified by the impurity surface coverage for competitive adsorption,

$$\theta_s = \frac{k_i c_i}{k_i c_i + k_p S + 1} \tag{9.1}$$

while the relative weight of the thermodynamic processes occurring at the surface, determinates the impurity activity given in terms of the β parameter (Chapter 6). The growth rate decrease relatively to pure solutions is proportional to the number of active sites occupied by the impurity. As a result, the relative growth rate in impure and pure systems is given by the following CAM equation:

$$\frac{R}{R_0} = 1 - \beta \frac{k_i c_i}{k_i c_i + k_p S + 1} \tag{9.2}$$

In Chapter 6, we discussed the action of single impurities during crystal growth, but in most applications, different impurities are present simultaneously and have a combined effect on the growth kinetics. In the industrial crystallization of sucrose, empirical equations are used to describe the variation of sucrose solubility and growth rate with the solution purity, generally expressed in terms of the non-sucrose to water ratio (NS/W). The estimated empirical parameters are valid for the specific composition of the syrup used on the measurements. It is reported that in beet sugar industry, raffinose is the most influencing impurity, while in cane sugar, oligosaccharides and the dextran polysaccharide are suspected to be the ones having a determinant role [1, 2]. From the study carried out by Smythe on the isolated influence of some of these species on the sucrose growth kinetics, one may expect active sugar beet impurities (high β) and poorly active sugar cane impurities (low β) [3]. Using crystal growth rates of sucrose measured in a pilot vacuum pan (evaporative crystallizer), an application example of the CAM is now given in order to characterize the kinetic influence of non-sucrose compounds in typical cane sugar syrups.

9.2 Experimental section

Crystal growth rates of sucrose were measured in a 50 L pilot vacuum pan at different NS/W levels. The detailed procedure and experimental apparatus are described in Chapters 2 and 3. The experiments were carried out at constant amount of water by means of an automatic control of the microwave density. Water was continuously admitted into the pan in order to balance the evaporation rate. Three types of syrups were used: industrial cane syrup from Cora Texas mill (Louisiana), synthetic syrup, prepared with refinery white sugar and tap water , and blended syrup obtained by adding 1 part of the industrial syrup to approximately 8 parts of synthetic syrup. Composition analysis indicates that the industrial syrup has 87.75% apparent purity (sucrose content measured by the polarization method), 65.42% of dissolved solids measured by refractometry, 1.12% of glucose and 1.16% of fructose measured by HPLC, and 2.22% of ash content. In the experiments with industrial syrup, different NS/W levels correspond to different boiling stages. Initially, the crystallized matter content (CC) is lower and the mother liquor purity is higher; as the crystallization proceeds, supersaturation is achieved by means of increasingly higher amounts of evaporated water, and the NS/W level is increased. Table 9.1 summarizes the main experimental conditions at which growth rates were measured.

Table 9.1. Experimental conditions of the sucrose growth experiments.

Experiment #	NS/W	Syrup	Average Temperature (ºC)	CC (%)	
				Min	Max
1	0	Synthetic	62.3	0	13.6
2	0	Synthetic	62.3	13.6	22.5
3	0.058	Blended	62.1	0	17.1
4	0.434	Cane	62.0	0	11.0
5	0.490	Cane	65.6	8.1	16.9
6	0.597	Cane	62.2	18.5	31.0

Our previous growth experiments at laboratory scale suggest a linear dependence of the overall growth rate of sucrose (R_G) on the instantaneous crystal size (L) (Chapter 8). Based on this premise, the kinetic effect of crystal size was normalized by calculating the crystal growth rates in a volumetric basis:

$$R_V = \frac{\beta}{\alpha}\frac{R_G}{L} = 6\rho_s \frac{R}{L} \tag{9.3}$$

where α and β are the volume and surface area shape factors. The volumetric growth rate is directly computed from the variation of the mass of crystals, regardless of their size, number and surface area during the experiments, according to the following definition:

$$R_V = \rho_s \frac{\Delta \ln m}{\Delta t} \tag{9.4}$$

The average supersaturation in the time interval Δt is calculated from the average dissolved sucrose concentration (c) in the same period, and from the sucrose solubility (c^*) obtained for the set of conditions of each experiment according to the method described in Chapter 3.

9.3 Results and discussion

Figure 9.1 shows the growth rate curves obtained with synthetic syrup ("pure" case) at different experimental conditions (see Table 9.1). Equally spaced data points are considered.

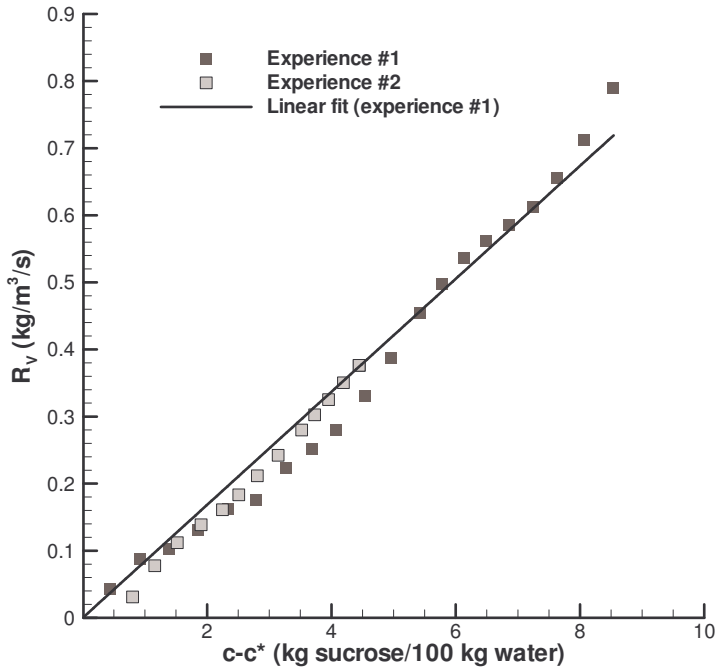

Figure 9.1. Volumetric growth rates of sucrose obtained with synthetic syrup ($NS/W \sim 0$).

Both curves are in good agreement, despite of the differences of crystal size and mass fraction, and of hydrodynamic conditions. This fact sustains the use of volumetric growth

rates to account for the kinetic influence of crystal size, as well as, our previous results reporting almost invariable mass transfer resistances at different hydrodynamic conditions inside the pan. (see Chapter 3 for more details). Variations on the volumetric growth rate of sucrose with NS/W can therefore be attributed to the impurities influence on the crystal growth kinetics. The differences found are represented in Figure 9.2. All the curves were well fitted by a rate law of the form

$$R_V = K_V \Delta c \tag{9.5}$$

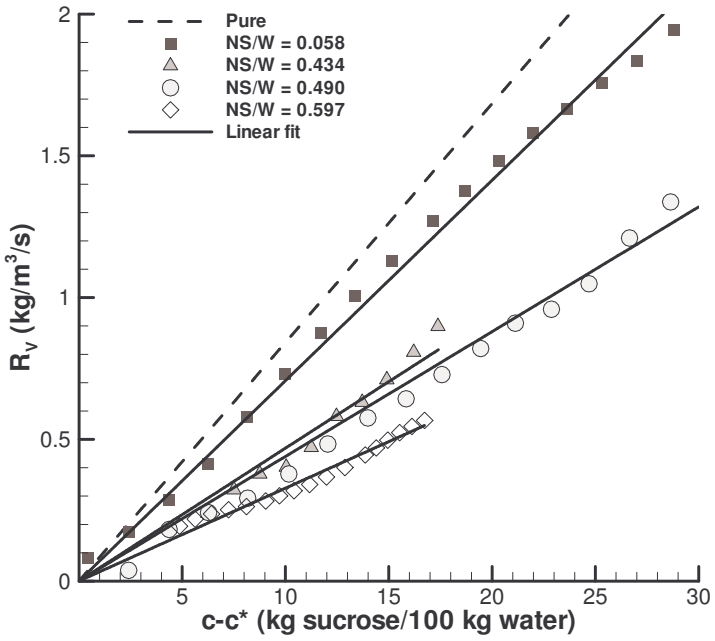

Figure 9.2. Volumetric growth rates of sucrose obtained at different NS/W levels.

A linear relationship between crystal growth rates and supersaturation was already reported by Wright and White in their mathematical model of vacuum pan crystallization [4]. At same time, they found an exponential dependence of the growth rate on NS/W:

$$\frac{R_1}{R_2} = \exp\left\{-1.75\left[\left(\frac{NS}{W}\right)_1 - \left(\frac{NS}{W}\right)_2\right]\right\} \tag{9.6}$$

Since the publication of the work of Wright and White, other authors have been proposing alternative empirical parameters for the same relationships [2, 5]. Using Eq. (9.6) and the equivalence given in Eq. (9.3), one can estimate the relative growth rate in impure and pure solutions, irrespective of the crystal size:

$$\frac{R_V}{R_{V_0}} = \exp\left(-1.75\frac{NS}{W}\right) \tag{9.7}$$

The form of Eq. (9.7) can be tested against the results of Figure 9.2. With that purpose, the relative volumetric growth rates were calculated using the rate constants that best fit the experimental curves (Table 9.2). The obtained results are plotted as a function of NS/W in Figure 9.3. A fairly good adjustment was obtained using an exponential constant of -1.45. This indicates a somewhat lower growth rate variation with NS/W than Eq. (9.7).

Table 9.2 Volumetric rate constants that best fitted the results of Figures 9.1 and 9.2, and relative volumetric growth rates, at different NS/W levels.

Experiment #	NS/W	K_V	R^2	R_V/R_{V_0}
1	0	0.0842	0.974	1
3	0.058	0.0707	0.994	0.840
4	0.434	0.0469	0.948	0.557
5	0.490	0.0440	0.980	0.522
6	0.597	0.0328	0.971	0.390

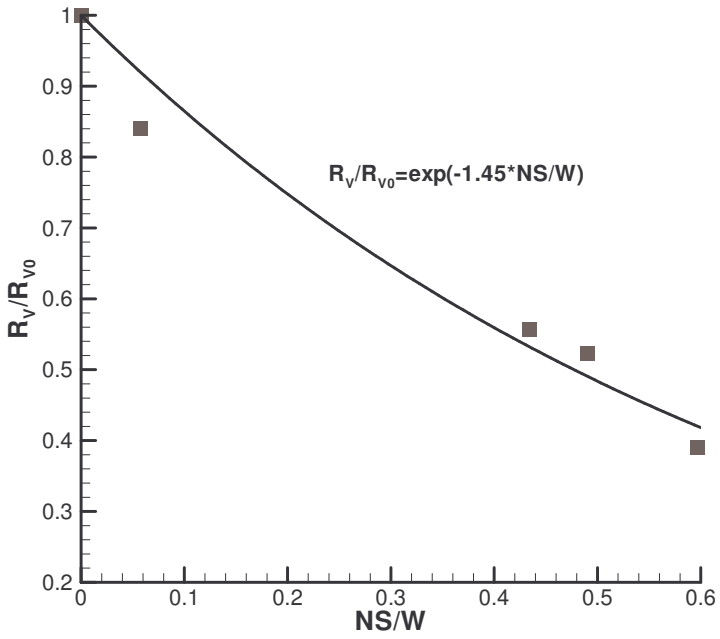

Figure 9.3. Influence of NS/W on the relative volumetric growth rates of sucrose, and respective fit using an exponential curve.

Although useful for sugar industry, the exponential-type equation correlating the relative growth rates and the impurity concentration lacks of physical meaning. The competitive adsorption theory can be applied to sugar crystallization by characterizing the overall action of the non-sucrose compounds through average CAM parameters. Linearizing Eq. (9.2) and expressing it in terms of volumetric rates yields:

$$\frac{1}{1-R_V/R_{V_0}} = \frac{1+k_pS}{\beta}\frac{1}{k_ic_i} + \frac{1}{\beta} \tag{9.8}$$

The dimensionless impurity concentration k_ic_i can be conveniently given as a function of the non-sucrose to water ratio, by letting $k_ic_i = k_i'(NS/W)$. The relative growth rates of sucrose are a strong function of NS/W but did not change significantly with supersaturation. At low supersaturations, this fact is explained by the simplified form of Eq. (9.8), admitting $k_pS \ll 1$:

$$\frac{1}{1-R_V/R_{V_0}} = \frac{1}{k_i'\beta}\frac{1}{NS/W} + \frac{1}{\beta} \tag{9.9}$$

The parameters β and k_i' are easily obtained by fitting Eq. (9.9) to the data of Table 9.2. In so doing, the average impurity activity of the compounds in the cane solutions is characterized by $\beta = 0.90$ and $k_i' = 2.64$. In Figure 9.4, the obtained influence of NS/W on the relative growth rates can be compared with the one given by the CAM using the fitted parameters. The good agreement found, confirms that the new model is a valuable alternative to the empirical correlations used so far in sugar industry. As expected, the impurities in sugar cane solutions are moderately active in suppressing the sucrose growth rate. Since $\beta < 1$, this example corresponds to a system exhibiting negative critical supersaturation (see Chapter 6 for more details):

$$S_c = \frac{k_ic_i(\beta-1)-1}{k_p} \tag{9.10}$$

The marked growth rate decrease is due do the extensive impurity adsorption in the considered range of NS/W. For example, for $NS/W = 0.6$, the overall surface coverage is given by

$$\theta_s \approx \frac{k_i'(NS/W)}{k_i'(NS/W)+1} = 0.61 \tag{9.11}$$

which is equivalent to say that, under these conditions, more than 60% of the sucrose crystal surface is covered by non-sucrose compounds.

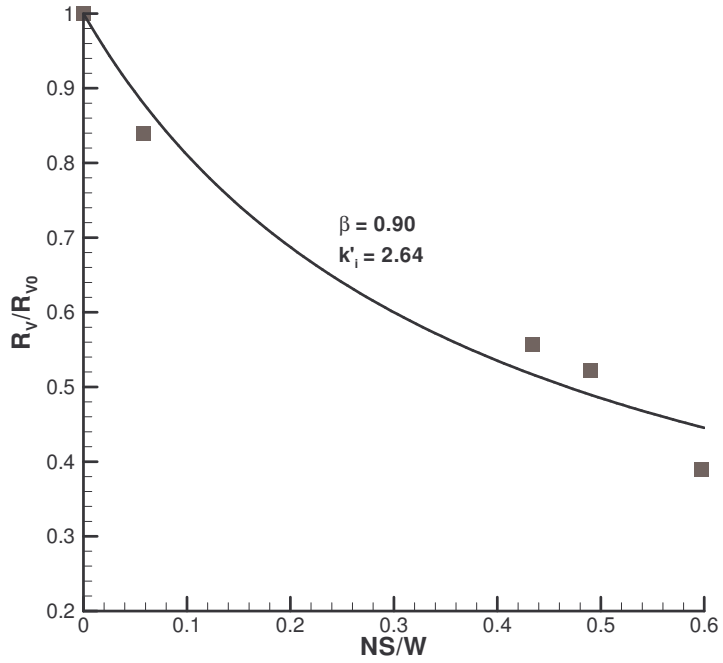

Figure 9.4. Experimental and theoretical influence of NS/W on the relative volumetric growth rates of sucrose. The CAM curve is represented for the parameters of Eq. (9.9) that best fit the experimental data.

9.4 Conclusions

Crystal growth rates of sucrose measured in a pilot vacuum pan at different impurity concentrations were well described by the CAM. The average activity of the non-sucrose compounds in cane sugar syrups was estimated to be $\beta = 0.90$, which confirms the low kinetic effect predicted in literature for these compounds. Using the fitted parameters, it was possible to calculate the fraction of the crystals surface occupied by adsorbed impurities as a function of their concentration in solution. This application example illustrates the robustness of the new model and demonstrates the CAM to be a valuable alternative to the empirical correlations used so far in sugar industry.

References

[1] Z. Bubnik, G. Vaccari, G. Mantovani, G. Sgualdino, and P. Kadlec, Effect of dextran, glucose and fructose on sucrose crystal elongation and morphology. *Zuckerindustrie*, **1992,** 117, 557-561.

[2] D. J. Love, Dynamic modelling and optimal control of sugar crystallisation in a multi-compartment continuous vacuum pan, Ph.D. Thesis, University of Natal, Durban, South Africa, **2002**.

[3] B. M. Smythe, Sucrose crystal growth.I. Rate of crystal growth in the presence of impurities. *Aust. J. Chem.*, **1967,** 20, 1097-1114.

[4] P. G. Wright and E. T. White, in *Proc. Int. Soc. Sugar Cane Technol.*, Australia, **1974**.

[5] Q. Li-Wu and A. B. Corripio, Experimental verification of a dynamic model of a vacuum pan. *J. Amer. Soc. Sugar Cane Technol.*, **1985,** 5, 77-84.

10. The influence of temperature and growth rate history on crystal growth

Overview

Crystallization experiments of sucrose are carried out in a batch crystallizer to study the effect of temperature and growth rate history on the crystal growth kinetics. In one of the growth methods adopted, the isothermal volumetric growth rate (R_V) is determined as a function of supersaturation (S) at 35, 40 and 45 ºC. In the other, crystals are allowed to grow at constant supersaturation by automatically controlling the solution temperature as the solute concentration decreased. Using the latter method, R_V is continuously calculated as the solution is cooled. The obtained results are interpreted using empirical, engineering and fundamental perspectives of crystal growth. Firstly, the overall activation energy (E_A) is determined from the empirical growth constants obtained in the isothermal method. The concept of falsified kinetics, widely used in chemical reaction engineering, is then extended to the crystal growth of sucrose in order to estimate the true activation energy (E_T) from the diffusion-affected constant, E_A. Considerably different $\ln R_V$ vs $1/T$ curves are obtained in the isothermal and constant supersaturation methods. The differences found are explained from the viewpoint of the spiral nucleation mechanism, taking into account different crystal surface properties caused by the growth rate history in each method. Finally, the crystal growth curve obtained in the batch crystallizer at 40 ºC is compared with the one obtained in a fluidized bed crystallizer at the same temperature. Apparently divergent results are explained

by the effects of crystal size, hydrodynamic conditions and growth rate history on the crystallization kinetics of sucrose.

10.1 Introduction

Crystal growth from solution has been described by empirical, engineering or fundamental models depending on the purposes and degree of detail envisaged. Theoretical relations between crystal growth rate and main variables such as supersaturation or temperature often involve complex parameters and mathematics which are not suitable for practical purposes [1]. In those cases, the simple arrangement in series of a volume diffusion step and the solute integration at crystal surface is preferred to describe crystal growth, since only kinetic and mass transfer parameters are involved [2]. As discussed in Chapters 4 and 5, for simple integration kinetics this two step model can be simplified to the form of the most widely used growth rate equation:

$$R_G = K_G S^g \tag{10.1}$$

In most applications the parameters of this equation are, however, assumed to be purely empirical [3, 4]. Modifications to Eq. (10.1) are frequently made to account for the effect of crystal size on the growth rates. Some of the correlations used were previously reviewed in the works of Abegg et al. [5], Mitrovic et al. [6] and White et al. [7]. According to Mitrovic et al. [6], there is no reason for using complex relations between growth rate and crystal size since this dependence is, in general, linear. Based on fundamental arguments supporting this linearity, one proposed the crystal growth rates to be expressed in terms of mass deposition rate per unit of crystal volume (Chapter 8),

$$R_V = \frac{1}{V}\frac{\Delta m}{\Delta t} = K_V S^{n_V} \tag{10.2}$$

so that R_G and R_V can be related using the volume and surface area shape factors (α and β, respectively):

$$R_V = \frac{\beta}{\alpha}\frac{R_G}{L} \tag{10.3}$$

The volumetric growth rate R_V can be directly computed from the variation of the mass of crystals with time, regardless of their size, number and surface area. The kinetic constant K_V is related with temperature by an Arrhenius-type equation:

$$K_V = K_{V0} \exp\left(-\frac{E_A}{RT}\right) \tag{10.4}$$

where K_{V0} is a constant and E_A is the overall activation energy.

In Chapter 4, an alternative engineering approach to the role of diffusional resistance during growth from solution was presented. The incorporation of molecules into the crystal lattice is assumed to be preceded by volume diffusion and solute adsorption along the stagnant film surrounding the particle. Based on these simultaneous resistances, a generalized growth rate expression was found relating R_G with supersaturation, mass transfer coefficient (k_d), and the kinetic parameters associated to the adsorption rate (k_r and r):

$$R_G = k_r S^r \cdot \frac{\eta}{r+1} \tag{10.5}$$

where η is called the effectiveness factor and corresponds to

$$\eta = \frac{2}{\phi_g}\left\{\frac{1}{\tanh\left(\phi_g\right)} - \frac{1}{\sinh\left(\phi_g\right)}\right\} \tag{10.6}$$

with

$$\phi_g = \sqrt{\frac{2}{r+1} \cdot \frac{k_r}{k_d} S^{r-1}} \tag{10.7}$$

The validity of this parallel step model (PSM) was confirmed against experimental data taken from literature and from growth experiments with sucrose in a batch crystallizer (Chapter 5).

In the last years, a great number of works have been published reporting the observation of growth features on crystal surfaces using atomic force microscopy. The new perspectives provided do not always confirm classical fundamental theories suggested more than 50 years ago. In Chapter 7, a new atomistic representation of crystal growth was proposed where classical concepts of two dimensional nucleation and spiral growth were combined with recent findings on the formation and development of steps from surface dislocations. Through the so-called spiral nucleation model (SNM), the crystal growth rate is

related with conventional variables such as supersaturation, temperature and crystal size, and with surface properties such as the interfacial tension (γ), and the width and height of steps (h and y_0, respectively):

$$\frac{R_G}{L} = \frac{2\pi\rho_s h^3}{y_0} n_{sp} v \exp\left(-\frac{W}{kT}\right) S \tag{10.8}$$

In this equation, n_{sp} corresponds to the fraction of total dislocation density on the surface λ, whose resulting spirals reached the thermodynamic barrier ΔG_c and continued on growing:

$$n_{sp} = \frac{\lambda y_0}{2\bar{l}} \exp\left(-\frac{\Delta G_c}{kT}\right) \tag{10.9}$$

and

$$\Delta G_c = 1.64h \frac{\gamma^2 \Omega}{kT \ln(1+S)} \tag{10.10}$$

Theoretical and empirical models are conventionally used in an unrelated way, which contributes to the existing gap between micro and macro scale models [8]. Equations (10.1), (10.5) and (10.8) provide three distinct definitions of R_G corresponding to increasingly refined perspectives of the crystal growth physics and chemistry. In this chapter, it is aimed to link up these definitions on the interpretation of the influence of temperature on the growth kinetics of sucrose. Additionally, differences between results obtained using different growth techniques are discussed in the light of the new theories under consideration.

10.2 Experimental section

10.2.1 Growth in a batch crystallizer at constant temperature

Crystal growth rates of sucrose were measured in a 3 L jacketed batch crystallizer as a function of supersaturation at 35, 40 and 45 ºC. The detailed experimental apparatus and procedures are described in Chapter 5. In these experiments, temperature was automatically controlled by regulating the hot to cold water ratio circulating in the crystallizer jacket via a three way electronic valve. The volumetric growth rate for a given time interval Δt was calculated from the variation of the logarithm of the mass of crystals during that period:

$$R_V = \rho_s \frac{\Delta \ln m}{\Delta t} \tag{10.11}$$

The corresponding supersaturation was estimated from the average mole fraction (x_b) during the time interval Δt and from the sucrose solubility expressed in terms of mole fraction (x_e). The sucrose solubility was calculated at the operating temperature according to the relation found by Maurandi et al. [9]. Significant variation of the crystal mass occurred throughout a period of about 5 h and it was preceded by a pre-growth period of about 40 min.

10.2.2 Growth in a batch crystallizer at constant supersaturation

The influence of temperature on the crystal growth rate of sucrose was measured at constant supersaturation ($S = 0.114$) by adopting an analogous procedure to that just described for isothermal growth rates. The automatic controller of the 3 L jacketed batch crystallizer was this time set to control the supersaturation, using as inputs the solute concentration and the sucrose solubility at the solution temperature. The aqueous solution of sucrose with $x_b = 0.1270$ was prepared at 60 ºC by dissolving refinery white sugar in ultra-pure water. Once the automatic control was started, the solution was cooled down to 44.0 ºC in order to achieve the supersaturation set-point. At that point, 5g of seed crystals with sieve sizes between 0.250 and 0.300 mm were introduced into the supersaturated solution and were allowed to grow at an agitation speed of 300 rpm. As the growth proceeded, the solution was slowly cooled down (Figure 10.1a) in order to balance the sucrose concentration decrease and keep the supersaturation constant (Figure 10.1b). Again, the volumetric growth rate for a given time interval Δt was calculated from Eq. (10.11), using the variation of the mass of crystals obtained by mass balance. The corresponding solution temperature is given by the average temperature during the time interval Δt. The growth experiment ended when the solution reached the room temperature.

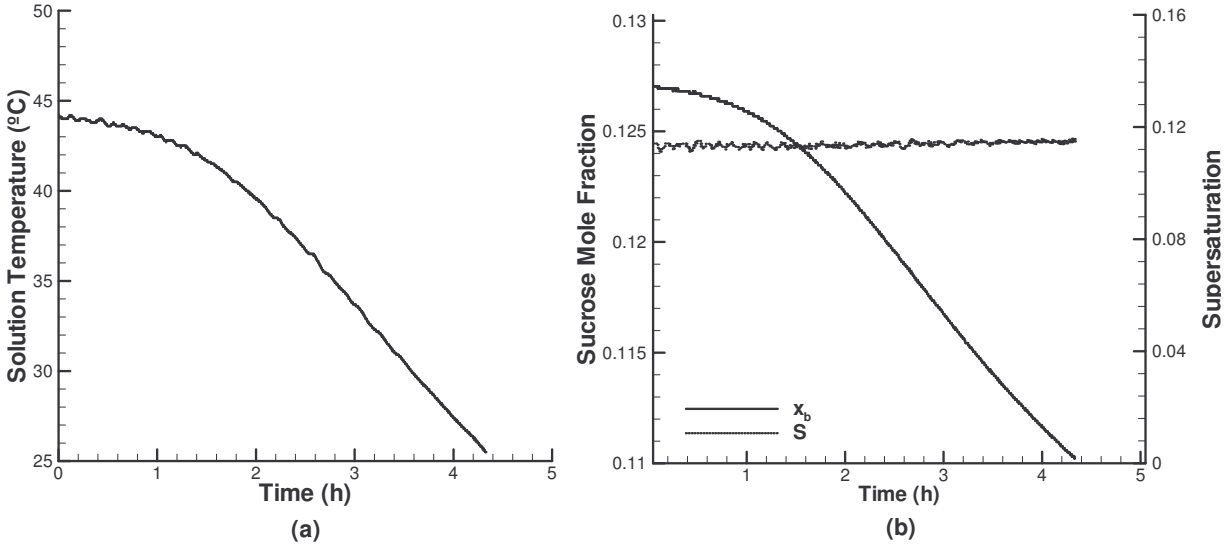

Figure 10.1. Evolution of (a) the solution temperature, and (b) the sucrose mole fraction and supersaturation during the batch growth experience at controlled supersaturation.

10.3 Results and discussion

Figure 10.2 shows the variation of the volumetric growth rate with supersaturation, for the three temperatures adopted in the isothermal method.

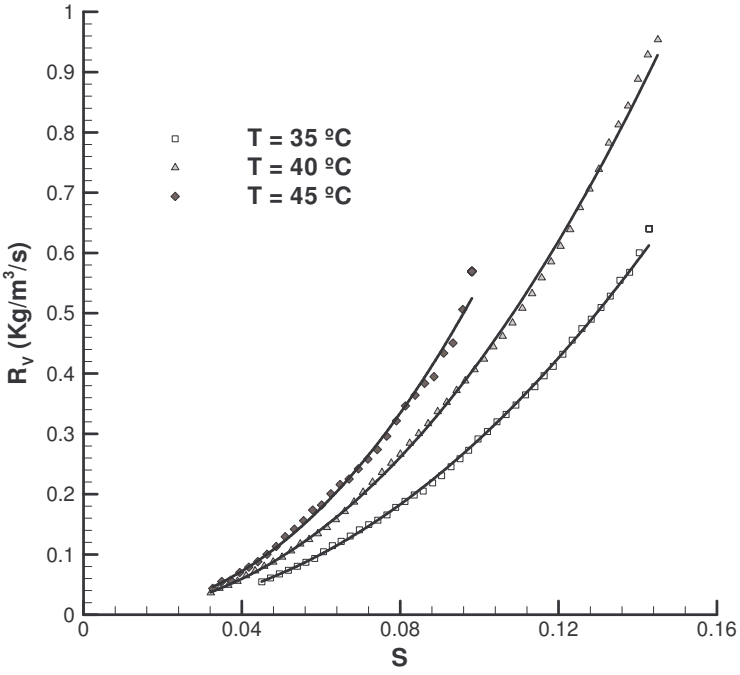

Figure 10.2. Volumetric growth rates of sucrose measured by the isothermal method at different temperatures.

The experimental data are represented for an average difference between successive mean supersaturations of 2.3×10^{-3}. Growth rate increases with both supersaturation and temperature. The first effect was well described through the supersaturation ranges by the semi-empirical relation given in Eq. (10.2). The respective fitting results are shown in Table 10.1.

Table 10.1. Parameters of Eq. (10.2) that best fit the experimental results presented in Figure 10.2.

Temperature (ºC)	K_V	n_V	R^2
35	35.5	2.08	0.999
40	57.4	2.13	0.999
45	88.9	2.21	0.998

The influence of the temperature on the growth rates is typically given by an Arrhenius relationship of the form of Eq. (10.4). The higher the overall activation energy E_A, the stronger is the influence of T on the volumetric growth constant K_V. The representation of the logarithm of K_V against $1/T$ provides a straight line with slope $-E_A/R$. The solid points in Figure 10.3 illustrate this behavior for the growth rate constants obtained at 35, 40 and 45 ºC (curve 1).

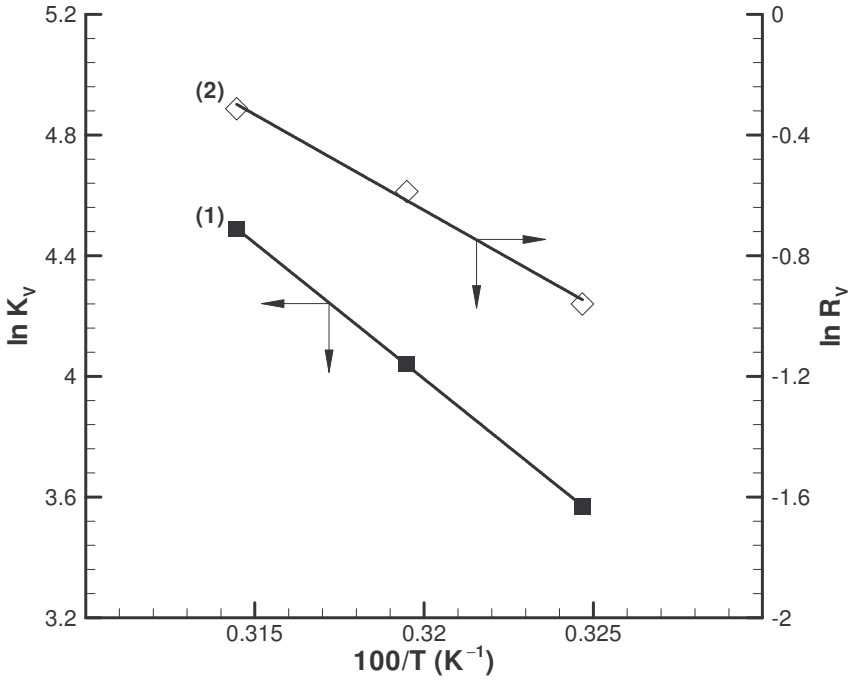

Figure 10.3. Effect of the inverse of temperature on the volumetric growth rate constant and on the volumetric growth rates inferred at $S = 0.114$.

The estimated overall activation energy $E_A = 74.8$ KJ/mol is slightly above the values found by Smythe [10] (62.8 KJ/mol) and by Maurandi et al [11] (69.8 KJ/mol), for temperatures below 40 ºC. In those works, a weighing method was employed to measure R_G at high crystal-solution velocities. According to the relationship between R_V and R_G given in Eq. (10.3), equivalent temperature dependences result from the use of both formalisms, as long as R_G is measured at constant average crystal size in all experiments:

$$\frac{\partial \ln\left(K_G\right)}{\partial\left(1/T\right)} = \frac{\partial \ln\left(\frac{\alpha L}{\beta} K_G\right)}{\partial\left(1/T\right)} = \frac{\partial \ln K_V}{\partial\left(1/T\right)} = -\frac{E_A}{R} \tag{10.12}$$

The open points in Figure 10.3 represent the influence of temperature on the volumetric growth rate itself (curve 2). According to Eqs. (10.3) and (10.4) one obtains:

$$\frac{\partial \ln R_V}{\partial\left(1/T\right)} = -\frac{E_A}{R} + \ln S \frac{\partial \ln n_V}{\partial\left(1/T\right)} \tag{10.13}$$

Accordingly, the difference between the slopes of the straight lines in Figure 10.3 provides the variation of the growth kinetic order n_V with temperature. If n_V was constant over the

temperature range, the slopes would both correspond to $-E_A/R$. In the present case, one obtained the slope of curve 1, −8999.8 K and of curve 2 −6345.1 K, which makes $\partial \ln n_V / \partial (1/T) = -1222.5$ K. The overall kinetic order is therefore expected to increase from about 2.0 to 2.3 when increasing the temperature from 35 to 45 ºC. This is roughly confirmed by the results of Table 10.1.

10.3.1 Falsified kinetics

In Chapter 5, the crystal growth rates of sucrose at 40 ºC were found to be strongly affected by mass transfer resistances. The variation of the growth kinetics with the agitation speed followed the behavior expected by the novel parallel step model (PSM) for the case of diffusional regime. In chemical reaction engineering, the concept of falsified kinetics is widely used to distinguish the reaction rate constants affected by diffusional limitations from the true, purely chemical, kinetic constants [12]. Extending this concept to the ongoing characterization of the sucrose growth rate dependence on temperature, one must consider the obtained activation energy as an apparent value. The true kinetic parameters are obtained from growth experiments carried out under sufficiently high crystal-solution velocities to eliminate the mass transfer resistances (chemical regime). In that case, the apparent and true activation energies are equivalent ($E_A = E_T$) and

$$K_{G_{chem}} = k_r = k_{r0} \exp\left(-\frac{E_T}{RT}\right) \tag{10.14}$$

Conversely, under diffusional regime the overall growth rate is given by

$$R_{G_{diff}} = \rho \sqrt{2 \frac{k_r k_d}{r+1} S^{r+1}} \tag{10.15}$$

so that the overall growth rate constant corresponds to $K_G = \rho \sqrt{2 k_r k_d / (r+1)}$. In the preceding equation k_d is the mass transfer coefficient during growth. This is a temperature-dependent constant given by

$$k_d = k_{d0} \exp\left(-\frac{E_D}{RT}\right) \tag{10.16}$$

If one assumes the true kinetic order r to be constant over the temperature range, the apparent activation energy in diffusional regime will correspond to the arithmetic mean of the activation energies for adsorption and diffusion:

$$\frac{\partial \ln K_G}{\partial (1/T)} = -\frac{E_A}{R} = -\frac{(E_T + E_D)/2}{R} \tag{10.17}$$

Using standard mass transfer correlations, Maurandi et al. estimated $E_D = 16.4$ KJ/mol for temperatures between 30 and 40 ºC and $E_D = 13.1$ KJ/mol for temperatures between 40 and 50 ºC. Assuming an average value of 15 KJ/mol for the working temperature range, and since $E_A = 74.8$ KJ/mol, it results from Eq. (10.17) that $E_T = 135$ KJ/mol. This value is considerably higher than E_D, indicating that the rate of the kinetic step during growth increases more strongly with temperature than the mass transfer rate. Therefore, the sucrose growth kinetics would remain highly affected by diffusional limitations for temperatures above 40 ºC, while for lower temperatures the process is expected to gradually become less influenced by diffusion.

In general terms, the true and apparent activation energies can be related once the effectiveness factor is known, i.e., once the role of the mass transfer resistance is established. In fact, if the overall growth rate order does not change significantly over the temperature range, it results from the definitions given in Eqs. (10.1), (10.5), (10.12) and (10.14) that

$$-\frac{E_A}{R} = -\frac{E_T}{R} + \frac{\partial \ln \eta}{\partial (1/T)} = -\frac{E_T}{R} + \frac{\partial \ln \eta}{\partial \ln \phi_g}\frac{\partial \ln \phi_g}{\partial (1/T)} \tag{10.18}$$

The constant kinetic order condition is verified in some works [11, 13, 14] but, as previously seen, one cannot assume it as a general rule. Substituting now the definitions of η (Eq. (10.6)) and ϕ_g (Eq. (10.7)) in Eq. (10.18) one obtains that

$$E_A = E_T + \frac{\phi_g - \sinh \phi_g}{\sinh \phi_g}\frac{(E_T - E_D)}{2} \tag{10.19}$$

This equation is plotted in Figure 10.4 in conjunction with the definition of the effectiveness factor given by Eq. (10.6). For small mass transfer resistances, the value of ϕ_g is also small and the apparent activation energy tends to the true one ($\eta = 1$). As the mass transfer resistances become higher, ϕ_g increases and the apparent activation energy tends to the arithmetic mean of E_T and E_D. This corresponds to the limit case of diffusional regime obtained with pure sucrose at 40 ºC. Parameter ϕ_g can be decreased by increasing the crystal-solution velocity (increasing k_d) and/or by decreasing the temperature (lowering the k_r/k_d ratio).

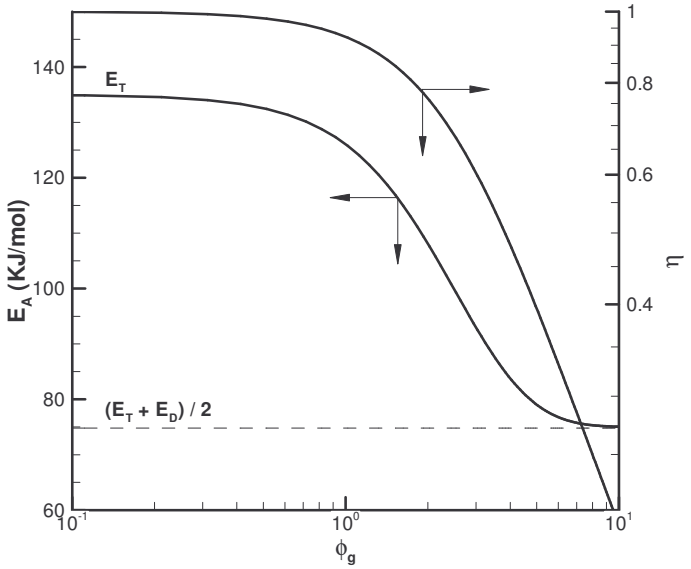

Figure 10.4. Influence of the parameter ϕ_g on the apparent activation energy and on the effectiveness factor for sucrose crystal growth.

10.3.2 Surface effects

So far, only the growth rate results obtained by the isothermal method have been discussed. In this work, the influence of temperature on the crystal growth rate was further characterized using an innovative measurement method in which R_V (or R_G) is obtained at constant supersaturation, as the temperature decreases. Figure 10.5 illustrates that the $\ln R_V$ vs $1/T$ curves resulting from both methods significantly differ. Apart from the fair agreement between growth rates verified in the beginning of the constant supersaturation experiment (at 44–40 ºC), as the temperature decreases, progressively lower rates are obtained by the novel method. Consequently, the absolute of the slope $\partial \ln R_V / \partial (1/T)$ is in this case higher than the obtained from the measurements at constant temperature. Both types of batch growth experiments were carried out under comparable experimental conditions so that the differences found cannot be explained by simple engineering models.

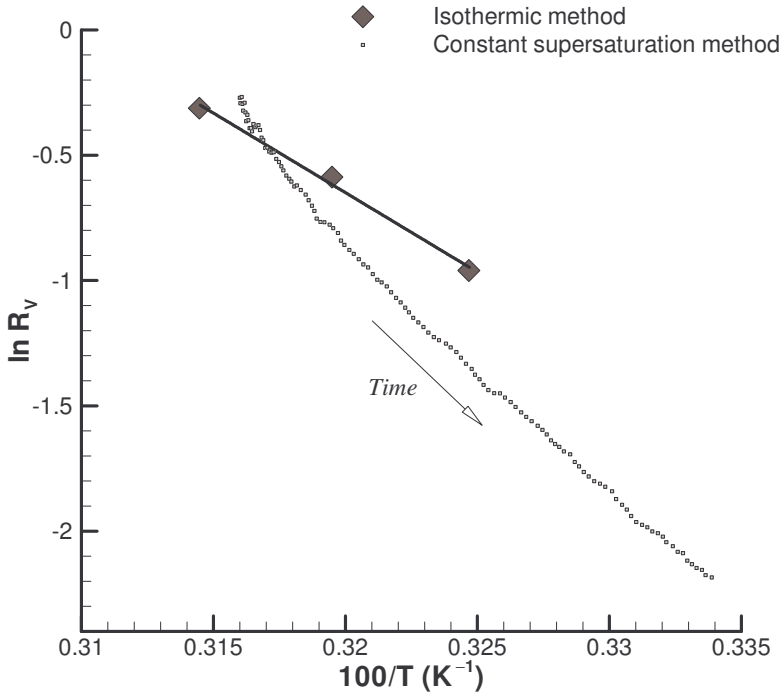

Figure 10.5. Effect of the reciprocal of temperature on the volumetric growth rates measured by the constant supersaturation method and by the isothermal method at $S = 0.114$.

The results of Figure 10.5 are likely to be explained by surface effects provoked by the different growth rate histories in each method. Following recent findings of Pantaraks and Flood [15], rapid crystal growth of sucrose causes a roughening of the crystal surface, so that subsequent growth occurs at lower rates than would be expected without this growth history. The same authors observed that posterior periods of growth at low growth rates may heal the surface after its roughening, and allow the crystal to return its normal kinetics. Nevertheless, the time required for healing is of the order of several hours. In the constant supersaturation method, the seed crystals are introduced at the highest temperature (T_i) of the studied range. Hence, the period at which crystals grow faster corresponds to the beginning of the experiment. This fact would certainly affect the surface features of the crystals during the remaining growth. In particular, at a given $T < T_i$ the surface roughness would be higher than if the crystals had been growing at the temperature T. As a result, the measured growth rates would be lower than the ones obtained isothermally. Since the process of crystal healing is slow comparatively to the cooling rate, the differences between rate histories, and thus, between the measured growth rates become more marked as the temperature decreases and $1/T$ increases (Figure 10.5).

Going a step further, the role of temperature and growth rate history will now be interpreted in the light of the fundamental perspective of the integration kinetics provided by the spiral nucleation model (SNM). From the definitions given in Eqs. (10.8), (10.9) and (10.10) the following result is obtained:

$$\frac{\partial \ln R_V}{\partial (1/T)} = -\frac{W}{k} - 2\frac{1.64\Omega h}{\ln(1+S)}\left(\frac{\gamma}{kT}\right)^2\left(\frac{\partial \ln \gamma}{\partial (1/T)} + T\right) \tag{10.20}$$

The term dependent on the adsorbing energy (W) accounts for the velocity of advancement of steps, while the second term stands for the activation energy of formation of stable spirals (ΔG_c). In the cases where the first term is not clearly dominant relatively to the second, $\partial \ln R_V / \partial (1/T)$ will change with T and S in a manner that is also function of the $\gamma(T,S)$ relationship. In this concern, the interfacial tension γ is normally thought to decrease linearly with T (Eötvös rule) [16], while the following $\gamma(S)$ function results, from the SNM, when the condition of constant growth kinetic order over the supersaturation range is observed (see Chapter 7 for more details):

$$\gamma = \sqrt{C_1 S - C_2 S \ln S} \tag{10.21}$$

where C_1 and C_2 are constants. Minor variations of the overall activation energy over the temperature and supersaturation ranges are expected form Eq. (10.20) when $W \gg \Delta G_c$. From our study in Chapter 7, $\Delta G_c / kT \sim 14$ at $S = 0.1$, which is of the same order of magnitude of estimations of $W/kT \sim 24$ [17]. In these cases of high energetic barrier for spiral nucleation, the importance of the interfacial tension on the growth kinetics is also reinforced. Changes on the surface properties of the crystal as the ones caused by different growth rate histories would affect R_V and its dependence on T. As seen, crystals having a history of fast growth have rougher surfaces and lower growth rates. The connection between surface roughness and crystal growth kinetics can be explained by combining the SNM with the Wenzel roughness factor (r_w), defined as the ratio between the true and the apparent (geometric) surface area of the solid [18-20]. The wetting properties of rough solids are directly proportional to r_w so as to account for the enhancement of the microscope surface area. Accordingly, the effective interfacial tension of a growing crystal is given by

$$\gamma = r_w \gamma_{SL} \tag{10.22}$$

where γ_{SL} is the solid-liquid interfacial tension on a smooth surface ($r_w = 1$). As the values of r_w and γ increase, the energetic barrier for spiral nucleation given by Eq. (10.10) increases

and the crystal tends to grow more slowly. Higher interfacial tensions would also increase the absolute of the slope $\partial \ln R_V / \partial (1/T)$ given by Eq. (10.20). This is well illustrated by the data of Figure 10.5 obtained by the constant supersaturation method. In a first phase of the experiment, there is a rapid surface roughening that leads to high values of γ. The strong decrease of the initial growth rate shown in Figure 10.5 reflects not only the temperature decrease but also the development of a more heterogeneous surface. As the growth proceeds at lower temperatures and growth rates, the crystals become gradually healed and r_w slowly decreases. As a consequence the $\partial \ln R_V / \partial (1/T)$ slope seems to progressively decrease as the experience progresses. If the surface properties were constant throughout the experiment, the slope would instead increase as the $1/T$ increases because of less dominant mass transfer resistances at lower temperatures. This trend was previously verified in the works of Smythe [10] and Maurandi et al. [11].

10.3.3 Comparison of crystal growth rates measured by different techniques

Scale up problems and low reproducibility are frequently associated to growth rate measurements using different techniques. In previous chapters, we have been focusing important (but sometimes overlooked) crystallization variables such as the mass transfer resistance (Chapter 5), interfacial properties (Chapter 7) and crystal size (Chapter 8) based on sucrose growth experiments at 40 ºC in a batch crystallizer. These studies were now complemented by characterizing the influence of temperature and growth rate history on the sucrose crystallization kinetics. At this point, we are able to investigate why growth rates measured at same supersaturation and temperature can be apparently very divergent when employing distinct growth techniques [21, 22]. In particular, the results of Figure 10.2 obtained by the isothermal method at 40 ºC will be compared with the crystal growth rates of sucrose measured by Guimarães et al. [23] in a 0.5 L fluidized bed crystallizer at the same temperature. In both cases, sieved white sugar with 99.98 % purity was used as seed crystals (sieve sizes between 0.250 and 0.300 mm in the batch experiment and between 0.710 and 0.850 mm in the fluidized bed case). The results taken from literature were converted into volumetric growth rates through Eq. (10.3), using the sucrose shape factors found by Bubnik and Kadlec [24], and $L = 0.853$ mm. By using the volumetric formalism it is aimed to normalize the effect of crystal size on both results. Even so, Figure 10.6 shows very distinct growth curves depending on the measurement technique employed.

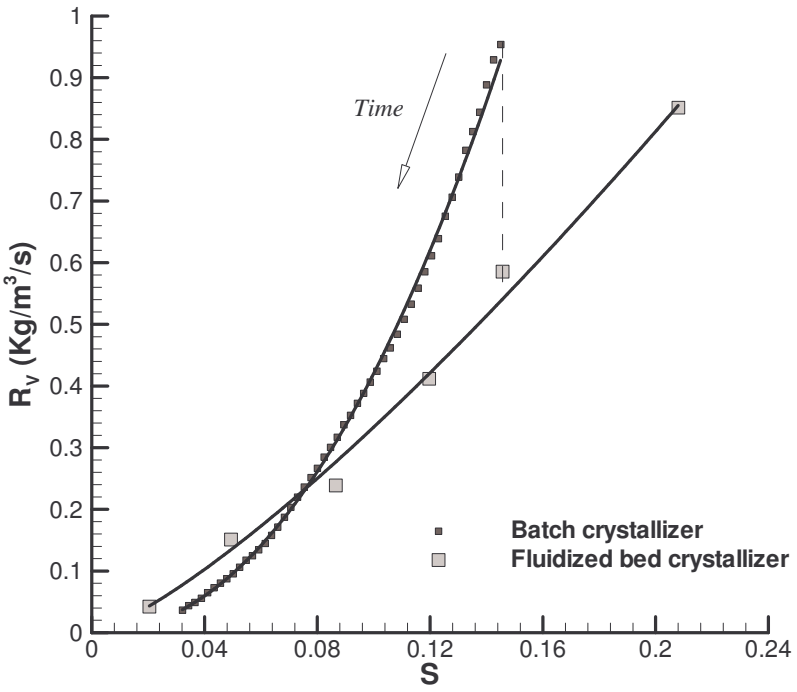

Figure 10.6. Volumetric growth rates of sucrose at 40 ºC measured in a batch crystallizer (isothermal method) and in a fluidized bed crystallizer [23].

The reasons previously suggested for the contrasting influence of T on R_V obtained in Figure 10.5 keep in essence valid for the results of Figure 10.6. The crystals growth rate history in each type of experiment is only comparable for $S \sim 0.14$, when the batch isothermal experience is starting. At that time, the seed crystals in the batch crystallizer had already grown during 40 min at a supersaturation slightly above 0.14. Although the subsequent growth occurs at progressively lower supersaturations, the surface properties of the crystals would keep associated to a fast growth history. In its turn, the fluidized bed experiments are carried at constant supersaturation and each point in Figure 10.6 corresponds to a different experiment of 40 min duration. The surface properties change is therefore limited to that growth period. Thinking in terms of the evolution of the roughness factor, high values of r_w are expected over the entire supersaturation range of the batch experiment. This happens because of the initial rapid growth period (roughening) and subsequent slow surface healing. On the other hand, in the measurements of Guimarães et al. the r_w factor is supposed to abruptly decrease as the supersaturation decreases; for $S < 0.14$, the crystals surface would be smoother than in the batch case, with the differences becoming more marked as the supersaturation decreases. In the case of the fluidized bed experiments, the growth rate

enhancement with supersaturation is partially opposed by the effect of r_w on the effective interfacial tension (Eq. (10.22)) and on the energetic barrier for growth (Eq. (10.10)). As a result, comparatively weaker R_V vs S dependence is obtained in Figure 10.6. Conversely, since r_w does not change significantly over the batch experiment the effect of the supersaturation on the volumetric growth rates is not masked, and a strong R_V vs S dependence is obtained.

Crystal surface properties affect the energetic barrier for integration, and thus the dependence of R_V on supersaturation. This explains the divergence between the apparent kinetic orders obtained with the literature results ($n_V = 1.3$) and in these experiments ($n_V = 2.1$). Nevertheless, one important question remains unanswered: why the growth rates are so different in the supersaturation range of comparable growth rate histories ($S \sim 0.08$)? Certainly the explanation for this fact is not related with the integration mechanism but instead with the relative weight of the mass transfer resistance in each method. While the batch growth experiment was carried out under vigorous agitation (300 rpm), in the fluidized bed crystallizer the crystals were suspended by the upwards flow of solution along with gentle agitation [23]. Following the previous studies in this work, the relationship between volumetric growth rates obtained under different hydrodynamic conditions is given by:

$$\frac{R_{V_1}}{R_{V_2}} = \sqrt{\frac{(R_D / L)_1}{(R_D / L)_2}} \tag{10.23}$$

In this equation R_D is the dissolution rate under corresponding hydrodynamic conditions of growth. These data are shown for the two methods in question in Figure 10.7 after normalizing R_D by the instantaneous (batch) or the average (fluidized bed) crystal size during the dissolution experiments. With the additional representation of dissolution rates obtained at 200 and 250 rpm it is aimed to demonstrate the strong influence of the agitation speed on the mass transfer resistance.

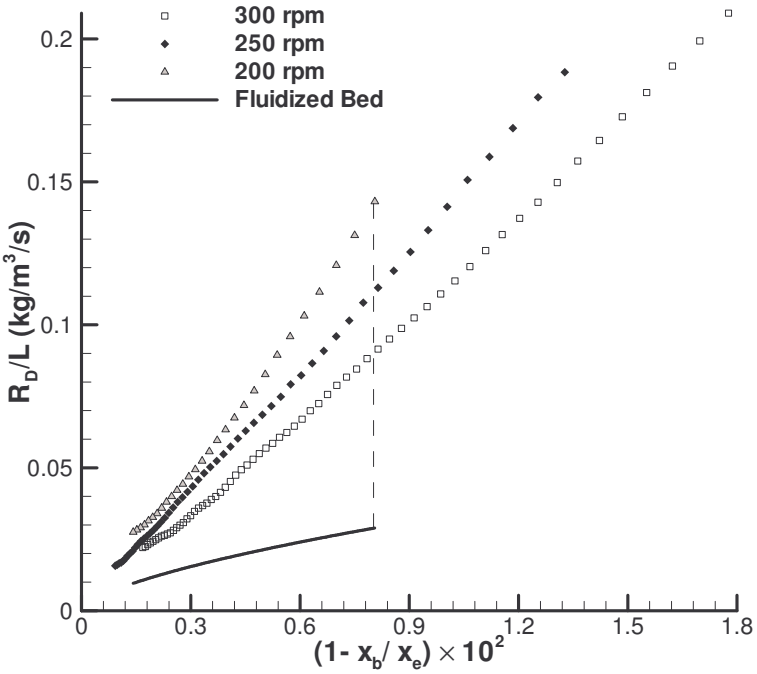

Figure 10.7. Comparison between the normalized dissolution rates of sucrose at 40 ºC measured in the batch crystallizer at different agitation speeds (Chapter 5) and the ones estimated for the fluidized bed crystallizer [25].

Comparing the differences between the growth rates highlighted in Figure 10.6 by a dashed line, and between the dissolution rates shown in Figure 10.7, one obtains that in fact

$$\frac{R_{V\,batch}}{R_{V\,fluid.bed}} \sim \sqrt{\frac{\left(R_D / L\right)_{batch}}{\left(R_D / L\right)_{fluid.bed}}} \sim 2 \tag{10.24}$$

As expected, this correspondence is obtained when the volumetric growth rates are evaluated at $S \sim 0.14$, i.e., for crystals with similar growth rate history. For $S < 0.14$, the differences between growth rates result from different diffusional conditions and crystal surface properties. The correspondence given in Eq. (10.24) confirms not only the diffusion-integration models from which the relationship was derived, but also the connection between growth rate history, surface properties and crystal growth rates suggested in this work. The significance of this conclusion is emphasized by the fact that growth results obtained by very distinct measurement techniques were used to its drawing.

10.4 Conclusions

Empirical, engineering and fundamental models of crystal growth were combined on the interpretation of the kinetic effect of temperature and growth rate history. Growth rate data obtained in a batch crystallizer at 35, 40 and 40 ºC by an isothermal method was used to determine the apparent activation energy. The temperature dependence of the empirical kinetic order n_V is determined from the slope of the plots of $\ln K_V$ and $\ln R_V$ as a function of $1/T$. Following the recently introduced parallel step model, a theoretical relationship between apparent and true activation energy is proposed (Eq. (10.19)). For small mass transfer resistances, E_A and E_T are equivalent. As the mass transfer resistances become higher, E_T tends to the arithmetic mean of the activation energies for adsorption and diffusion. The influence of temperature on the sucrose growth rate was measured by an alternative method, by allowing the crystals to grow at constant supersaturation ($S = 0.114$) as the temperature decreased from ~44 to 25 ºC. The different results obtained by the isothermal and constant supersaturation methods were explained by different surface roughness of the crystals in each type of experiments. Crystals with a history of rapid growth are believed to have higher roughness factors, and therefore, higher effective interfacial tensions. According to the spiral nucleation mechanism, this increases the energetic barrier for growth and decreases the crystal growth rate. Information about the growth rate dependence on the crystal size, hydrodynamic conditions and growth rate history was used to explain the sucrose growth rate curves obtained at 40 ºC in a batch crystallizer and in a fluidized bed crystallizer. The differences found by employing the two techniques satisfactorily correspond to the theoretical predictions.

References

[1] M. Ohara and R. C. Reid, Modelling crystal growth rates from solution, Prentice-Hall, Inc., New Jersey, **1973**.

[2] J. Garside, The concept of effectiveness factors in crystal growth. *Chem. Eng. Sci.*, **1971,** 26, 1425-1431.

[3] J. W. Mullin, Crystallization, 4th ed.; Butterworth-Heinemann, Oxford, **2001**.

[4] C. Y. Tai, Crystal growth kinetics of two-step growth process in liquid fluidized-bed crystallizers. *J. Cryst. Growth*, **1999,** 206, 109-118.

[5] X. F. Abegg, J. D. Stevens, and M. A. Larson, Crystal size distributions in continous crystallizers when growth rate is size dependent. *AIChE J.*, **1968,** 14, 118-122.

[6] M. M. Mitrovic, A. A. Zekic, and M. M. Napijalo, Correlation between the crystal size and crystal growth rate of KDP and Rochelle salt crystals. *J. Cryst. Growth*, **2000,** 216, 437-442.

[7] E. T. White, L. L. Bending, and M. A. Larson, in *Analysis and design of crystallization processes*, (R. W. Rousseau, M. A. Larson, eds.), AIChE Symposium Series, New-York, **1976**.

[8] T. S. Li, I. Livk, and D. Ilievski, Supersaturation and temperature dependency of gibbsite growth in laminar and turbulent flows. *J. Cryst. Growth*, **2003,** 258, 409-419.

[9] V. Maurandi, G. Mantovani, G. Vaccari, and A. Rossi, Kinetics and technology of low boiling massecuite exhaustion. *Zuckerindustrie*, **1988,** 113, 791-794.

[10] B. M. Smythe, Sucrose crystal growth.I. Rate of crystal growth in pure solutions. *Aust. J. Chem.*, **1967,** 20, 1087-1095.

[11] V. Maurandi, G. Mantovani, and G. Vaccari, Sucrose crystal growth activation energies from pure and impure solutions. *Zuckerindustrie*, **1984,** 109, 734-739.

[12] H. S. Fogler, Elements of Chemical Reaction Engineering, 3rd ed.; Prentice Hall International Inc., Upper Saddle River, NJ, **1999**.

[13] N. A. Clontz, R. T. Johnson, W. L. McCabe, and R. W. Rousseau, Growth of magnesium sulphate heptahydrate crystals from solution. *Ind. Eng. Chem. Fundam.*, **1972,** 11, 368-373.

[14] J. Garside, J. W. Mullin, and S. N. Das, Growth and dissolution kinetics of potassium sulfate crystals in an agitated vessel. *Ind. Eng. Chem. Fundam.*, **1974,** 13, 299-305.

[15] P. Pantaraks and A. E. Flood, Effect of growth rate history on current crystal growth: A second look at surface effects on crystal growth rates. *Cryst. Growth Des.*, **2005,** 5, 365-371.

[16] G. Wedler, Manual de Química Física, Fundação Calouste Gulbenkian, Lisbon, **1997**.

[17] W. K. Burton, N. Cabrera, and F. C. Frank, The growth of crystals and the equilibrium structure of their surfaces. *Phil. Trans. Roy. Soc. London*, **1951,** 243, 299-358.

[18] N. R. Wenzel, Resistance of solid surfaces to wetting by water. *Ind. Eng. Chem.*, **1936,** 28, 988-994.

[19] T. S. Meiron, A. Marmur, and I. S. Saguy, Contact angle measurement on rough surfaces. *J. Colloid Interface Sci.*, **2004,** 274, 637-644.

[20] G. Mhale and M. I. Newton, Frenkel's method and the dynamic wetting of heterogeneous planar surfaces. *Colloid Surf. A-Physicochem. Eng. Asp.*, **2002,** 206, 193-201.

[21] J. W. Mullin and J. Garside, Crystallization of aluminium potassium sulphate: a study in the assessment of crystallizer design data: II: - Growth in a fluidized bed crystallizer. *Trans. Inst. Chem. Eng.*, **1967,** 45, T291-T295.

[22] M. Kohl, F. Puel, J. P. Klein, C. Hoff, and O. Monnier, Investigation of the growth rate of [beta]-cyclodextrin in water during both flow-cell and batch experiments. *J. Cryst. Growth*, **2004,** 270, 633-645.

[23] L. Guimarães, S. Sá, L. S. M. Bento, and F. Rocha, Investigation of crystal growth in a laboratory fluidized bed. *Int. Sugar J.*, **1995,** 97, 199-204.

[24] Z. Bubnik and P. Kadlec, Sucrose crystal shape factors. *Zuckerindustrie*, **1992,** 117, 345-350.

[25] S. Sá, L. Guimarães, F. Rocha, and L. S. M. Bento, in *13th Symposium on Industrial Crystallization*, Toulouse, France, **1996**.

11. General conclusions and suggestions for future work

11.1 General conclusions

The measurement of reliable crystal growth kinetics and subsequent rational interpretation were discussed according to classical and newly proposed perspectives. The crystallization of sucrose is used as a case study in laboratory and pilot scale experiments. Departing from identified limitations of the existing crystal growth theories, alternatives were proposed to characterize the influence of growth parameters such as supersaturation, temperature, hydrodynamic conditions, impurity concentration and crystal size. Developments on the molecular description of the crystal growth phenomenon provided new tools for the determination of interfacial and topological properties from growth rate data.

Practical difficulties found in industry-like environment were the starting point for a systematic study of the factors affecting crystal growth. In Part I of the thesis, new methods were proposed for characterization and management of sugar evaporative crystallizers: by the **mass balance method**, the vacuum pan content of sucrose, impurities, and water was dynamically computed using typical sugar boiling data and the initial parameters of the cane syrups. This way, the evolution of the crystal content, mass of crystals, liquor purity, and liquor non-sucrose to water ratio was possible to be determined during sugar boiling runs. Using modern image processing techniques, the progress of the mean crystal size in the first phases of sugar boiling experiments was followed. The results obtained in this **image analysis**

method compared well with the ones calculated by mass balance. The next challenge was to process the obtained supplementary boiling data so as to estimate sucrose growth kinetics in other conditions than of conventional laboratory experiments. This was firstly done by determining equilibrium data at the particular conditions of the pilot pan experiments. The **estimation of sucrose solubility from crystallization curves** was accomplished by fitting the derived theoretical concentration profile to the sucrose concentration curves calculated by the mass balance method. The resulting sucrose solubility coefficients were in good agreement with published data measured at similar conditions of sugar cane boiling. Then, a new **growth rate measurement method** was proposed, where the measured evolution of mass of crystals with time was used to calculate the corresponding variation of the sucrose growth rate. The used equation takes into account the variation of the crystal surface area, instead of assuming a mean surface area over the growth period. Kinetic curves were obtained by representing the sucrose growth rates as a function of the liquor supersaturation during the experiments. The methods for equilibrium and kinetic data determination proved to be robust and of direct application to large-scale sugar crystallization.

A number of different factors affected the growth rates of sucrose obtained in the first part of thesis. Thus, the isolated role of important variables such as supersaturation, crystal size, impurity concentration, hydrodynamic conditions, etc, is difficult to be inferred from those results. In the succeeding chapters, new theoretical and experimental studies focusing some of the most important crystallization variables were presented. In spite of the importance of the transport phenomena during crystal growth, significant limitations of typical diffusion-reaction models were identified when confronting the theory against experimental data. An attempt was made to fulfil this gap by means of the novel **parallel step model**. In this model, the existence of interfacial adsorption is considered not only in physical terms, but also in the mathematical derivation of the growth rate equations. Adopting a methodology comparable to the derivation of the Brunauer-Emmett-Teller isotherm, it was concluded that the rate at which molecules integrate the crystal lattice corresponds to the net adsorption velocities extended to the thickness of the adsorbed multilayer. Consequently, simultaneous occurrence of solute diffusion and adsorption was assumed to occur before the integration of the adsorbed molecules at crystal surface. Different situations were analysed concerning the crystal shape, integration kinetic order and diffusional resistance, and a generalized overall growth rate equation was proposed. The **comprehensive test of the new**

model was carried out using crystallization data obtained under different and well-defined diffusional conditions, and available information about limiting cases of pure chemical and diffusional regimes. Mass transfer coefficients were determined from the growth rate data using the conventional two-step model and the parallel step model. In the first case, an unrealistic variation of the coefficients with the relative crystal-solution velocity was obtained when compared with the behaviour expected from standard mass transfer correlations. Conversely, the mass transfer coefficients obtained by the parallel step model were confirmed both in their order of magnitude and in the way they were influenced by the hydrodynamic conditions. Closely controlled **laboratory experiments were conceived** to study the influence of agitation speed on the sucrose growth rates in a batch crystallizer. Contrarily to what happened in the pilot-scale runs, this procedure allowed accurate investigations on the kinetic influence of isolated growth variables. As predicted by the parallel step model, the presence of a thick adsorbed layer around the sucrose crystals is likely to have affected the solute molecular diffusivity in the medium. According to that, the results obtained were well described by the parallel step model.

The other engineering approach in Part II consists in a new **competitive adsorption model** to describe the growth of crystals in impure solutions. A dispute between the crystallizing solute and the impurity was considered to exist for the surface coverage and for the occupation of energetically favourable places at surface steps. The impurity effect on the crystal growth rates is characterized by a Langmuirian isotherm for competitive adsorption and by the parameter β, accounting for the impurity ability to move across the surface and occupy a stable position at the active sites. Published experimental data showing different types of impurity-affected kinetics were adequately described by the competitive adsorption model. The contribution of the new model on explaining unresolved mechanistic and kinetic evidences was highlighted.

Regardless of the advancements on crystal growth characterization provided by the new engineering models, many questions can only be answered through molecular scale fundamentals of the phenomenon. In Part III of the thesis, the limitations of classical two-dimensional nucleation models and of the Burton-Cabrera-Frank theory were recalled in view of recent observations of growth features using modern microscopic techniques. An alternative theory was proposed in which new and classical concepts were combined in the so-called "**spiral nucleation model**". Initial growth nuclei are assumed to result from the organization of adsorbed molecules in spirals around surface dislocations. The energetic

barrier for the activation of the spiral nuclei is considerably lower than the admitted in other energy-activated mechanisms. Stable nuclei evolve into bigger growth hillocks in supersaturated media through the incorporation of adsorbed units into their steps. The displacement velocity of steps in solution and vapour growth is calculated under different kinetic premises, taking into consideration the importance of surface diffusion in each process. A generalized expression was obtained relating the crystal growth rate with main variables such as supersaturation, temperature, crystal size, surface topology and interfacial properties. An application example was given, where the **supersaturation-dependence of the interfacial tension** is determined from the crystal growth kinetics of sucrose at 40 ºC. Additionally, the spiral nucleation model was applied on the estimation of the **optimum interstep distance and of critical parameters of the growing hillocks** without the use of microscopic techniques. The published data in this field support the consistency of those findings.

Finally, in Part IV of the thesis, the potential of the new fundamental end engineering models was illustrated in several application examples. The occurrence of **size-dependent growth** in the crystallization of sucrose was investigated according to the new insights provided by the spiral nucleation model. Laboratory growth experiments carried out with crystals of different size confirmed that the integration rate is linearly dependent on the crystal characteristic dimension. Accordingly, an innovative growth rate definition was put forward by expressing the mass deposition rate per crystal volume units. The **volumetric growth rates** demonstrated to be size independent over the considered supersaturation range. Moreover, this formalism is of great practical interest since it can be used in situations of unknown crystal number and size. Since crystal size also affects the mass transfer processes, the parallel step model was recalled for the diffusional effect quantification. The conventional growth rates measured in the sugar boiling experiments of Part I were conveniently converted into volumetric growth rates to study the isolated **influence of cane sugar impurities on the sucrose growth kinetics**. Empirical correlations used in sugar industry satisfactorily described the growth rate decrease with the non-sucrose compounds concentration. On the other hand, besides being consistent with the experimental findings, the proposed competitive adsorption model additionally contributed for the logical understanding of the impurities action. The estimated model parameters indicate that cane sugar impurities can be greatly adsorbed at the sugar crystal surface, even though their kinetic effectiveness is low. In a

concluding example, empirical, engineering and fundamental models were combined on the interpretation of the **effect of temperature** and **growth rate history** on the growth kinetics. The apparent and true activation energies of sucrose were determined from the growth rate curves measured at different temperatures. A theoretical relationship between the two activation energies was derived from the parallel step model. The influence of temperature on the crystal growth rates was measured by the innovative **constant supersaturation method** by allowing the crystals to grow at controlled supersaturation and decreasing temperature. Differences between the results of the isothermal and constant supersaturation methods were explained from the viewpoint of the spiral nucleation mechanism, taking into account **different crystal surface properties** caused by the growth rate history in each case. The same framework was used to explain the growth rate curves measured in the batch crystallizer and in a fluidized bed crystallizer at the same temperature. Apparently divergent results were successfully described by the combined effects of crystal size, hydrodynamic conditions and growth rate history that have been proposed throughout this thesis.

11.2 Suggestions for future work

More than setting the end of the thesis, the conclusions summarized above are expected to provide some of the guidelines for future works in this field. Desirably, the presented methods and theories will continue to be developed through their application to new systems and purposes.

In the near future, it is intended to implement the mass balance method in sugar evaporative crystallizers for on-line measurement of important process variables. The results of Chapter 2 were obtained at the end of the sugar boiling runs, after processing the experimental data according to the set of equations of the model. By incorporating these equations in the pan automation software, it would be possible to follow the progress of supersaturation, crystal content, mass of crystals, liquor purity and liquor non-sucrose to water ratio as the run evolves. Nowadays, there is a great interest in sugar industry to improve the monitoring techniques and considerable research has been devoted to the variables discussed here. In its turn, the image analysis method should also be improved in terms of the results accuracy and in the method application range. Improvements can be made in the image acquisition probe to allow good crystals differentiation at crystal mass fractions above 10%. The potential of the method in following the crystal size distribution with time may well be

used on the study of the crystallization kinetics, size-dependent growth, crystal growth dispersion, primary nucleation, particle agglomeration, etc.

From the literature reviews made, the new engineering models will be very welcomed in other systems than sucrose. For example, the parallel step model demonstrated to be of great applicability in the crystallization of inorganic salts from solution, and the competitive adsorption model adequately described uncharacteristic crystal growth curves in the presence of impurities. In addition, the parallel step model can be further explored in view of straightforward determinations of the diffusional resistance. It would be interesting to combine the parallel step model and the competitive adsorption model on the investigation of the impurity effect at different mass transfer resistances. A natural follow-up of the competitive adsorption model would be the study of non-equilibrium impurity adsorption during crystal growth. In this concern, the occurrence in some systems of growth rate hysteresis is a good experimental evidence of the impurity adsorption kinetics. So far, the existing theoretical models did not give a completely satisfactory justification for this fact, possibly because the competitive nature of surface adsorption has been disregard.

The fundamental views provided by the spiral nucleation model can be extended through many branches of crystal growth science. In this thesis, some application examples were given by applying the new theory to crystal growth from solution, using the pure sucrose system. In the future, the spiral nucleation model might be useful in varied fields such as molecular beam epitaxy, chemical vapour deposition, crystal growth of metals, minerals, semiconductors, superconductors, magnetics and biological substances, either in bulk or as thin films. The availability of new microscopic techniques (e.g., atomic force microscopy, electron microscopy, X-ray diffraction, etc) represents a valuable tool for consolidating the theoretical concepts introduced here. Advances in the molecular modeling of the crystals structure can be suitably combined with the spiral nucleation model on the investigation of less studied variables like the surface mobility of adsorbed molecules, dislocation density and other interfacial properties. The new atomistic model can as well be improved to account for the phenomena of step bunching and non-spiral growth occurring at high supersaturations. The current quest for large protein crystals with low defect contents is believed to be a privileged application field of the new growth theories. Such crystals are of key importance in contemporary molecular biology or in drug discovery, for suitable protein structure determinations by diffraction of X-rays, electrons or neutrons. A good understanding of the

factors influencing crystal growth is therefore essential for biochemical and biomedical research, and can contribute to find alternatives to the expensive microgravity techniques of producing well grown crystals.